



NUREG/CR-7194
ORNL/TM-2014/240

Technical Basis for Peak Reactivity Burnup Credit for BWR Spent Nuclear Fuel in Storage and Transportation Systems

AVAILABILITY OF REFERENCE MATERIALS IN NRC PUBLICATIONS

NRC Reference Material

As of November 1999, you may electronically access NUREG-series publications and other NRC records at NRC's Public Electronic Reading Room at <http://www.nrc.gov/reading-rm.html>. Publicly released records include, to name a few, NUREG-series publications; *Federal Register* notices; applicant, licensee, and vendor documents and correspondence; NRC correspondence and internal memoranda; bulletins and information notices; inspection and investigative reports; licensee event reports; and Commission papers and their attachments.

NRC publications in the NUREG series, NRC regulations, and Title 10, "Energy," in the *Code of Federal Regulations* may also be purchased from one of these two sources.

1. The Superintendent of Documents
U.S. Government Printing Office
Mail Stop SSOP
Washington, DC 20402-0001
Internet: bookstore.gpo.gov
Telephone: 202-512-1800
Fax: 202-512-2250
2. The National Technical Information Service
Springfield, VA 22161-0002
www.ntis.gov
1-800-553-6847 or, locally, 703-605-6000

A single copy of each NRC draft report for comment is available free, to the extent of supply, upon written request as follows:

Address: U.S. Nuclear Regulatory Commission
Office of Administration
Publications Branch
Washington, DC 20555-0001

E-mail: DISTRIBUTION.RESOURCE@NRC.GOV
Facsimile: 301-415-2289

Some publications in the NUREG series that are posted at NRC's Web site address <http://www.nrc.gov/reading-rm/doc-collections/nuregs> are updated periodically and may differ from the last printed version. Although references to material found on a Web site bear the date the material was accessed, the material available on the date cited may subsequently be removed from the site.

Non-NRC Reference Material

Documents available from public and special technical libraries include all open literature items, such as books, journal articles, transactions, *Federal Register* notices, Federal and State legislation, and congressional reports. Such documents as theses, dissertations, foreign reports and translations, and non-NRC conference proceedings may be purchased from their sponsoring organization.

Copies of industry codes and standards used in a substantive manner in the NRC regulatory process are maintained at—

The NRC Technical Library
Two White Flint North
11545 Rockville Pike
Rockville, MD 20852-2738

These standards are available in the library for reference use by the public. Codes and standards are usually copyrighted and may be purchased from the originating organization or, if they are American National Standards, from—

American National Standards Institute
11 West 42nd Street
New York, NY 10036-8002
www.ansi.org
212-642-4900

Legally binding regulatory requirements are stated only in laws; NRC regulations; licenses, including technical specifications; or orders, not in NUREG-series publications. The views expressed in contractor-prepared publications in this series are not necessarily those of the NRC.

The NUREG series comprises (1) technical and administrative reports and books prepared by the staff (NUREG-XXXX) or agency contractors (NUREG/CR-XXXX), (2) proceedings of conferences (NUREG/CP-XXXX), (3) reports resulting from international agreements (NUREG/IA-XXXX), (4) brochures (NUREG/BR-XXXX), and (5) compilations of legal decisions and orders of the Commission and Atomic and Safety Licensing Boards and of Directors' decisions under Section 2.206 of NRC's regulations (NUREG-0750).

DISCLAIMER: This report was prepared as an account of work sponsored by an agency of the U.S. Government. Neither the U.S. Government nor any agency thereof, nor any employee, makes any warranty, expressed or implied, or assumes any legal liability or responsibility for any third party's use, or the results of such use, of any information, apparatus, product, or process disclosed in this publication, or represents that its use by such third party would not infringe privately owned rights.



United States Nuclear Regulatory Commission

Protecting People and the Environment

NUREG/CR-7194
ORNL/TM-2014/240

Technical Basis for Peak Reactivity Burnup Credit for BWR Spent Nuclear Fuel in Storage and Transportation Systems

Manuscript Completed: December 2014

Date Published: April 2015

Prepared by:

William (B.J.) Marshall

Brian J. Ade

Stephen M. Bowman

Ian C. Gauld

Germina Ilas

Ugur Merturek

Georgeta Radulescu

Oak Ridge National Laboratory

Managed by UT-Battelle, LLC

Oak Ridge, TN 37831-6170

M. Aissa, NRC Project Manager

NRC Job Code V6452

Office of Nuclear Regulatory Research

ABSTRACT

Criticality safety analyses of pressurized-water-reactor (PWR) spent nuclear fuel (SNF) assemblies in storage and transportation casks frequently take credit for reactivity reduction during depletion. This credit is commonly referred to as “burnup credit” (BUC) as outlined in U.S. Nuclear Regulatory Commission (NRC) Interim Staff Guidance (ISG) 8, Revision 3, “Burnup Credit in the Criticality Safety Analyses of PWR Spent Fuel in Transportation and Storage Casks.” However, such credit for boiling-water reactor (BWR) SNF is not addressed in ISG 8. The focus of this report is to document studies performed to provide a technical basis for the application of BUC in storage and transportation casks using BWR peak reactivity methods.

Most BWR fuel assemblies contain gadolinium oxide (Gd_2O_3 , or gadolinium) burnable absorber in some fuel rods. The gadolinium absorber depletes more rapidly than the fuel during the initial part of its irradiation, which causes the fuel assembly reactivity to increase and reach a maximum value at an assembly average burnup typically less than 20 gigawatt days per metric ton of uranium (GWd/MTU). Then the reactivity decreases for the remainder of fuel assembly irradiation. Criticality analyses of BWR spent fuel pools (SFPs) typically employ what are known as peak reactivity methods to account for this behavior in the SNF. Some peak reactivity methods correlate the peak reactivity value in storage to the infinite multiplication factor (k_{inf}) in the standard cold core geometry (SCCG). The SCCG is an infinite planar array of fuel assemblies in reactor geometry, typically a 6-inch pitch, flooded with full density water at 20°C. The peak reactivity methods are also sometimes referred to as “gadolinium credit.”

This report reviews the most commonly used peak reactivity methods in SFP analyses for BWR SNF to provide technical background for potential application to storage and transportation casks, including (1) an examination of the fuel assembly lattice design and operating parameters that affect the burnup and reactivity of the peak reactivity in storage and transportation configurations, (2) validation of these reactivity calculations, and (3) validation of the depleted isotopic inventories in BWR SNF at burnups associated with peak reactivity. Each of these three areas is investigated in detail in this report. This report is focused on peak reactivity, so it applies to fuel assemblies with average burnups of approximately 20 GWd/MTU or less. Burnup credit for BWR fuel assemblies with typical discharge burnups will be addressed in future reports planned over the next few years.

The following parameters have been studied, and their impact on the reactivity of BWR SNF has been quantified for determining potentially limiting conditions: initial fuel composition, number and loading of gadolinium pins, control blade insertion (referred to as “rodded” vs. “unrodded” conditions), moderator void fraction (unrodded and rodded), fuel temperature, specific power, and operating history. The depletion parameters used and the nuclides credited in an analysis will depend on the methodology developed and implemented by the applicant.

A suitable number of critical experiments has been identified to support validation of peak reactivity analysis of BWR SNF. All experiments identified in this report are low-enriched uranium (LEU), water-moderated pin array experiments. Penalty factors have been developed for the unvalidated transuranic, gadolinium, and fission product nuclides included in generic BUC cask (GBC)-68 models used in this report. The sum of these three factors is less than 0.5% Δk .

The physics of BWR fuel depletion are well understood, reliable, and predictable in their effects on discharged fuel reactivity near peak reactivity. This study confirms that a conservative set of analysis conditions can be identified and implemented to allow criticality safety analysis of BWR SNF for peak reactivity BUC in storage and transportation casks.

CONTENTS

	<u>Page</u>
ABSTRACT.....	iii
LIST OF FIGURES.....	vii
LIST OF TABLES.....	xi
LIST OF ACRONYMS AND UNITS.....	xiii
1 INTRODUCTION.....	1
2 CURRENT PEAK REACTIVITY METHODS.....	3
2.1 GENERAL CONSIDERATIONS FOR PEAK REACTIVITY ANALYSES.....	3
2.2 SCCG LIMIT WITH GADOLINIUM CREDIT.....	7
2.3 SCCG LIMIT WITHOUT GADOLINIUM CREDIT.....	10
2.4 OTHER METHODS.....	15
3 FACTORS AFFECTING PEAK REACTIVITY IN STORAGE AND TRANSPORTATION CASKS.....	17
3.1 SENSITIVITY STUDY METHODOLOGY.....	17
3.2 CALCULATIONAL METHODS, MODELS, AND CODES.....	18
3.2.1 Triton.....	19
3.2.2 CSAS/KENO.....	19
3.2.3 Cask Application Model.....	22
3.3 FUEL DESIGN TYPES.....	23
3.4 RESULTS.....	25
3.4.1 Isotopic Modeling during Depletion.....	25
3.4.2 Gadolinium Loading.....	31
3.4.3 Gadolinium Pattern.....	43
3.4.4 Void Fraction.....	48
3.4.5 Control Blade Insertion.....	52
3.4.6 Operating Parameters.....	60
3.4.7 Three-Dimensional Modeling.....	71
3.5 SUMMARY OF FACTORS AFFECTING PEAK REACTIVITY.....	74
3.5.1 Summary of Sensitivity Studies.....	74
3.5.2 Recommended Minimum Analyses.....	78
3.5.3 Areas for Further Study.....	78
4 VALIDATION OF CASK REACTIVITY CALCULATIONS.....	81
4.1 CODES AND METHODS.....	81
4.2 METHODOLOGY FOR VALIDATION STUDIES.....	82
4.3 SDF SOURCES.....	83
4.4 POTENTIALLY APPLICABLE EXPERIMENTS.....	84
4.4.1 Vanished Lattice with Actinide-Only Modeling.....	84
4.4.2 Vanished Lattice with Actinide and Fission Product Modeling.....	86
4.4.3 Full Lattice with Actinide and Fission Product Modeling.....	90
4.5 BIAS AND UNCERTAINTY DETERMINATION.....	92
4.5.1 Bias and Uncertainty without Trending Analysis.....	94
4.5.2 Traditional Trending Analysis.....	94
4.5.3 c_k Trending.....	96

4.6	PENALTIES FOR UNVALIDATED NUCLIDES	97
4.6.1	Plutonium.....	98
4.6.2	Residual Gadolinium.....	99
4.6.3	Fission Products and Minor Actinides.....	100
4.7	SUMMARY OF VALIDATION OF CASK REACTIVITY CALCULATIONS.....	101
5	VALIDATION OF SPENT FUEL NUCLIDE COMPOSITIONS.....	103
5.1	APPLICATION MODEL	103
5.2	NUCLIDE IMPORTANCE TO REACTIVITY.....	105
5.3	CODES AND METHODS.....	107
5.4	APPLICABLE EXPERIMENTAL DATA	108
5.5	OECD/NEA BWR BENCHMARK.....	111
5.6	BIAS AND UNCERTAINTY DETERMINATION	112
5.6.1	Nuclide Uncertainty Analysis	112
5.6.2	k_{eff} Bias and Uncertainty Analysis	114
5.6.3	k_{eff} Bias and Uncertainty Results	115
5.7	CONCLUSIONS AND RECOMMENDATIONS	116
6	SUMMARY AND CONCLUSIONS.....	119
6.1	CURRENT PEAK REACTIVITY METHODS FOR SPENT FUEL POOLS	119
6.2	PEAK REACTIVITY ANALYSIS SUMMARY.....	120
6.3	VALIDATION OF CASK REACTIVITY CALCULATIONS SUMMARY.....	121
6.4	ISOTOPIC VALIDATION SUMMARY	121
6.5	CONCLUSIONS	122
7	REFERENCES	125
	APPENDIX A. TRITON DEPLETION MODELING DETAILS	A-1
	APPENDIX B. GADOLINIUM PATTERNS	B-1
	APPENDIX C. EXPERIMENTS CONSIDERED.....	C-1
	APPENDIX D. CRITICAL EXPERIMENTS WITH C_k VALUES NO LESS THAN 0.8.....	D-1
	APPENDIX E. VALIDATION DATA	E-1
	APPENDIX F. ISOTOPIC VALIDATION DATA	F-1

LIST OF FIGURES

	<u>Page</u>
Figure 2.1. Example BWR fuel assembly containing seven lattices [5].	5
Figure 2.2. Reactivity trajectories for a BWR fuel assembly with different gadolinium loadings.	6
Figure 2.3. Sample correlation of k_{rack} and SCCG k_{inf} [3]. (used by permission)	8
Figure 2.4. Correlations of k_{rack} vs. SCCG k_{inf} for a range of fuel design types [7].	11
Figure 2.5. Variation in k_{inf} (SCCG) with burnup without gadolinium for 4.90% fuel [8].	12
Figure 2.6. k_{rack} vs. burnup for a range of gadolinium loadings [4].	13
Figure 2.7. Interpolation of minimum gadolinium loading requirement [4].	14
Figure 3.1. SCALE sequences, modules, and codes used for calculations.	18
Figure 3.2. Example of GBC-68 half cask model.	22
Figure 3.3. Detailed representation of a single storage cell in the GBC-68 cask model.	22
Figure 3.4. GE14 full and vanished lattices in reactor geometry.	24
Figure 3.5. Full and vanished lattice layouts for the GE14 assembly [5].	25
Figure 3.6. 2D Cask k_{inf} as a function of burnup for fuel with no initial gadolinium loading and three nuclide sets, AEAI modeling strategy.	27
Figure 3.7. 2D Cask k_{inf} as a function of burnup for fuel initially containing six pins with 2 wt% gadolinium and four nuclide sets, AEAI modeling strategy.	29
Figure 3.8. Gadolinium-free lattice layout for the full and vanished lattices.	32
Figure 3.9. Two gadolinium pin layout for the full and vanished lattices.	33
Figure 3.10. Four gadolinium pin layout for the full and vanished lattices.	33
Figure 3.11. Six gadolinium pin layout for the full and vanished lattices.	34
Figure 3.12. Eight gadolinium pin layout for the full and vanished lattices.	34
Figure 3.13. TRITON eigenvalue trajectories for the PEPI isotopic strategy varying the gadolinium content and number of gadolinium pins.	36
Figure 3.14. Dominating cross sections in gadolinium-bearing fuel pins.	37
Figure 3.15. (a) Percentage of ^{155}Gd remaining as a function of radial location in the fuel pin for the 6×2Gd, 6×4Gd, 6×6Gd, 6×8Gd, and 6×10Gd cases at 10 GWd/MTU and (b) eigenvalue trajectories for the 6-gadolinium pin cases.	38
Figure 3.16. Cask k_{inf} as a function of burnup for 2 wt% gadolinium in a range of pins, AO nuclides.	39
Figure 3.17. Cask k_{inf} as a function of burnup for 2 wt% gadolinium in a range of pins, AFP nuclides.	40
Figure 3.18. Cask k_{inf} as a function of burnup for gadolinium pins with a range of initial gadolinium loadings, AO nuclides.	41
Figure 3.19. Cask k_{inf} as a function of burnup for six gadolinium pins with a range of initial gadolinium loadings, AFP nuclides.	42
Figure 3.20. Cask k_{inf} as a function of burnup for all 15 patterns, AO nuclide set.	44
Figure 3.21. Cask k_{inf} as a function of burnup for all 15 patterns, AFP nuclide set.	45
Figure 3.22. Gadolinium patterns 2 (P2).	46
Figure 3.23. Gadolinium patterns 3 (P3).	47
Figure 3.24. Gadolinium patterns 9 (P9).	47
Figure 3.25. Gadolinium patterns 5 (P5).	48
Figure 3.26. Cask k_{inf} as a function of burnup for several depletion moderator void fractions, AO nuclide set.	49
Figure 3.27. ^{239}Pu atom density as a function of burnup for several depletion moderator void fractions.	50

Figure 3.28.	Cask k_{inf} as a function of burnup for several depletion moderator void fractions, AFP nuclide set	51
Figure 3.29.	^{155}Gd atom density as a function of burnup for several depletion moderator void fractions.	52
Figure 3.30.	Cask k_{inf} as a function of burnup for several depletion moderator void fractions and rodde depletion, AO nuclide set.....	53
Figure 3.31.	^{239}Pu atom density as a function of burnup for several depletion moderator void fractions, rodde depletion.	54
Figure 3.32.	Cask k_{inf} as a function of burnup for several depletion moderator void fractions, rodde depletion, AFP nuclide set.	55
Figure 3.33.	Cask k_{inf} as a function of burnup for several depletion moderator void fractions and the AFP nuclide set, comparing rodde and unrodde depletion.....	56
Figure 3.34.	^{235}U concentration difference (in percent) between rodde and unrodde cases.....	57
Figure 3.35.	^{155}Gd concentration difference (in percent) between rodde and unrodde cases.	57
Figure 3.36.	^{155}Gd atom density as a function of burnup for several depletion moderator void fractions and rodde depletion.....	58
Figure 3.37.	^{155}Gd atom density over a range of burnup for rodde and unrodde depletion with 0% and 80% void.	59
Figure 3.38.	Cask k_{inf} as a function of burnup at 25 W/g for different fuel temperatures, AO nuclide set.....	61
Figure 3.39.	Cask k_{inf} as a function of burnup at 25 W/g for different fuel temperatures, AFP nuclide set.....	63
Figure 3.40.	Cask k_{inf} as a function of burnup for different specific powers with 950 K fuel temperature, AO nuclide set.	65
Figure 3.41.	Cask k_{inf} as a function of burnup for different specific powers with 950 K fuel temperature, AFP nuclide set.....	67
Figure 3.42.	Cask k_{inf} as a function of burnup for four different operating histories, AO nuclide set.....	70
Figure 3.43.	Cask k_{inf} as a function of burnup for four different operating histories, AFP nuclide set.....	71
Figure 3.44.	Cask reactivity as a function of burnup, unrodde depletion with 40% void fraction, all nuclide sets.....	72
Figure 3.45.	Cask reactivity as a function of burnup, rodde depletion with 0% void fraction, all nuclide sets.	73
Figure 4.1.	c_k values for critical experiments compared to GBC-68 with vanished lattice and AO nuclides.	85
Figure 4.2.	c_k values greater than or equal to 0.8 with vanished lattice and AO nuclides.	86
Figure 4.3.	c_k values for critical experiments compared to GBC-68 with vanished lattice and AFP nuclides.....	87
Figure 4.4.	c_k values greater than or equal to 0.8 with vanished lattice and AFP nuclides.	88
Figure 4.5.	Sensitivity profile comparison for ^{155}Gd between GBC-68 with vanished lattice and LEU-COMP-THERM-005-010.	89
Figure 4.6.	Values for critical experiments compared to GBC-68 with full lattice and AFP nuclides.....	90
Figure 4.7.	c_k values greater than or equal to 0.8 with full lattice and AFP nuclides.	91
Figure 4.8.	Changes in c_k values between vanished lattice and full lattice.	92
Figure 4.9.	C/E trend and limits as a function of enrichment.....	95
Figure 4.10.	C/E trend and limits as a function of EALF.	96
Figure 4.11.	C/E trend and limits as a function of c_k	97
Figure 5.1.	Illustration of the BWR fuel assembly in application model and fuel rod mixture locations.....	105

Figure 5.2.	Relative neutron absorption fractions in typical UO ₂ fuel with gadolinium. [38]	106
Figure 5.3.	k_{eff} relative sensitivity coefficients (absolute) for the BWR application model at peak reactivity for actinides, fission products, and residual ¹⁵⁵ Gd.	107
Figure A.1.	Lattice layout highlighting the three different sets of Dancoff factors used in this SCALE/TRITON analysis.	A-1
Figure A.2.	PEPI lattice layout (left) and SCALE/TRITON representation (right).	A-2
Figure A.3.	AEPI lattice layout (left) and SCALE/TRITON representation (right).	A-3
Figure A.4.	Visual depiction of the grouping of depletion mixtures based on Dancoff factor for 4.40 wt% fuel.	A-3
Figure A.5.	PEAI lattice layout (left) and SCALE/TRITON representation (right).	A-4
Figure A.6.	AEAI lattice layout (left) and SCALE/TRITON representation (right).	A-4
Figure B.1.	Gadolinium patterns 0 (same as used in the Gd-loading study, P0).	B-1
Figure B.2.	Gadolinium patterns 1 (P1).	B-1
Figure B.3.	Gadolinium patterns 2 (P2).	B-2
Figure B.4.	Gadolinium patterns 3 (P3).	B-2
Figure B.5.	Gadolinium patterns 4 (P4).	B-3
Figure B.6.	Gadolinium patterns 5 (P5).	B-3
Figure B.7.	Gadolinium patterns 6 (P6).	B-4
Figure B.8.	Gadolinium patterns 7 (P7).	B-4
Figure B.9.	Gadolinium patterns 8 (P8).	B-5
Figure B.10.	Gadolinium patterns 9 (P9).	B-5
Figure B.11.	Gadolinium patterns 10 (P10).	B-6
Figure B.12.	Gadolinium patterns 11 (P11).	B-6
Figure B.13.	Gadolinium patterns 12 (P12).	B-7
Figure B.14.	Gadolinium patterns 13 (P13).	B-7
Figure B.15.	Gadolinium patterns 14 (P14).	B-8
Figure F.1.	Burnup vs. enrichment for available BWR RCA data.	F-2
Figure F.2.	Effect of void fraction change (-10%) on isotopic content for 5 GWd/MTU BWR fuel.	F-3
Figure F.3.	JPDR core map [F1].	F-6
Figure F.4.	JPDR samples axial locations [F1].	F-7
Figure F.5.	Illustration of SCALE/TRITON model for JPDR assembly.	F-8
Figure F.6.	Diagram of assembly C16 enrichment profile [F1].	F-9
Figure F.7.	Illustration of SCALE/TRITON model for Gundremmingen sample C16-B3.	F-11
Figure F.8.	Radial loading diagram of assembly 2F2DN23.	F-13
Figure F.9.	Measurement positions for rod SF99.	F-13
Figure F.10.	Illustration of SCALE/TRITON model for Fukushima Daini-2 SF99 samples.	F-15
Figure F.11.	Illustration of SCALE/TRITON model for Ohi-2 assembly.	F-18
Figure F.12.	Variation with burnup of (C/M-1) for ²³⁵ U and ²³⁹ Pu.	F-20

LIST OF TABLES

	<u>Page</u>
Table 3.1. Nuclides included in the three sets of BUC isotopes considered.....	20
Table 3.2. All TRITON default nuclides included in depletion calculations (ALL) (94 total nuclides, TRITON “addnux=2” nuclides) [11].....	20
Table 3.3. Uncertainty in k_{eff} due to uncertainty in nuclear data for BUC application models	21
Table 3.4. Change in cask k_{inf} , AEAI-AEPI, zero initial gadolinium	27
Table 3.5. Change in cask k_{inf} , AEAI-PEAI, zero initial gadolinium	28
Table 3.6. Change in cask k_{inf} , AEAI-PEPI, zero initial gadolinium.....	28
Table 3.7. Change in cask k_{inf} , AEAI-AEPI, six rods with 2 wt% initial gadolinium	30
Table 3.8. Change in cask k_{inf} , AEAI-PEAI, six rods with 2 wt% initial gadolinium	30
Table 3.9. Change in cask k_{inf} , AEAI-PEPI, six rods with 2 wt% initial gadolinium.....	30
Table 3.10. Number of pins and gadolinium content per pin.....	32
Table 3.11. Cask k_{inf} values for various patterns with the AO nuclide set.....	44
Table 3.12. Cask k_{inf} values for various patterns with the AFP nuclide set	46
Table 3.13. Fuel temperatures, specific powers, and operating histories	60
Table 3.14. Cask Δk_{inf} values for 25 W/g depletion case, 950 K base case, AO nuclide set	62
Table 3.15. Cask Δk_{inf} values for 35 W/g depletion case, 950 K base case, AO nuclide set	62
Table 3.16. Cask Δk_{inf} values for 45 W/g depletion case, 950 K base case, AO nuclide set	62
Table 3.17. Cask Δk_{inf} values for 25 W/g case, 1100 K – 850 K, AO nuclide set.....	62
Table 3.18. Cask Δk_{inf} values for 25 W/g depletion case, 950 K base case, AFP nuclide set.....	64
Table 3.19. Cask Δk_{inf} values for 35 W/g depletion case, 950 K base case, AFP nuclide set.....	64
Table 3.20. Cask Δk_{inf} values for 45 W/g depletion case, 950 K base case, AFP nuclide set.....	64
Table 3.21. Cask Δk_{inf} values for 25 W/g case, 1100 K–850 K, AFP nuclide set	64
Table 3.22. Cask Δk_{inf} values for 35 W/g and 45 W/g, 850 K fuel temperature, AO nuclide set.....	66
Table 3.23. Cask Δk_{inf} values for 35 W/g and 45 W/g 950 K fuel temperature, AO nuclide set	66
Table 3.24. Cask Δk_{inf} values for 35 W/g and 45 W/g 1100 K fuel temperature, AO nuclide set.....	66
Table 3.25. ^{235}U and ^{239}Pu number densities for different specific powers and 950 K fuel temperature	67
Table 3.26. Cask Δk_{inf} values for 35 W/g and 45 W/g, 850 K fuel temperature, AFP nuclide set	68
Table 3.27. Cask Δk_{inf} values for 35 W/g and 45 W/g, 950 K fuel temperature, AFP nuclide set	68
Table 3.28. Cask Δk_{inf} values for 35 W/g and 45 W/g, 1100 K fuel temperature, AFP nuclide set	68
Table 3.29. ^{149}Sm number densities at a range of specific powers and 950 K fuel temperature.....	69
Table 3.30. Difference between 2D cask k_{inf} and 3D cask k_{eff} , unrodded depletion with 40% void fraction.....	73
Table 3.31. Difference between 2D cask k_{inf} and 3D cask k_{eff} , rodded depletion with 0% void fraction	74
Table 3.32. Summary of parameters affecting discharged reactivity for BWR peak reactivity analysis considering the AO nuclide set.....	75
Table 3.33. Summary of parameters affecting discharged reactivity for BWR peak reactivity analysis considering the AFP nuclide set	76
Table 4.1. Bias and bias uncertainty values	94
Table 4.2. Uncertainty contributions from major transuranic nuclides	99
Table 4.3. Uncertainty contribution from ^{155}Gd	100
Table 4.4. Uncertainty contribution from major fission products and minor actinides	101
Table 5.1. Evaluated experimental spent fuel nuclide data.....	110

Table 5.2.	Isotopic bias and bias uncertainty values associated with calculated BWR isotopic concentrations	113
Table 5.3.	k_{eff} results and margin for uncertainty for the GBC-68 cask model	116
Table C.1.	Critical experiments considered for validation	C-1
Table D.1.	Experiments with a c_k no less than 0.8, vanished lattice – actinide only	D-1
Table D.2.	Experiments with a c_k no less than 0.8, vanished lattice – actinides and fission products	D-2
Table D.3.	Experiments with a c_k no less than 0.8, full lattice – actinides and fission products	D-3
Table E.1.	Validation data for vanished lattice with actinides and fission products	E-1
Table F.1.	Sources of RCA data for BWR isotopic validation	F-1
Table F.2.	Selected RCA isotopic validation data set	F-4
Table F.3.	JPDR assembly design data [F1, F2]	F-6
Table F.4.	JPDR samples data [F1, F2]	F-7
Table F.5.	Comparison calculation-measurement for JPDR samples	F-8
Table F.6.	Gundremmingen-A assembly design data	F-10
Table F.7.	Gundremmingen-A samples data	F-10
Table F.8.	Comparison calculation-measurement for Gundremmingen-A samples	F-11
Table F.9.	Fukushima-Daini-2 assembly design data	F-14
Table F.10.	Fukushima-Daini-2 samples data	F-14
Table F.11.	Comparison calculation-measurement for Fukushima Daini-2 samples	F-15
Table F.12.	Ohi-2 assembly design data [F8]	F-17
Table F.13.	Ohi-2 samples data	F-17
Table F.14.	Comparison calculation-measurement for Ohi-2 samples (actinides)	F-19
Table F.15.	Comparison calculation-measurement for Ohi-2 samples (Gd)	F-19
Table F.16.	Statistical data for the BWR samples (BUC nuclides)	F-20

LIST OF ACRONYMS AND UNITS

2D	two-dimensional
3D	three-dimensional
ADSNF	assay data of spent nuclear fuel
AE	average enrichment
AEAI	average enrichment with average isotopics
AEPI	average-enrichment with pin-wise isotopics
AFP	actinides and fission products (includes minor actinides and major fission products)
AFPNG	actinides and fission products with no gadolinium
AI	average isotopics
ALL	all nuclides in depletion calculations
ANS	American Nuclear Society
ANSI	American National Standards Institute
AO	actinide-only
BOL	beginning of life
BUC	burnup credit
BWR	boiling water reactor
C/E	calculated-to-expected
CFR	<i>Code of Federal Regulations</i>
COMP	solid composition (fuel form)
CSN	Consejo de Seguridad Nuclear [Spanish Nuclear Safety Council]
DICE	Database for the International Criticality Safety Benchmark Evaluation Project
EALF	energy of average lethargy of fission
EGBUC	Expert Group on Burnup Credit Criticality Safety
FHP	full power followed by half power
FP	full power
FTHP	full power followed by three-quarter power followed by half-power
GBC	generic burnup credit cask
GWd	gigawatt days
HFP	hot full power
HP	half power
HTC	French Haut Taux de Combustion
IHECSBE	International Handbook of Evaluated Criticality Safety Benchmark Experiments
ISG	Interim Staff Guidance
JAEA	Japanese Atomic Energy Agency
JAERI	Japanese Atomic Energy Research Institute
JENDL	Japanese Evaluated Nuclear Data Library
JPDR	Japan Power Demonstration Reactor
LCT	LEU-COMP-THERM
LEU	low enriched uranium
MCT	MIX-COMP-THERM
MIX	mixed uranium/plutonium

MOX	mixed oxide
MST	MIX-SOL-THERM
MTU	metric ton of uranium
NEA	Nuclear Energy Agency
NRA	Nuclear Regulation Authority [Japan]
NRC	U.S. Nuclear Regulatory Commission
NSC	Nuclear Science Committee
OECD	Organisation for Economic Co-operation and Development
ORNL	Oak Ridge National Laboratory
PE	pin-wise initial enrichment
PEAI	pin-wise enrichment with average isotopics
PEPI	pin-wise enrichment with pin-wise isotopics
PI	pin-wise isotopics
PIE	postirradiation examination
PLE	plenum
PSZ	power shaping zone
PWR	pressurized water reactor
RCA	radiochemical assay
REGAL	Rod Extremity and Gadolinia AnaLysis
SAMS	Sensitivity Analysis Module for SCALE
SCALE	Standardized Computer Analyses for Licensing Evaluation
SCCG	standard cold core geometry
SCK•CEN	Studiecentrum voor Kernenergie
SDF	sensitivity data file
SFCOMPO	Spent Fuel Isotopic Composition Database
SFP	spent fuel pool
SNF	spent nuclear fuel
S/U	sensitivity/uncertainty
SWAT	Step Wise Burnup Analysis Code System
TEPCO	Tokyo Electric Power Company
THERM	thermal (flux spectrum)
TRITON	two-dimensional transport and depletion module for characterization of spent nuclear fuel
TSUNAMI	Tools for Sensitivity and Uncertainty Analysis Methodology Implementation
TSUNAMI-IP	TSUNAMI-Indices and Parameters
USL	upper safety limit
USLSTATS	Upper Safety Limit Statistics
VALID	Verified, Archived Library of Inputs and Data (SCALE)
V	vanished rod location
WPNCs	Working Party of Nuclear Criticality Safety
WR	water rod (location)

1 INTRODUCTION

Criticality safety analyses of fuel assemblies in spent nuclear fuel (SNF) storage and transportation systems are performed to demonstrate that these systems are adequately subcritical per the requirements of Title 10 of the Code of Federal Regulations (CFR) Parts 71 and 72 [1]. The U.S. Nuclear Regulatory Commission (NRC) staff reviews analyses of pressurized water reactor (PWR) SNF that credit the reduction in assembly reactivity caused by depletion of fissile nuclides and buildup of neutron absorbing nuclides during power operation using guidance in the Division of Spent Fuel Storage and Transportation Interim Staff Guidance (ISG) 8, Revision 3 [2]. This credit for reactivity reduction during depletion is commonly referred to as “burnup credit” (BUC). Such credit for boiling-water reactor (BWR) SNF is not addressed in ISG-8. The focus of this report is to document studies performed to provide a technical basis for the review of BWR peak reactivity methods in dry storage casks and transportation packages, hereafter referred to as “casks.”

The analysis of SNF in spent fuel pools (SFPs), as regulated by 10 CFR Part 50, allows a combination of BUC and credit for residual burnable absorber in BWR fuel. However, analysis of BWR SNF in casks currently assumes fresh fuel with no burnable absorber. Most BWR fuel assemblies contain gadolinium oxide (Gd_2O_3 , or gadolinium) burnable absorber in some fuel rods, so reactivity increases early in assembly irradiation before reaching a peak and subsequently decreases until end of life. The early increase in reactivity results from the more rapid depletion of the burnable absorber than the fuel. A BWR BUC method that takes credit for gadolinium must consider this effect. This type of analysis is known as a peak reactivity method.

Some peak reactivity methods correlate the peak reactivity value in storage to the infinite multiplication factor (k_{inf}) in the standard cold core geometry (SCCG). These techniques are also referred to as using an SCCG approach. The SCCG is an infinite planar array of fuel assemblies in reactor geometry, typically a 6-inch pitch, flooded with full density water at 20°C. The peak reactivity methods are also sometimes called “gadolinium credit,” as some residual burnable absorber material is typically credited. The peak reactivity methods used most frequently in SFP analyses for BWR SNF are reviewed in Section 2 as a background for development of a technical basis for the application of peak reactivity methods to BWR SNF casks.

This report presents (1) an examination of the lattice design and operating parameters that affect the burnup and the effective multiplication factor (k_{eff}) value associated with the peak reactivity in storage and transportation configurations, (2) validation of these reactivity calculations, and (3) validation of the BWR SNF nuclide concentrations in terms of impact on k_{eff} . Each of these three areas is investigated in this report. The analysis of design and depletion parameters affecting peak reactivity is presented in Section 3, “Factors Affecting Peak Reactivity,” while the validations of reactivity determinations and isotopic inventories are presented in Section 4, “Validation of Cask Reactivity Calculations,” and Section 5, “Validation of BWR Isotopic Concentrations near Peak Reactivity.” A final summary is presented in Section 6, “Summary and Conclusions.”

2 CURRENT PEAK REACTIVITY METHODS

Although no BUC methods are currently applied to BWR SNF casks, a range of methods has been developed and implemented over the last 20 years for analysis of BWR fuel in SFPs at nuclear power plants. Two different methods have been used to qualify the vast majority of the current discharged inventory. The methods create a correlation between the neutron multiplication factor (k_{inf} or k_{eff}) in the storage rack and the SCCG k_{inf} [3, 4]. For simplicity, this report will refer to the storage rack k_{inf} or k_{eff} as “ k_{rack} .” This correlation is used to determine the maximum SCCG k_{inf} that can be shown to meet the regulatory limits for the storage rack; thus, implementation is based on limiting the SCCG k_{inf} . The primary advantages of this methodology are that a single limit exists that covers storage of fuel at any burnup and that the SCCG k_{inf} is calculated by BWR fuel vendors as part of the reload analysis process. Because the maximum SCCG k_{inf} over all burnups is shown to be lower than the limit, it can therefore be implemented as a constraint on bundle design to ensure that all assemblies can be stored at the plant. These two most common methods will be discussed in Sections 2.2 and 2.3.

For completeness, other peak reactivity methods are also noted. These methods are either under development or in limited use currently at BWR power plants.

2.1 GENERAL CONSIDERATIONS FOR PEAK REACTIVITY ANALYSES

All of the peak reactivity methods used in SFP analyses share common characteristics and approaches. These similarities are driven by the physics of the BWR fuel being analyzed and by the regulatory requirements that must be met.

BWR fuel assemblies consist of multiple axial zones. Each unique axial zone is identified by the number of fuel rods, the enrichment of the fuel in each lattice location, and the number and loading of gadolinium rods. Each unique axial zone within the same assembly is referred to as a “lattice.” Modern BWR designs include part-length fuel rods. Lower lattices contain fuel rods in all locations, but lattices at higher elevations have empty fuel rod locations. The top and bottom axial zones contain reduced or natural enrichment blankets that are typically about 6 inches long. The full lattices above the bottom blanket are usually referred to as “power-shaping zone” and “dominant” lattices. Lattices with empty fuel rod locations are referred to as “vanished” lattices; some fuel designs contain multiple vanished lattices with differing numbers of fuel rods. Additionally, plenum lattices exist in axial elevations in the plenum region of the part-length rods. An example of a fuel assembly layout with seven unique lattices is shown in Figure 2.1, adapted from Fensin, “Optimum BWR Fuel Design Strategies to Enhance Reactor Shutdown by the Standby Liquid Control System” [5].

The reactivity behavior of BWR fuel assemblies as a function of fuel burnup is the primary consideration in all analyses and is thus examined here in additional detail. As mentioned previously, nearly all BWR fuel contains gadolinium burnable absorber fuel rods. The gadolinium loading in each assembly is determined by selecting the number of rods containing gadolinium and the enrichment in weight percent of gadolinium loaded in each rod. The location of the gadolinium rods within the assembly lattice also affects the depletion of the absorber. For

example, gadolinium loaded in areas of increased moderation, such as areas near water holes or bypass channels, depletes faster because of its large thermal absorption cross section. These differences impact the fuel assembly reactivity trajectory as a function of burnup. This reactivity trajectory is of utmost importance in peak reactivity methods because the reactivity of the fuel assembly at the peak is dependent upon the burnup where the peak occurs.

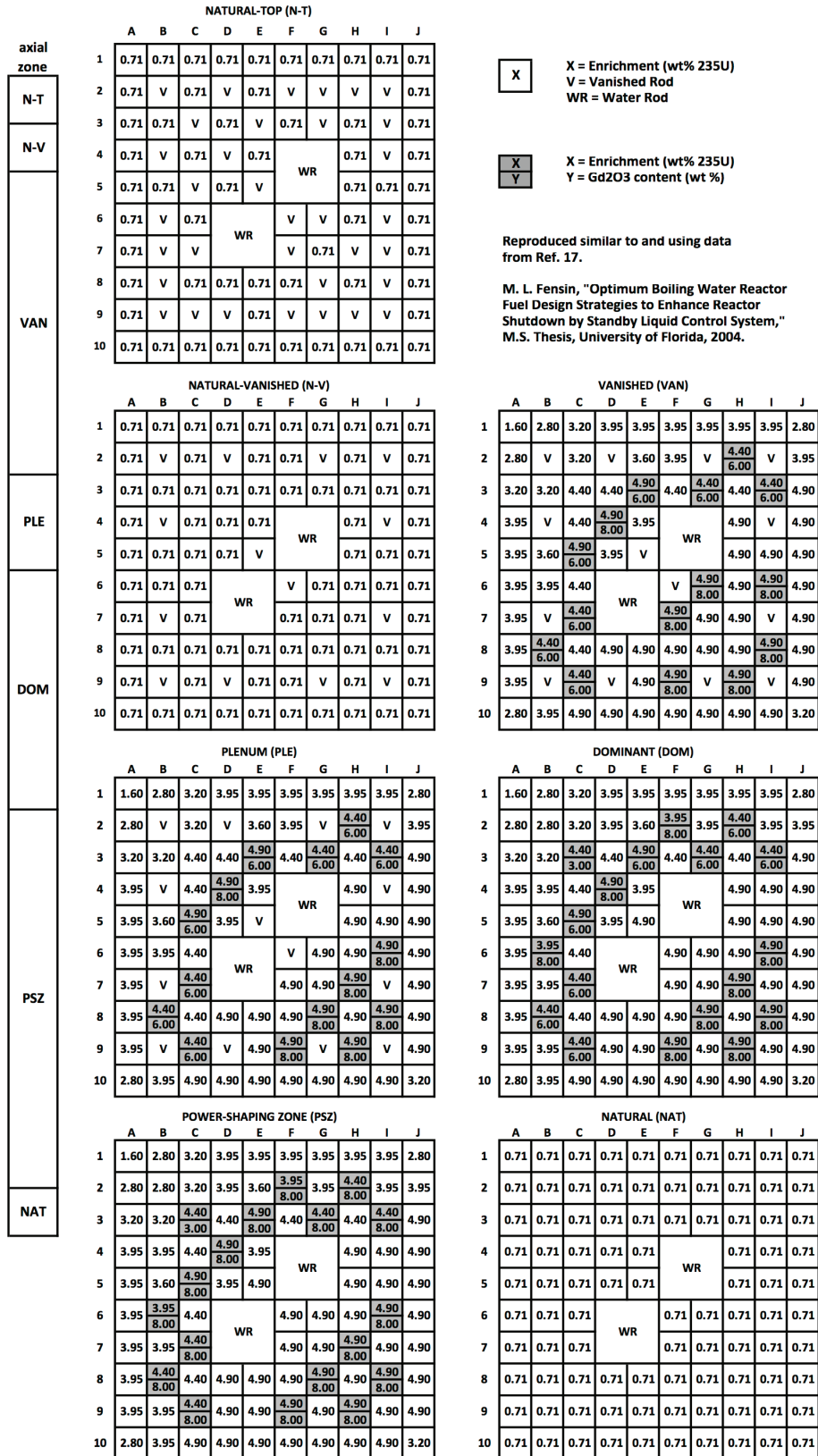


Figure 2.1. Example BWR fuel assembly containing seven lattices [5].

Peak reactivity typically occurs at burnups less than ~20 gigawatt days per metric ton of uranium (GWd/MTU) for modern fuel assembly designs. After equilibrium xenon is established, during the first ~100 hours at full power, the reactivity of fuel without gadolinium decreases nearly linearly. The addition of gadolinium to the fuel results in a lower initial reactivity that increases to a peak as the gadolinium depletes, then merges with a similar trajectory to that of fuel without gadolinium until the end of life. Examples of this behavior are shown in Figure 2.2, which compares depletion of fuel without gadolinium and with two different gadolinium loadings. The reactivity curves of the gadolinium-loaded assemblies are virtually the same as the gadolinium-free assembly after peak reactivity. A comparison of light and heavy gadolinium loadings shows that the earlier peak for the light loading (less gadolinium rods with lower gadolinium enrichment) is significantly higher than the later peak experienced in the heavier loading (more gadolinium rods with higher gadolinium enrichment). The factors that affect gadolinium depletion are the most important parameters for peak reactivity analyses because they impact when the peak occurs and thus the magnitude of the peak reactivity. The design and depletion parameters affecting peak reactivity are explored in detail in Section 3.

Figure 2.2 also illustrates the relative importance of credits for both fuel burnup and residual gadolinium. The credit for burnup is essentially the reactivity difference between fresh fuel conditions and the conditions at the assumed burnup of peak reactivity for the fuel without gadolinium. The credit for residual gadolinium is the difference in reactivity between the fuel with and without gadolinium at the burnup of peak reactivity. Although this figure shows the relative magnitudes of these credits for different core depletion conditions, the magnitudes of these credits in rack conditions are similar.

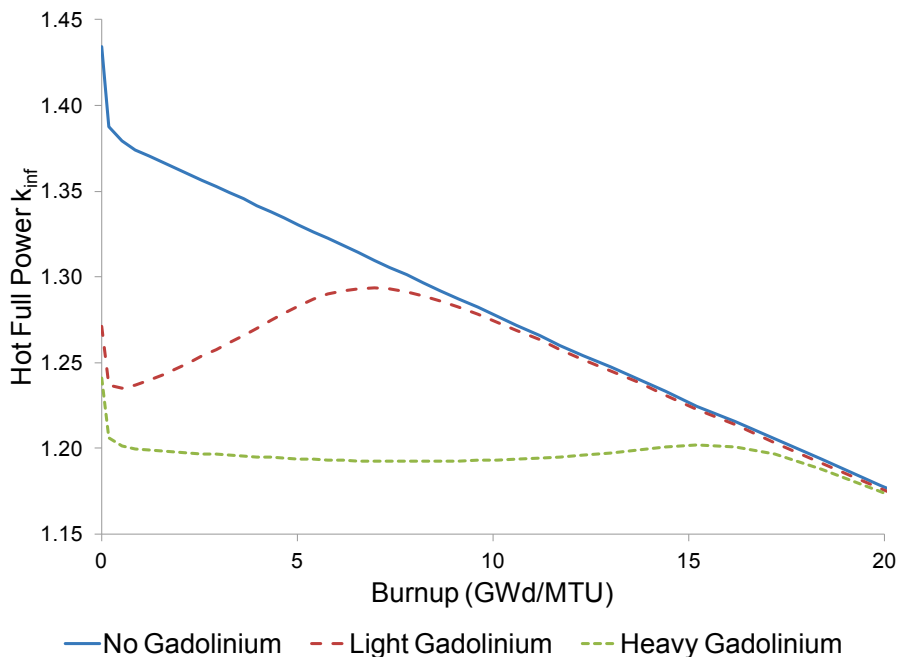


Figure 2.2. Reactivity trajectories for a BWR fuel assembly with different gadolinium loadings.

Little information is available in the open literature on the nuclides credited in peak reactivity methods. Typical commercial lattice codes include TGBLA, CASMO, or PHOENIX. The nuclides included in the BWR SNF compositions depend on the depletion code and code version. More recently, BWR SFP analyses have implemented a generic depletion uncertainty of 5% of the reactivity difference between fresh fuel with no gadolinium and fuel at peak reactivity based on the Kopp Letter [6].

Each method includes reactivity allowances for biases and uncertainties. The biases typically come from the criticality code validation. The uncertainties are typically derived from manufacturing tolerances on the fuel assembly and on the storage rack, the uncertainty in the code bias, an allowance for eccentric positioning of assemblies in the storage cells, the use of different codes to calculate SCCG k_{inf} and k_{rack} , and uncertainty in the Monte Carlo estimate of k_{rack} . The number of allowances used, the processes used to determine them, and their magnitudes vary among the various methods. The uncertainties are typically combined using the square root of the sum of the squares of the independent uncertainty allowances. The calculated best estimate k_{rack} value is then combined with these allowances to demonstrate that the regulatory limit of 0.95 specified in 10 CFR 50.68 [1] is met. The evaluation of these biases and uncertainties is an essential part of the criticality analysis but is not described in detail in this section, as the same general techniques are used for all methods currently implemented in BWR SFP analyses.

The storage rack calculation is typically performed for a two-dimensional (2D) model of the storage rack and fuel assembly using the most reactive lattice with reflective boundary conditions, but some three-dimensional (3D) models have also been used. The resulting calculated k_{rack} values can therefore be either k_{inf} (2D models) or k_{eff} (3D models). The conservatism of the 2D model compared to the 3D model is examined in Section 3.4.7.

There are two primary SCCG methods, and each uses a different approach. One method uses a range of operating conditions and different lattices as well as credit for residual gadolinium. The other method uses limiting operating conditions and does not credit gadolinium. These methods are described in the following two subsections.

2.2 SCCG LIMIT WITH GADOLINIUM CREDIT

The SCCG-limit-with-gadolinium-credit method gives credit for residual gadolinium and examines several different lattices including a range of enrichments, gadolinium loadings, and gadolinium patterns over multiple burnups. This method is described in a case study presented in “Uncertainty Contribution to Final In-Rack $k(95/95)$ from the In-Core k_{∞} Criterion Methodology for Spent Fuel Storage Rack Criticality Safety Analyses” (Hannah et al) [3]. The k_{rack} calculations use a range of fuel lattice designs, enrichments, and gadolinium loadings. A range of depletion conditions is studied, including different lattice types, burnups, enrichments, gadolinium loadings, and void fractions. The SCCG k_{inf} and the k_{rack} are calculated for each lattice at a range of burnups, and these data are used to create a single correlation between k_{rack} and SCCG k_{inf} . The correlation is intended to cover the full range of lattices, enrichment, and gadolinium loadings that could conceivably be used in the core, and therefore includes a variety of designs to cover each of these parameters. A limiting case is identified from the calculated results as a peak reactivity that is near but greater than the desired SCCG k_{inf} limit. Finally, this

case is demonstrated to meet regulatory requirements for fuel storage. Each of these steps is examined further, and then a summary of the method is presented.

This method uses a lattice average enrichment. The considered lattice average enrichments range from 2.8 to 4.9 wt% ^{235}U [3]. Various gadolinium loadings are considered, including a case with no burnable absorber loading. The void fraction is the only depletion parameter that is explicitly varied.

The results from these calculations are used to generate a correlation between k_{rack} and SCCG k_{inf} . The uncertainty in the correlation is determined to establish a 95% confidence, 95% probability (95/95) upper bound on the correlation [3]. Figure 2.3 [3] shows the best estimate correlation as a solid line and the 95%/95% upper bound as a dashed line. The nominal value for k_{rack} is determined through the nominal correlation, and the uncertainty is combined with the other applicable uncertainties in the analysis generated with the design basis lattice.

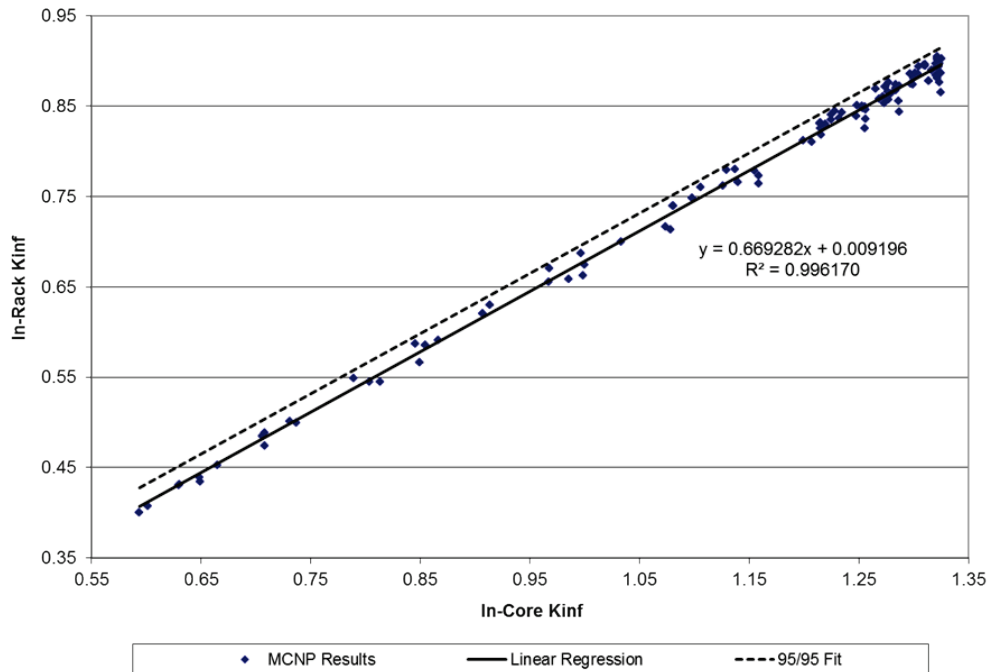


Figure 2.3. Sample correlation of k_{rack} and SCCG k_{inf} [3]. (used by permission)

As described above, this design basis lattice is selected from points on the correlation that are near but greater than the proposed SCCG k_{inf} limit. The consideration of only points that are above the proposed SCCG k_{inf} limit ensures that a reactive lattice is used and adds conservatism to the analysis by explicitly demonstrating that an assembly that should not be placed in the rack can be stored safely. The lattice that generates the highest rack efficiency of the candidates near but over the limit is selected as the design basis lattice. The rack efficiency is calculated by dividing k_{rack} by the SCCG k_{inf} , and it serves to normalize the k_{rack} values for differences in SCCG k_{inf} . The rack efficiency changes from one lattice to another based on neutron spectrum and residual gadolinium content, which impact the worth of the neutron absorber panels in the rack and communication among assemblies. For example, two lattices with the same k_{rack} values

might have different SCCG k_{inf} values; the lattice with the lower SCCG k_{inf} is of more concern and is properly identified because of its higher efficiency. The goal is to identify the lattice with the highest k_{rack} value that also has a SCCG k_{inf} at or just above the proposed limit. This design basis lattice is used in the evaluation of manufacturing tolerances, biases, and uncertainties.

The final step is to combine the biases and uncertainties calculated for the design basis assembly, the code predictions, and the correlation method to demonstrate that the design basis lattice meets regulatory requirements for fuel storage. The terms are combined as described in the following equation:

$$K(95/95) = K_{Nominal} + \Delta K_{Bias} + \Delta K_{Tolerance} + \Delta K_{Uncertainty} \quad (3)$$

The $K_{Nominal}$ term is derived from the correlation, and the remaining terms $\Delta K_{Tolerance}$, ΔK_{Bias} , and $\Delta K_{Uncertainty}$ are determined by the tolerance calculations, the code prediction validation study, and the correlation uncertainty, respectively. If the resulting $K(95\%/95\%)$ value does not meet the regulatory requirements, a new lower SCCG k_{inf} limit is proposed, and the process is repeated.

This method has some benefits. First, it uses real lattice designs in the generation of the correlation curve. This is feasible as the method is used by a BWR fuel vendor, and thus the analysts have access to a large number of lattice designs. The method also explicitly considers a range of assembly design and operating conditions including gadolinium loadings, enrichment, and void fractions. The inclusion of the uncertainty of the fit in the assessment of $K(95\%/95\%)$ is also a strength. The method also allows storage of fuel with comparison against one limit. Other methods in SFP analysis use a combination of two or three limits on enrichment, gadolinium loading, and/or SCCG k_{inf} . The use of a single limit simplifies implementation and reduces the probability of mischaracterizing an assembly relative to the limit.

There are also potential areas of concern. The most significant area of concern is the use of potentially non-limiting depletion conditions in the generation of the correlation of k_{rack} to SCCG k_{inf} . This concern applies to the use of multiple void fractions during depletion. A study such as the one documented in Section 3.4.4 could be performed to identify the limiting void fraction. Using only this single void fraction in the depletion calculations could provide additional confidence that the correlation is conservative. The use of potentially non-limiting points is of concern as these points would act to lower the correlation. Although these points may also increase the uncertainty in the fit, this is likely to be a small effect. A second area of concern is the use of points that are far from limiting reactivities. As shown in Figure 2.3, some points used in generating the correlation have k_{rack} values as low as about 0.4. It is highly desirable that the correlation be generated using only points that are near the limit, so that the correlation is based on points of direct relevance to the limit. There is significant scatter in the data for these points near the limit, although this may be a result of the limited number of lattices considered in the case study presented [Fig. 2 of Reference 3].

The SCCG-limit-with-gadolinium-credit methodology has been implemented in several SFPs over the last 20 years. The method requires a large number of lattice designs, but the use of real lattice designs provides a degree of accuracy in the analysis that is lacking in some of the other methods. However, the use of a sizeable number of real lattice designs may be problematic for

implementation by a cask vendor without ready access to a reliable collection of such design information. The SCCG-limit-with-gadolinium-credit method attempts to balance some of the conservatisms of the peak reactivity methods, such as considering all assemblies to be identical and all at peak reactivity, with a less conservative depletion analysis including non-limiting depletion conditions and lattices. In summary, the SCCG k_{inf} with gadolinium credit method provides a fairly straightforward approach to demonstrating safe storage of BWR fuel assemblies.

2.3 SCCG LIMIT WITHOUT GADOLINIUM CREDIT

The SCCG-limit-*without*-gadolinium credit method uses different limits in different implementations. In some cases [7], it includes a maximum enrichment limit, a minimum gadolinium requirement limit, and an SCCG k_{inf} limit. In other cases [8], it uses only the minimum gadolinium requirement and SCCG limits. The development and application of each of these limits are discussed in this section of the report.

The SCCG-limit-*without*-gadolinium-credit method has historically included a bias of 1% Δk , along with the other bias and uncertainty terms. This conservatism is primarily intended to cover potential discrepancies between SFP criticality vendor calculations of SCCG k_{inf} and fuel vendor calculations of SCCG k_{inf} using a different computational code and different gadolinium loadings and patterns [4].

The maximum enrichment limit is calculated using fresh fuel with no gadolinium. It is simply the highest fresh fuel enrichment with a reactivity that satisfies the regulatory requirement for storage. For lattices with average enrichments at or below this limit, no further comparisons are necessary to qualify the lattice for storage. The limit is determined by calculating k_{rack} over a range of enrichments in the storage configuration to determine the limiting enrichment. This method is essentially the same one used in licensing BWR storage and transportation casks currently under the fresh fuel assumption.

The SCCG limit is generated in this method in a manner similar to the SCCG-limit-with-gadolinium-credit method described in the previous section; however, there are some key differences in the methodology details. As with the other SCCG limit, correlations are constructed between k_{rack} and SCCG k_{inf} . However, this method explicitly generates a separate correlation for each fuel design type. An example set of correlations is provided in Figure 2.4. Once again, an SCCG k_{inf} limit is proposed and ultimately shown to meet storage requirements with k_{rack} and appropriate biases and uncertainties.

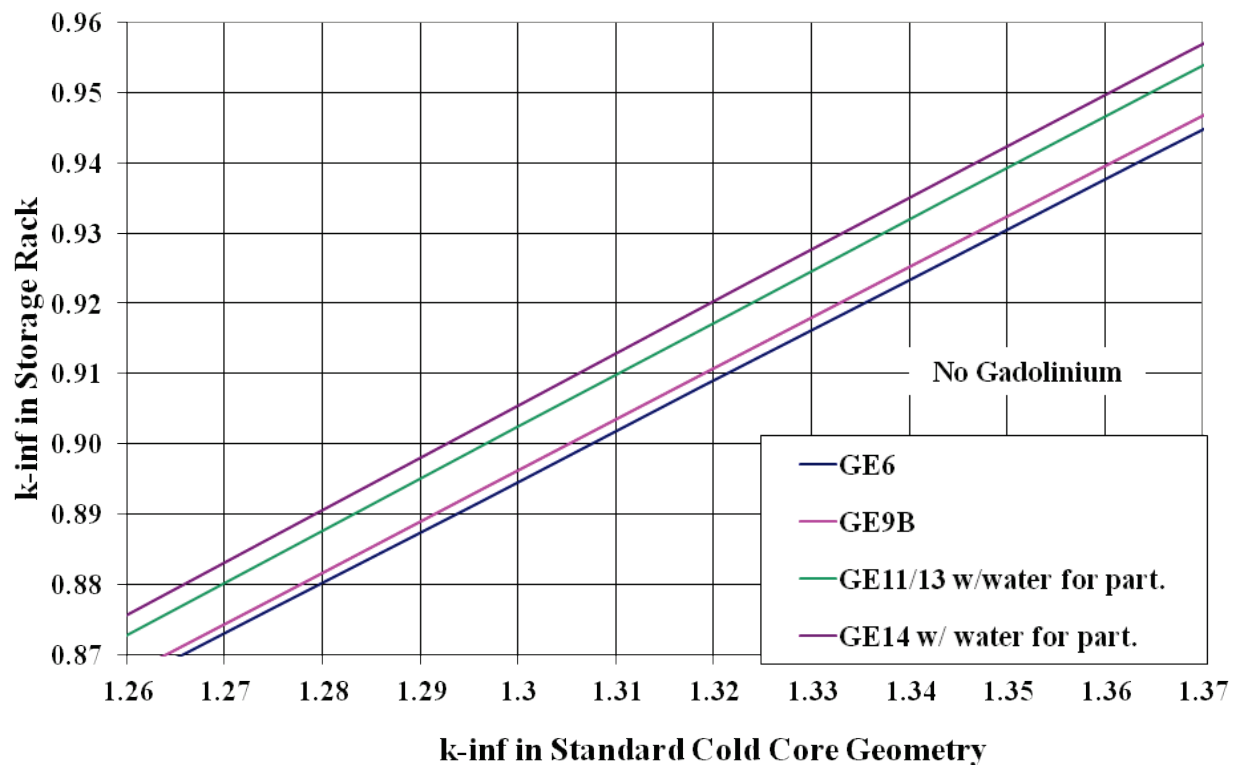


Figure 2.4. Correlations of k_{rack} vs. SCCG k_{inf} for a range of fuel design types [7].

The correlation is developed by determining k_{rack} and the SCCG k_{inf} for a range of different burnups for a uniform lattice of fuel rods without gadolinium using the maximum enrichment that occurs in that lattice. The points for this correlation exhibit much more linear behavior than that shown in Figure 2.3 because the points come from the depletion of fuel without burnable absorbers. Separate depletion calculations are performed for each assembly type of interest, as shown in Figure 2.4, and explicit calculations are performed to generate separate correlations for full and vanished lattices as necessary. Only the most reactive correlation is used in setting the storage limit. Another difference is that sensitivity studies are performed to determine the depletion conditions that create the most reactive correlation, and only these limiting depletion conditions are used. Because these depletion calculations are performed without gadolinium, the limiting conditions will be different from those where the fuel with burnable absorber is modeled.

For assemblies with enrichments greater than the maximum enrichment limit, a minimum gadolinium loading requirement is needed in the current SFP implementation for fuel with burnups below the minimum burnup where fuel without burnable absorbers meets the SCCG k_{inf} limit (Fig. 2.5). For the analysis illustrated in this figure, the minimum burnup for which fuel could be stored solely with the SCCG k_{inf} limit is 12.6 GWd/MTU.

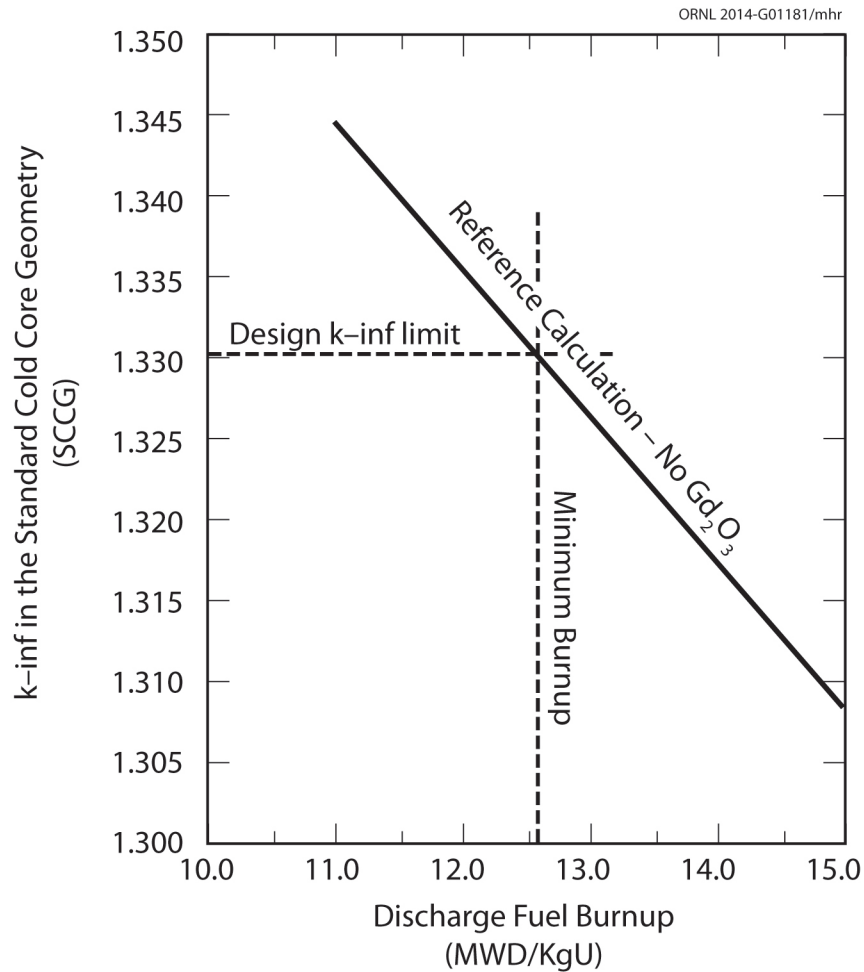


Figure 2.5. Variation in k_{inf} (SCCG) with burnup without gadolinium for 4.90% fuel [8].

Two different approaches have been used to determine the gadolinium loading requirement. Generally, a single combination of minimum rods and minimum gadolinium loading is determined, while in some instances, multiple combinations are used to meet regulatory requirements. The more common approach generates a limit by performing depletion calculations for various combinations of (1) the number of gadolinium-bearing rods and (2) the number of gadolinium loadings per rod, as illustrated in the example in Figure 2.6.

The peak value of k_{rack} is plotted versus the gadolinium concentration for each unique number of gadolinium-bearing rods, and interpolation is performed to determine at what concentration k_{rack} satisfies regulatory requirements. An example using the results from Figure 2.6 is provided in Figure 2.7. In this example from *Criticality Safety Evaluation for the Nine Mile Point 2 Rack Installation Project*, it was shown that six rods with 4.2 wt% gadolinium would meet the loading requirements [7]. The less common approach simply selects combinations that meet the loading limit. For example, if the limit on k_{rack} is 0.92, then Figure 2.6 would indicate that either six rods with 5 wt% gadolinium would be acceptable or eight rods with 4 wt% gadolinium would be acceptable. In both approaches, additional gadolinium rods and/or additional gadolinium loading

increases the reactivity margin, so these gadolinium loading specifications are the minimum requirements.

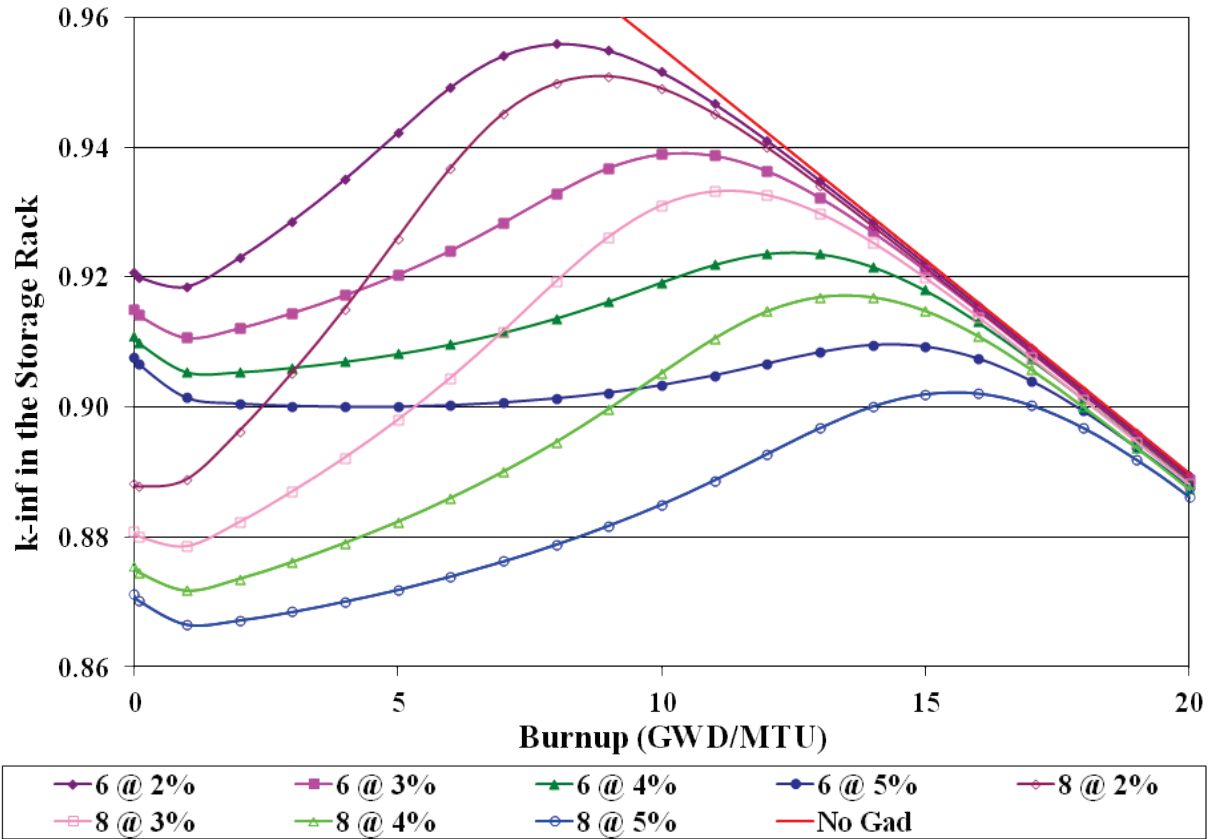


Figure 2.6. k_{rack} vs. burnup for a range of gadolinium loadings [4].

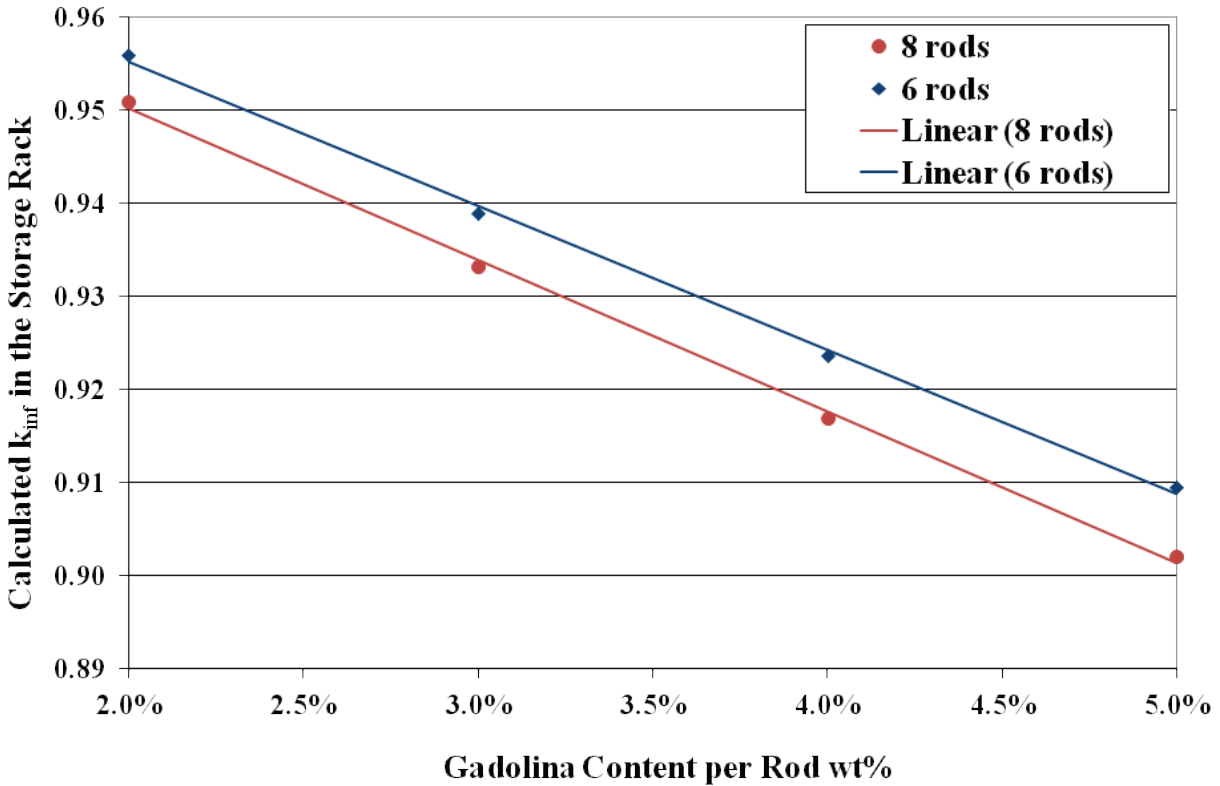


Figure 2.7. Interpolation of minimum gadolinium loading requirement [4].

The SCCG-limit-without-gadolinium-credit method has some benefits. The method adds conservatism relative to the other peak reactivity methods beyond the minimum required burnup by not modeling gadolinium poison in the fuel. The margin added by neglecting the residual gadolinium poison is small, but this approach allows the use of a single lattice for each fuel design type. This simplifies the analysis by significantly reducing the number of depletion calculations needed to generate the correlation between k_{rack} and SCCG k_{inf} . The use of only limiting depletion conditions is also conservative, and using a single set of depletion conditions eliminates scatter in the correlation of k_{rack} and SCCG k_{inf} . Furthermore, using the correlation from the bounding assembly design type and lattice adds another layer of conservatism, and it also simplifies the analysis by eliminating interface conditions between different assembly design types in storage.

This method also presents areas of concern. It is a more complicated method for implementation as it requires multiple limits that apply in different burnup regimes. For this method to be executed properly, the depletion conditions used to determine the gadolinium loading requirements would be different from those without gadolinium that are used to determine the SCCG k_{inf} correlation. Sensitivity studies would need to be performed and documented to demonstrate that both sets of depletion conditions are conservative in their respective areas of applicability. No basis has been presented for the magnitude of the 1% penalty for differences between calculated SCCG k_{inf} values. A method that does not credit residual gadolinium in

storage also presents an advantage since validation of the depleted gadolinium is not required because the material is not credited.

The primary drawback to this method is the complexity of multiple limits and the differing depletion conditions necessary in the analysis. The simplicity of performing depletion calculations only for fuel with no burnable absorbers is offset by the requirement to consider the presence of gadolinium at low burnup. The use of different sets of depletion parameters for different limits may increase the complexity of the necessary validation effort for depleted number density calculations because both sets of conditions must be validated.

The SCCG-limit-without-gadolinium-credit method is used to demonstrate the criticality safety of BWR fuel assemblies in SFPs. There are subtle but important differences between this method and the SCCG-limit-with-gadolinium-credit method described in the previous section. The primary difference is that in this method, the SCCG limit is based on a correlation created without credit for gadolinium. The storage of fresh and low burnup fuel requires that a separate gadolinium requirement be determined and met in the burnup range in which the reactivity of unpoisoned fuel is too high. The method has some advantages in terms of conservatism, and even with the additional limit, it is still simple to implement in power plant operations. This method has been widely used in the nuclear power industry for about the last 20 years.

2.4 OTHER METHODS

Other methods have been proposed or used in SFP analysis for BWR fuel, but limited information is available for some of these methods in the open literature. Additional methods are likely to be developed for storage and transportation cask applications. One recent example is provided in *Gadolinium Credit Application for Transportation and Storage Casks loaded with BWR UO₂ Assemblies* [9].

3 FACTORS AFFECTING PEAK REACTIVITY IN STORAGE AND TRANSPORTATION CASKS

As discussed in Section 2.1, several different depletion and lattice design parameters can influence the burnup of peak reactivity, thus influencing the reactivity of the fuel lattice at the peak. This section describes sensitivity studies performed to identify the factors most important to conservative determinations of peak reactivity for various sets of nuclides modeled in the storage and transportation configuration. These studies are intended not only to determine the most important parameters affecting peak reactivity analysis, but also to determine the conservative direction for each of these parameters. All studies are performed within the generic BUC (GBC)-68 cask model [10]. The models used for the GBC-68 cask include reflective boundary conditions, and thus they effectively model an infinite array of casks. For this reason, all reactivity calculation results reported in this section are infinite multiplication factors and are referred to as cask k_{inf} values.

This section provides an overview of the methodology used in the sensitivity studies, a review of the codes and methods used to perform the calculations, and a discussion of the BWR fuel design type used for this work. The detailed results for the studies are presented, and a summary is provided at the conclusion of the section.

3.1 SENSITIVITY STUDY METHODOLOGY

The methodology used in these studies is intended to identify the factors most important to conservative reactivity determinations for discharged BWR fuel. Some of these studies would likely need to be repeated as a part of any BWR peak reactivity analysis for a specific storage or transportation cask design. The sensitivity studies would need to be performed within the methodology used for the application and thus may generate differences in the magnitude of reactivity effects documented in this report. It is expected, however, that the primary parameters controlling fuel assembly reactivity near its peak will be common among any methods used.

The first studies performed in this section relate to the modeling of the BWR fuel both during depletion and in the storage/transportation configuration. To establish a technical basis for peak reactivity BUC, these studies have been performed to identify an acceptable approach for modeling the complex initial and depleted distributions of fissile and absorbing nuclides within the fuel assembly. Detailed, complicated models are constructed for baseline calculations to investigate the conservatism of simplified models that can be generated and executed more quickly. The results of these studies provide a basic modeling approach used for the remaining sensitivity studies.

The remaining studies are mainly focused on the impact of lattice design and operational parameters on fuel assembly reactivity. The effects of gadolinium loading are investigated by varying (1) the number of gadolinium-bearing rods and the gadolinium content of these rods, (2) the gadolinium rod pattern, (3) void fraction, (4) control blade insertion, and (5) core operating parameters. As described in Section 3.2, depletion calculations are performed with the same nuclide set for each set of conditions being modeled. The depleted isotopic number densities are then decayed for five years to represent an approximate minimum post-irradiation

cooling time prior to cask loading which would represent the maximum reactivity. Various sets of nuclides are then modeled in the storage/transportation configuration as discussed in Section 3.2. The reactivity effect of each parameter is thus established for actinide-only (AO) models, as well as for models including actinide and fission product (AFP) nuclides. The effect of including different nuclide sets in the criticality safety model is thus studied directly.

3.2 CALCULATIONAL METHODS, MODELS, AND CODES

This section presents the methods, codes, and models used in generating the results presented in Section 3.4. A description of the general approach to the sensitivity studies is presented, followed by a discussion of the SCALE sequences used for depletion and cask modeling. The models used for each step are also discussed in this section. The last portion of this section includes a discussion of the fuel assembly type considered in this work; the GE14 fuel assembly type is the base model considered, as it is the most common fuel assembly type used in domestic BWR plants today and includes features common to other advanced fuel design types.

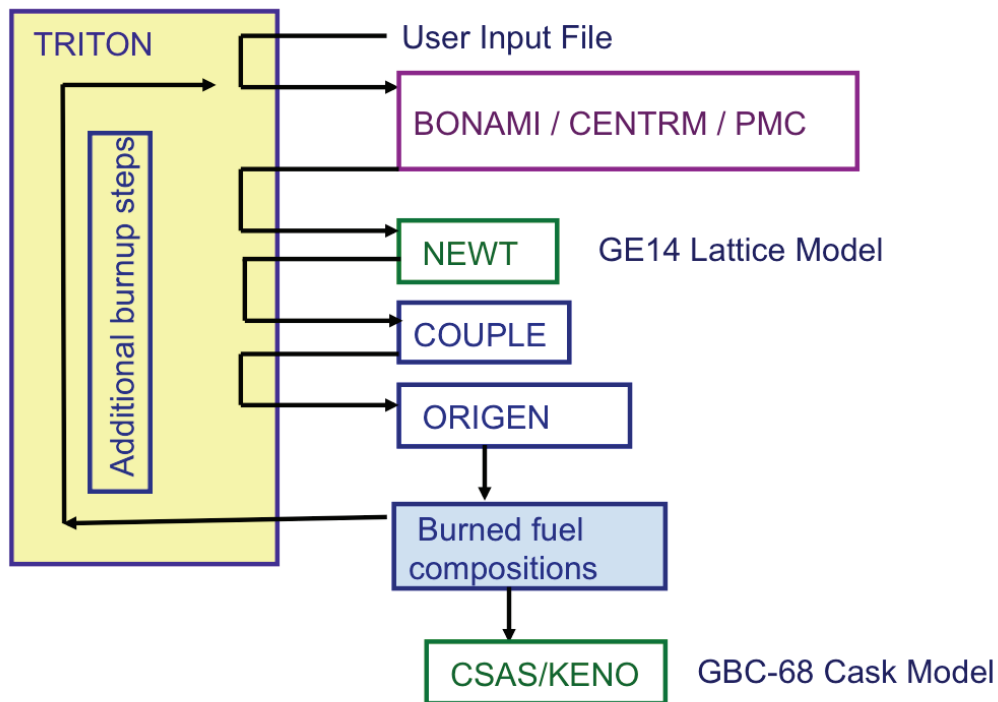


Figure 3.1. SCALE sequences, modules, and codes used for calculations.

The calculations were performed with the publicly available version 6.1.2 of SCALE [11]. TRITON/NEWT was used to perform 2D lattice depletion calculations for various operating conditions. Isotopic concentrations corresponding to burnup points at or near the reactivity peak were then extracted from the TRITON output files. The nuclide concentrations were then decayed for five years using ORIGEN. The resulting nuclide concentration values (in the form of SCALE composition input) were passed to KENO in order to perform the cask criticality

calculations. Figure 3.1 is a simplified flowchart showing how the calculations were performed with SCALE for these BWR BUC sensitivity studies.

3.2.1 Triton

TRITON is a multipurpose SCALE control module for transport, depletion, and sensitivity and uncertainty analysis. TRITON can be used to provide automated, problem-dependent cross-section processing, followed by multigroup transport calculations for 1D, 2D, and 3D configurations. This functionality can be used in tandem with the ORIGEN depletion module to predict isotopic concentrations, source terms, and decay heat, as well as to generate few-group homogenized cross sections for nodal core calculations. In the context of this work, TRITON is used for automating resonance self-shielding (CENTRM/BONAMI), 2D neutron transport (NEWT), and fuel depletion calculations (ORIGEN), which constitute a single time step of the depletion calculations. Many of these steps are simulated in order to perform the full depletion calculations.

For this project, TRITON was used to perform 2D lattice depletion calculations over a range of varying conditions. A set of 94 nuclides was included in the transport model, corresponding to the “addnux=2” option (default in TRITON), while more than 2000 nuclides were tracked during the ORIGEN depletion and decay calculations. Seven equal-area radial rings were used in the gadolinium-bearing fuel pins to capture radial depletion of gadolinium. Seven equal-area rings provide the necessary solution accuracy in a reasonable computational time [12]. The ENDF/B-VII.0 238-group cross-section library was used with the “parm=weight” option in TRITON to collapse the 238-group library to a 49-group working library. Details of the TRITON models are documented in Appendix A. After depletion calculations were complete, the output files generated during the TRITON depletion calculations were post-processed to generate depleted and decayed fuel composition files to be used in subsequent criticality calculations.

3.2.2 CSAS/KENO

The CSAS/KENO criticality sequence was used for reactivity calculations for the GBC-68. Although KENO is a 3D code, it will essentially perform 2D calculations by using reflective axial boundary conditions. The sequence provides automated, problem-dependent cross-section processing, followed by multi-group Monte Carlo transport to solve the k_{eff} eigenvalue problem. Most of the calculations performed to support this report used reflective axial boundary conditions to create a model that is effectively 2D, as the model is both infinite and uniform in axial extent, for simplicity and conservatism. All calculations were performed using the 238-group neutron library based on ENDF/B-VII.0.

Four different sets of nuclides are considered in the fuel modeling in the CSAS models: (1) major AO, (2) major and minor AFPs; (3) major and minor actinides with no credit for gadolinium (AFPNG); and (4) TRITON “addnux=2” set of 94 nuclides modeled in the transport portion of the depletion calculations (ALL). The nuclides used in the AO and AFP nuclide sets are taken from NUREG/CR-7109 [13] and are the same as those typically used in PWR BUC. The BUC nuclides considered in the AO, AFP, and AFPNG sets are provided in Table 3.1. The AFPNG set is included to study the possibility of AFP BUC without credit for residual

gadolinium poison. The nuclides in the ALL set from TRITON, which approximates modeling all actinides and fission products that would impact k_{eff} , are provided in Table 3.2.

Table 3.1. Nuclides included in the three sets of BUC isotopes considered

Actinide-only (AO) nuclides (10 nuclides)									
²³⁴ U	²³⁵ U	²³⁸ U	²³⁸ Pu	²³⁹ Pu	²⁴⁰ Pu	²⁴¹ Pu	²⁴² Pu	²⁴¹ Am	¹⁶ O
Major and minor AFPs (29 total nuclides)									
²³⁴ U	²³⁵ U	²³⁶ U	²³⁸ U	²³⁷ Np	²³⁸ Pu	²³⁹ Pu	²⁴⁰ Pu	²⁴¹ Pu	²⁴² Pu
²⁴¹ Am	²⁴³ Am	⁹⁵ Mo	⁹⁹ Tc	¹⁰¹ Ru	¹⁰³ Rh	¹⁰⁹ Ag	¹³³ Cs	¹⁴⁷ Sm	¹⁴⁹ Sm
¹⁵⁰ Sm	¹⁵¹ Sm	¹⁵² Sm	¹⁴³ Nd	¹⁴⁵ Nd	¹⁵¹ Eu	¹⁵³ Eu	¹⁵⁵ Gd	¹⁶ O	
Major and minor AFPNG (28 total nuclides)									
²³⁴ U	²³⁵ U	²³⁶ U	²³⁸ U	²³⁷ Np	²³⁸ Pu	²³⁹ Pu	²⁴⁰ Pu	²⁴¹ Pu	²⁴² Pu
²⁴¹ Am	²⁴³ Am	⁹⁵ Mo	⁹⁹ Tc	¹⁰¹ Ru	¹⁰³ Rh	¹⁰⁹ Ag	¹³³ Cs	¹⁴⁷ Sm	¹⁴⁹ Sm
¹⁵⁰ Sm	¹⁵¹ Sm	¹⁵² Sm	¹⁴³ Nd	¹⁴⁵ Nd	¹⁵¹ Eu	¹⁵³ Eu	¹⁶ O		

Table 3.2. All TRITON default nuclides included in depletion calculations (ALL) (94 total nuclides, TRITON “addnux=2” nuclides) [11]

²³⁴ U	²³⁵ U	²³⁶ U	²³⁸ U	²³⁷ Np	²³⁸ Pu	²³⁹ Pu	²⁴⁰ Pu	²⁴¹ Pu	²⁴² Pu
²⁴¹ Am	²⁴² Am	²⁴³ Am	²⁴² Cm	²⁴³ Cm	²⁴⁴ Cm	¹ H	¹⁰ B	¹¹ B	¹⁴ N
¹⁶ O	⁸³ Kr	⁹³ Nb	⁹⁵ Nb	⁹¹ Zr	⁹³ Zr	⁹⁴ Zr	⁹⁵ Zr	⁹⁶ Zr	⁹⁵ Mo
⁹⁷ Mo	⁹⁸ Mo	⁹⁹ Mo	¹⁰⁰ Mo	⁹⁹ Tc	¹⁰¹ Ru	¹⁰² Ru	¹⁰³ Ru	¹⁰⁴ Ru	¹⁰⁶ Ru
¹⁰³ Rh	¹⁰⁵ Rh	¹⁰⁵ Pd	¹⁰⁷ Pd	¹⁰⁸ Pd	¹⁰⁹ Ag	¹¹³ Cd	¹¹⁵ In	¹²⁶ Sn	¹²⁷ I
¹²⁹ I	¹³⁵ I	¹³¹ Xe	¹³³ Xe	¹³⁵ Xe	¹³³ Cs	¹³⁴ Cs	¹³⁵ Cs	¹³⁷ Cs	¹³⁹ La
¹⁴⁰ Ba	¹⁴¹ Ce	¹⁴² Ce	¹⁴³ Ce	¹⁴⁴ Ce	¹⁴¹ Pr	¹⁴³ Pr	¹⁴³ Nd	¹⁴⁴ Nd	¹⁴⁵ Nd
¹⁴⁶ Nd	¹⁴⁷ Nd	¹⁴⁸ Nd	¹⁴⁷ Pm	¹⁴⁸ Pm	¹⁴⁹ Pm	¹⁴⁷ Sm	¹⁴⁹ Sm	¹⁵⁰ Sm	¹⁵¹ Sm
¹⁵² Sm	¹⁵³ Sm	¹⁵¹ Eu	¹⁵³ Eu	¹⁵⁴ Eu	¹⁵⁵ Eu	¹⁵⁶ Eu	¹⁵² Gd	¹⁵⁴ Gd	¹⁵⁵ Gd
¹⁵⁶ Gd	¹⁵⁷ Gd	¹⁵⁸ Gd	¹⁶⁰ Gd						

Table 3.3 (Table 6.10 from Reference 13) provides the uncertainty in k_{eff} for several BUC models containing PWR or BWR SNF due to nuclide cross-section uncertainties. Differences in these values largely represent differences in the sensitivities of the system k_{eff} to the nuclides listed because the same cross-section covariance data are used for both types of fuel. The minor actinides and fission products for the BWR SFP model have similar sensitivities to the PWR SFP model, indicating that the inclusion of these same nuclides from PWR BUC is reasonable for this evaluation of BWR BUC at peak reactivity.

Table 3.3. Uncertainty in k_{eff} due to uncertainty in nuclear data for BUC application models

Model	BUC model k_{eff} uncertainty (Δk)		
	SFP	GBC-32	BWR
Burnup (GWd/MTU)	10	10	11
All nuclides	0.00471	0.00468	0.00402
Major actinides (9)	0.00463	0.00455	0.00393
²³⁴ U	0.00000	0.00000	0.00000
²³⁵ U	0.00270	0.00246	0.00293
²³⁸ U	0.00250	0.00246	0.00211
²³⁸ Pu	0.00000	0.00000	0.00000
²³⁹ Pu	0.00281	0.00292	0.00154
²⁴⁰ Pu	0.00017	0.00018	0.00011
²⁴¹ Pu	0.00008	0.00007	0.00003
²⁴² Pu	0.00001	0.00001	0.00000
²⁴¹ Am	0.00000	0.00003	0.00000
Minor actinides (3)	0.00007	0.00007	0.00013
²⁴³ Am	0.00000	0.00000	0.00000
²³⁷ Np	0.00002	0.00002	0.00001
²³⁶ U	0.00007	0.00007	0.00013
FP (16)	0.00022	0.00024	0.00023
⁹⁵ Mo	0.00001	0.00001	0.00002
⁹⁹ Tc	0.00002	0.00002	0.00003
¹⁰¹ Ru	0.00002	0.00002	0.00003
¹⁰³ Rh	0.00004	0.00006	0.00008
¹⁰⁹ Ag	0.00000	0.00000	0.00000
¹³³ Cs	0.00005	0.00005	0.00008
¹⁴⁷ Sm	0.00000	0.00002	0.00000
¹⁴⁹ Sm	0.00015	0.00016	0.00010
¹⁵⁰ Sm	0.00001	0.00001	0.00002
¹⁵¹ Sm	0.00008	0.00008	0.00006
¹⁵² Sm	0.00002	0.00002	0.00003
¹⁴³ Nd	0.00011	0.00012	0.00014
¹⁴⁵ Nd	0.00004	0.00004	0.00008
¹⁵¹ Eu	0.00000	0.00000	0.00000
¹⁵³ Eu	0.00001	0.00001	0.00002
¹⁵⁵ Gd	0.00000	0.00001	*
Other actinides	0.00003	0.00000	0.00000
Other FP	0.00015	0.00008	0.00014
Structural materials	0.00081	0.00106	0.00080

*Gadolinium is included in structural materials because most is residual gadolinium from gadolinium fuel rods (i.e., gadolinium FP concentration is negligible at short decay times).

3.2.3 Cask Application Model

The cask model used in this work is the GBC-68 cask, which was developed as a computational benchmark for BWR BUC studies [10]. The cask models used in this study represent 2D slices of the cask loaded with SNF. The cask basket, absorber panels, and cask body are modeled explicitly, as shown in Figure 3.2, as well as the fuel, cladding, water tubes, and assembly channel. Figure 3.3 shows a detailed view of a single storage cell containing a GE14 fuel assembly model of the vanished lattice. A more complete description of the GE14 assembly and its full and vanished lattices is provided in Section 3.3.

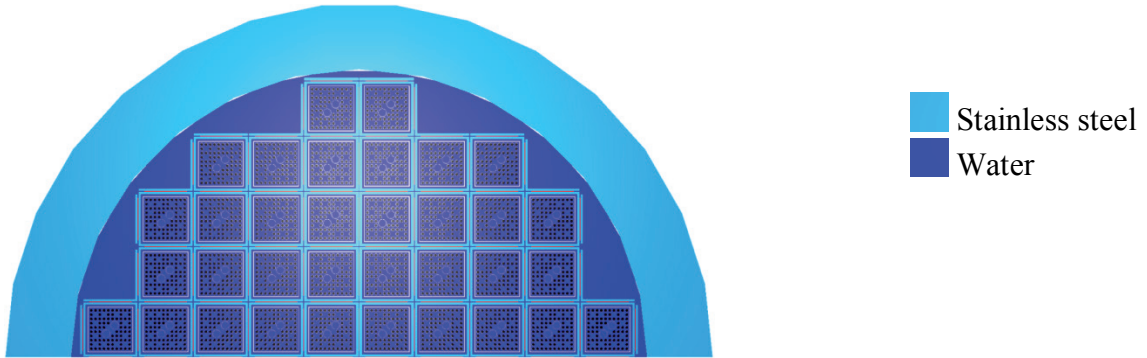


Figure 3.2. Example of GBC-68 half cask model.

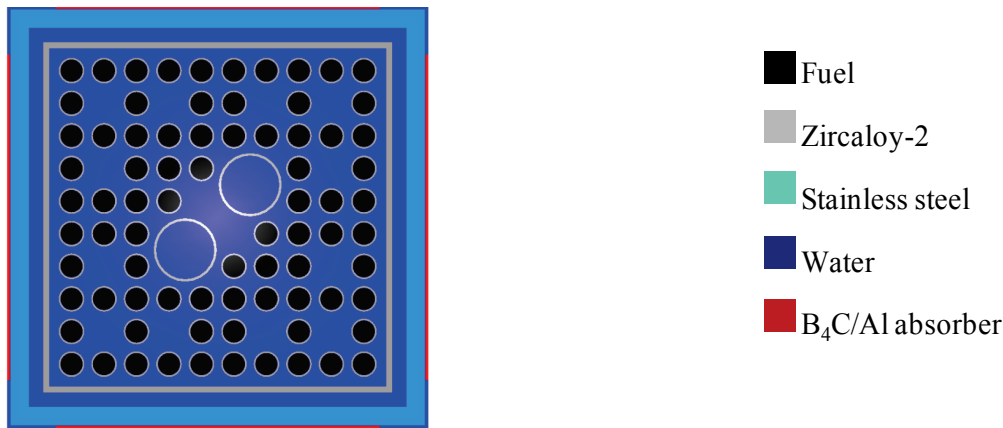


Figure 3.3. Detailed representation of a single storage cell in the GBC-68 cask model.

The fuel compositions are provided at specific burnups after extraction from the TRITON-generated output files (“ft71f001” files, ORIGEN concentration files). The burnups at which compositions were extracted were chosen based on the location of the peak reactivity in the 2D assembly model with points ranging within ± 5 GWd/MTU of the peak reactivity burnup. If no significant peak existed in the eigenvalue trajectory, then compositions were extracted for a default set of burnup values between 5–15 GWd/MTU. ORIGEN was used to extract the compositions from the ft71f001 files and decay the compositions for five years, which is a representative minimum cooling time in the SFP before transfer to a storage or transportation cask. The fuel cladding, water tubes, and assembly channel are modeled as Zircaloy-2 using the default SCALE specification. All water in the model is assumed to be full density, and the cask

is assumed to be fully flooded. Full density water is also modeled in the gap between the fuel pellet and the fuel cladding. These assumptions are typical of criticality safety analysis models and are not expected to have significant impacts on the sensitivity results presented in Section 3.4. Additional discussion of the depleted fuel and gadolinium composition modeling is provided in Section 3.4.1.

The cask calculations were performed using multigroup KENO. All fuel rods without gadolinium are modeled using the LATTICECELL treatment for multigroup resonance self-shielding calculations. The gadolinium pins are modeled with the same seven rings used in the depletion calculations. A MULTIREGION cell is used to process the multigroup cross sections for these rods. The KENO calculations considered 10,000 particles per generation, skipping the first 100 generations. The desired uncertainty was set to be no more than $0.0001 \Delta k$.

Calculations were performed for a range of burnups around the peak reactivity burnup determined in the depletion calculations. KENO calculations were performed for each of the four nuclide sets shown in Tables 3.1 and 3.2 at each burnup considered. With the removal of gadolinium in the AO and AFPNG sets, no reactivity peak occurs. The calculations are intended to provide an estimate of the conservatism due to the use of the AO, AFP, and AFPNG nuclide sets compared to the ALL set. Comparisons of the AFP and AFPNG results provide a direct measure of the residual gadolinium credit. This could be important when validation of depleted compositions, including the residual gadolinium, is considered.

3.3 FUEL DESIGN TYPES

The primary fuel assembly model used in this study was the GE14 fuel assembly. This assembly has a 10×10 array of fuel pins and contains two large central water rods. Each water rod displaces four fuel rods. In addition, the assembly has a channel box with rounded corners that are slightly thicker than the sidewalls. Modeling data for the GE14 assembly, including fuel enrichment and gadolinium loading, were taken from Reference 5. The GE14 fuel assembly can contain many axial levels with varying fuel enrichment and gadolinium loading. Due to the presence of part-length fuel rods which terminate at approximately half the total height of the fuel assembly, the GE14 fuel assembly contains two primary axial zones (or levels). These two axial regions are full and vanished zones. A 2D slice through one of these axial zones is referred to as a "lattice." As the name implies, the full lattice has a fuel rod occupying every position in the fuel pin array, and the vanished lattices are located above the part-length rods, so these rods are vanished from the lattice. SCALE/TRITON representations of GE14 full and vanished lattices with an eight-gadolinium-pin layout are illustrated in core geometry, with the control blade present, in Figure 3.4.

The GE14 fuel assembly was chosen as the main fuel assembly for the studies herein because (1) it is a common fuel assembly in U.S. BWRs, (2) it contains advanced geometry features commonly seen in modern BWR fuel assemblies (water rods, rounded channel corners, part-length rods, etc.), (3) it is commonly loaded with relatively highly enriched fuel pins (near 5.0 w/o ^{235}U), and (4) it typically contains many gadolinium-bearing fuel pins. Studying various characteristics in a modern, highly heterogeneous fuel lattice such as the GE14 allows extension of the basic results to other highly heterogeneous fuel configurations. Previous studies [4, 14]

have shown that the GE14 bundle design is more reactive than smaller GE lattices (7×7, 8×8, and 9×9) at burnups at which peak reactivity occurs.

The fuel assembly design in Reference 5 was used as a basis for further model modifications. Various studies, such as those investigating gadolinium fuel pin loading and gadolinium fuel pin patterns, were implemented by modification of the original lattice design to suit the needs of the sensitivity studies.

The fuel enrichment and gadolinium layouts for the full and vanished lattices are illustrated in Figure 3.5 [5]. A box with a single number signifies the fuel pin enrichment in wt% ^{235}U , and a box with two numbers signifies the enrichment (top) and gadolinium content in wt% gadolinium (bottom). The large boxes labeled “WR” specify the large central water rod, and boxes with a “V” specify a vanished fuel pin.

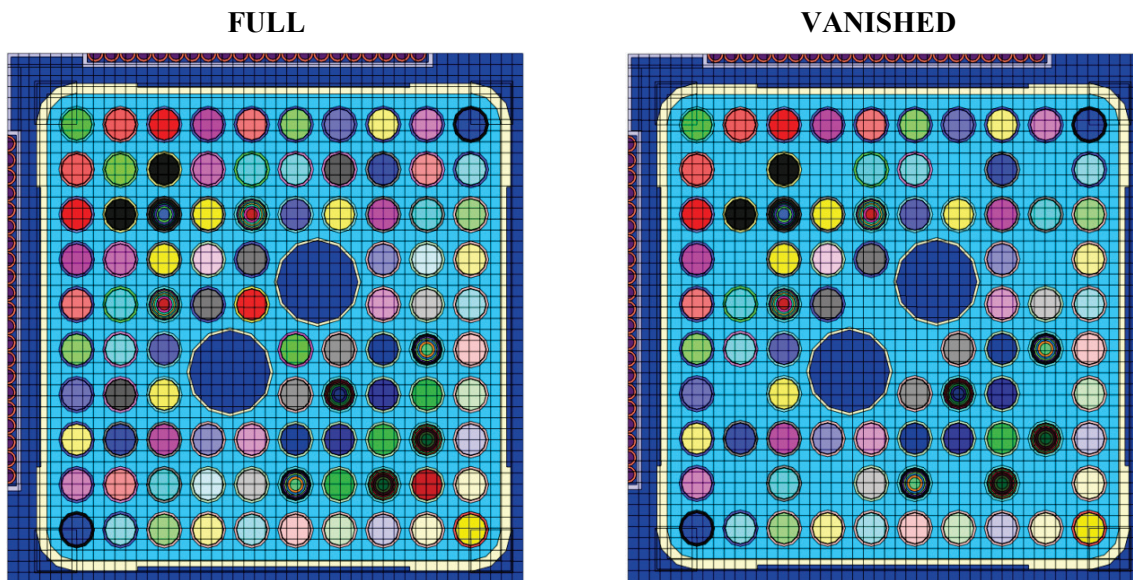


Figure 3.4. GE14 full and vanished lattices in reactor geometry.

FULL										VANISHED											
1.60	2.80	3.20	3.95	3.95	3.95	3.95	3.95	3.95	2.80	1.60	2.80	3.20	3.95	3.95	3.95	3.95	3.95	3.95	2.80		
2.80	2.80	3.20	3.95	3.60	3.95	3.95	4.40	3.95	3.95	2.80	V	3.20	V	3.60	3.95	V	4.40	V	3.95		
3.20	3.20	4.40	4.40	4.90	4.40	4.40	4.40	4.40	4.90	3.20	3.20	4.40	4.40	4.90	4.40	4.40	4.40	4.40	4.90		
3.95	3.95	4.40	4.90	3.95	WR			4.90	4.90	4.90	3.95	V	4.40	4.90	3.95	WR			4.90	V	4.90
3.95	3.60	4.90	3.95	4.40	WR			4.90	4.90	4.90	3.95	3.60	4.90	3.95	V	WR			4.90	4.90	4.90
3.95	3.95	4.40	WR		4.90	4.90	4.90	4.90	4.90	3.95	3.95	4.40	WR		V	4.90	4.90	4.90	4.90	4.90	
3.95	3.95	4.40	WR		4.90	4.90	4.90	4.90	4.90	3.95	V	4.40	WR		4.90	4.90	4.90	V	4.90		
3.95	4.40	4.40	4.90	4.90	4.90	4.90	4.90	4.90	4.90	3.95	4.40	4.40	4.90	4.90	4.90	4.90	4.90	4.90	4.90		
3.95	3.95	4.40	4.90	4.90	4.90	4.90	4.90	4.90	4.90	3.95	V	4.40	V	4.90	4.90	V	4.90	V	4.90		
2.80	3.95	4.90	4.90	4.90	4.90	4.90	4.90	4.90	3.20	2.80	3.95	4.90	4.90	4.90	4.90	4.90	4.90	4.90	4.90	3.20	

Figure 3.5. Full and vanished lattice layouts for the GE14 assembly [5].

3.4 RESULTS

This section presents the results of the sensitivity studies, which in turn support the recommendations presented in Section 3.5. These studies are intended to determine general trends for the representative fuel lattices used. They are not intended to provide absolute results to be used in licensing actions. Some of the results indicate areas in which application-specific studies may be needed to demonstrate that conservative or appropriate modeling assumptions have been used in the criticality safety analysis. Each study is presented in a separate subsection; the first few studies—which are related to fuel modeling, gadolinium loading, and gadolinium rod patterns—are necessary to support the selection of base models used for the remaining studies on void fraction, control blade insertion, and operating parameters.

3.4.1 Isotopic Modeling during Depletion

When using a general-purpose lattice depletion tool such as TRITON, the user has a significant number of modeling choices to make, which could impact the isotopic content produced from simulation of the model. In other software specifically designed for lattice depletion and nodal data generation, such as CASMO [15] or fuel vendor software, the user might not have the multitude of options available for modeling choices. In the interest of covering all the options that a user might select for isotopic modeling, four isotopic modeling strategies were chosen and used throughout this work. The strategies were used consistently in the TRITON depletion and KENO reactivity calculations so that whichever strategy was used to generate a particular set of depleted fuel isotopics was also used in the cask model including those depleted compositions.

The four chosen options are (1) pin-wise enrichment with pin-wise isotopics (PEPI), (2) pin-wise enrichment with average isotopics (PEAI), (3) average-enrichment with pin-wise isotopics (AEPI), and (4) average-enrichment with average isotopics (AEAI). “Pin-wise enrichment” refers to explicitly modeling the actual fuel enrichment in each fuel pin location in the lattice, while “average enrichment” refers to using the average fuel enrichment over the lattice for every fuel pin location in the lattice. “Pin-wise isotopics” refers to explicitly modeling the fuel depletion in each individual fuel pin in the lattice, while “average isotopics” refers to modeling a

group of like-enrichment fuel pins as a single depletion material in the model. The average enrichment for the lattices modeled in this study is 4.305 wt% ^{235}U .

PEPI is the most accurate method of modeling depletion in the fuel lattice, as the initial enrichment is modeled in each fuel pin and the isotopics are tracked separately in each fuel pin. PEAI is slightly less accurate: each fuel pin contains the correct initial fuel enrichment, but each like-enrichment group is tracked as a single mixture in the depletion calculation. In AEPI, the average enrichment for the lattice is calculated and used in each fuel pin, but the isotopics are individually tracked in each fuel pin. This method is feasible within TRITON, but it erases any impact that the differing initial loadings might have on these pin-wise depleted compositions. In AEAI, the average enrichment for the lattice is calculated and used in each fuel pin, and the isotopics are tracked as a single group. In both average enrichment scenarios, the gadolinium content is discrete (loaded only in certain fuel pins) rather than being averaged over the entire lattice. In both the average isotopics cases (AEAI and PEAI), one mixture is used for each radial ring in all gadolinium-bearing fuel pins. That is, in all gadolinium-bearing pins, the outer ring of a gadolinium-bearing pin contains identical isotopics to all the other gadolinium-bearing pins, but the isotopics in each radial ring are tracked separately. Conversely, in the pin-wise isotopics cases (PEPI and AEPI), every radial ring in every gadolinium-bearing pin is depleted as a separate mixture.

The choice of the isotopic modeling strategies impacts the depleted isotopic concentrations and resulting reactivity calculations, so it is important to determine which of these strategies is most (and least) conservative from a reactivity standpoint.

The results for the vanished lattice containing no gadolinium rods are shown in Figure 3.6 for the AO, AFP, and ALL nuclide sets using the AEAI modeling strategy.

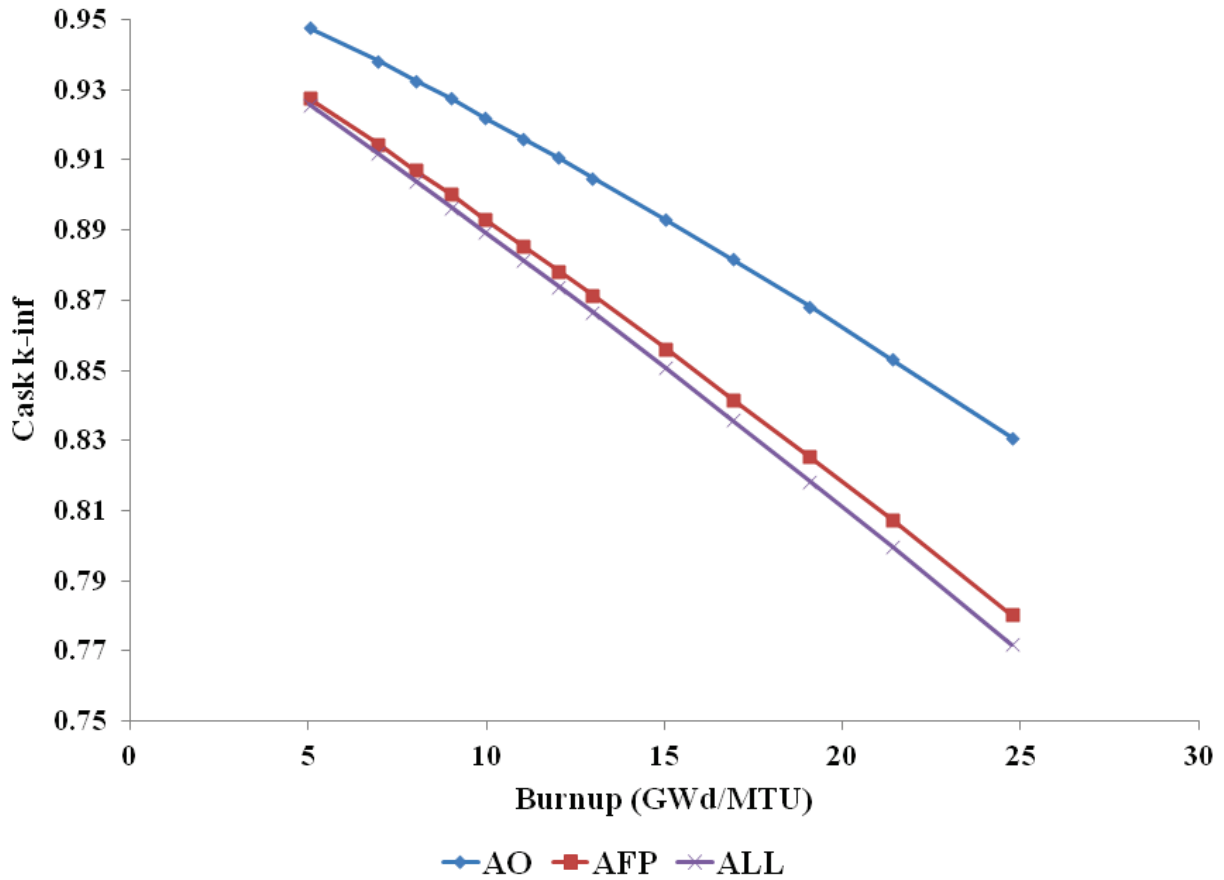


Figure 3.6. 2D Cask k_{inf} as a function of burnup for fuel with no initial gadolinium loading and three nuclide sets, AEAI modeling strategy.

The reactivity change is nearly linear over the burnup range of interest because no gadolinium was loaded in the fresh fuel. Calculations are performed for the same lattice at the same burnups, assuming AEPI, PEAI, and PEPI modeling. The difference in calculated cask k_{inf} for each of the isotopic modeling strategies is provided in Tables 3.4–3.6.

Table 3.4. Change in cask k_{inf} , AEAI-AEPI, zero initial gadolinium

Burnup (GWd/MTU)	AO		AFP		ALL	
	Δk_{inf}	σ	Δk_{inf}	σ	Δk_{inf}	σ
5.04	-0.00017	0.00014	-0.00041	0.00014	0.00012	0.00014
6.96	-0.00015	0.00014	-0.00039	0.00014	-0.00043	0.00014
8.00	-0.00025	0.00014	-0.00070	0.00014	-0.00051	0.00014
9.01	-0.00014	0.00014	-0.00032	0.00014	-0.00069	0.00014
9.97	-0.00040	0.00014	-0.00108	0.00014	-0.00056	0.00014
11.02	-0.00017	0.00014	-0.00041	0.00014	0.00012	0.00014

Table 3.5. Change in cask k_{inf} , AEAI-PEAI, zero initial gadolinium

Burnup (GWd/MTU)	AO		AFP		ALL	
	Δk_{inf}	σ	Δk_{inf}	σ	Δk_{inf}	σ
5.04	0.00305	0.00014	0.00302	0.00014	0.00335	0.00014
6.96	0.00300	0.00014	0.00278	0.00014	0.00304	0.00014
8.00	0.00279	0.00014	0.00271	0.00014	0.00278	0.00014
9.01	0.00286	0.00014	0.00291	0.00014	0.00272	0.00014
9.97	0.00280	0.00014	0.00268	0.00014	0.00263	0.00014
11.02	0.00305	0.00014	0.00302	0.00014	0.00335	0.00014

Table 3.6. Change in cask k_{inf} , AEAI-PEPI, zero initial gadolinium

Burnup (GWd/MTU)	AO		AFP		ALL	
	Δk_{inf}	σ	Δk_{inf}	σ	Δk_{inf}	σ
5.04	0.00311	0.00014	0.00303	0.00014	0.00323	0.00014
6.96	0.00327	0.00014	0.00284	0.00014	0.00294	0.00014
8.00	0.00280	0.00014	0.00283	0.00014	0.00267	0.00014
9.01	0.00311	0.00014	0.00285	0.00014	0.00266	0.00014
9.97	0.00253	0.00014	0.00221	0.00014	0.00272	0.00014
11.02	0.00264	0.00014	0.00238	0.00013	0.00251	0.00014

Similar results for the vanished lattice containing six gadolinium rods with 2 wt% gadolinium in gadolinium fuel pins are shown in Figure 3.7 for the AO, AFP, AFPNG, and ALL nuclide sets using the AEAI modeling strategy.

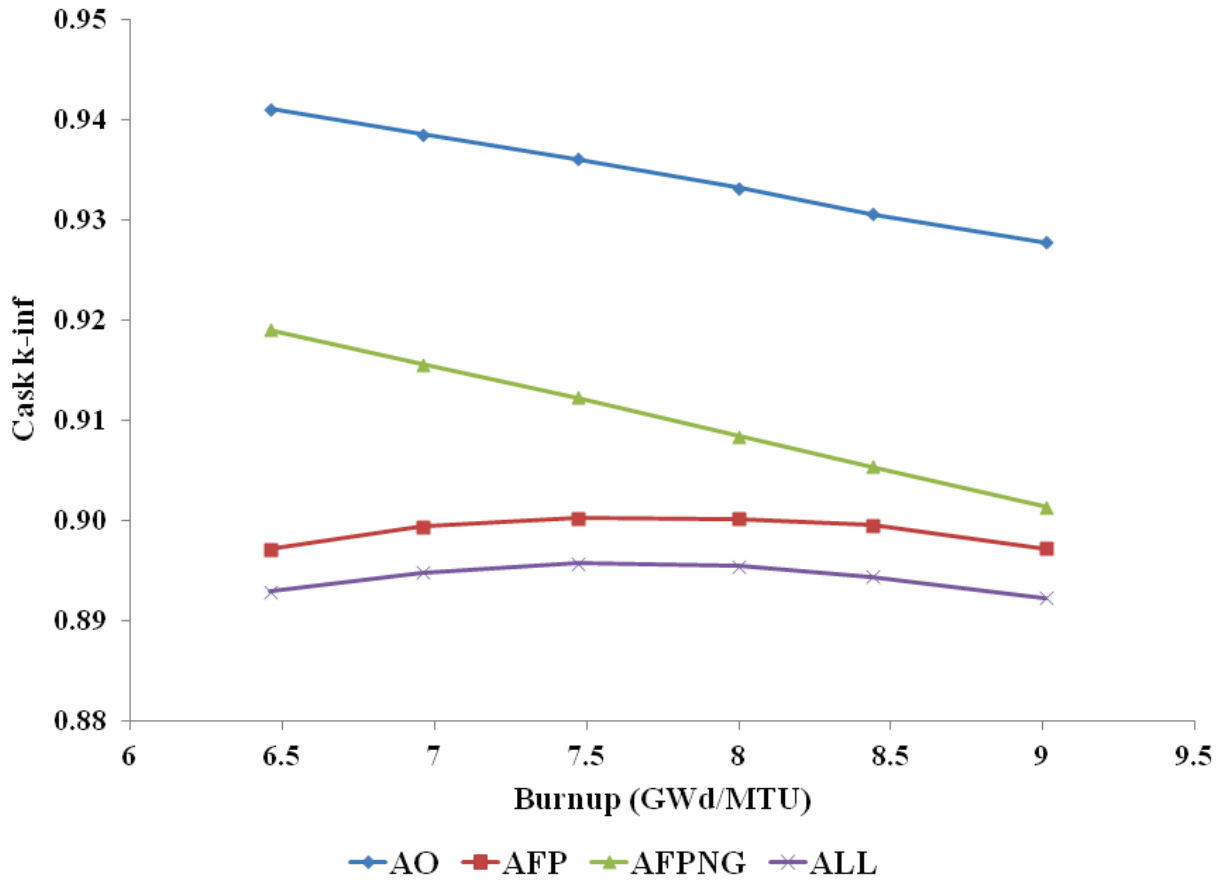


Figure 3.7. 2D Cask k_{inf} as a function of burnup for fuel initially containing six pins with 2 wt% gadolinium and four nuclide sets, AEAI modeling strategy.

The AO and AFPNG nuclide sets show a nearly linear depletion because the residual gadolinium is not included in the model. The AFP and ALL sets include the gadolinium and therefore show a reactivity peak at approximately 7.5 GWd/MTU. At this burnup, the residual gadolinium is worth about 1.25% Δk . The minor actinides, residual ^{155}Gd , and top 16 fission products are worth 3.6% Δk . The remaining fission products are worth approximately 0.4% Δk . The difference in calculated cask k_{inf} for each of the isotopic modeling strategies is provided in Tables 3.7–3.9.

Table 3.7. Change in cask k_{inf} , AEAI-AEPI, six rods with 2 wt% initial gadolinium

Burnup (GWd/MTU)	AO		AFP		AFPNG		ALL	
	Δk_{inf}	σ						
6.46	-0.00046	0.00014	-0.00021	0.00014	-0.00063	0.00014	-0.00002	0.00014
6.96	-0.00032	0.00014	0.00018	0.00014	-0.00064	0.00014	0.00009	0.00014
7.47	-0.00011	0.00014	-0.00002	0.00014	-0.00008	0.00014	0.00000	0.00014
8.00	-0.00030	0.00014	-0.00025	0.00014	-0.00048	0.00014	0.00017	0.00014
8.44	-0.00072	0.00014	0.00001	0.00014	-0.00057	0.00014	-0.00028	0.00014
9.01	-0.00045	0.00014	-0.00035	0.00014	-0.00061	0.00014	-0.00001	0.00014

Table 3.8. Change in cask k_{inf} , AEAI-PEAI, six rods with 2 wt% initial gadolinium

Burnup (GWd/MTU)	AO		AFP		AFPNG		ALL	
	Δk_{inf}	σ						
6.46	0.00324	0.00014	0.00403	0.00014	0.00301	0.00014	0.00413	0.00014
6.96	0.00308	0.00014	0.00435	0.00014	0.00285	0.00014	0.00420	0.00014
7.47	0.00319	0.00014	0.00401	0.00014	0.00311	0.00014	0.00391	0.00014
8.00	0.00297	0.00014	0.00373	0.00014	0.00296	0.00014	0.00392	0.00014
8.44	0.00291	0.00014	0.00384	0.00014	0.00283	0.00014	0.00371	0.00014
9.01	0.00306	0.00014	0.00346	0.00014	0.00279	0.00014	0.00354	0.00014

Table 3.9. Change in cask k_{inf} , AEAI-PEPI, six rods with 2 wt% initial gadolinium

Burnup (GWd/MTU)	AO		AFP		AFPNG		ALL	
	k_{inf}	σ	k_{inf}	σ	k_{inf}	σ	k_{inf}	σ
6.46	0.00323	0.00014	0.00447	0.00014	0.00306	0.00014	0.00503	0.00014
6.96	0.00322	0.00014	0.00526	0.00014	0.00287	0.00014	0.00536	0.00014
7.47	0.00322	0.00014	0.00550	0.00014	0.00311	0.00014	0.00543	0.00014
8.00	0.00305	0.00014	0.00533	0.00014	0.00284	0.00014	0.00551	0.00014
8.44	0.00266	0.00014	0.00516	0.00014	0.00259	0.00014	0.00491	0.00014
9.01	0.00309	0.00014	0.00446	0.00014	0.00282	0.00014	0.00469	0.00014

For the cases both with and without gadolinium, the AEPI results are generally statistically equivalent to the AEAI results. The AEPI method requires many more depletion calculations than the AEAI method to calculate and track pin-wise isotopics. Because the two methods show nearly identical k_{inf} results, use of the AEAI strategy is preferable because it requires less computational resources, and the strategy is self-consistent using assembly averages for both the initial enrichment loading and the tracking of isotopic depletion.

It is clear that the PEAI and PEPI pin-wise enrichment modeling approaches result in lower k_{inf} values that are similar to each other. These modeling approaches accurately represent the zoning designed into the lattice to help control power peaking near the periphery of the bundle. The PEAI and PEPI approaches are statistically equivalent in the AO and AFPNG cases, indicating that there is little impact of averaging the depleted fuel isotopics given a detailed depletion model. The PEAI results are more reactive than the PEPI results near peak reactivity for the 6×2Gd AFP and ALL cases, indicating that the average gadolinium modeling results in a conservative reactivity determination. The significantly reduced reactivity estimates resulting from the pin-wise enrichment modeling compared to the average enrichment modeling indicate that the latter approach is not only simpler but is also more conservative. The AEAI modeling

strategy is used for the remainder of the cask k_{inf} results presented in this report unless noted otherwise. This strategy is adopted as it is simple and conservative.

This conclusion should be true for realistic BWR assembly designs because the driving consideration in assembly designs is the control of pin power peaking during power operations. A BWR assembly could be designed with higher enrichment near the periphery that would challenge the average enrichment assignment, but the design would result in unacceptable peaking near the gap between assemblies. This is especially true for most of the currently operating BWR plants that have larger gaps on the control blade side of the assembly than on the detector side. Some designs have symmetric gaps, which likely reduce the magnitude of enrichment zoning; this would act to lower the difference between average initial enrichment (AE) and pin-wise initial enrichment (PE) approaches but not reverse it.

3.4.2 Gadolinium Loading

The gadolinium loading in each assembly is controlled with two independent parameters: the number of pins containing gadolinium and the loading of the absorber in each of those pins. Assembly designs often contain different loadings in different gadolinium rods within the same lattice. For simplicity, all poisoned rods in a lattice contain the same gadolinium loading in this study. Lattices involving multiple gadolinium loadings should see similar effects, but the specific modeling used would need to be described and justified for each application. As discussed in Section 2.1, additional gadolinium tends to push the reactivity peak toward higher burnups and thus reduce the magnitude of the peak.

3.4.2.1 Depletion Studies

The gadolinium loading study consisted of running a number of cases based on the lattice in Figure 3.4, but varying the number of gadolinium-bearing pins and the concentration in those pins. This study is primarily intended to show the sensitivity of peak reactivity (absolute reactivity and location of the peak) as determined in the depletion calculations to the number of pins and the concentration of gadolinium. The number and content of gadolinium pins in the as-designed lattice (an example is shown in Figure 3.4) result in a peak reactivity that is significantly lower (less limiting) than for lattices that contain fewer gadolinium pins with a lower gadolinium content. In the interest of generating results for more limiting cases, the number of pins and the gadolinium content in those pins were modified from the as-designed case by varying the number of gadolinium-bearing pins from 2 to 8 and the gadolinium content from 2 to 10 wt% gadolinium, as listed in Table 3.10. The locations of the gadolinium pins are a subset of the pin locations in the as-designed case. For each number of pins (2, 4, 6, and 8), five cases were run with each of the five different gadolinium loadings listed (2, 4, 6, 8, and 10), for a total of 20 cases considered for each lattice design. In addition, a gadolinium-free lattice was also simulated for comparison purposes. Throughout this document, the $N \times W \text{Gd}$ format is used to specify various gadolinium-bearing lattices, where N is the number of pins and W is the weight percent of gadolinium in those pins.

Table 3.10. Number of pins and gadolinium content per pin

Number of Pins	Gadolinium wt%
2	2
4	4
6	6
8	8
	10

The lattice layouts for the full and vanished lattices used in the gadolinium study can be found in Figures 3.8–3.12. In these figures, the numbers represent the fuel pin enrichment in that lattice location, and shaded boxes highlight gadolinium-bearing fuel pins.

FULL										VANISHED											
1.60	2.80	3.20	3.95	3.95	3.95	3.95	3.95	3.95	3.95	2.80	1.60	2.80	3.20	3.95	3.95	3.95	3.95	3.95	3.95	3.95	2.80
2.80	2.80	3.20	3.95	3.60	3.95	3.95	4.40	3.95	3.95	2.80	V	3.20	V	3.60	3.95	V	4.40	V	3.95		
3.20	3.20	4.40	4.40	4.90	4.40	4.40	4.40	4.40	4.90	3.20	3.20	4.40	4.40	4.90	4.40	4.40	4.40	4.40	4.90		
3.95	3.95	4.40	4.90	3.95	WR		4.90	4.90	4.90	3.95	V	4.40	4.90	3.95	WR		4.90	V	4.90		
3.95	3.60	4.90	3.95	4.40	WR		4.90	4.90	4.90	3.95	3.60	4.90	3.95	V	WR		4.90	4.90	4.90		
3.95	3.95	4.40	WR		4.90	4.90	4.90	4.90	4.90	3.95	3.95	4.40	WR		V	4.90	4.90	4.90	4.90		
3.95	3.95	4.40	WR		4.90	4.90	4.90	4.90	4.90	3.95	V	4.40	WR		4.90	4.90	4.90	V	4.90		
3.95	4.40	4.40	4.90	4.90	4.90	4.90	4.90	4.90	4.90	3.95	4.40	4.40	4.90	4.90	4.90	4.90	4.90	4.90	4.90		
3.95	3.95	4.40	4.90	4.90	4.90	4.90	4.90	4.90	4.90	3.95	V	4.40	V	4.90	4.90	V	4.90	V	4.90		
2.80	3.95	4.90	4.90	4.90	4.90	4.90	4.90	4.90	3.20	2.80	3.95	4.90	4.90	4.90	4.90	4.90	4.90	4.90	3.20		

Figure 3.8. Gadolinium-free lattice layout for the full and vanished lattices.

FULL										VANISHED											
1.60	2.80	3.20	3.95	3.95	3.95	3.95	3.95	3.95	2.80	1.60	2.80	3.20	3.95	3.95	3.95	3.95	3.95	3.95	2.80		
2.80	2.80	3.20	3.95	3.60	3.95	3.95	4.40	3.95	3.95	2.80	V	3.20	V	3.60	3.95	V	4.40	V	3.95		
3.20	3.20	4.40	4.40	4.90	4.40	4.40	4.40	4.40	4.90	3.20	3.20	4.40	4.40	4.90	4.40	4.40	4.40	4.40	4.90		
3.95	3.95	4.40	4.90 Gd	3.95	WR			4.90	4.90	4.90	3.95	V	4.40	4.90 Gd	3.95	WR			4.90	V	4.90
3.95	3.60	4.90	3.95	4.40	WR			4.90	4.90	4.90	3.95	3.60	4.90	3.95	V	WR			4.90	4.90	4.90
3.95	3.95	4.40	WR		4.90	4.90	4.90	4.90	4.90	3.95	3.95	4.40	WR		V	4.90	4.90	4.90	4.90		
3.95	3.95	4.40	WR		4.90	4.90	4.90	4.90	4.90	3.95	V	4.40	WR		4.90	4.90	4.90	V	4.90		
3.95	4.40	4.40	4.90	4.90	4.90	4.90	4.90 Gd	4.90	4.90	3.95	4.40	4.40	4.90	4.90	4.90	4.90	4.90 Gd	4.90	4.90		
3.95	3.95	4.40	4.90	4.90	4.90	4.90	4.90	4.90	4.90	3.95	V	4.40	V	4.90	4.90	V	4.90	V	4.90		
2.80	3.95	4.90	4.90	4.90	4.90	4.90	4.90	4.90	3.20	2.80	3.95	4.90	4.90	4.90	4.90	4.90	4.90	4.90	3.20		

Figure 3.9. Two gadolinium pin layout for the full and vanished lattices.

FULL										VANISHED											
1.60	2.80	3.20	3.95	3.95	3.95	3.95	3.95	3.95	2.80	1.60	2.80	3.20	3.95	3.95	3.95	3.95	3.95	3.95	2.80		
2.80	2.80	3.20	3.95	3.60	3.95	3.95	4.40	3.95	3.95	2.80	V	3.20	V	3.60	3.95	V	4.40	V	3.95		
3.20	3.20	4.40	4.40	4.90 Gd	4.40	4.40	4.40	4.40	4.90	3.20	3.20	4.40	4.40	4.90 Gd	4.40	4.40	4.40	4.40	4.90		
3.95	3.95	4.40	4.90	3.95	WR			4.90	4.90	4.90	3.95	V	4.40	4.90	3.95	WR			4.90	V	4.90
3.95	3.60	4.90 Gd	3.95	4.40	WR			4.90	4.90	4.90	3.95	3.60	4.90 Gd	3.95	V	WR			4.90	4.90	4.90
3.95	3.95	4.40	WR		4.90	4.90	4.90	4.90 Gd	4.90	3.95	3.95	4.40	WR		V	4.90	4.90	4.90 Gd	4.90		
3.95	3.95	4.40	WR		4.90	4.90	4.90	4.90	4.90	3.95	V	4.40	WR		4.90	4.90	4.90	V	4.90		
3.95	4.40	4.40	4.90	4.90	4.90	4.90	4.90	4.90	4.90	3.95	4.40	4.40	4.90	4.90	4.90	4.90	4.90	4.90	4.90		
3.95	3.95	4.40	4.90	4.90	4.90 Gd	4.90	4.90	4.90	4.90	3.95	V	4.40	V	4.90	4.90 Gd	V	4.90	V	4.90		
2.80	3.95	4.90	4.90	4.90	4.90	4.90	4.90	4.90	3.20	2.80	3.95	4.90	4.90	4.90	4.90	4.90	4.90	4.90	3.20		

Figure 3.10. Four gadolinium pin layout for the full and vanished lattices.

FULL										VANISHED									
1.60	2.80	3.20	3.95	3.95	3.95	3.95	3.95	3.95	2.80	1.60	2.80	3.20	3.95	3.95	3.95	3.95	3.95	3.95	2.80
2.80	2.80	3.20	3.95	3.60	3.95	3.95	4.40	3.95	3.95	2.80	V	3.20	V	3.60	3.95	V	4.40	V	3.95
3.20	3.20	4.40	4.40	4.90 Gd	4.40	4.40	4.40	4.40	4.90	3.20	3.20	4.40	4.40	4.90 Gd	4.40	4.40	4.40	4.40	4.90
3.95	3.95	4.40	4.90	3.95	WR		4.90	4.90	4.90	3.95	V	4.40	4.90	3.95	WR		4.90	V	4.90
3.95	3.60	4.90 Gd	3.95	4.40	WR		4.90	4.90	4.90	3.95	3.60	4.90 Gd	3.95	V	WR		4.90	4.90	4.90
3.95	3.95	4.40	WR		4.90	4.90	4.90	4.90 Gd	4.90	3.95	3.95	4.40	WR		V	4.90	4.90	4.90 Gd	4.90
3.95	3.95	4.40	WR		4.90	4.90	4.90	4.90	4.90	3.95	V	4.40	WR		4.90	4.90	4.90	V	4.90
3.95	4.40	4.40	4.90	4.90	4.90	4.90	4.90	4.90 Gd	4.90	3.95	4.40	4.40	4.90	4.90	4.90	4.90	4.90	4.90 Gd	4.90
3.95	3.95	4.40	4.90	4.90	4.90 Gd	4.90	4.90 Gd	4.90	4.90	3.95	V	4.40	V	4.90	4.90 Gd	V	4.90 Gd	V	4.90
2.80	3.95	4.90	4.90	4.90	4.90	4.90	4.90	4.90	3.20	2.80	3.95	4.90	4.90	4.90	4.90	4.90	4.90	4.90	3.20

Figure 3.11. Six gadolinium pin layout for the full and vanished lattices.

FULL										VANISHED									
1.60	2.80	3.20	3.95	3.95	3.95	3.95	3.95	3.95	2.80	1.60	2.80	3.20	3.95	3.95	3.95	3.95	3.95	3.95	2.80
2.80	2.80	3.20	3.95	3.60	3.95	3.95	4.40	3.95	3.95	2.80	V	3.20	V	3.60	3.95	V	4.40	V	3.95
3.20	3.20	4.40 Gd	4.40	4.90 Gd	4.40	4.40	4.40	4.40	4.90	3.20	3.20	4.40 Gd	4.40	4.90 Gd	4.40	4.40	4.40	4.40	4.90
3.95	3.95	4.40	4.90	3.95	WR		4.90	4.90	4.90	3.95	V	4.40	4.90	3.95	WR		4.90	V	4.90
3.95	3.60	4.90 Gd	3.95	4.40	WR		4.90	4.90	4.90	3.95	3.60	4.90 Gd	3.95	V	WR		4.90	4.90	4.90
3.95	3.95	4.40	WR		4.90	4.90	4.90	4.90 Gd	4.90	3.95	3.95	4.40	WR		V	4.90	4.90	4.90 Gd	4.90
3.95	3.95	4.40	WR		4.90	4.90 Gd	4.90	4.90	4.90	3.95	V	4.40	WR		4.90	4.90 Gd	4.90	V	4.90
3.95	4.40	4.40	4.90	4.90	4.90	4.90	4.90	4.90 Gd	4.90	3.95	4.40	4.40	4.90	4.90	4.90	4.90	4.90	4.90 Gd	4.90
3.95	3.95	4.40	4.90	4.90	4.90 Gd	4.90	4.90 Gd	4.90	4.90	3.95	V	4.40	V	4.90	4.90 Gd	V	4.90 Gd	V	4.90
2.80	3.95	4.90	4.90	4.90	4.90	4.90	4.90	4.90	3.20	2.80	3.95	4.90	4.90	4.90	4.90	4.90	4.90	4.90	3.20

Figure 3.12. Eight gadolinium pin layout for the full and vanished lattices.

As discussed in Section 3.3, “V” denotes the location of a vanished rod in the lattice, and “WR” shows the location of the two water rods. The location of the gadolinium pins remains constant, while the concentration is varied using the values shown in Table 3.9.

TRITON depletion calculations were performed for all cases (including all isotopic modeling strategies) using 40% void fraction (core average condition) in the moderator and representative

fuel, clad, and moderator temperatures for BWRs. Eigenvalue trajectories (k_{inf} vs. burnup) for the PEPI isotopic strategy (most precise modeling) and the vanished lattices (most reactive lattices) were extracted from the output files and plotted in Figure 3.13. Each subfigure (a–e) corresponds to a certain gadolinium concentration (2–10 wt% gadolinium, respectively) in the gadolinium pins, and each line corresponds to the number of gadolinium pins in the lattice. The black line in each of the figures is the eigenvalue trajectory for the gadolinium-free lattice. The results from the PEPI depletions are used in this figure because they are the most accurate. Results from the AEAI strategy were similar. Figure 3.13 shows that the lattice reactivity as a function of burnup is strongly correlated to the gadolinium concentration and number of gadolinium pins.

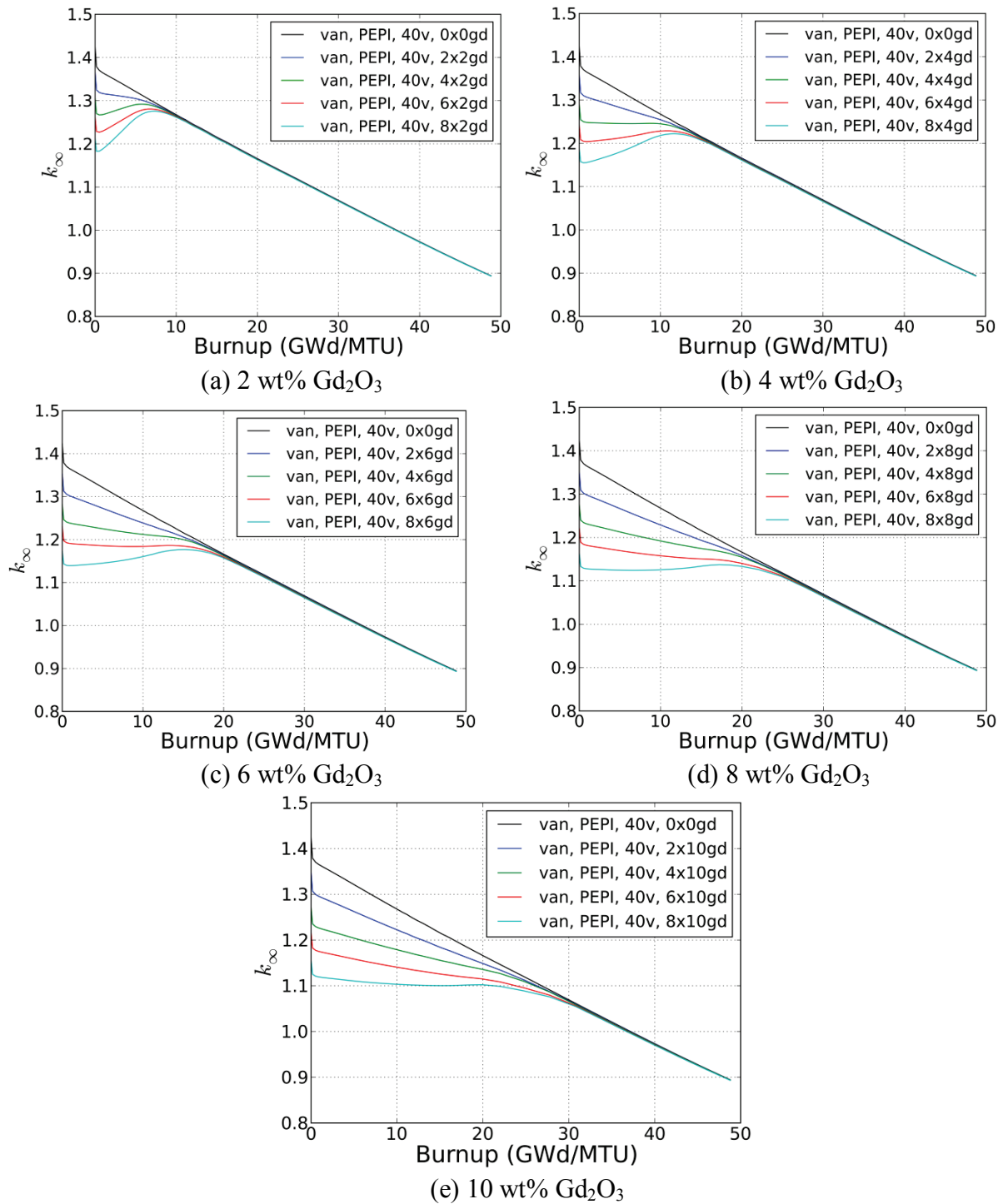


Figure 3.13. TRITON eigenvalue trajectories for the PEPI isotopic strategy varying the gadolinium content and number of gadolinium pins.

In all cases, after gadolinium has been depleted, the trajectories closely follow the gadolinium-free trajectory. The number of gadolinium fuel pins has a significant impact on the initial

reactivity of the lattice, but it has a relatively small impact on the location (burnup) and value (height) of peak reactivity. This is due to the spatial self-shielding in gadolinium fuel pins. Because gadolinium is a very strong neutron absorber (primarily ^{155}Gd and ^{157}Gd), very few thermal neutrons reach the interior of the gadolinium pins near beginning of life (BOL)—most neutrons are absorbed in the outermost radial region of the fuel pellet, meaning that more gadolinium fuel pins leads to a significant change in initial reactivity. Even when the gadolinium concentration is relatively low, the parasitic absorption by gadolinium is much more likely than fission in ^{235}U as the gadolinium absorption cross sections are 2 to 3 orders of magnitude greater than ^{235}U fission. This can be clearly observed in Figure 3.14, which plots the continuous energy cross sections for ^{155}Gd , ^{157}Gd , ^{238}U (capture, n-gamma), and ^{235}U (fission) (ENDF/B-VII.0, available in SCALE 6.1.2).

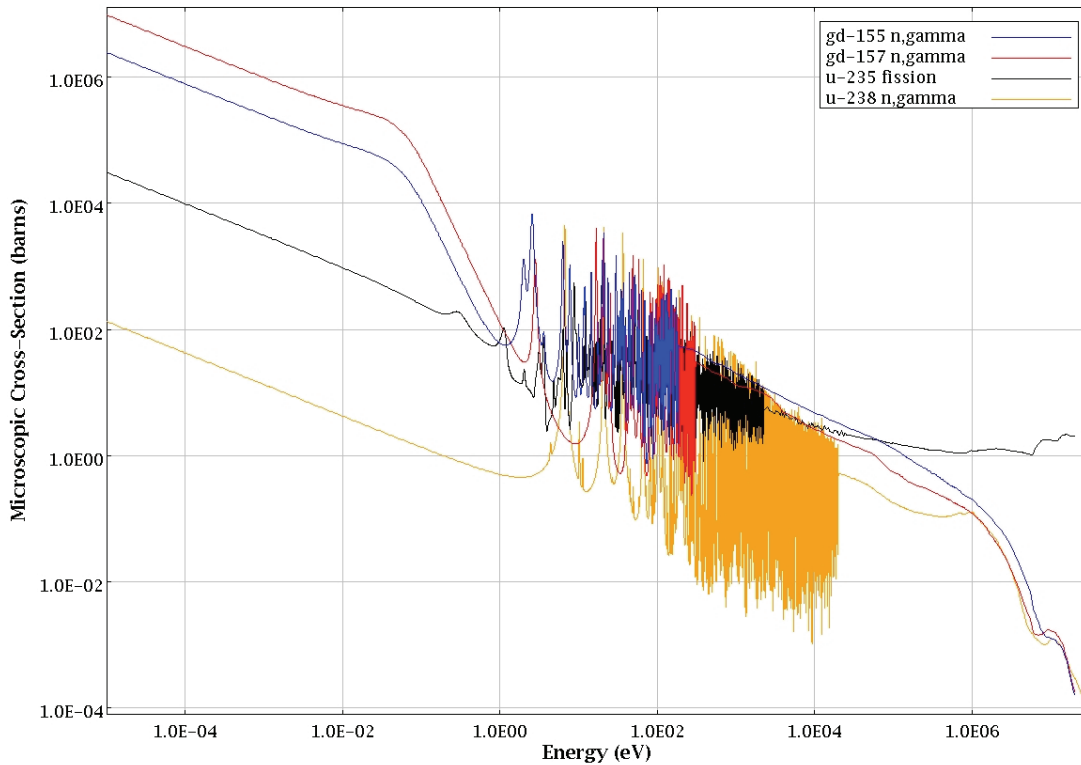


Figure 3.14. Dominating cross sections in gadolinium-bearing fuel pins.

Conversely, the gadolinium concentration has a relatively small impact on the initial reactivity, but it has a significant impact on the location (burnup) and value (height) of the reactivity peak. Because gadolinium is a very strong absorber, nearly all neutrons entering a gadolinium-bearing fuel pin will be absorbed by gadolinium, which explains the minimal impact on changing the initial gadolinium concentration. However, the concentration of gadolinium has a significant effect on the spatial depletion of gadolinium (the onion skin effect). Higher concentrations of gadolinium mean that gadolinium in the central portion of the pin will be shielded from neutrons by the outer region of the fuel pin for a longer period of time. This geometric self-shielding results in a slower overall depletion of gadolinium, which moves the reactivity peak to higher burnup, and thus, lower values further along the gadolinium-free trajectory.

This effect is illustrated in Figure 3.15(a), which shows the percent of ^{155}Gd remaining in the radial regions of gadolinium-bearing fuel pins for the 6-pin cases with concentrations ranging from 2 wt% to 10 wt% gadolinium at a burnup of 10 GWd/MTU. Figure 3.15(b) plots the eigenvalue trajectories for the cases in Figure 3.15(a). Figure 3.15 shows that for higher gadolinium fractions, the depletion of the gadolinium occurs more slowly for the inner regions of the fuel pin – this is due to the larger spatial self-shielding for the higher concentrations cases as compared to the lower concentration cases. The impact is directly observed in Figure 3.15(b) – initial k_{inf} is similar for the five cases, but the burnup and magnitude of peak reactivity is significantly changed with increasing gadolinium concentration.

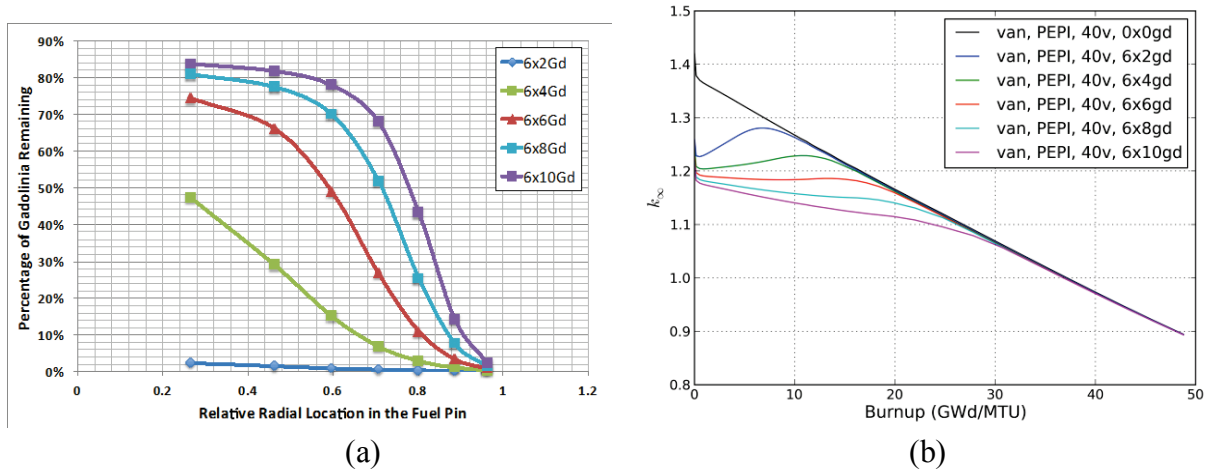


Figure 3.15. (a) Percentage of ^{155}Gd remaining as a function of radial location in the fuel pin for the 6×2Gd, 6×4Gd, 6×6Gd, 6×8Gd, and 6×10Gd cases at 10 GWd/MTU and (b) eigenvalue trajectories for the 6-gadolinium pin cases.

3.4.2.2 Cask Reactivity Studies

The depleted number densities for each of the twenty cases discussed in 3.4.2.1 are modeled in the cask using the AEAI strategy to investigate the effect of gadolinium loadings on discharged fuel reactivity. The results presented in the previous section document the effects of gadolinium loading on lattice reactivity during depletion, but the impact may vary in the storage/transportation cask. The results also depend on the nuclides included in the criticality safety model, and thus must be investigated.

The results for 2 wt% gadolinium per pin and a varying number of pins are shown for the AO nuclide set in Figure 3.16 and for the AFP nuclide set in Figure 3.17. Both figures also contain a line showing the reactivity of the assembly with no gadolinium initially loaded and the same nuclides included in the cask model. The results for the AO set, including only the nuclides listed for this set in Table 3.1, show that the number of pins has essentially no effect on the calculated cask k_{inf} . These results indicate that the number of gadolinium pins has very little impact on cask reactivity for AO analysis in the burnup range at which peak reactivity occurs for these gadolinium loadings. The results for the AFP set show that as the gadolinium loading increases, the reactivity peak is lower and it occurs at slightly higher burnups. The 2-pin and 4-pin loadings do not have sufficient gadolinium to create a peak, but instead they show a fairly uniform

reactivity through about 7 GWd/MTU before reactivity falls. The results also show that at burnups beyond the peak, the reactivity curve is similar to the gadolinium-free lattice. These results are in good agreement with expectations, and they indicate that higher gadolinium loadings, given the same number of pins, cause the reactivity peak to occur at higher burnups with lower k_{inf} values.

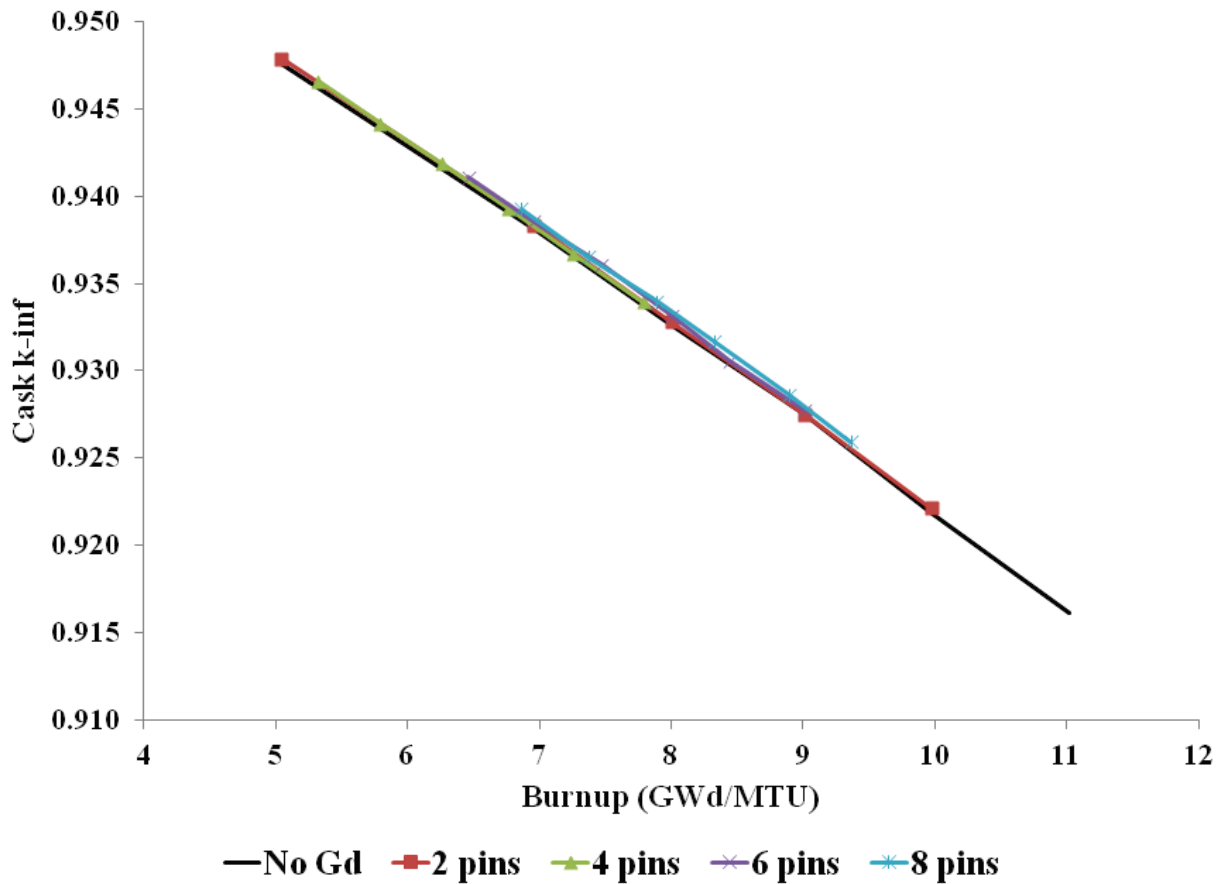


Figure 3.16. Cask k_{inf} as a function of burnup for 2 wt% gadolinium in a range of pins, AO nuclides.

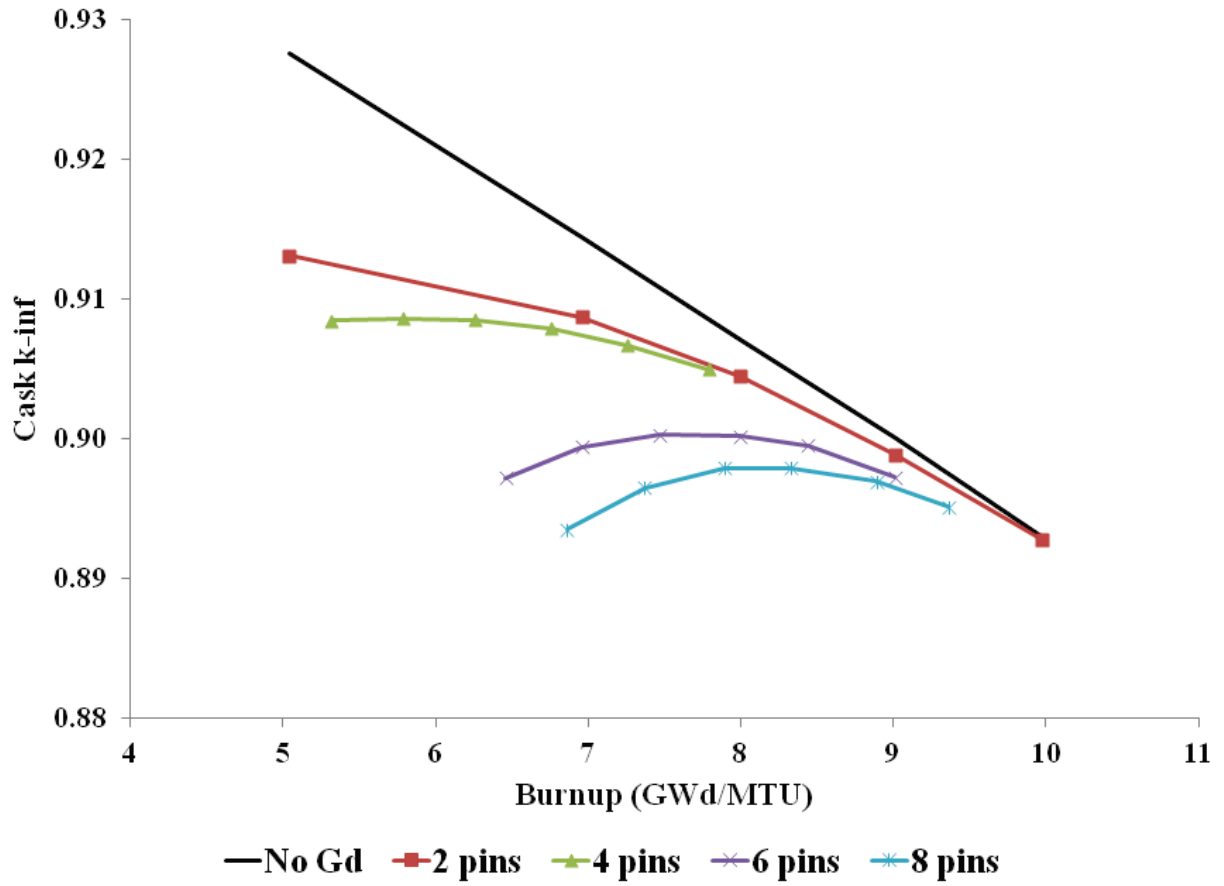


Figure 3.17. Cask k_{inf} as a function of burnup for 2 wt% gadolinium in a range of pins, AFP nuclides.

The results for six gadolinium pins and a variable gadolinium loading per pin are shown in Figure 3.18 for the AO nuclides, along with the reactivity of the assembly with no initial gadolinium.

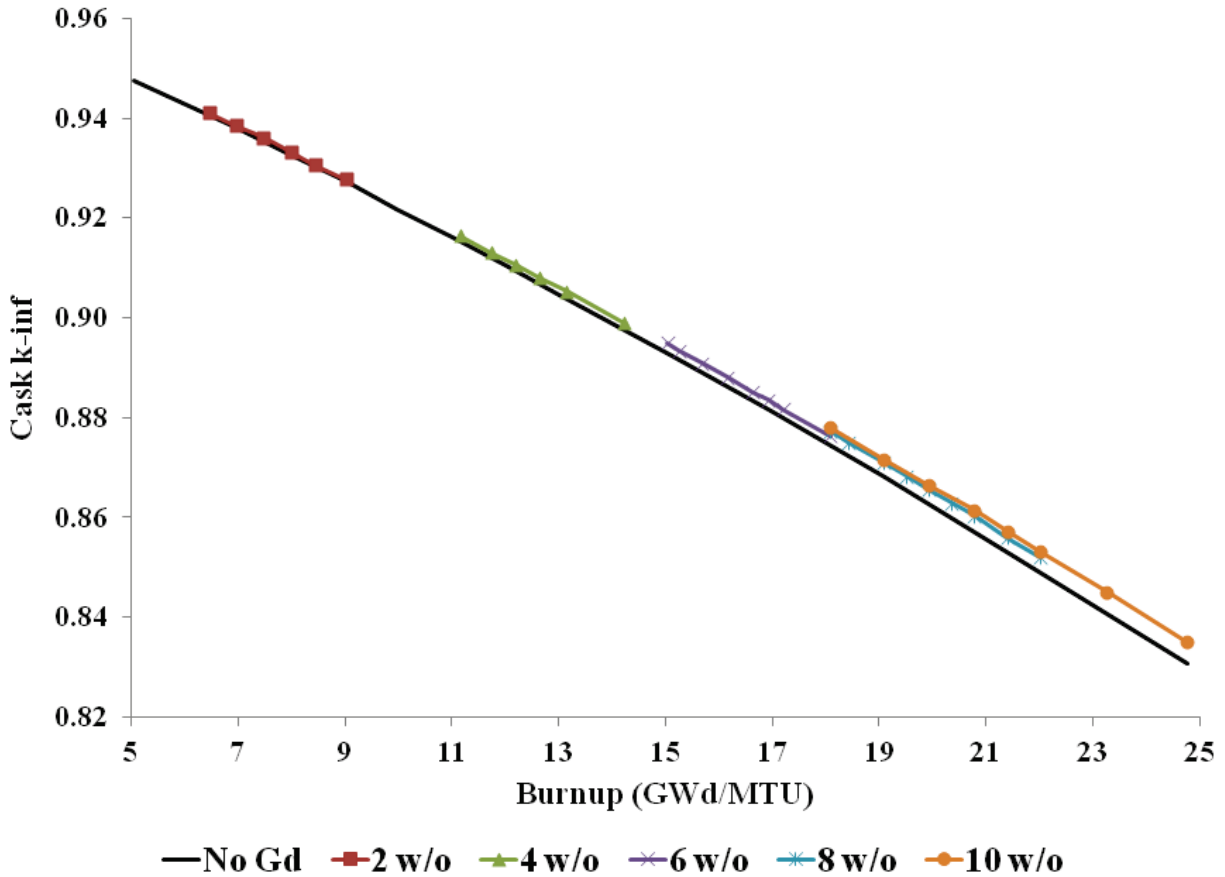


Figure 3.18. Cask k_{inf} as a function of burnup for gadolinium pins with a range of initial gadolinium loadings, AO nuclides.

The results for the AO nuclides show that for small gadolinium loadings, there is no effect; however, at higher loadings, the reactivity is slightly higher than for the assembly without initial gadolinium. This difference is caused by the spectral hardening effect of the gadolinium increasing the ^{239}Pu production. At 21.4 GWd/MTU, the $6 \times 10\text{Gd}$ fuel compositions have slightly less ^{235}U , but they have 2% to 4% more plutonium than the compositions depleted without gadolinium. This high burnup is of interest because it is near peak reactivity of this relatively heavily loaded assembly; note that the cask k_{inf} is below 0.88 at this point. The increase in plutonium production rate due to heavy gadolinium loadings may be an important phenomenon, depending upon the assembly enrichment and burnup.

The results using the AFP nuclide set are shown in Figure 3.19, along with the reactivity of the assembly with no initial gadolinium. The results show that as the loading per pin increases, the reactivity peak comes at significantly higher burnups and much lower k_{inf} values. This is in good agreement with expectations and the depletion studies. The heavier gadolinium loadings show a

generally flat trajectory to burnups of greater than 20 GWd/MTU before reactivity starts to fall. As discussed in Section 2.1, the cause of this behavior is the additional burnup required to deplete the gadolinium and the lower remaining fuel reactivity at these higher burnups.

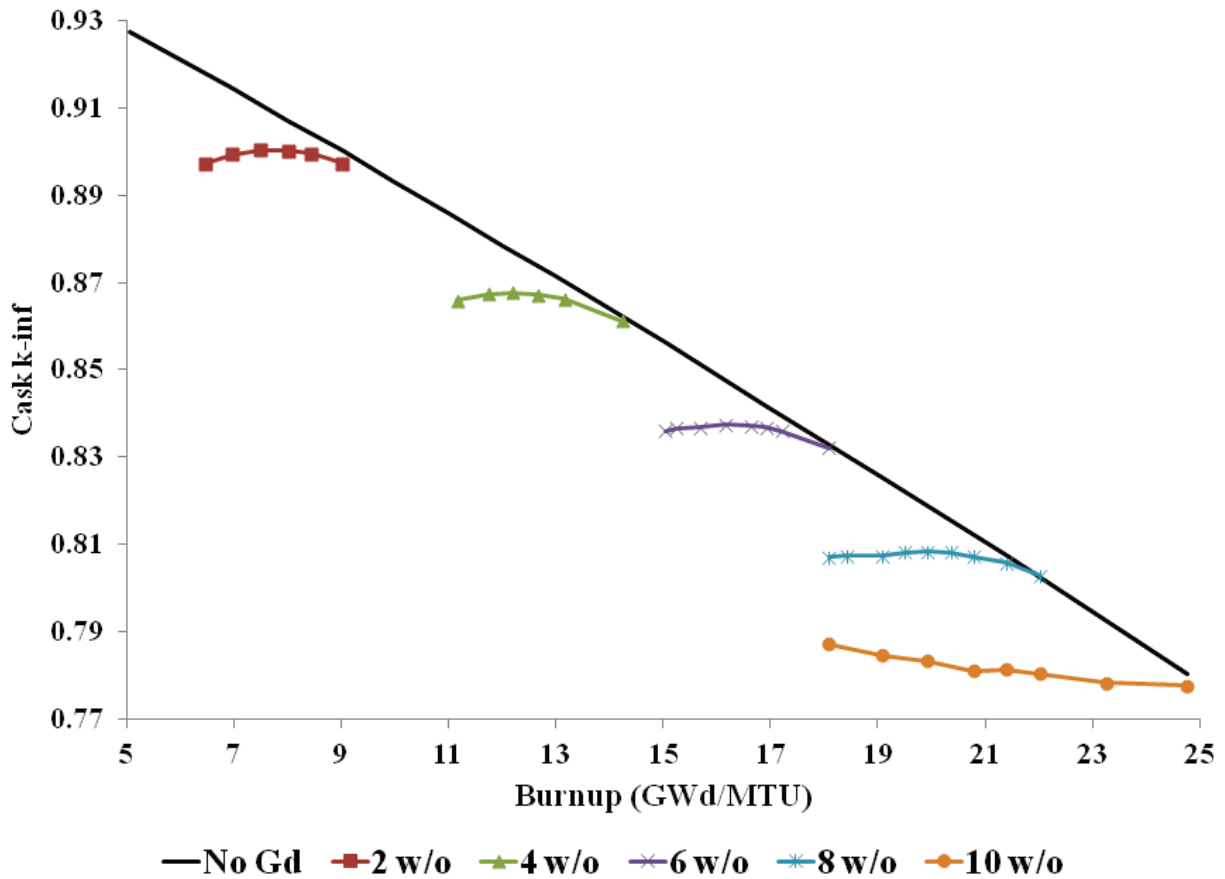


Figure 3.19. Cask k_{inf} as a function of burnup for six gadolinium pins with a range of initial gadolinium loadings, AFP nuclides.

The results of the depletion studies presented in Section 3.4.2.1 and the cask studies presented in this section are consistent and support the same conclusions. It is clear that increasing the gadolinium loading will cause the peak reactivity to be lower and to occur at a higher burnup.

Based on the results presented in this section, the 6×2Gd loading is selected for use in the remainder of the sensitivity studies. The 6×2Gd pattern was selected for use in remaining studies for four primary reasons: (a) it provides a definitive peak in reactivity; (b) the peak reactivity occurs at a burnup that is representative of those seen in SFP use of peak reactivity methods; (c) the peak is at low burnup resulting in a peak that has a large magnitude compared to other higher-gadolinium cases; and (d) six gadolinium pins provide a sufficient number of pins to enable a significant number of patterns for the gadolinium pattern study.

3.4.3 Gadolinium Pattern

In order to study the impact of the gadolinium pin pattern on reactivity, the full and vanished lattice gadolinium patterns were modified from the original 6×2Gd pattern to 14 additional patterns, for a total of 15 patterns. To conserve masses of fuel and poison, only the 4.9 wt% ²³⁵U enriched fuel pins were used as gadolinium-bearing fuel pins, and the gadolinium concentration was held at 2 wt% for all cases. Vanished fuel pin lattice positions were not used for any gadolinium-pin locations so that the vanished and full lattices would have corresponding gadolinium patterns. Lattice and core design experience was used to determine potentially realistic fuel pin patterns; the 15 gadolinium patterns are shown in Appendix B.

The gadolinium patterns shown in Appendix B are fairly typical of BWR designs. In GE14 lattices, there are typically a greater number of gadolinium-bearing pins in the northwest and southeast quadrants of the assemblies due to the orientation of the water rods. The orientation of the water rods cause power peaking in these regions of the assembly, so more poison is needed in these regions. Gadolinium rods are also used in both the northeast and southwest quadrants when a high number of gadolinium pins is required, but moving pins to these regions is unlikely to affect the results of this study. Modern BWR designs contain many gadolinium pins (10 to 18) ranging in gadolinium concentration from 2–9 wt% gadolinium. The cases studied here cover a realistic design space. However, if the gadolinium pattern varies significantly from normal, it could warrant further study. It is possible that credit could be taken for restrictions on gadolinium pin placement enforced by fuel vendors during lattice design, but these rules would likely need to be captured in the safety analysis report.

The cask k_{inf} results for the 15 patterns with the AO nuclide set are shown in Figure 3.20. The sensitivity of the calculated cask k_{inf} is low; the spread from maximum to minimum k_{inf} is less than 0.1% Δk and is largely insensitive to burnup. The individual patterns are virtually indistinguishable because the k_{inf} values are within 2 to 3 standard deviations of each other.

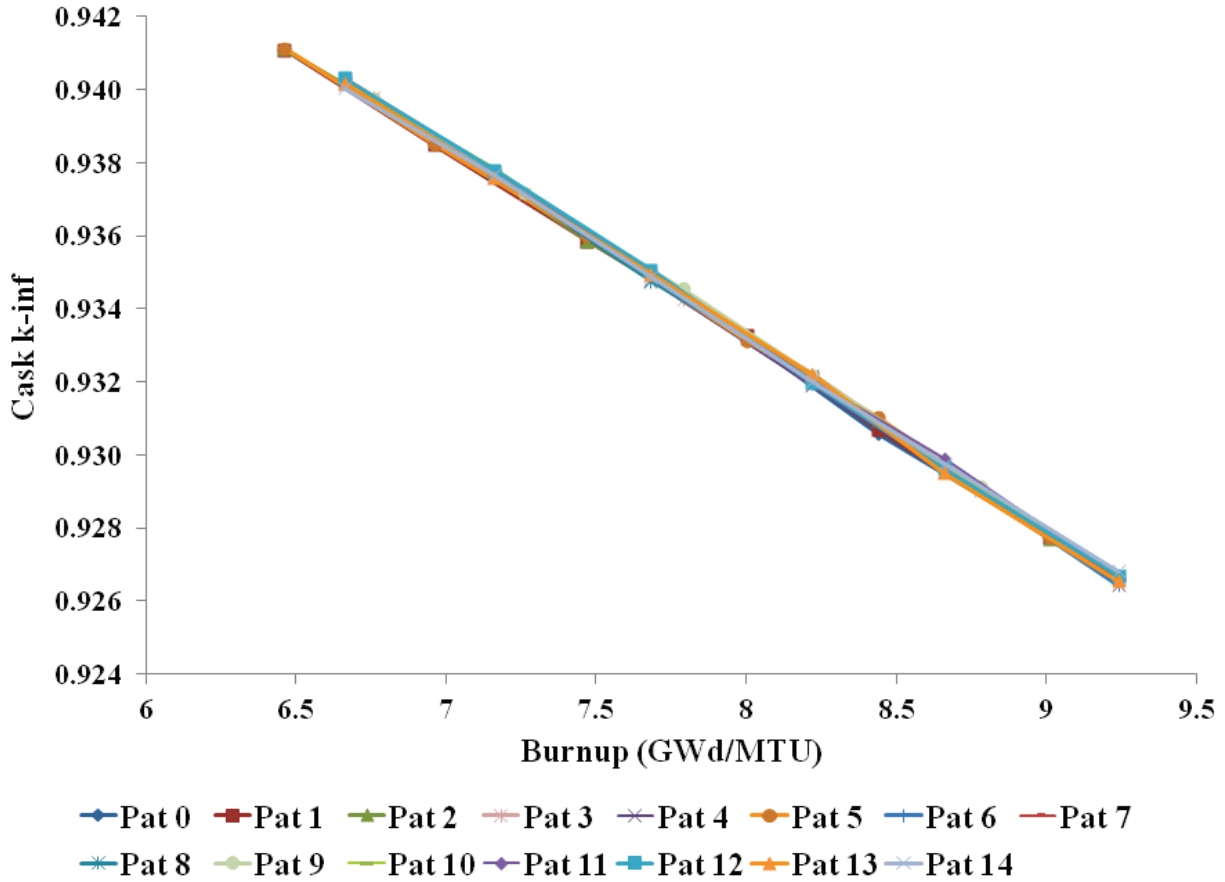


Figure 3.20. Cask k_{inf} as a function of burnup for all 15 patterns, AO nuclide set.

Table 3.11 provides the maximum cask k_{inf} and the pattern from which it results for each burnup, along with the base case (Pattern 0) cask k_{inf} . The base case pattern results in statistically equivalent reactivity with the maximum k_{inf} pattern for most burnups considered, and that the impact of the gadolinium pattern on cask k_{inf} with the AO nuclide set is negligible.

Table 3.11. Cask k_{inf} values for various patterns with the AO nuclide set

Burnup (GWd/MTU)	Max k_{inf}	Limiting Pattern	Pattern 0 k_{inf}	Uncertainty (1 σ)
6.96	0.93879	12	0.93854	0.00010
7.47	0.93609	0	0.93609	0.00010
8.00	0.93331	9	0.93317	0.00010
8.44	0.93103	5	0.93058	0.00010
9.01	0.92804	9	0.92775	0.00010

The cask k_{inf} results for all 15 patterns with the AFP nuclide set are shown in Figure 3.21. The calculated spread from maximum to minimum k_{inf} is about 0.4% Δk near peak reactivity (near 7.5 GWd/MTU) and decreases at higher burnups. At about 6.5 GWd/MTU, the full range is nearly 0.7% Δk , but it drops to only about 0.2% Δk by 9 GWd/MTU. This behavior is plausible since the differences in gadolinium worth are diminishing as the gadolinium burns out in each pattern and the reactivity of all the lattices approaches the no-gadolinium fuel reactivity depletion

trajectory. The peak reactivity occurs for most patterns at around 7.5 GWd/MTU, though for some it occurs at around 8 GWd/MTU.

Patterns 2, 3, 9, and 12 show the highest reactivity peaks near 0.902. This is about 0.2% Δk higher than the base case Pattern 0. These patterns have less residual gadolinium remaining and hence a higher k_{inf} . The gadolinium in Pattern 2 is more depleted because the pins are more spread out than in the base case. Pattern 3 experiences more gadolinium depletion because of the separation of the pins and because two of the pins are near the water tubes with additional thermal flux nearby. Pattern 9 has more depleted gadolinium because five of the gadolinium pins are very near the central water tubes. Pattern 12 has four of the six gadolinium pins near the water tubes, which results in faster gadolinium depletion than the base case.

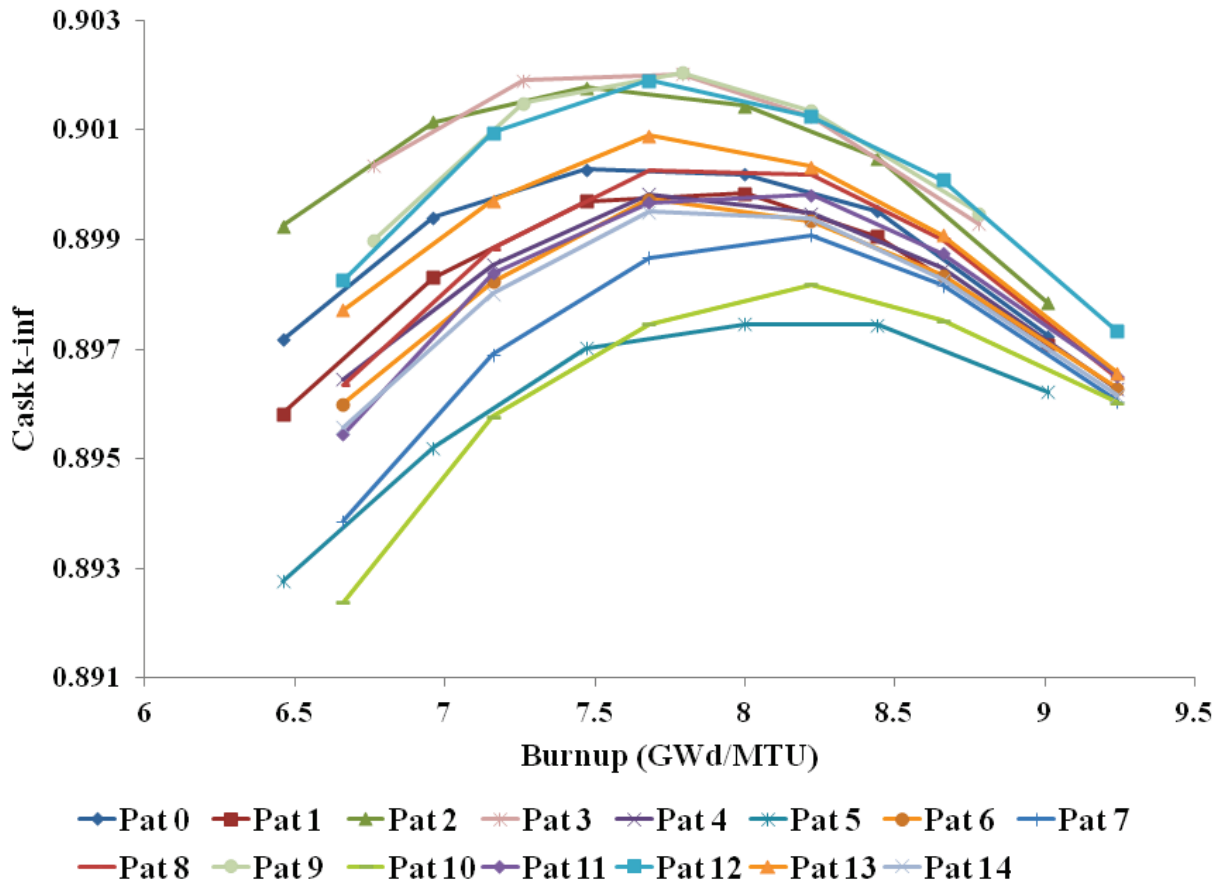


Figure 3.21. Cask k_{inf} as a function of burnup for all 15 patterns, AFP nuclide set.

Conversely, Pattern 10 has low reactivity because it has a large amount of residual gadolinium. Pattern 5 has the lowest peak k_{inf} value, and also has a significantly higher residual gadolinium concentration. The large residual is caused by the relatively close grouping of the pins in the southeast quadrant; the proximity of the pins causes a suppression in the thermal flux near this group of rods, leaving a higher residual gadolinium content. Table 3.12 provides k_{inf} values for Patterns 0, 5, and 3 (representing nominal, low, and high reactivity cases, respectively) for several burnups in the range of interest.

Table 3.12. Cask k_{inf} values for various patterns with the AFP nuclide set

Burnup (GWd/MTU)	Pattern 0		Pattern 5		Burnup (GWd/MTU)	Pattern 3	
	Cask k_{inf}	σ	Cask k_{inf}	σ		Cask k_{inf}	σ
6.46	0.89718	0.00010	0.89276	0.00010	6.26	0.89759	0.00010
6.96	0.89940	0.00010	0.89520	0.00010	6.76	0.90035	0.00010
7.47	0.90028	0.00010	0.89702	0.00010	7.26	0.90191	0.00010
8.00	0.90019	0.00010	0.89746	0.00010	7.79	0.90203	0.00010
8.44	0.89953	0.00010	0.89745	0.00010	8.22	0.90125	0.00010
9.01	0.89724	0.00010	0.89622	0.00010	8.78	0.89929	0.00010

The most reactive patterns—2, 3, and 9—are shown in Figures 3.22, 3.23, and 3.24, respectively. The least reactive Pattern 5 is shown in Figure 3.25.

The results indicate that the reactivity of the base case pattern is near the middle of the field of cask reactivities resulting from a 6×2Gd loading, and it is used for the remaining studies in this report. The gadolinium pattern has a more significant effect on cask reactivity for the AFP nuclide set than it does for the AO set, but the magnitude of the effect is still small, at approximately ±0.25% Δk of Pattern 0 k_{inf} value. This conclusion is limited to the number of pins and gadolinium loadings in this study.

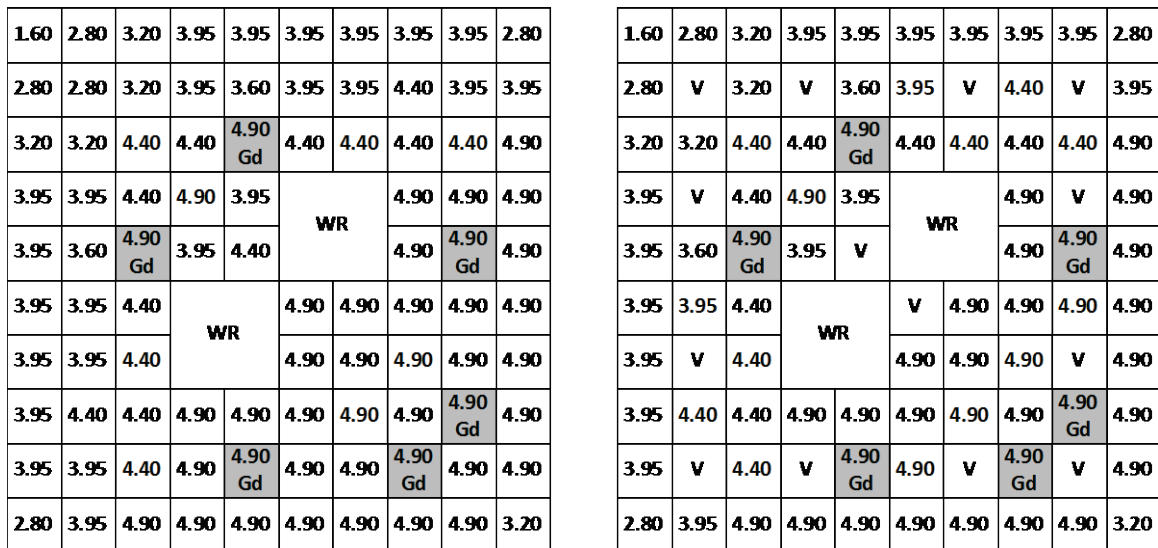


Figure 3.22. Gadolinium patterns 2 (P2).

1.60	2.80	3.20	3.95	3.95	3.95	3.95	3.95	3.95	2.80
2.80	2.80	3.20	3.95	3.60	3.95	3.95	4.40	3.95	3.95
3.20	3.20	4.40	4.40	4.90 Gd	4.40	4.40	4.40	4.40	4.90
3.95	3.95	4.40	4.90	3.95	WR		4.90	4.90	4.90
3.95	3.60	4.90 Gd	3.95	4.40	WR		4.90 Gd	4.90	4.90
3.95	3.95	4.40	WR		4.90	4.90	4.90	4.90	4.90
3.95	3.95	4.40	WR		4.90	4.90	4.90	4.90	4.90
3.95	4.40	4.40	4.90	4.90 Gd	4.90	4.90	4.90	4.90 Gd	4.90
3.95	3.95	4.40	4.90	4.90	4.90	4.90	4.90 Gd	4.90	4.90
2.80	3.95	4.90	4.90	4.90	4.90	4.90	4.90	4.90	3.20

1.60	2.80	3.20	3.95	3.95	3.95	3.95	3.95	3.95	2.80
2.80	V	3.20	V	3.60	3.95	V	4.40	V	3.95
3.20	3.20	4.40	4.40	4.90 Gd	4.40	4.40	4.40	4.40	4.90
3.95	V	4.40	4.90	3.95	WR		4.90	V	4.90
3.95	3.60	4.90 Gd	3.95	V	WR		4.90 Gd	4.90	4.90
3.95	3.95	4.40	WR		V	4.90	4.90	4.90	4.90
3.95	V	4.40	WR		4.90	4.90	4.90	V	4.90
3.95	4.40	4.40	4.90	4.90 Gd	4.90	4.90	4.90	4.90 Gd	4.90
3.95	V	4.40	V	4.90	4.90	V	4.90 Gd	V	4.90
2.80	3.95	4.90	4.90	4.90	4.90	4.90	4.90	4.90	3.20

Figure 3.23. Gadolinium patterns 3 (P3).

1.60	2.80	3.20	3.95	3.95	3.95	3.95	3.95	3.95	2.80
2.80	2.80	3.20	3.95	3.60	3.95	3.95	4.40	3.95	3.95
3.20	3.20	4.40	4.40	4.90	4.40	4.40	4.40	4.40	4.90
3.95	3.95	4.40	4.90 Gd	3.95	WR		4.90 Gd	4.90	4.90
3.95	3.60	4.90	3.95	4.40	WR		4.90	4.90	4.90
3.95	3.95	4.40	WR		4.90	4.90 Gd	4.90	4.90	4.90
3.95	3.95	4.40	WR		4.90 Gd	4.90	4.90	4.90	4.90
3.95	4.40	4.40	4.90 Gd	4.90	4.90	4.90	4.90 Gd	4.90	4.90
3.95	3.95	4.40	4.90	4.90	4.90	4.90	4.90	4.90	4.90
2.80	3.95	4.90	4.90	4.90	4.90	4.90	4.90	4.90	3.20

1.60	2.80	3.20	3.95	3.95	3.95	3.95	3.95	3.95	2.80
2.80	V	3.20	V	3.60	3.95	V	4.40	V	3.95
3.20	3.20	4.40	4.40	4.90	4.40	4.40	4.40	4.40	4.90
3.95	V	4.40	4.90 Gd	3.95	WR		4.90 Gd	V	4.90
3.95	3.60	4.90	3.95	V	WR		4.90	4.90	4.90
3.95	3.95	4.40	WR		V	4.90 Gd	4.90	4.90	4.90
3.95	V	4.40	WR		4.90 Gd	4.90	4.90	V	4.90
3.95	4.40	4.40	4.90 Gd	4.90	4.90	4.90	4.90 Gd	4.90	4.90
3.95	V	4.40	V	4.90	4.90	V	4.90	V	4.90
2.80	3.95	4.90	4.90	4.90	4.90	4.90	4.90	4.90	3.20

Figure 3.24. Gadolinium patterns 9 (P9).

1.60	2.80	3.20	3.95	3.95	3.95	3.95	3.95	3.95	2.80
2.80	2.80	3.20	3.95	3.60	3.95	3.95	4.40	3.95	3.95
3.20	3.20	4.40	4.40	4.90	4.40	4.40	4.40	4.40	4.90
3.95	3.95	4.40	4.90 Gd	3.95	WR		4.90	4.90	4.90
3.95	3.60	4.90	3.95	4.40	WR		4.90	4.90	4.90
3.95	3.95	4.40	WR		4.90	4.90	4.90	4.90 Gd	4.90
3.95	3.95	4.40	WR		4.90	4.90 Gd	4.90	4.90	4.90
3.95	4.40	4.40	4.90	4.90	4.90	4.90	4.90	4.90 Gd	4.90
3.95	3.95	4.40	4.90	4.90	4.90 Gd	4.90	4.90	4.90	4.90
2.80	3.95	4.90	4.90	4.90	4.90	4.90	4.90	4.90	3.20

1.60	2.80	3.20	3.95	3.95	3.95	3.95	3.95	3.95	2.80
2.80	V	3.20	V	3.60	3.95	V	4.40	V	3.95
3.20	3.20	4.40	4.40	4.90	4.40	4.40	4.40	4.40	4.90
3.95	V	4.40	4.90 Gd	3.95	WR		4.90	V	4.90
3.95	3.60	4.90	3.95	V	WR		4.90	4.90	4.90
3.95	3.95	4.40	WR		V	4.90	4.90	4.90 Gd	4.90
3.95	V	4.40	WR		4.90	4.90 Gd	4.90	V	4.90
3.95	4.40	4.40	4.90	4.90	4.90	4.90	4.90	4.90 Gd	4.90
3.95	V	4.40	V	4.90	4.90 Gd	V	4.90 Gd	V	4.90
2.80	3.95	4.90	4.90	4.90	4.90	4.90	4.90	4.90	3.20

Figure 3.25. Gadolinium patterns 5 (P5).

3.4.4 Void Fraction

BWR cores contain a range of coolant void fractions, from near zero at the core inlet to nearly 80% at the core exit in some cases. Higher exit void fractions may be experienced in some cores, but the range of void fractions studied here is broad enough to identify reactivity trends as a function of void fraction for this study. The range of void fractions would need to be studied by the license applicant to determine the impact it has on fuel reactivity, as the most reactive 2D slice must be considered in peak reactivity methods. An appropriate void fraction value would need to be selected and defended as part of the analysis. A series of depletion calculations was performed for five discrete void fractions using the base case 6×2Gd lattice ranging from 0 to 80%, and the depleted compositions were used in the cask model with differing nuclide sets and the AEAI strategy. Note that the cask model is flooded with full density water in all cases; the effect being studied here is the moderator density during depletion.

The results for the AO nuclide set at each of the five void fractions are shown in Figure 3.26 for a range of burnups. The burnups selected surround the peak reactivity in the cask model with the AFP nuclide set. It is clear from the figure that the reactivity of the cask is monotonically increasing with higher void fractions. This is a result of the hardening neutron spectrum at increasing void fractions. The harder spectrum causes additional ²³⁹Pu generation, which is a significant contributor to reactivity even at these relatively low burnups.

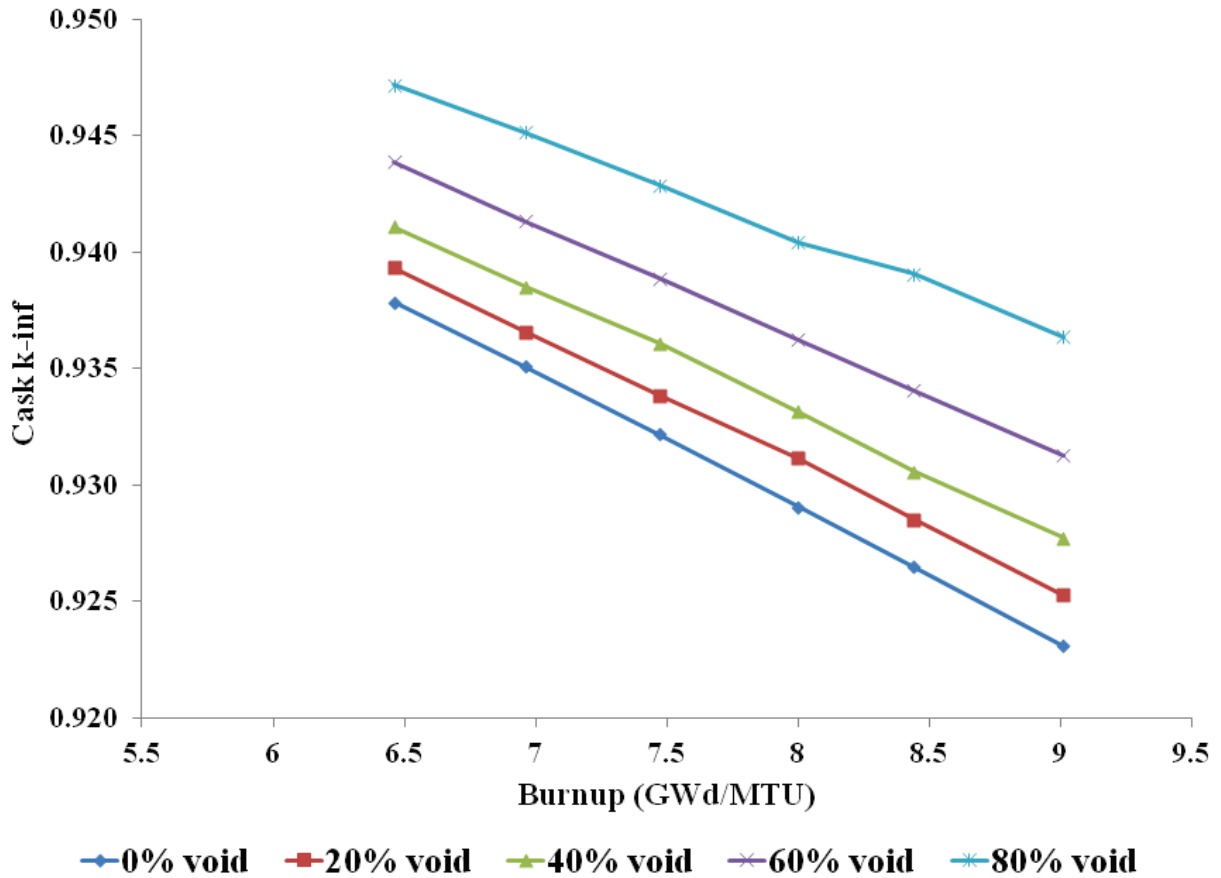


Figure 3.26. Cask k_{inf} as a function of burnup for several depletion moderator void fractions, AO nuclide set.

The ^{239}Pu number densities for fuel rods in the central portion of the assembly for these calculations are shown in Figure 3.27, and they clearly demonstrate the results of the spectral hardening effect of higher void fractions. The overall reactivity change from 0% to 80% void is greater than 1% Δk at about 7.5 GWd/MTU; this is a significant impact that must be properly accounted for during depletion calculations for AO BUC.

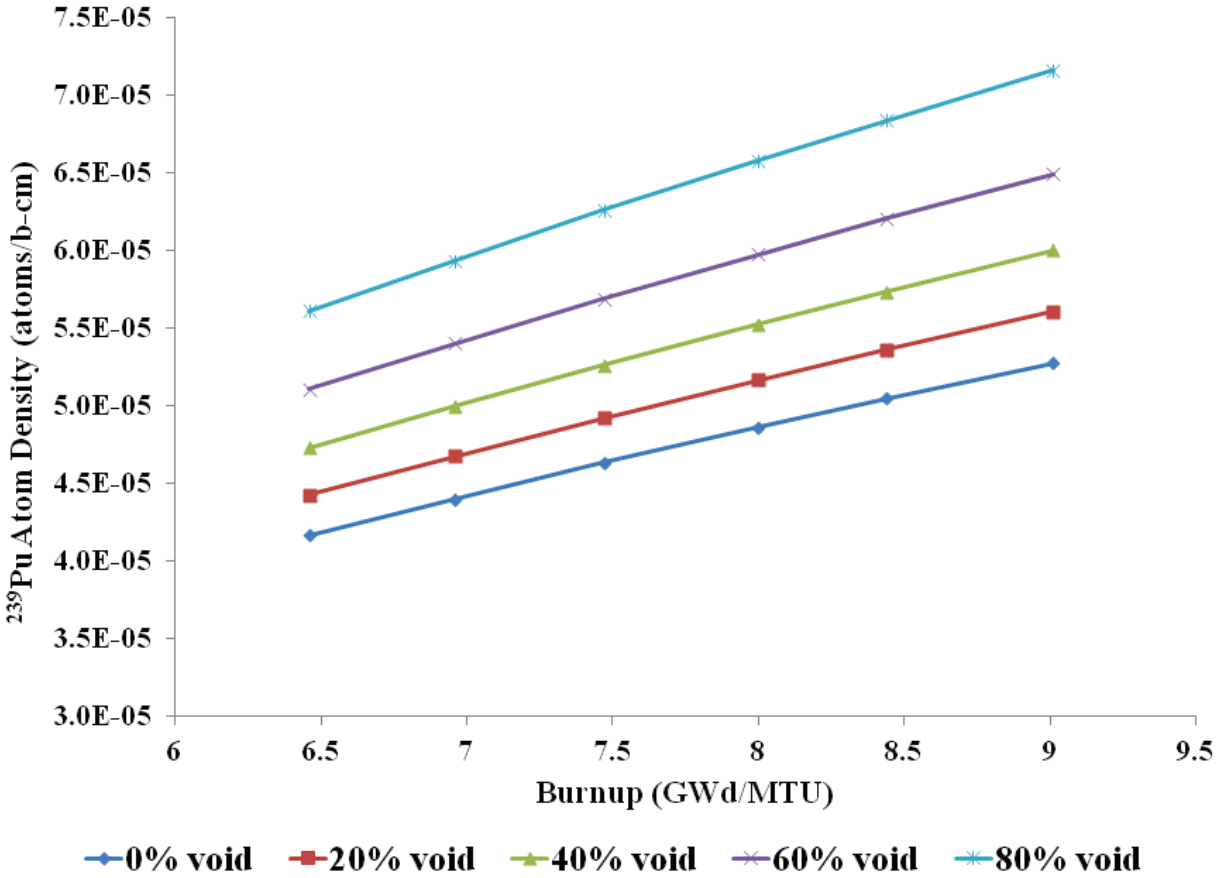


Figure 3.27. ^{239}Pu atom density as a function of burnup for several depletion moderator void fractions.

Results for the AFP nuclide set at each of the five void fractions are shown in Figure 3.28 for a range of burnups. The results are completely reversed in this case. The driving effect for the AFP nuclides is the amount of residual gadolinium, which is decreased by a more thermal spectrum because of the larger thermal absorption cross section for gadolinium (see Figure 3.14). The accelerated absorber depletion caused by the more thermal spectrum causes the assembly to reach peak reactivity at lower burnups, and thus at higher k_{inf} values. As the void fraction increases, the gadolinium depletion is slower, causing a reduction in the reactivity peak and a shift to higher burnups. This is a key manifestation of the peak reactivity phenomenon.

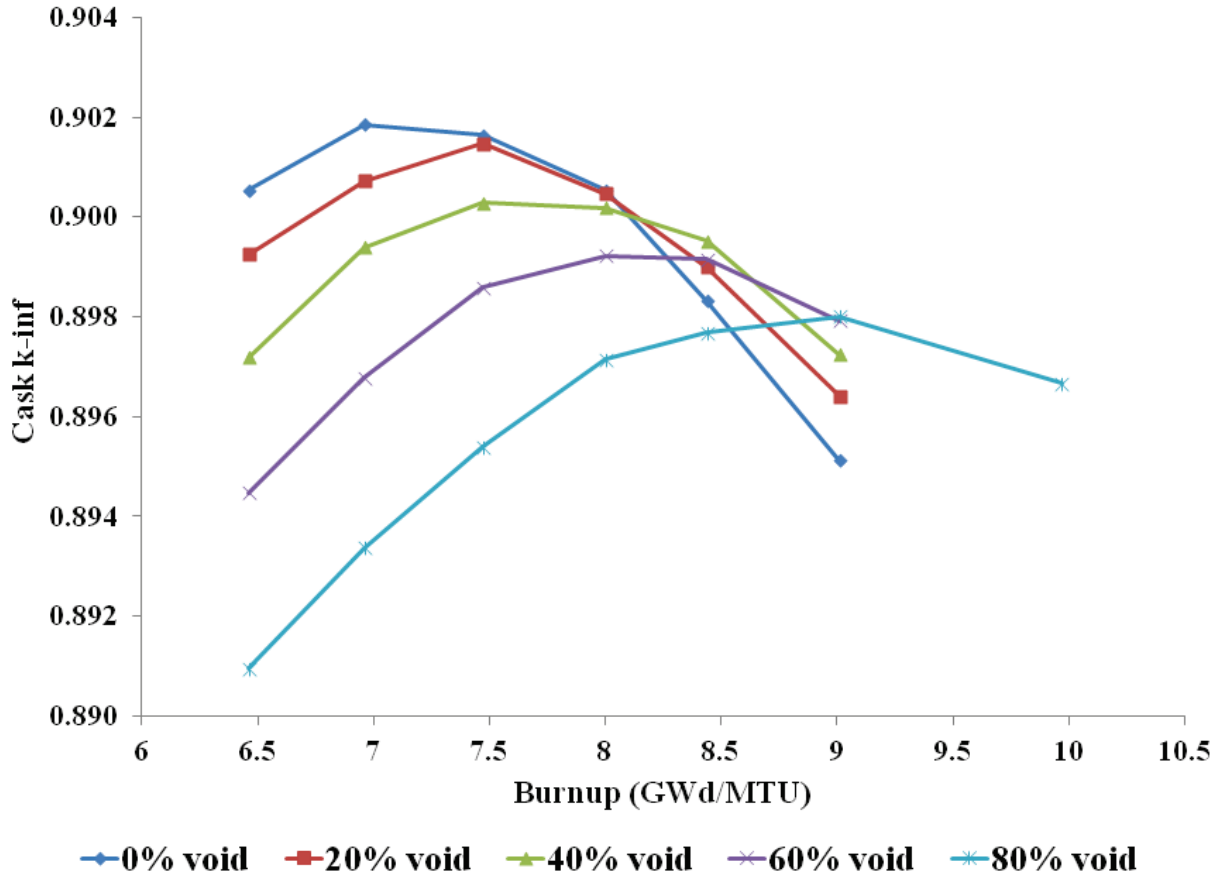


Figure 3.28. Cask k_{inf} as a function of burnup for several depletion moderator void fractions, AFP nuclide set.

The volume-average ^{155}Gd number density in the gadolinium pins is shown in Figure 3.29, demonstrating the impact of the void fraction on residual gadolinium concentration. The results also show that the residual gadolinium effect is stronger than the ^{239}Pu effect, which is the primary driver for the AO nuclide set. The peak reactivity of the cask drops by about 0.4% Δk from the 0% void fraction case to the 80% void fraction case. This is equivalent to about a $\pm 0.2\%$ Δk effect relative to the base case with a 40% void fraction. Clearly, the low void fraction case is bounding for the AFP nuclide set.

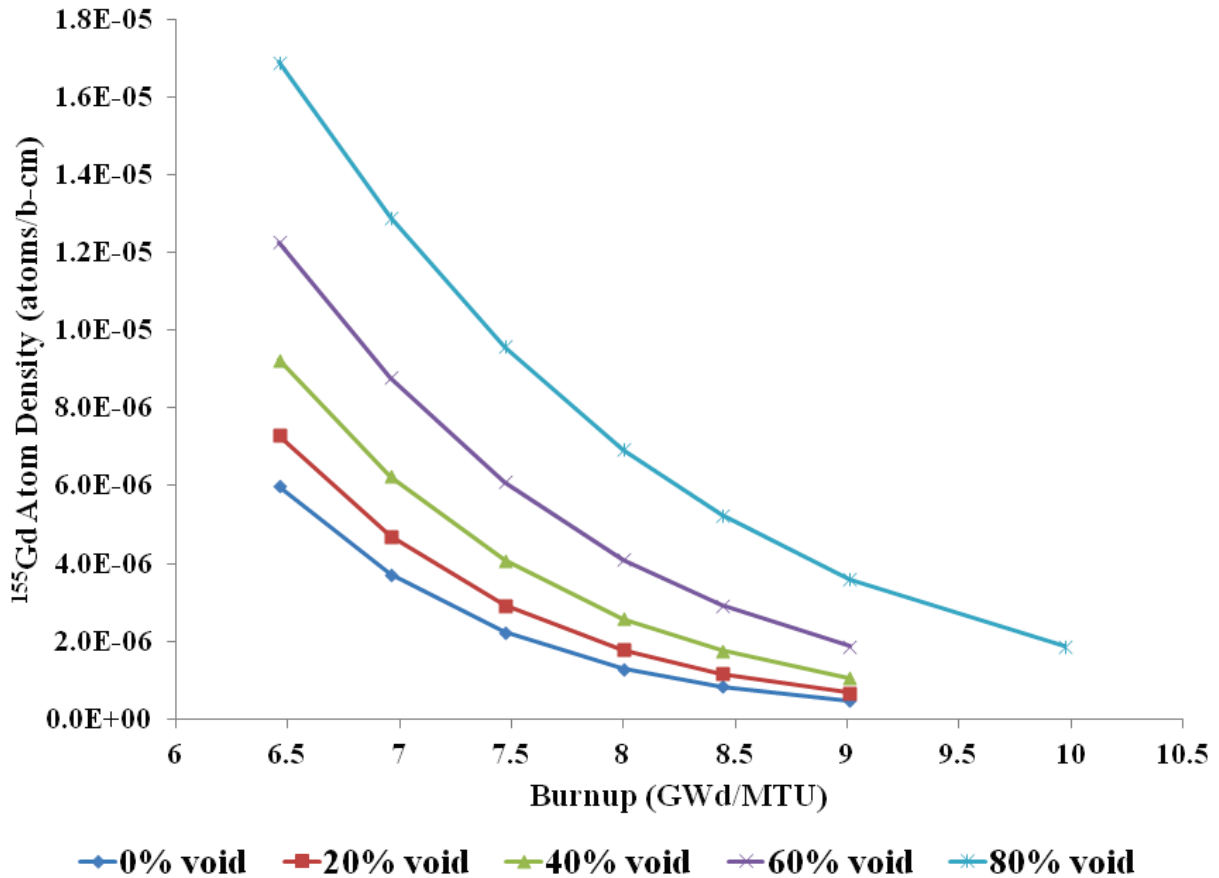


Figure 3.29. ^{155}Gd atom density as a function of burnup for several depletion moderator void fractions.

3.4.5 Control Blade Insertion

BWR cores operate with some control blades, or rods, inserted (“rodded”) to control reactivity and power distributions. The control blades are inserted in the gaps between fuel assemblies; each assembly has two faces toward a blade and two faces away from a blade inserted between adjacent assemblies. The control blade can be seen in Figure 3.4, along the north and west faces of the assembly. The absorber in most BWR control blades is boron carbide (B_4C), which has a strong thermal absorption cross section. Some control blades contain hafnium, which has similar control properties. Depletion under the rodded condition hardens the flux spectrum due to the absorption of thermal neutrons and induces radial burnup variation in both fuel and gadolinium pins that will likely influence discharged assembly reactivity. The presence of the control blade also hardens the neutron spectrum by displacing water in the control blade gap. A series of depletion calculations was performed with the control blade inserted for the full depletion for the same five discrete void fractions used in Section 3.4.4. The depleted compositions were used in the cask model with differing nuclide sets and the AEAI strategy. In all cases, the KENO model is flooded with full density water at room temperature (293 K). The effect being studied is the control blade insertion during depletion; this study will also determine if the impact of control blade insertion varies as a function of moderator void fraction in the depletion model.

The rodded depletion results for the AO nuclide set at each of the five void fractions are shown in Figure 3.30 for a range of burnups. The burnups selected surround the peak reactivity in the cask model with the AFP nuclide set. It is clear from the figure that the reactivity of the cask is monotonically increasing with higher void fractions. Comparison with the unrodded depletion results presented in Figure 3.26 shows that the presence of the control blade during depletion increases cask k_{inf} up to 1% Δk . These results are driven by the hardening neutron spectrum at increasing void fractions and a significant spectral shift caused by the presence of the control blade during depletion. The harder spectrum causes additional ^{239}Pu generation, which is a significant contributor to reactivity even at these relatively low burnups. The control blade effect on cask k_{inf} is similar in magnitude to the reactivity increase caused by changing void fraction from 0% to 80% in the unrodded case.

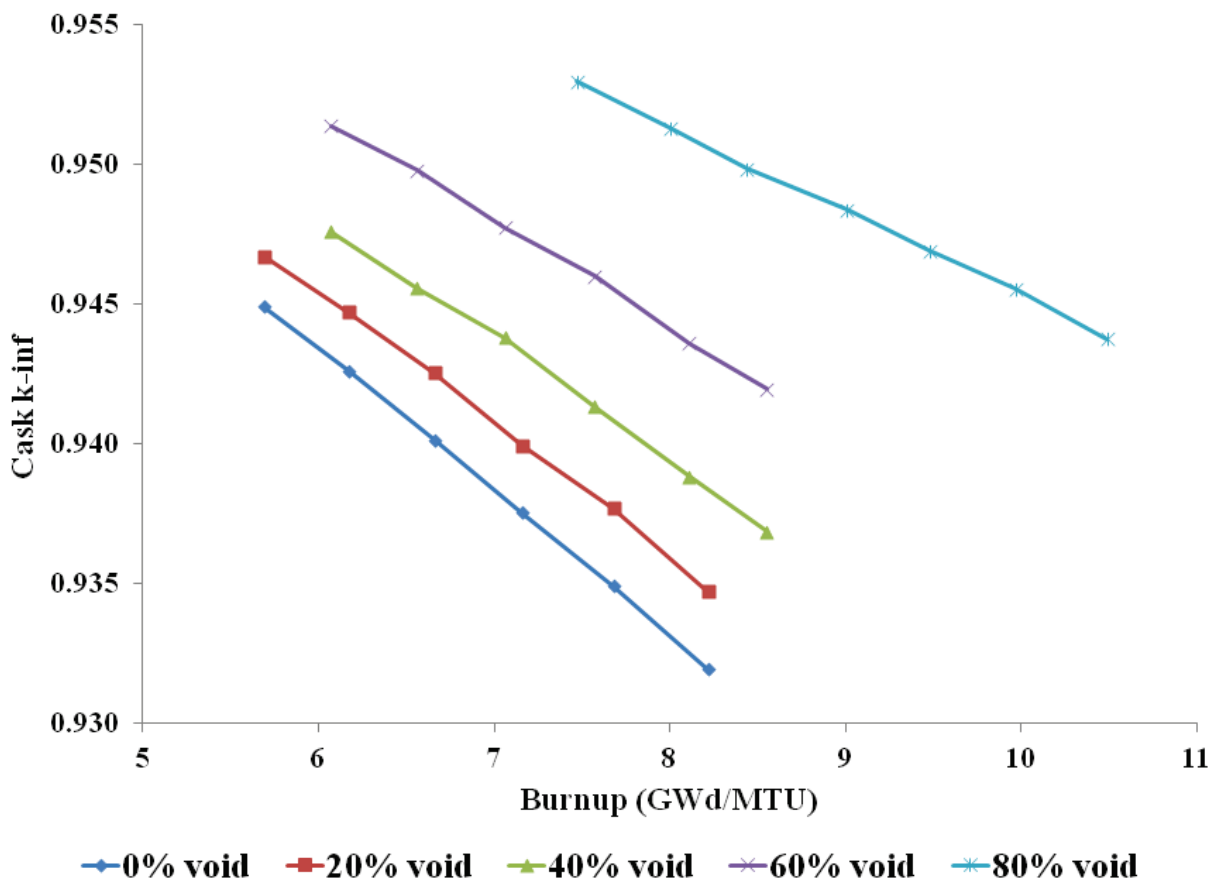


Figure 3.30. Cask k_{inf} as a function of burnup for several depletion moderator void fractions and rodded depletion, AO nuclide set.

The ^{239}Pu number densities for fuel rods in the central portion of the assembly for these calculations are shown in Figure 3.31, clearly demonstrating the results of the spectral hardening effect of higher void fractions and, by comparison with Figure 3.27, control blade insertion.

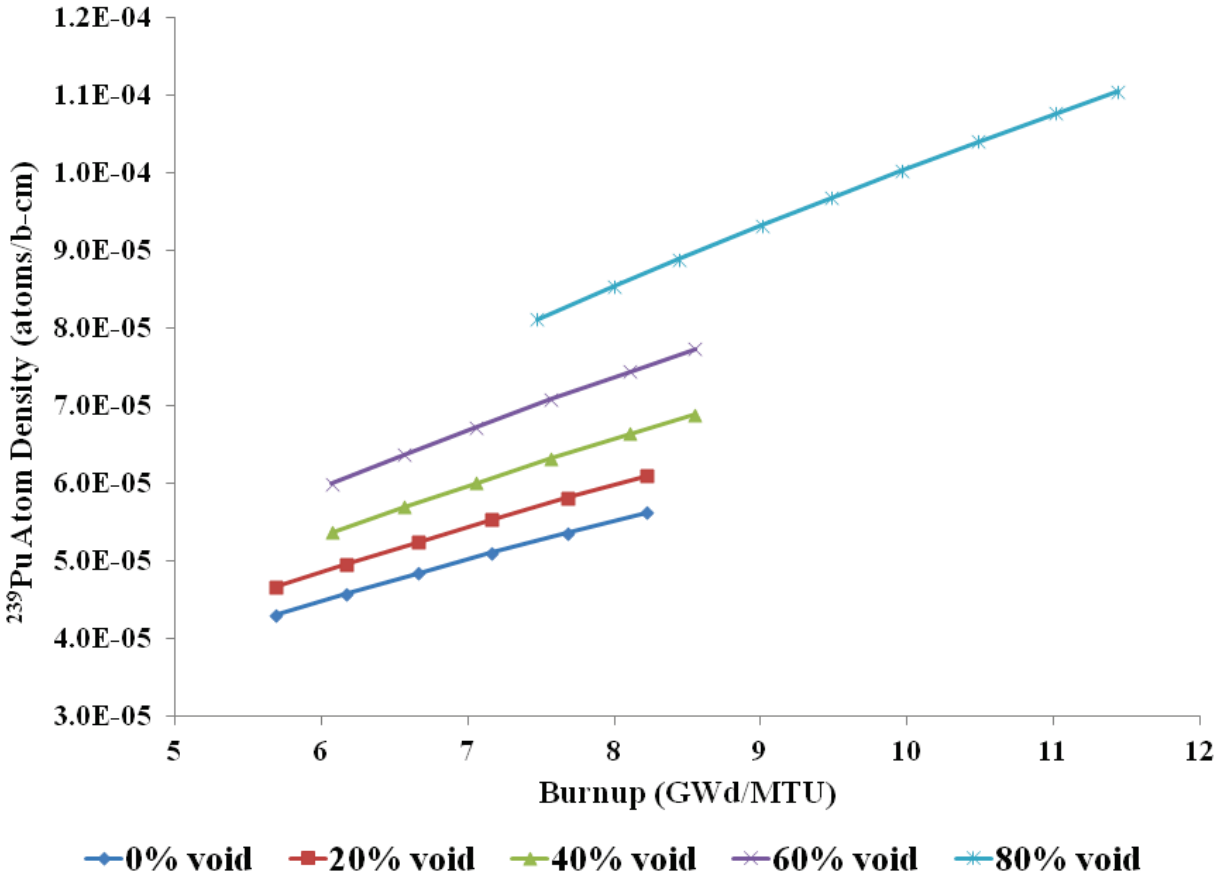


Figure 3.31. ²³⁹Pu atom density as a function of burnup for several depletion moderator void fractions, rodded depletion.

As with the unrodded depletions, the sensitivity to void fraction increases with higher void fractions. The reactivity increase caused by control blade insertion is larger at higher void fractions. The results for the AFP nuclide set at each of the five void fractions are shown in Figure 3.32 for a range of burnups.

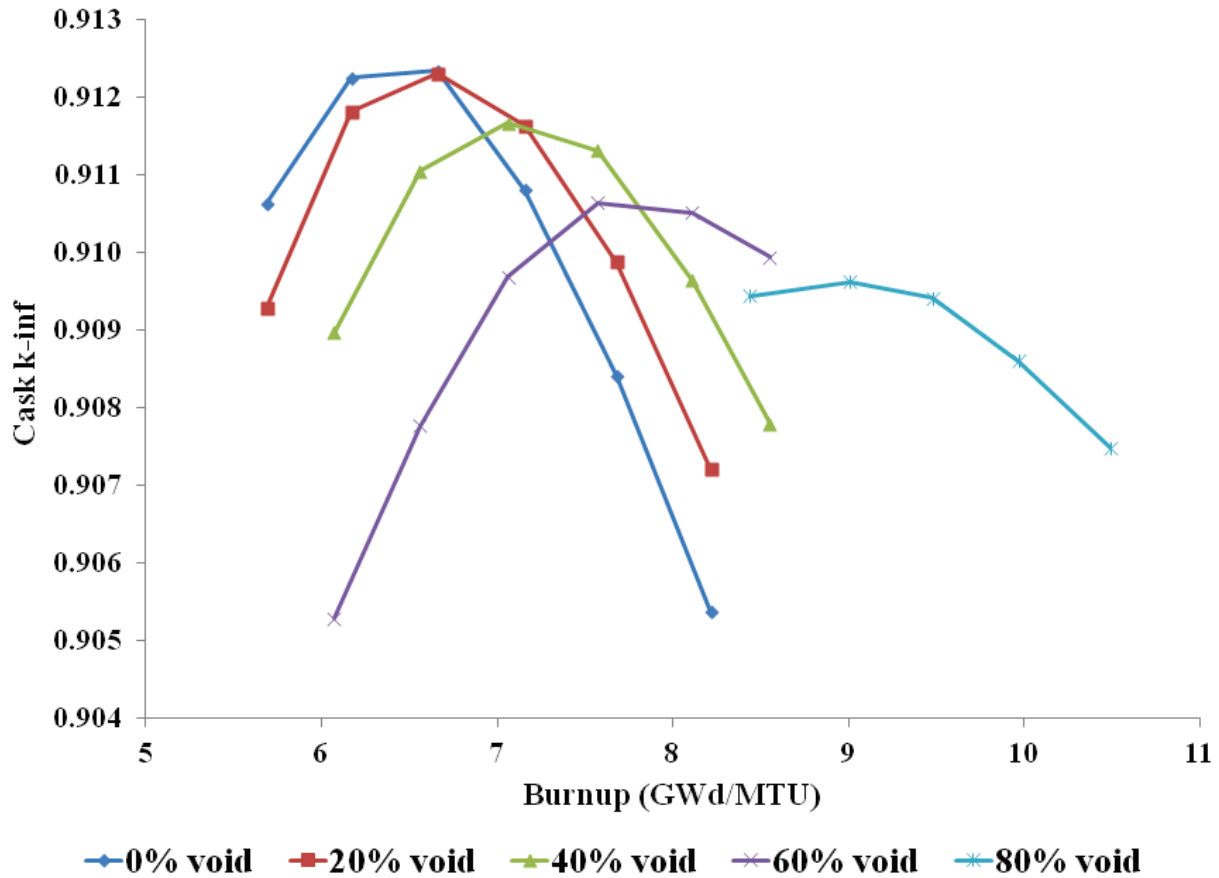


Figure 3.32. Cask k_{inf} as a function of burnup for several depletion moderator void fractions, rodded depletion, AFP nuclide set.

As with the unrodded results, the impact of void fraction is completely reversed compared to the AO nuclide set with highest reactivity for no void or low void (20%) cases. A comparison of the results for the unrodded and rodded cases, shown in Figure 3.33, indicates that control blade insertion results in a significant increase in cask k_{inf} , by approximately 1% Δk . The reactivity peak occurs at lower burnups for smaller void fractions but at higher burnup for 80% void fraction.

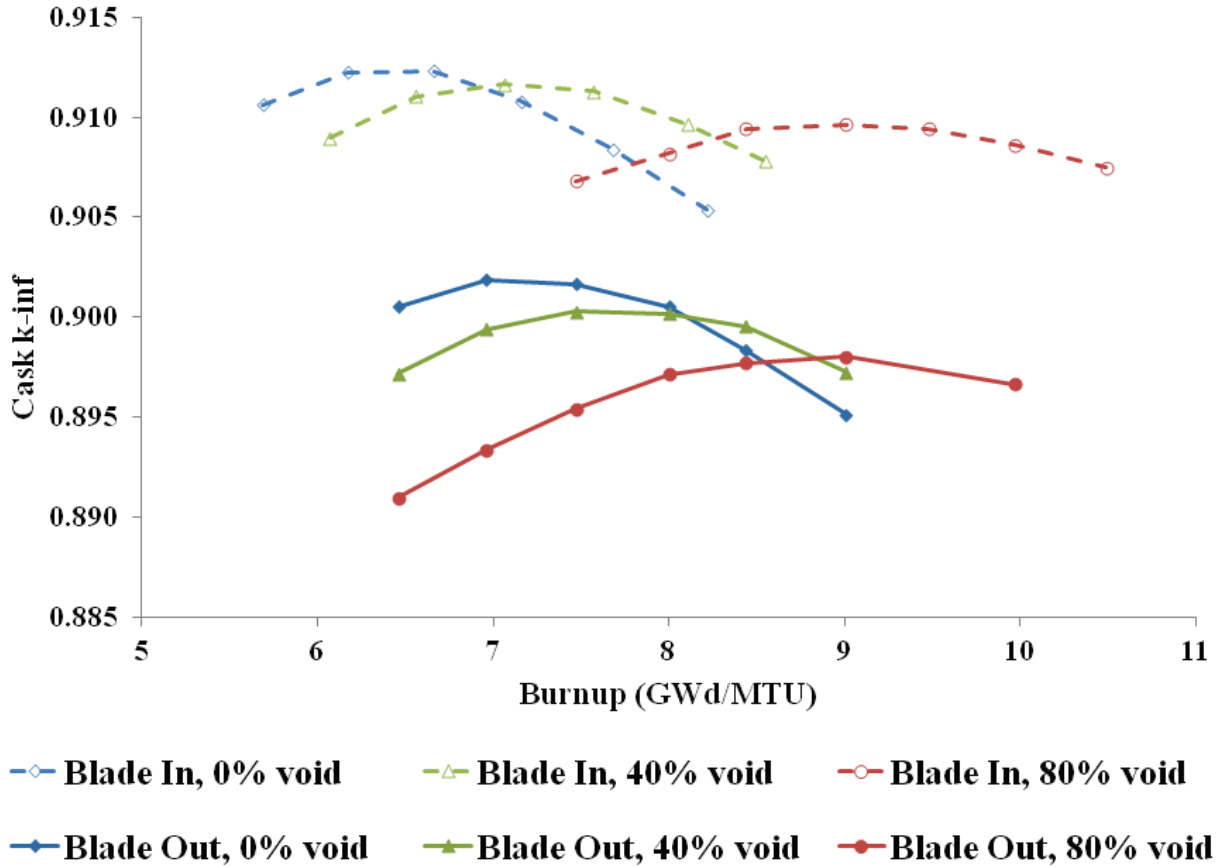


Figure 3.33. Cask k_{inf} as a function of burnup for several depletion moderator void fractions and the AFP nuclide set, comparing rodded and unrodded depletion.

An important phenomenon in these cases is the impact of the control blade insertion on the depletion of the gadolinium rods. The gadolinium pattern used is shown in Figure 3.11 and contains four pins in the southeast quadrant of the assembly and two pins in the northwest quadrant. The presence of the control blade in the northwest corner of the lattice suppresses power on that half of the assembly, thus increasing the power and flux in the southeast half. The increased power and flux causes more depletion locally in the southeast quadrant. Figure 3.34 shows the percent change in the pin-wise ^{235}U number densities in the depleted fuel (10.1 GWd/MTU) from the rodded depletion to the unrodded depletion. In the 3D plot on the left, the height and color of the bar correspond to the percentage differences. The legend on the right applies to both the 3D and 2D plots. Positive values indicate larger number densities following rodded depletion.

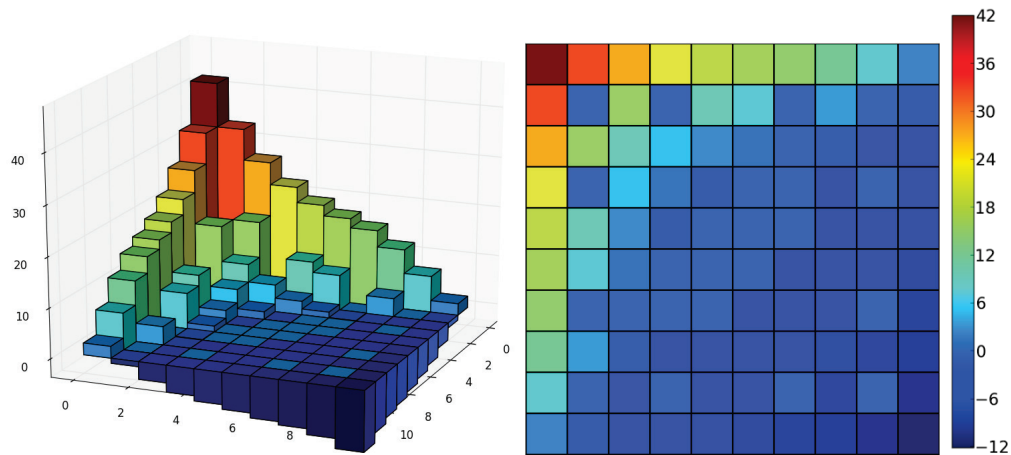


Figure 3.34. ^{235}U concentration difference (in percent) between rodded and unrodded cases.

Figure 3.35 shows the same information for ^{155}Gd ; the large bars show the difference in residual gadolinium in the absorber rods and the fission product gadolinium in all fuel rods. The figure clearly illustrates the higher depletion of the gadolinium in the southeast quadrant of the assembly away from the control blade. The pin-wise isotopics were not used in the cask model, but are used to illustrate the radial burnup shift and its impact on average uranium and residual gadolinium concentrations. In the 3D plot on the left, the height and color of the bar correspond to the percent differences. The legend on the right applies to both the 3D and 2D plots. Positive values indicate larger number densities following rodded depletion.

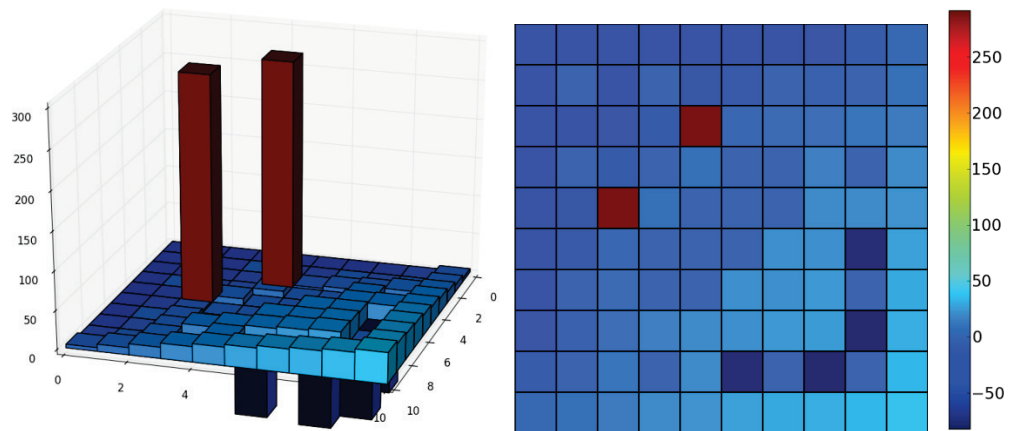


Figure 3.35. ^{155}Gd concentration difference (in percent) between rodded and unrodded cases.

The volume averaged ^{155}Gd concentration for the rodded cases is shown in Figure 3.36, and a comparison between the rodded and unrodded cases is shown for the 0% and 80% void fractions in Figure 3.37.

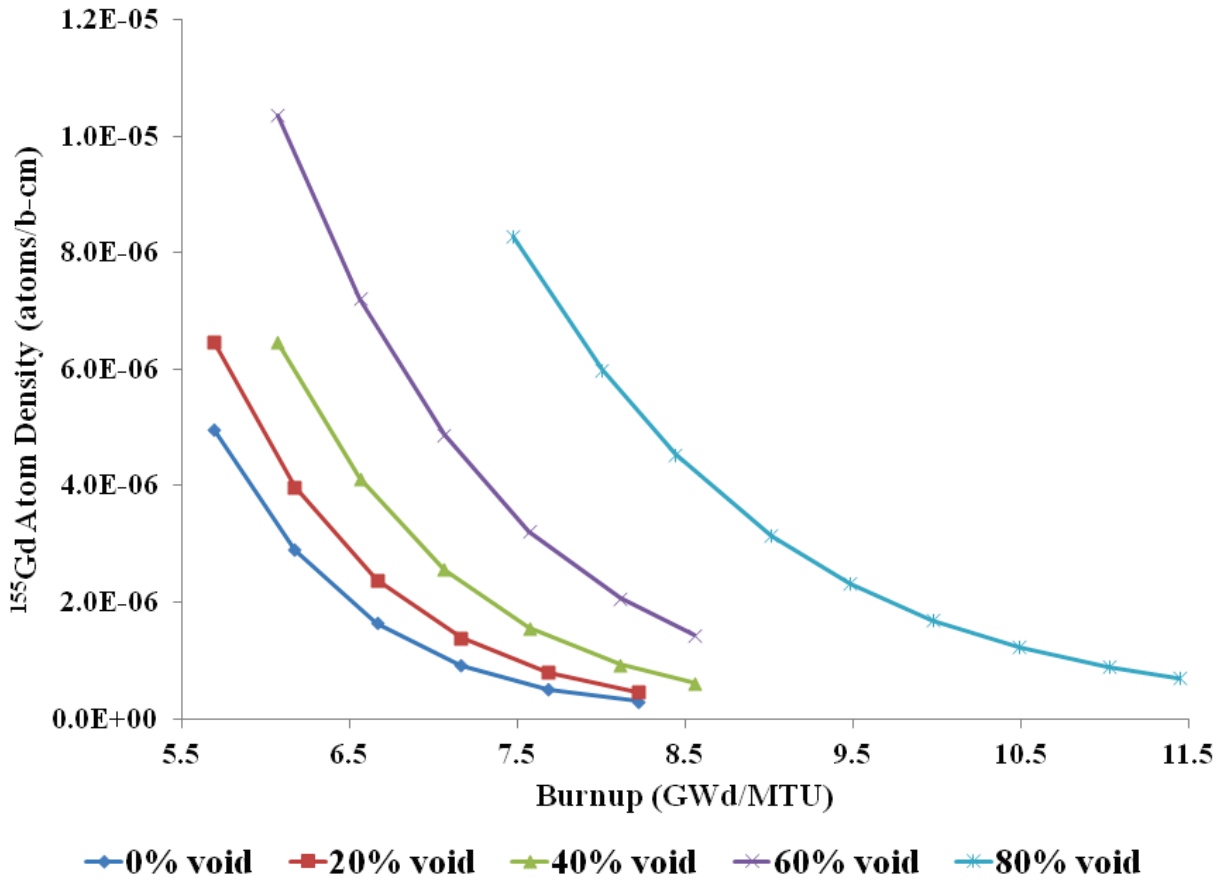


Figure 3.36. ^{155}Gd atom density as a function of burnup for several depletion moderator void fractions and rodded depletion.

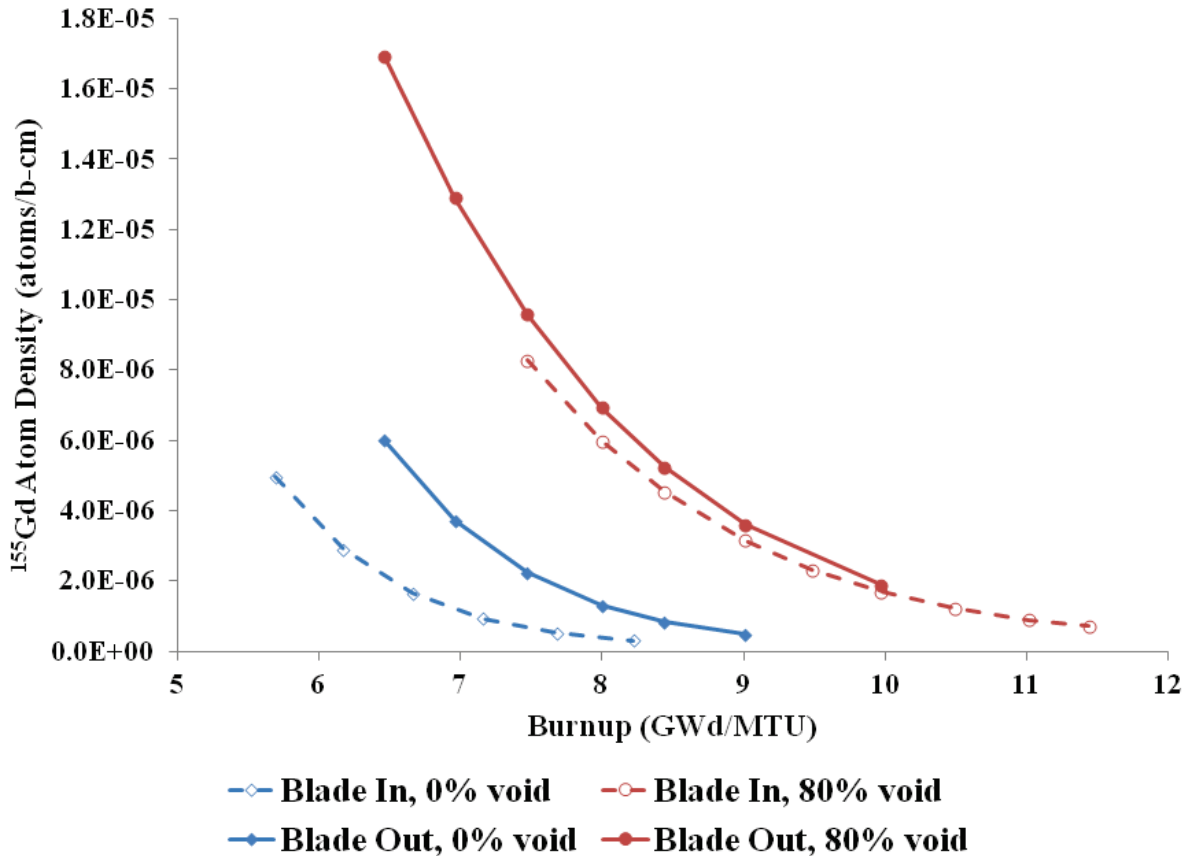


Figure 3.37. ^{155}Gd atom density over a range of burnup for rodded and unrodded depletion with 0% and 80% void.

These results indicate that the effect of control blade insertion is potentially dependent on the gadolinium pattern. If the majority of the gadolinium rods were on the rodded side of the assembly, the average residual gadolinium poison in the assembly would increase. Patterns that contain many gadolinium pins on the rodded side of the assembly are unlikely for assemblies designed for power operations since radial enrichment zoning is generally used to lower reactivity on the rodded side of the assembly and less gadolinium is therefore needed to control power peaking in these regions. Such patterns are certainly possible in criticality safety analysis, however, as the patterns developed by criticality safety analysts are not intended to meet power peaking limits, but rather are intended to maximize reactivity.

In summary, control blade insertion during depletion increases reactivity of discharged fuel for both the AO and the AFP nuclide sets with the gadolinium pattern used in this study. The AO rodded results increase with higher void fraction, while AFP rodded results increase with lower void fraction. It is conservative to model gadolinium pins on the opposite side of the assembly from the control blade, as this will deplete them faster. The maximum reactivity for discharged fuel occurs for AFP rodded depletion with zero and 20% void fractions during depletion. The presence of the control blade during depletion increases cask k_{inf} by approximately 1% Δk for the AFP cases using the 6x2 gadolinium pattern.

3.4.6 Operating Parameters

The reactor operating parameters influence the depleted fuel compositions and thus the discharged fuel reactivity. This section presents sensitivity studies investigating the impact of fuel temperature, specific power, and operating history on cask k_{inf} values. No studies are performed relating to moderator temperature as the core operates at the saturation temperature. Any change in power or coolant flow would result in void fraction changes, which were studied in Section 3.4.4.

The operating parameters were studied by performing a matrix of calculations as shown in Table 3.13. All depletion calculations were performed unrodded with the 6×2 gadolinium pattern shown in Figure 3.11, and all cask calculations used the AEAI modeling strategy. Three fuel temperatures, three specific powers, and four operating histories were used. The following sections present results for each of the operating parameters investigated. Although all 36 combinations of operating conditions were considered, not all of the results are presented, as the trends are similar across the range investigated.

Table 3.13. Fuel temperatures, specific powers, and operating histories

Fuel Temperatures (K)	Specific Powers (W/g)	Operating Histories
850	25	100% power
950	35	50% power
1100	45	100% power (5 GWd/MTU), 50% power (5 GWd/MTU), 100% power
		100% power (3 GWd/MTU), 75% power (3 GWd/MTU), 50% power (4 GWd/MTU), 100% power

3.4.6.1 Fuel Temperature

The models used in all the studies presented in sections 3.4.1 through 3.4.5 of this report have assumed a fuel temperature of 950 K. This fuel temperature was used because it is typical of BWR fuel at hot full power (HFP) conditions; it was not chosen to be a bounding value. The sensitivity of cask k_{inf} to fuel temperature was determined by performing unrodded depletion calculations at 850 K, 950 K, and 1100 K for each of the specific powers and operating histories shown in Table 3.13. The results for the AO nuclide set are shown for the three fuel temperatures and a specific power of 25 W/g in Figure 3.38.

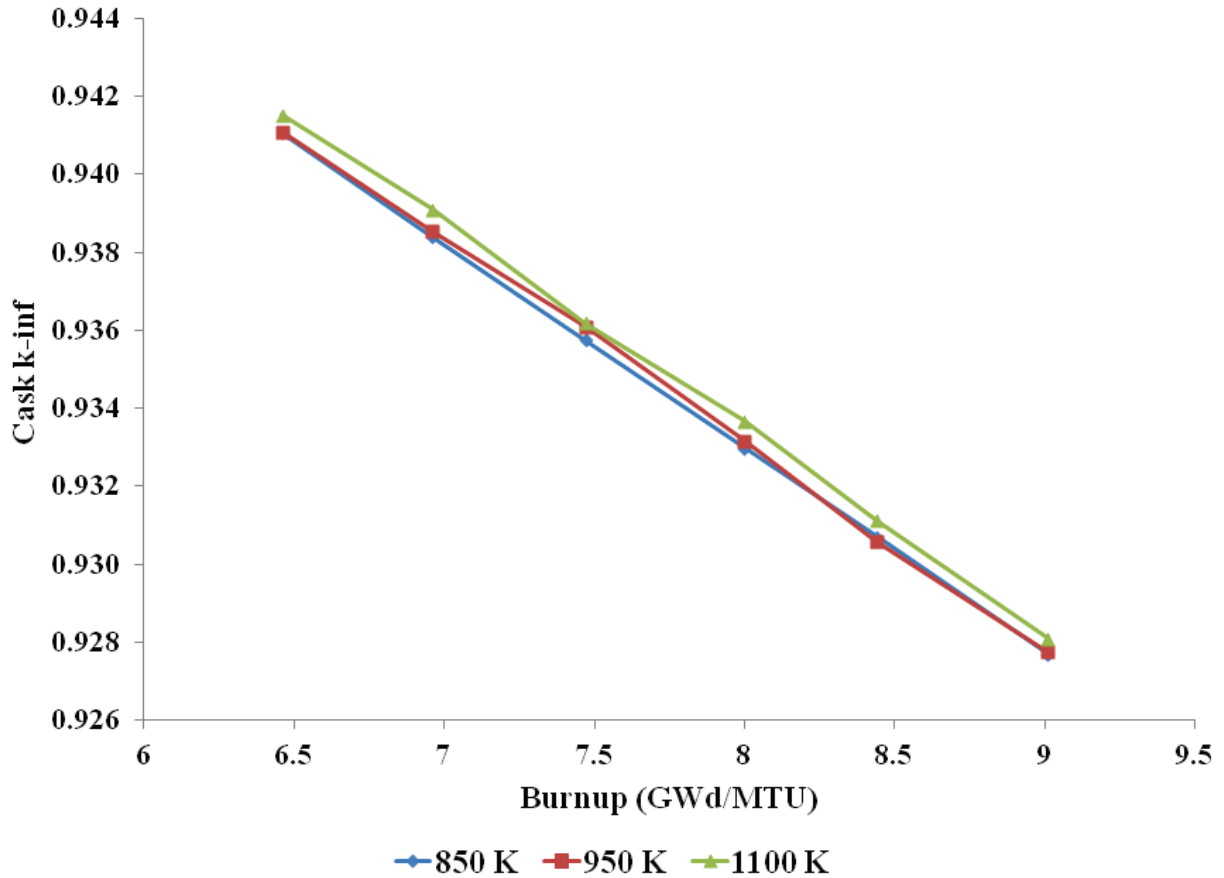


Figure 3.38. Cask k_{inf} as a function of burnup at 25 W/g for different fuel temperatures, AO nuclide set.

The burnups selected surround the cask peak reactivity burnup with the AFP nuclide set. The change in cask k_{inf} for the 850 K and 1100 K cases relative to the 950 K base case is shown for the 25 W/g, 35 W/g, and 45 W/g cases in Tables 3.14–3.16. The differences between the 1100 K and 850 K cases are shown in Table 3.17 for the 25 W/g case.

Table 3.14. Cask Δk_{inf} values for 25 W/g depletion case, 950 K base case, AO nuclide set

Burnup (GWd/MTU)	Δk_{inf}	Δk_{inf}	Δk_{inf}	Δk_{inf}
	850 K – 950 K (Δk)	850 K – 950 K ($ \Delta k/\sigma $)	1100 K – 950 K (Δk)	1100 K – 950 K ($ \Delta k/\sigma $)
6.46	-0.00001	0.09	0.00043	3.09
6.96	-0.00014	0.98	0.00056	4.01
7.47	-0.00033	2.38	0.00010	0.74
8.00	-0.00019	1.33	0.00050	3.59
8.44	0.00011	0.82	0.00055	3.93
9.01	-0.00004	0.32	0.00035	2.52

Table 3.15. Cask Δk_{inf} values for 35 W/g depletion case, 950 K base case, AO nuclide set

Burnup (GWd/MTU)	Δk_{inf}	Δk_{inf}	Δk_{inf}	Δk_{inf}
	850 K – 950 K (Δk)	850 K – 950 K ($ \Delta k/\sigma $)	1100 K – 950 K (Δk)	1100 K – 950 K ($ \Delta k/\sigma $)
6.46	-0.00016	1.16	0.00019	1.37
6.96	-0.00046	3.31	0.00028	2.01
7.47	-0.00008	0.60	0.00052	3.68
8.00	0.00000	0.03	0.00048	3.44
8.44	-0.00023	1.67	0.00037	2.66
9.01	-0.00019	1.37	0.00021	1.52

Table 3.16. Cask Δk_{inf} values for 45 W/g depletion case, 950 K base case, AO nuclide set

Burnup (GWd/MTU)	Δk_{inf}	Δk_{inf}	Δk_{inf}	Δk_{inf}
	850 K – 950 K (Δk)	850 K – 950 K ($ \Delta k/\sigma $)	1100 K – 950 K (Δk)	1100 K – 950 K ($ \Delta k/\sigma $)
6.46	-0.00020	1.39	0.00012	0.87
6.96	-0.00015	1.11	0.00014	1.03
7.47	-0.00031	2.18	0.00004	0.29
8.00	-0.00035	2.48	0.00025	1.76
8.44	-0.00026	1.87	0.00020	1.46
9.01	-0.00009	0.63	0.00050	3.56

Table 3.17. Cask Δk_{inf} values for 25 W/g case, 1100 K – 850 K, AO nuclide set

Burnup (GWd/MTU)	Δk_{inf} 1100 K – 850 K (Δk)	Δk_{inf} 1100 K – 850 K ($ \Delta k/\sigma $)
	6.46	0.00044
6.96	0.00070	4.98
7.47	0.00044	3.12
8.00	0.00069	4.91
8.44	0.00043	3.10
9.01	0.00040	2.84

In each of the tables, the differences are shown both in actual k_{inf} change, Δk , and in terms of the number of standard deviations, $n=|\Delta k/\sigma|$, that this difference represents. The comparison in terms of standard deviations helps provide context for the magnitude of the differences. Generally, differences that are less than 2σ are considered statistically equivalent. There is evidence of a

weak trend of reactivity variation with increasing fuel temperatures at the lower two specific power levels. There is no clear indication of a trend as a function of burnup at any of the specific power levels. The comparison from maximum to minimum fuel temperatures presented in Table 3.17 supports the conclusion that cask reactivity increases with increasing fuel temperatures during depletion, but it does not show any clear trends as a function of burnup. It can therefore be concluded that cask k_{inf} increases slightly ($\sim 0.0020\% \Delta k / 100 \text{ K}$) with increasing fuel temperature for the AO nuclide set in this study.

Figure 3.39 shows the results for the AFP nuclide set for the three fuel temperatures and a specific power of 25 W/g.

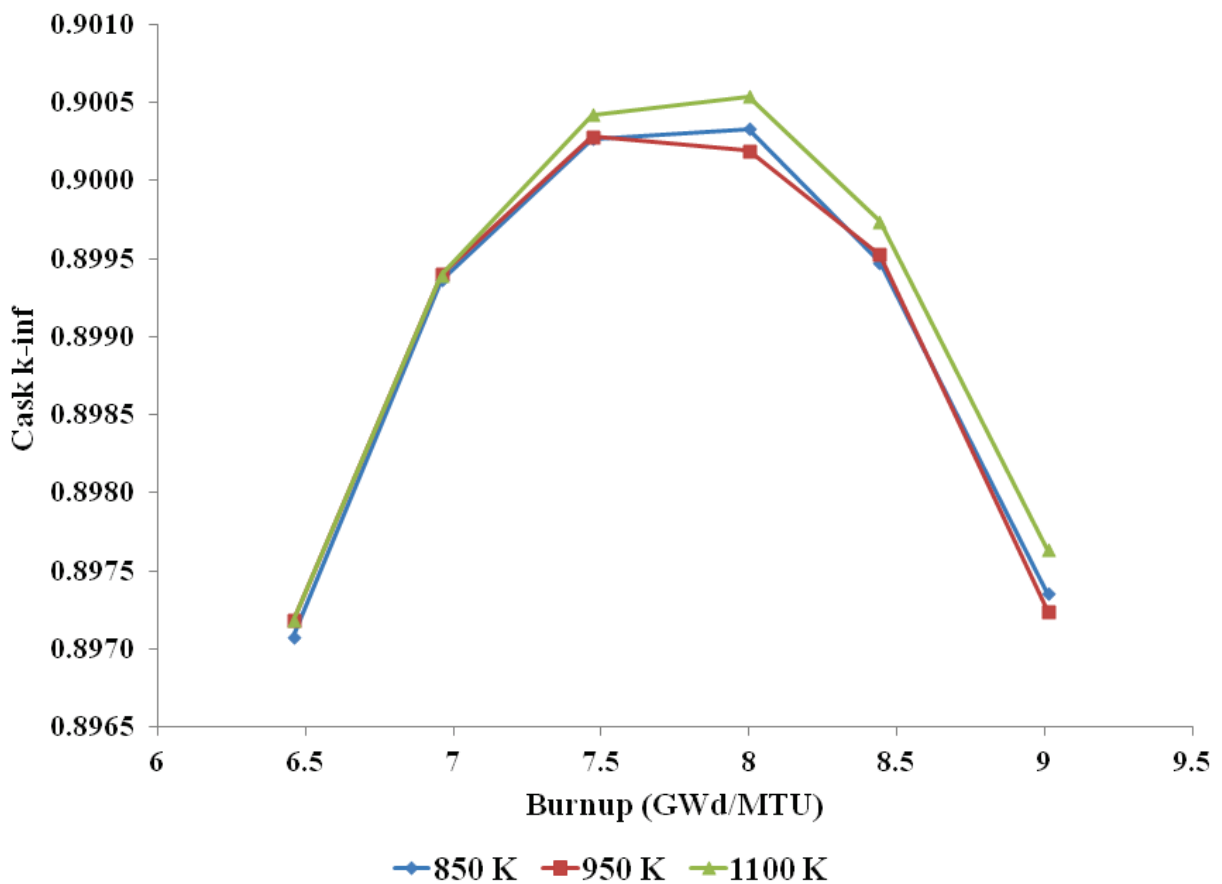


Figure 3.39. Cask k_{inf} as a function of burnup at 25 W/g for different fuel temperatures, AFP nuclide set.

Tables 3.18–3.20 show the change in cask k_{inf} for the 850 K and 1100 K cases relative to the 950 K base case for the 25 W/g, 35 W/g, and 45 W/g cases. The differences between the 1100 K and 850 K cases are shown in Table 3.21 for the 25 W/g case. As with the results for the AO set, the differences are shown both in actual k_{inf} change and in terms of the number of standard deviations this difference represents. No clear statistical trends are evident in the results, but it

appears that k_{inf} may increase slightly with increasing fuel temperature for the AFP nuclide set as well. This conclusion may change at the higher burnups considered for extended BUC.

Table 3.18. Cask Δk_{inf} values for 25 W/g depletion case, 950 K base case, AFP nuclide set

Burnup (GWd/MTU)	Δk_{inf} , 850 K – 950 K (Δk)	Δk_{inf} , 850 K – 950 K ($ \Delta k/\sigma $)	Δk_{inf} , 1100 K – 950 K (Δk)	Δk_{inf} , 1100 K – 950 K ($ \Delta k/\sigma $)
6.46	-0.00010	0.73	0.00000	0.01
6.96	-0.00004	0.26	0.00000	0.02
7.47	-0.00001	0.09	0.00014	1.00
8.00	0.00014	1.01	0.00035	2.49
8.44	-0.00005	0.35	0.00021	1.50
9.01	0.00011	0.80	0.00040	2.88

Table 3.19. Cask Δk_{inf} values for 35 W/g depletion case, 950 K base case, AFP nuclide set

Burnup (GWd/MTU)	Δk_{inf} , 850 K – 950 K (Δk)	Δk_{inf} , 850 K – 950 K ($ \Delta k/\sigma $)	Δk_{inf} , 1100 K – 950 K (Δk)	Δk_{inf} , 1100 K – 950 K ($ \Delta k/\sigma $)
6.46	-0.00015	1.11	0.00008	0.56
6.96	-0.00004	0.32	0.00025	1.78
7.47	0.00030	2.15	0.00031	2.22
8.00	-0.00007	0.52	0.00007	0.52
8.44	-0.00021	1.46	0.00010	0.74
9.01	0.00006	0.45	0.00053	3.87

Table 3.20. Cask Δk_{inf} values for 45 W/g depletion case, 950 K base case, AFP nuclide set

Burnup (GWd/MTU)	Δk_{inf} , 850 K – 950 K (Δk)	Δk_{inf} , 850 K – 950 K ($ \Delta k/\sigma $)	Δk_{inf} , 1100 K – 950 K (Δk)	Δk_{inf} , 1100 K – 950 K ($ \Delta k/\sigma $)
6.46	-0.00008	0.55	-0.00015	1.07
6.96	-0.00017	1.21	0.00009	0.64
7.47	-0.00002	0.15	0.00021	1.46
8.00	-0.00009	0.66	0.00009	0.61
8.44	-0.00011	0.80	0.00014	1.00
9.01	-0.00009	0.67	0.00024	1.74

Table 3.21. Cask Δk_{inf} values for 25 W/g case, 1100 K–850 K, AFP nuclide set

Burnup (GWd/MTU)	Δk_{inf} , 1100 K – 850 K (Δk)	Δk_{inf} , 1100 K – 850 K ($ \Delta k/\sigma $)
6.46	0.00010	0.72
6.96	0.00003	0.24
7.47	0.00015	1.08
8.00	0.00021	1.49
8.44	0.00026	1.85
9.01	0.00028	2.06

3.4.6.2 Specific Power

The models used in all studies presented in sections 3.4.1–3.4.5 of this report assumed a specific power of 25 W/g. This specific power was used because it is typical of BWR fuel; it is not chosen to be a bounding value. The sensitivity of cask k_{inf} to specific power was determined by performing unrodded depletion calculations at 25, 35, and 45 W/g for each of the fuel temperatures and operating histories shown in Table 3.13.

The results for the AO nuclide set are shown in Figure 3.40 for the three specific powers and at a fuel temperature of 950 K. The burnups selected surround the cask peak reactivity burnup with the AFP nuclide set.

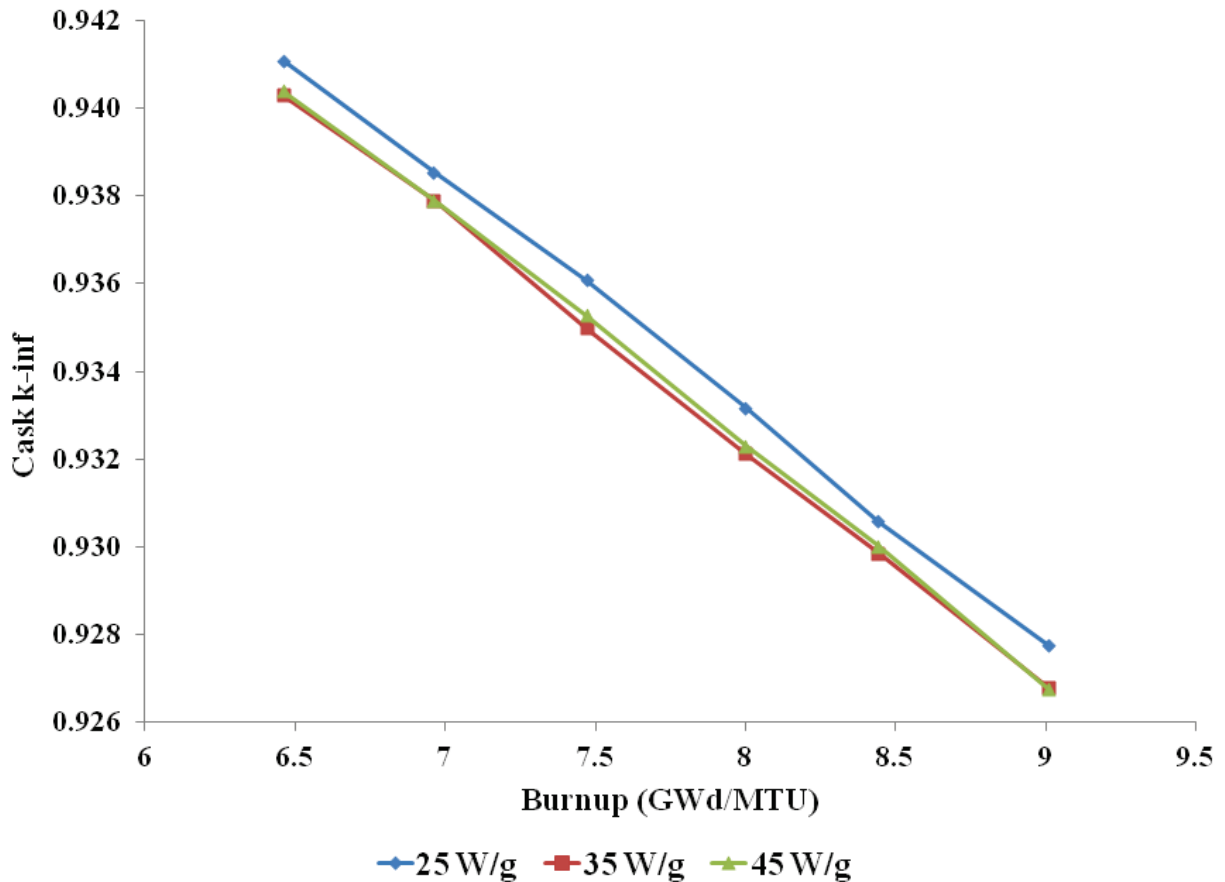


Figure 3.40. Cask k_{inf} as a function of burnup for different specific powers with 950 K fuel temperature, AO nuclide set.

The change in cask k_{inf} for the 35 W/g and 45 W/g cases relative to the 25 W/g base case is shown for the 850 K, 950 K, and 1100 K cases in Tables 3.22–3.24. In each of the tables, the differences are shown both in actual k_{inf} change and in the number of standard deviations.

Table 3.22. Cask Δk_{inf} values for 35 W/g and 45 W/g, 850 K fuel temperature, AO nuclide set

Burnup (GWd/MTU)	$\Delta k_{inf} (\Delta k)$	$\Delta k_{inf} (\Delta k/\sigma)$	$\Delta k_{inf} (\Delta k)$	$\Delta k_{inf} (\Delta k/\sigma)$
	35 W/g – 25W/g	35 W/g – 25W/g	45 W/g – 25W/g	45 W/g – 25W/g
6.46	-0.00095	6.75	-0.00088	6.25
6.96	-0.00096	6.83	-0.00065	4.67
7.47	-0.00085	6.02	-0.00077	5.51
8.00	-0.00084	6.02	-0.00103	7.32
8.44	-0.00107	7.65	-0.00094	6.72
9.01	-0.00110	7.84	-0.00104	7.39

Table 3.23. Cask Δk_{inf} values for 35 W/g and 45 W/g 950 K fuel temperature, AO nuclide set

Burnup (GWd/MTU)	$\Delta k_{inf} (\Delta k)$	$\Delta k_{inf} (\Delta k/\sigma)$	$\Delta k_{inf} (\Delta k)$	$\Delta k_{inf} (\Delta k/\sigma)$
	35 W/g – 25W/g	35 W/g – 25W/g	45 W/g – 25W/g	45 W/g – 25W/g
6.46	-0.00079	5.68	-0.00069	4.95
6.96	-0.00063	4.50	-0.00064	4.54
7.47	-0.00110	7.83	-0.00080	5.71
8.00	-0.00103	7.38	-0.00086	6.17
8.44	-0.00072	5.16	-0.00056	4.01
9.01	-0.00095	6.83	-0.00099	7.09

Table 3.24. Cask Δk_{inf} values for 35 W/g and 45 W/g 1100 K fuel temperature, AO nuclide set

Burnup (GWd/MTU)	$\Delta k_{inf} (\Delta k)$	$\Delta k_{inf} (\Delta k/\sigma)$	$\Delta k_{inf} (\Delta k)$	$\Delta k_{inf} (\Delta k/\sigma)$
	35 W/g – 25W/g	35 W/g – 25W/g	45 W/g – 25W/g	45 W/g – 25W/g
6.46	-0.00104	7.39	-0.00100	7.13
6.96	-0.00091	6.48	-0.00106	7.50
7.47	-0.00069	4.89	-0.00086	6.20
8.00	-0.00105	7.53	-0.00112	8.00
8.44	-0.00089	6.46	-0.00090	6.51
9.01	-0.00109	7.81	-0.00085	6.04

Cask reactivity clearly drops slightly between 25 and 35 W/g at all three fuel temperatures. It appears that there is no statistically significant difference in cask reactivity between 35 and 45 W/g, though reactivity may be slightly higher at 45 W/g. This may be evidence for a nonlinear relationship between specific power and reactivity, as noted for PWR BUC [16]. A review of depleted number densities shows that at higher specific powers, the ^{235}U is slightly more depleted, but that slightly more ^{239}Pu has been generated. The depleted number densities for non-gadolinium fuel pins in the interior region of the fuel assembly are shown in Table 3.25. Note that the depleted ^{235}U concentrations for the 35 and 45 W/g cases are nearly identical. Thus it appears that, at the burnups of interest for peak reactivity methods, the increase in ^{235}U depletion is the primary cause of the reduction in cask reactivity between 25 and 35 W/g, and there is no significant change between 35 and 45 W/g. As with the fuel temperature sensitivity, it is possible that a different trend could manifest at the higher burnups associated with extended BWR BUC beyond peak reactivity.

Table 3.25. ^{235}U and ^{239}Pu number densities for different specific powers and 950 K fuel temperature

Burnup (GWd/MTU)	^{235}U Number Density (a/b-cm)			^{239}Pu Number Density (a/b-cm)		
	25 W/g	35 W/g	45 W/g	25 W/g	35 W/g	45 W/g
6.46	8.548E-04	8.504E-04	8.503E-04	4.727E-05	4.857E-05	4.874E-05
6.96	8.436E-04	8.391E-04	8.390E-04	4.996E-05	5.124E-05	5.143E-05
7.47	8.321E-04	8.275E-04	8.275E-04	5.261E-05	5.391E-05	5.410E-05
8.00	8.204E-04	8.156E-04	8.156E-04	5.525E-05	5.656E-05	5.676E-05
8.44	8.107E-04	8.058E-04	8.058E-04	5.735E-05	5.867E-05	5.888E-05
9.01	7.983E-04	7.933E-04	7.933E-04	5.999E-05	6.131E-05	6.153E-05

The results for the AFP nuclide set are shown for three specific powers and a fuel temperature of 950 K in Figure 3.41.

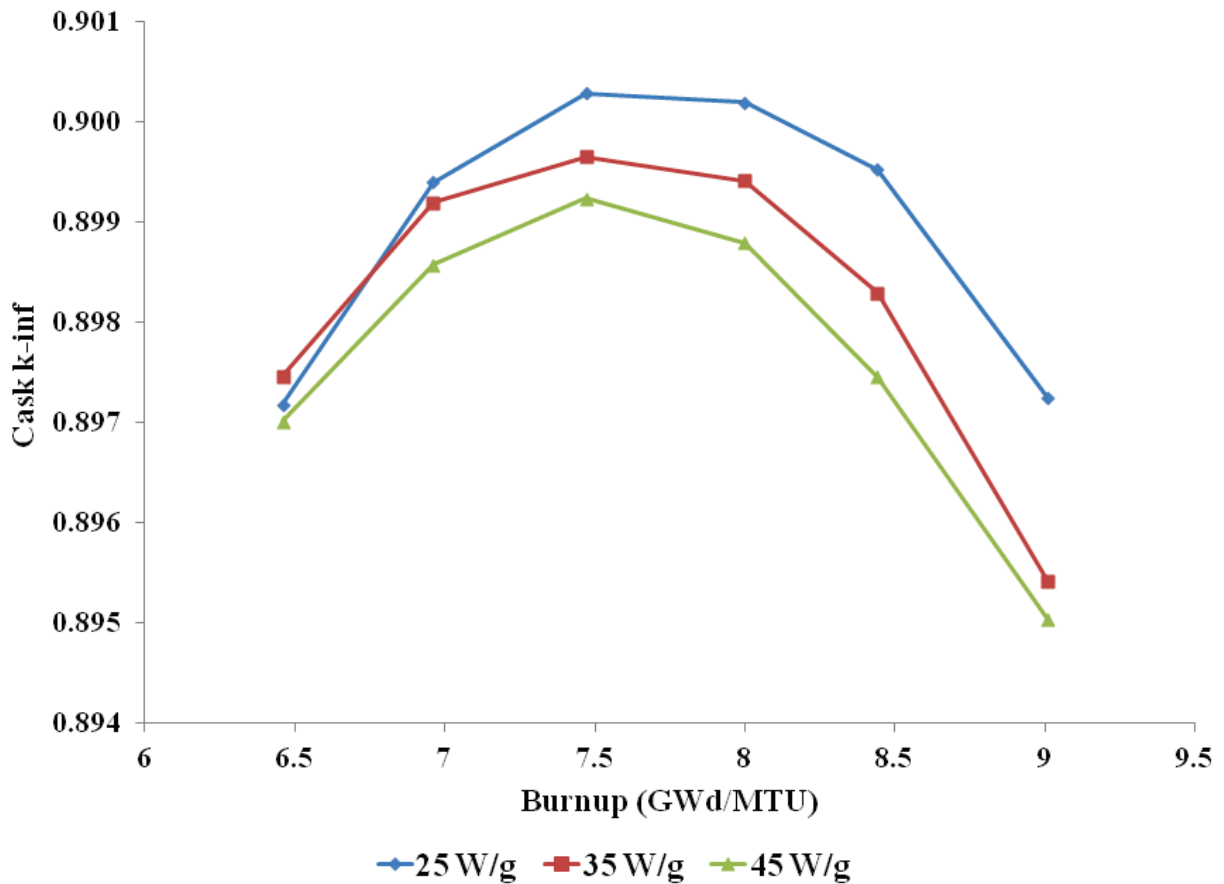


Figure 3.41. Cask k_{inf} as a function of burnup for different specific powers with 950 K fuel temperature, AFP nuclide set.

The change in cask k_{inf} for the 35 W/g and 45 W/g cases relative to the 25 W/g base case is shown for the 850 K, 950 K, and 1100 K cases in Tables 3.26–3.28.

Table 3.26. Cask Δk_{inf} values for 35 W/g and 45 W/g, 850 K fuel temperature, AFP nuclide set

Burnup (GWd/MTU)	$\Delta k_{inf} (\Delta k)$	$\Delta k_{inf} (\Delta k/\sigma)$	$\Delta k_{inf} (\Delta k)$	$\Delta k_{inf} (\Delta k/\sigma)$
	35 W/g – 25W/g	35 W/g – 25W/g	45 W/g – 25W/g	45 W/g – 25W/g
6.46	0.00023	1.66	-0.00015	1.04
6.96	-0.00021	1.53	-0.00096	6.85
7.47	-0.00032	2.27	-0.00105	7.48
8.00	-0.00099	7.10	-0.00163	11.64
8.44	-0.00139	9.91	-0.00214	15.48
9.01	-0.00188	13.41	-0.00241	17.21

Table 3.27. Cask Δk_{inf} values for 35 W/g and 45 W/g, 950 K fuel temperature, AFP nuclide set

Burnup (GWd/MTU)	$\Delta k_{inf} (\Delta k)$	$\Delta k_{inf} (\Delta k/\sigma)$	$\Delta k_{inf} (\Delta k)$	$\Delta k_{inf} (\Delta k/\sigma)$
	35 W/g – 25W/g	35 W/g – 25W/g	45 W/g – 25W/g	45 W/g – 25W/g
6.46	0.00028	2.00	-0.00017	1.22
6.96	-0.00021	1.47	-0.00083	5.90
7.47	-0.00063	4.54	-0.00104	7.50
8.00	-0.00078	5.57	-0.00140	9.97
8.44	-0.00123	8.76	-0.00207	14.81
9.01	-0.00183	13.25	-0.00220	15.74

Table 3.28. Cask Δk_{inf} values for 35 W/g and 45 W/g, 1100 K fuel temperature, AFP nuclide set

Burnup (GWd/MTU)	$\Delta k_{inf} (\Delta k)$	$\Delta k_{inf} (\Delta k/\sigma)$	$\Delta k_{inf} (\Delta k)$	$\Delta k_{inf} (\Delta k/\sigma)$
	35 W/g – 25W/g	35 W/g – 25W/g	45 W/g – 25W/g	45 W/g – 25W/g
6.46	-0.00032	2.29	-0.00032	2.29
6.96	-0.00073	5.24	-0.00073	5.24
7.47	-0.00098	6.99	-0.00098	6.99
8.00	-0.00166	11.80	-0.00166	11.80
8.44	-0.00215	15.24	-0.00215	15.24
9.01	-0.00236	17.16	-0.00236	17.16

Cask reactivity decreases with increased specific power. The differences among the specific powers are small at low burnups, but they grow noticeably with increasing burnup. The ^{239}Pu number densities show a slight increase with increased specific power, and the ^{155}Gd number densities show a slight decrease with increasing specific power. Both of these trends would indicate a small positive relationship between specific power and cask k_{inf} . The number densities for the most important fission products—including ^{149}Sm , ^{103}Rh , and ^{143}Nd [13]—are higher for higher specific powers. The ^{149}Sm number densities shown in Table 3.29 indicate an increase of about 9% at 35 W/g compared to the 25 W/g base case and a total increase of about 18% at 45 W/g. The effect of these increased absorbers overwhelms the slight differences in plutonium and gadolinium and creates a slight negative relationship that increases with burnup.

Table 3.29. ^{149}Sm number densities at a range of specific powers and 950 K fuel temperature

Burnup (GWd/MTU)	^{149}Sm, 25 W/g (a/b-cm)	^{149}Sm, 35 W/g (a/b-cm)	Percent change from 25 W/g	^{149}Sm, 45 W/g (a/b-cm)	Percent change from 25 W/g
6.46	1.08E-07	1.18E-07	8.95%	1.27E-07	17.34%
6.96	1.09E-07	1.18E-07	9.02%	1.28E-07	17.59%
7.47	1.09E-07	1.19E-07	9.10%	1.28E-07	17.83%
8.00	1.09E-07	1.19E-07	9.27%	1.29E-07	18.07%
8.44	1.09E-07	1.19E-07	9.44%	1.29E-07	18.33%
9.01	1.09E-07	1.20E-07	9.61%	1.30E-07	18.66%

The increasing fission product inventory at higher burnups also explains the burnup dependence of this effect, providing additional confidence that increased fission product generation at higher specific powers causes the cask reactivity to decrease. The effect is fairly small at peak reactivity (less than 0.1% Δk), but the effect increases to about 0.25% Δk by 9 GWd/MTU. This provides a clear indication that there is likely to be sensitivity to specific power for extended BWR BUC beyond peak reactivity. For peak reactivity methods, there is a small sensitivity indicating that lower specific powers lead to higher discharged reactivities as shown in Figure 3.41.

3.4.6.3 Operating History

The models used in all the studies presented in sections 3.4.1–3.4.5 of this report assumed a full power (FP) operating history. This assumption is typical for depletion calculations; the actual operating history of a fuel assembly, even if the reactor operates at FP for an entire cycle, is more complex. The sensitivity of cask k_{inf} to other operating histories was determined by performing unrodded depletion calculations using each of the four power histories shown in Table 3.12 for each of the fuel temperatures and specific powers listed as well. In this section, the operating histories will be referred to as FP, half power (HP), full power followed by half power (FHP), and full power followed by three-quarter power followed by half power (FTHP).

The results for the AO nuclide set are shown for the four operating histories and a fuel temperature of 950 K in Figure 3.42.

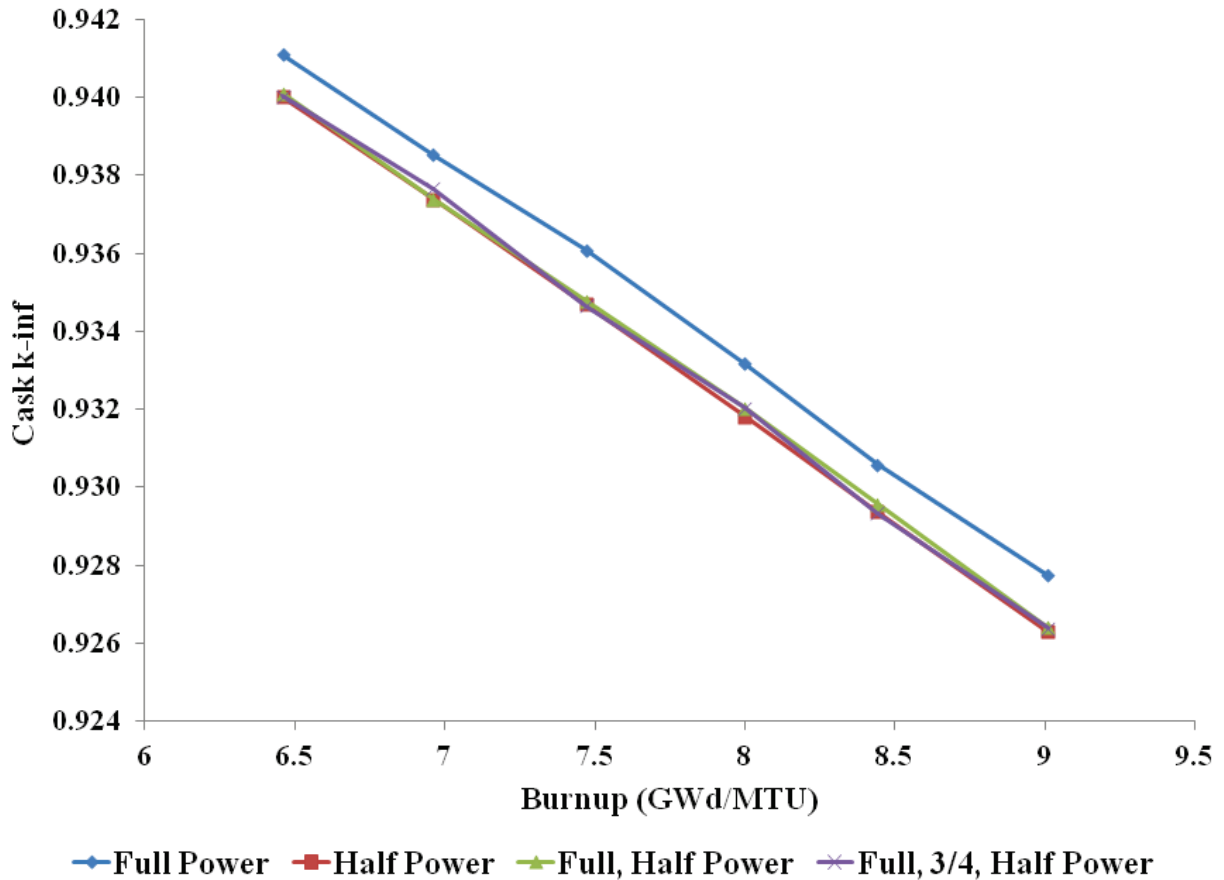


Figure 3.42. Cask k_{inf} as a function of burnup for four different operating histories, AO nuclide set.

The burnups selected surround the cask peak reactivity burnup with the AFP isotope set. The results indicate that the FP operating history yields the highest discharge reactivity, while the other histories lead to lower cask k_{inf} values that are statistically equivalent. The small magnitude of the changes among the different part-power histories for the AO set is consistent with the small magnitude of the sensitivity to specific power with the same nuclide set. The effect is reduced because the change among the histories is less dramatic than shifts of 10 W/g for the entire depletion. The FP operating history is limiting for cask k_{inf} with the AO nuclide set.

The results for the AFP nuclide set are shown for the four operating histories and a fuel temperature of 950 K in Figure 3.43.

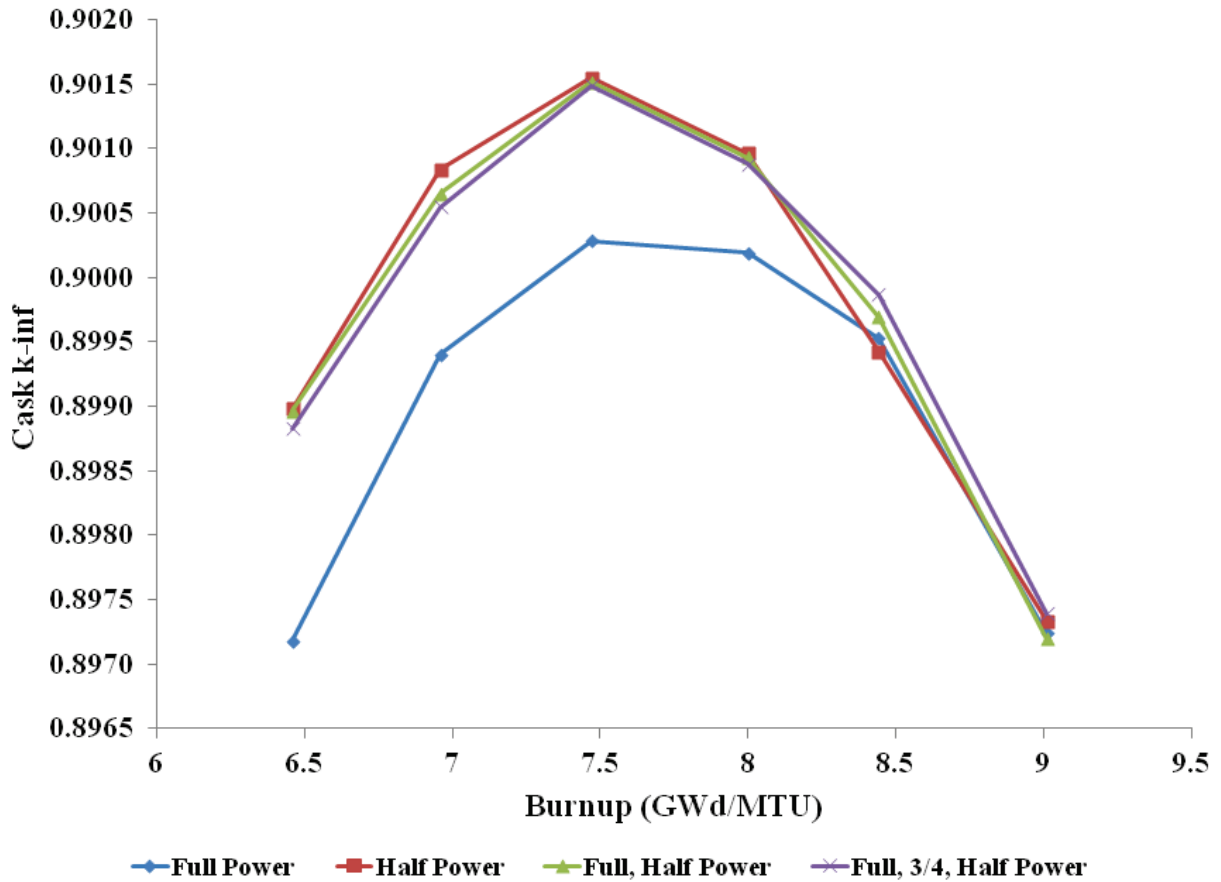


Figure 3.43. Cask k_{inf} as a function of burnup for four different operating histories, AFP nuclide set.

In this case, the FP history is the least reactive result. The HP history provides an upper bound on cask reactivity, and the FHP and FTHP histories yield results largely between the two. The peak reactivity burnup is largely unaffected by the power history, and the magnitude of the peak reactivity only shifts by about 0.2% Δk . The AFP operating history results are in good agreement with the AFP-specific power results presented in Section 3.4.6.2. The HP history is essentially equivalent to a specific power of 12.5 W/g, which would be expected to be more reactive than the 25 W/g FP history. A variable operating history is bounded by a constant history with an appropriate low specific power for the AFP nuclide set.

3.4.7 Three-Dimensional Modeling

A final sensitivity study was performed to investigate the practice of using a 3D cask model containing a fuel assembly represented by a 2D lattice slice extruded to the full fuel assembly length. The axial features of the fuel assembly and cask are used as specified in the GBC-68 definition [10]. Two sets of depleted fuel isotopics are modeled: the base case and the limiting case identified in the studies presented in this report for the AFP nuclide set. The base case is unrodded depletion with 40% moderator void fraction and the 6×2Gd pattern shown in Figure

3.11. The limiting case is rodded depletion with 0% void and the same 6×2Gd pattern. Both scenarios used 950 K fuel temperatures and a constant 25 W/g specific power depletion.

The results for the base case are shown in Figure 3.44 and for the limiting case in Figure 3.45. Both figures show all four nuclide sets for the 2D and 3D models.

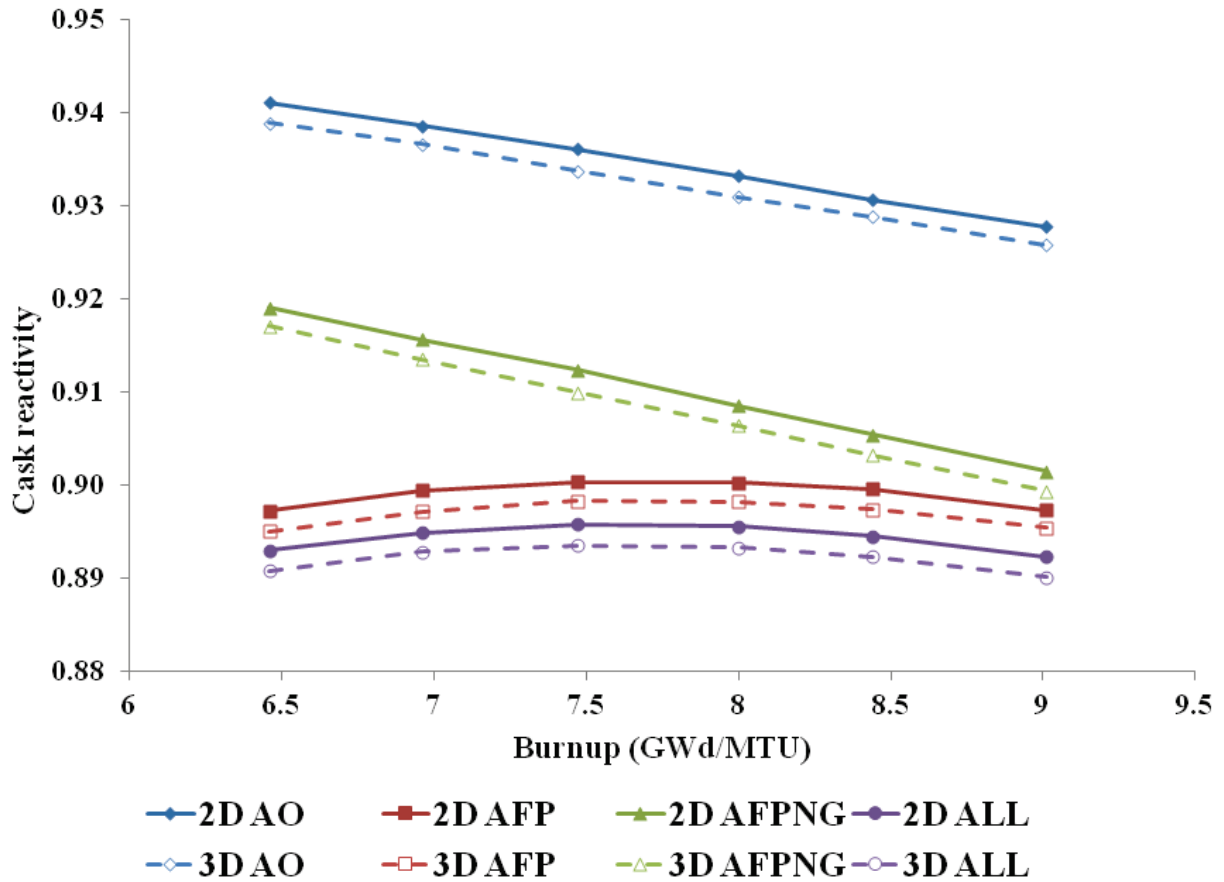


Figure 3.44. Cask reactivity as a function of burnup, unrodded depletion with 40% void fraction, all nuclide sets.

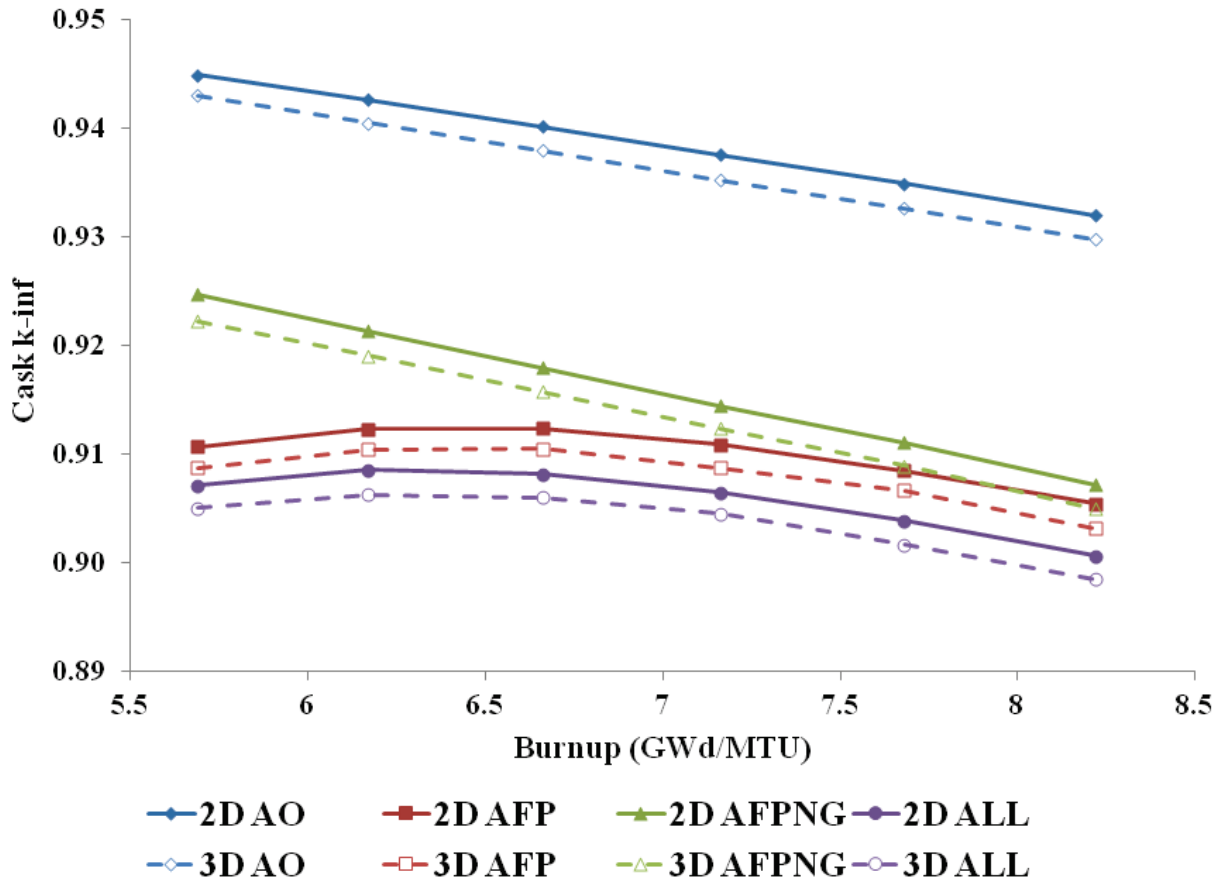


Figure 3.45. Cask reactivity as a function of burnup, rodded depletion with 0% void fraction, all nuclide sets.

The change in cask k_{inf} values (Δk) is presented for the AO and AFP nuclide sets for the base case fuel model in Table 3.30 and for the rodded depletion in Table 3.31. The results show that the extruded lattice models result in slightly lower cask reactivities than the 2D models. The margin inherent in the 2D models compared to the 3D models is small. In these cases the difference in reactivity is about 0.2% Δk .

Table 3.30. Difference between 2D cask k_{inf} and 3D cask k_{eff} , unrodded depletion with 40% void fraction

Burnup (GWd/MTU)	AO		AFP		AFPNG		ALL	
	Δk	σ						
6.46	0.00219	0.00014	0.00218	0.00014	0.00198	0.00014	0.00221	0.00014
6.96	0.00196	0.00014	0.00230	0.00014	0.00211	0.00014	0.00202	0.00014
7.47	0.00238	0.00014	0.00204	0.00014	0.00241	0.00014	0.00227	0.00014
8.00	0.00226	0.00014	0.00204	0.00014	0.00207	0.00014	0.00222	0.00014
8.44	0.00181	0.00014	0.00221	0.00014	0.00219	0.00014	0.00217	0.00014
9.01	0.00198	0.00014	0.00187	0.00014	0.00213	0.00014	0.00225	0.00014

Table 3.31. Difference between 2D cask k_{inf} and 3D cask k_{eff} , rodde depletion with 0% void fraction

Burnup (GWd/MTU)	AO		AFP		AFPNG		ALL	
	Δk	σ						
5.69	0.00193	0.00014	0.00197	0.00014	0.00243	0.00014	0.00208	0.00014
6.17	0.00215	0.00014	0.00186	0.00014	0.00226	0.00014	0.00224	0.00014
6.66	0.00219	0.00014	0.00192	0.00014	0.00221	0.00014	0.00213	0.00014
7.16	0.00233	0.00014	0.00213	0.00014	0.00206	0.00014	0.00194	0.00014
7.68	0.00230	0.00014	0.00178	0.00014	0.00213	0.00014	0.00224	0.00014
8.22	0.00215	0.00014	0.00228	0.00014	0.00223	0.00014	0.00214	0.00014

3.5 SUMMARY OF FACTORS AFFECTING PEAK REACTIVITY

The purpose of this section is to examine the impacts of important BWR design and operating parameters on reactivity, up to the peak reactivity. Sensitivity calculations have been performed over a range of parameters, including gadolinium loadings and assembly patterns, void fraction, control blade insertion, fuel temperature, specific power, and operating history. This section summarizes the sensitivity studies results, lists recommended analyses that should be presented as part of a criticality safety evaluation, and defines areas of future study. Conclusions for the report are presented in Section 6.

3.5.1 Summary of Sensitivity Studies

A range of parameters were studied to identify the important parameters for BWR peak reactivity and to quantify the potential sensitivity of calculated cask reactivity to these parameters. The primary fuel assembly model used in this study was the GE14 fuel assembly, which has a 10×10 array of fuel pins and contains two large central water rods which each displace four fuel rods. Full and vanished lattices with no gadolinium-poisoned pins were used as the base case for AO BUC sensitivity studies. For the AFP BUC sensitivity studies, six gadolinium-poisoned fuel pins with 2.0 wt% gadolinium were used as the base case. The results of the sensitivity studies are summarized below and shown in Tables 3.32 and 3.33 for AO and AFP, respectively.

Table 3.32. Summary of parameters affecting discharged reactivity for BWR peak reactivity analysis considering the AO nuclide set

Parameter	Range Studied	Reactivity Impact (% Δk)
Fuel composition modeling	AEAI, PEAI, PEPI	0.3 (AEAI)
Number of gadolinium pins	0 to 8 pins (0 pins base case)	~ 0 (≤ 0.06 at 7 GWd/MTU)
Loading of gadolinium pins	0 to 10 wt%	0 to 0.5 (9 – 25 GWd/MTU)
Gadolinium pattern	15 patterns	~ 0 (± 0.03 at 7 GWd/MTU)
Moderator void fraction, unrodded	0 to 80% (40% base case)	-0.4 to +0.7 (0% void to 80% void)
Moderator void fraction, rodded	0 to 80% (40% base case)	-0.6 to +1.1 (0% void to 80% void)
Control blade insertion	unrodded vs. rodded (full depletion)	≤ 1 (rodded)
Fuel temperature	850 to 1100 K (950 K base case)	$\sim 0.0020\% \Delta k / 100 \text{ K}$
Specific power	25 to 45 W/g (25 W/g base case)	0.1 (35 and 45 W/g)
Operating history	4 histories (FP base case)	-0.1
Cask model dimension	2D, 3D (2D base case)	-0.2

Table 3.33. Summary of parameters affecting discharged reactivity for BWR peak reactivity analysis considering the AFP nuclide set

Parameter	Range Studied	Reactivity Impact (% Δk)
Fuel composition modeling	AEAI, PEAI, PEPI	0.5 (AEAI)
Number of gadolinium pins	2 to 8 pins (6 pins base case)	+1.3 to -0.2 (2 to 8 pins)
Loading of gadolinium pins	2 to 10 wt% (2 wt% base case)	-3 to -11 (4 wt% to 10 wt%)
Gadolinium pattern	15 patterns	± 0.25 at peak reactivity (~ 7.5 GWd/MTU)
Moderator void fraction, unrodded	0 to 80% (40% base case)	+0.2 to -0.2 (0% void to 80% void)
Moderator void fraction, rodded	0 to 80% (40% base case)	+0.1 to -0.2 (0% void to 80% void)
Control blade insertion	unrodded vs. rodded (full depletion)	~ 1.0 (rodded)
Fuel temperature	850 to 1100 K (950 K base case)	0
Specific power	25 to 45 W/g (25 W/g base case)	-0.1 (peak reactivity)
Operating history	4 histories (FP base case)	0.1 (HP case)
Cask model dimension	2D, 3D (2D base case)	-0.2

Most of the parameters studied affect reactivity through changes in the depleted fuel compositions. Two modeling approaches were examined for fuel compositions within the lattice: (1) the modeling of the initial enrichment zoning within a fuel assembly, and (2) the depletion and representation of the different depleted fuel mixtures in the cask. The initial enrichment zoning can be represented with PE or AE. The depleted compositions in the cask criticality model can use pin-wise isotopics (PI) or average isotopics (AI). The AE cases provide higher discharged reactivity than the PE cases by effectively moving fissile material to higher thermal flux regions around the periphery of the assembly and near the water tubes. There does not appear to be a strong dependence on the depleted fuel representation, but PI may lead to a slightly higher reactivity than AI. The AEPI approach is not recommended, however, because a significant contribution to the differences among the depleted fuel pins would be due to differences in initial concentrations that are not realistic. Therefore, the AEAI modeling strategy was chosen because of the moderate level of conservatism and the ease of modeling. The PE approaches would require additional effort to model the assembly more accurately.

The number and initial loading of gadolinium pins has negligible impact on AO BUC, because gadolinium is not included in the cask model. However, they impact both the magnitude of peak reactivity and the burnup at which it occurs for AFP BUC, as shown in Figures 3.17 and 3.19. The 6 \times 2Gd pattern was selected for the AFP base case because it provides a definitive peak in reactivity, and the peak is at a relatively low burnup resulting in a peak that has a large

magnitude compared to other higher gadolinium cases. A series of 15 gadolinium loading patterns (Appendix B) were examined to determine impacts on cask reactivity. The reactivity of the base case pattern was approximately average of the range of cask reactivities resulting from a $6 \times 2\text{Gd}$ loading, but the magnitude of the effect was small at approximately $\pm 0.25\% \Delta k$ at peak reactivity for AFP.

The impact of the void fraction on cask reactivity differs significantly between AO and AFP BUC cases. Cask reactivity increases with higher void fractions for the AO cases due to the hardening neutron spectrum at increasing void fractions. The overall reactivity change from 0% to 80% void is greater than $1\% \Delta k$ at about 7.5 GWd/MTU for unrodded cases and greater than 1.5% for rodded cases. This is a significant impact that must be properly accounted for during depletion calculations for AO BUC. The results for the AFP nuclide set are completely reversed: the low void fraction case is bounding. The driving effect for the AFP cases is the amount of residual gadolinium (the AO cases do not include residual gadolinium in the cask model), which is decreased by a more thermal spectrum because of the larger thermal absorption cross section for gadolinium. As the void fraction increases, the gadolinium depletion is slower, causing a reduction in the reactivity peak and a shift to higher burnups. The peak reactivity of the cask drops by about $0.4\% \Delta k$ from 0% void fraction to 80% void fraction ($\pm 0.2\% \Delta k$ relative to the 40% void fraction base case) for unrodded cases, and slightly less for rodded cases.

Depletion cases were run with control blades inserted for 0 to 80% void fraction cases to compare with the unrodded void fraction cases. The presence of the control blade during depletion increases cask k_{inf} up to $1\% \Delta k$ for AO cask reactivity cases. These results are driven by the hardening neutron spectrum at increasing void fractions and by a significant spectral shift caused by the presence of the control blade during depletion. The harder spectrum causes additional ^{239}Pu generation, which is a significant contributor to reactivity, even at these relatively low burnups. For the AFP nuclide set, the maximum reactivity for discharged fuel occurs for rodded depletion with zero void fractions during depletion. The presence of the control blade during depletion increases cask k_{inf} by approximately $1\% \Delta k$ for AFP cases.

Fuel temperature effects were studied by performing depletion cases at 850 K and 1100 K in addition to the base case at 950 K. For AO cases, the cask reactivity increases slightly with increasing fuel temperatures during depletion. The cask k_{inf} increases $\sim 0.0020\% \Delta k / 100 \text{ K}$ with increasing fuel temperature for the AO cases. The AFP cases also appeared to show slightly higher cask k_{inf} values with increasing fuel temperature during depletion, although there was no statistical trend.

The sensitivity of cask k_{inf} to specific power was determined by performing unrodded depletion calculations at 25, 35, and 45 W/g for each of the three fuel temperatures and four operating histories, FP, HP, FHP, and FTHP. Cask reactivity drops slightly for the AO cases between 25 and 35 W/g at all three fuel temperatures. It appears that there is no statistically significant difference in cask reactivity between 35 and 45 W/g. For AFP cases, cask reactivity decreases with increased specific power. The differences among the specific powers are small at low burnups, but grow with increasing burnup. The effect is fairly small at peak reactivity ($\sim 0.1\% \Delta k$) but increases to about $0.25\% \Delta k$ by 9 GWd/MTU.

The FP operating history is limiting for cask k_{inf} with the AO nuclide set. The part-power histories produce cask k_{inf} values that are approximately 0.1% lower. The results for the AFP nuclide set are different in that the FP history is the least reactive result. The HP history provides an upper bound on cask reactivity (0.1% Δk), and the FHP and FTHP histories yield results largely between the two. It appears that an appropriately bounding low specific power is limiting for the AFP nuclide set.

Regarding 2D vs. 3D modeling, the 2D model represents all cask and fuel components with a uniform height and uses reflecting boundary conditions in the axial direction to mimic a 2D slice. The 3D model represents the cask and fuel assembly with the heights specified for the GBC-68 computational benchmark model. The fuel is represented as a 2D slice extruded to the axial extent specified in the model definition. The results show that the 3D model is about 0.2% Δk less reactive than the 2D model. The 3D model is a more accurate representation of the system, but the 2D model includes only a small margin of conservatism.

3.5.2 Recommended Minimum Analyses

A range of parameters has been investigated in this report, and one set of conclusions that can be drawn relates to which parameters are sufficiently variable or interdependent so that examination is recommended for each licensing analysis performed. The primary parameters of interest in this category are the gadolinium pattern used in the analysis and the way it interacts with control blade insertion. It is conceivable that some gadolinium patterns will be more reactive than others. More importantly, the power distribution shifts caused by control blade insertion drive the changes in residual gadolinium, and hence discharged fuel reactivity. These effects will be sensitive to the gadolinium pattern. Certain other key parameters do not need to be studied further to identify the direction of conservatism, but justification that the values used are appropriate should be provided as part of an application. The parameters that do not need further investigation for the GE14 design considered in this work include initial or depleted composition modeling, void fraction, fuel temperature, and operating history.

3.5.3 Areas for Further Study

Several areas related to peak reactivity BUC could be further studied to provide additional confidence in the results generated in this report, clarify causes and relationships among parameters, or extend the area of applicability beyond the parameters, ranges, and fuel types studied here. One essential area that requires assessment is validation of reactivity calculations and depleted fuel isotopics. These validation assessments are provided in Sections 4 and 5, respectively. Other areas that could be studied further include the following:

- A wider range of lattice enrichment zoning patterns
- Additional gadolinium patterns, potentially including less constrained pattern development
- Expansion of the study of the interaction between gadolinium patterns and control blade effects

- Control blade programs, including both rodded and unrodded depletion during operation
- Additional fuel assembly design types
- 3D depletion calculations to investigate interactions between lattices
- Fuel assembly orientation within the cask
- Depletion effects of asymmetric gaps between assemblies in the core
- Parameter interdependencies and potential competing effects

4 VALIDATION OF CASK REACTIVITY CALCULATIONS

Consistent with industry standards [17] and regulatory guidance [2], criticality safety calculations must be validated against critical experiments to demonstrate the reliability of the computational methods and models and also to determine a bias and uncertainty applicable to the code and methods used. Validation of BUC is challenging due to the lack of critical experiments containing the appropriate AFP compositions [13]. The reactivity of typical BWR fuel lattices typically peak at less than ~20 GWD/MTU, which is significantly lower than the range of discharged assembly burnups. This provides unique challenges for validating BWR calculations [13].

The French Haut Taux de Combustion (HTC) experiments [18] provide a highly representative set of actinide compositions for validation of PWR BUC. These experiments are designed to have actinide compositions similar to a PWR fuel assembly with an initial enrichment of 4.5 wt% ^{235}U and a discharged burnup of 37.5 GWd/MTU. This burnup is significantly higher than typical BWR peak reactivity values, resulting in higher plutonium fractions and a different distribution of plutonium nuclides than would be expected in the BWR design basis fuel composition. Nevertheless, the HTC experiments will be considered here for validation of BWR peak reactivity calculations, along with several other experiments drawn from the *International Handbook of Evaluated Criticality Safety Benchmark Experiments* (IHECSBE) [19].

This section provides an overview of studies performed to establish a basis for validating cask reactivity calculations for BWR peak reactivity methods implemented in a storage and transportation cask. Items in this section include (1) the methodology used, (2) a description of the codes and methods used, (3) a description of the three primary sources for sensitivity data files (SDFs) used to assess similarity between critical experiments and application models, (4) a list of potentially applicable experiments identified in this work, (5) estimates for the bias and bias uncertainty using SCALE 6.1.2, (6) a discussion of potential penalties for unvalidated nuclides, and (7) a summary of the validation of cask reactivity calculations.

4.1 CODES AND METHODS

The majority of the work presented in this section is performed using tools from the SCALE code system's Tools for Sensitivity and Uncertainty Analysis Methodology Implementation (TSUNAMI) suite. SDFs are generated using the TSUNAMI-3D sequence, which combines the KENO Monte Carlo code with the Sensitivity Analysis Module for SCALE (SAMS) code. Similarity assessments are performed with TSUNAMI - Indices and Parameters (TSUNAMI-IP).

The TSUNAMI-3D sequence is the control module for 3D cross-section sensitivity and uncertainty analysis. The sequence provides automated processing of material input and cross-section data, forward and adjoint neutron transport, calculation of sensitivity coefficients (i.e., sensitivity of k_{eff} to nuclear data variation), and determination of uncertainty in k_{eff} due to cross-section covariances. The SAMS module computes sensitivities based on the forward and adjoint fluxes calculated by KENO and generates an SDF containing the nuclide-, energy-, and reaction-dependent k_{eff} sensitivity coefficients. These energy-dependent sensitivities are determined for each nuclide in the model using linear perturbation theory.

The three GBC-68 cask models used in these analyses are modeled in KENO V.a. Critical experiment models that were previously prepared using either KENO V.a or KENO-VI and are available from a variety of sources (as discussed below) are used in this work for convenience. The use of benchmark models from different criticality codes is not appropriate for application-specific validation since the validation must be performed with the same code as the licensing calculations. The geometry representation and tracking algorithms are different between the two KENO versions, so they implement different computational methods. The pooling of results from both codes is acceptable for this work because its primary purpose is to demonstrate validation feasibility.

TSUNAMI-IP is used to evaluate the similarity of critical experiments and application models and to determine uncertainties in cask reactivity due to cross-section covariance data. The similarity metric calculated in the c_k value is a correlation coefficient and can therefore be determined by dividing the covariance between the experiment and application by the product of the uncertainties in the experiment and the application [11], as shown in Equation 1.

$$c_k = \frac{\sigma_{AppExp}^2}{\sigma_{App} \sigma_{Exp}} \quad (1)$$

Where: c_k is the similarity between an application and an experiment
 σ_{AppExp}^2 is the covariance between the application and the experiment
 σ_{App} is the uncertainty in the application k_{eff} due to cross-section covariances
 σ_{Exp} is the uncertainty in the experiment k_{eff} due to cross-section covariances

A c_k value of 1 indicates that the k_{eff} values for two compared systems would be affected identically by nuclear data errors, which are the primary contributors to computational method bias. A c_k value ≥ 0.8 is considered a high enough degree of similarity to be acceptable for use in validation studies [20] and is used as the cutoff for the acceptably similar experiments identified in Section 4.4.

4.2 METHODOLOGY FOR VALIDATION STUDIES

The goal of this criticality validation study is to identify applicable experiments for the validation of criticality calculations that incorporate BUC up to peak reactivity for BWR fuel in storage and transportation casks.

Three GBC-68 cask models with full and vanished lattices were compared with a large number of critical experiment models using TSUNAMI-IP to determine how similar each experiment is to each application model. A significant advantage of this approach is that the cross-section uncertainties provide input to the similarity assessment; shared sensitivities with large uncertainties contribute more to c_k than shared sensitivities with small uncertainties. A disadvantage is that an SDF must be generated for each experiment and each application for a comparison to be made. Fortunately, a large number of SDFs have been generated [21] by the Organisation for Economic Cooperation and Development/Nuclear Energy Agency (OECD/NEA) for use in scoping studies such as this one. The majority of the low-enriched, pin-lattice critical experiments contained in the IHECSBE [19] have provided sensitivity data available in the public domain.

Once potentially applicable experiments have been identified, a brief validation study is presented using traditional trending methods and c_k trending. While this validation study is not sufficiently rigorous to be considered as an example for any specific application, it is intended to demonstrate that a sufficient population of experiments has been identified. These studies include methods drawn from previous NUREG/CR reports on validation [22, 23].

The penalties developed for unvalidated nuclides (i.e., nuclides not well represented in the validation experiment set) are based on cross-section uncertainty values propagated with model sensitivity data to determine reactivity uncertainty due to cross-section uncertainties. The uncertainty in the storage/transportation configuration calculated reactivity is determined from TSUNAMI-IP and/or TSUNAMI-3D. This method is based on techniques similar to those used to determine the fission product penalty factor recommended for use in ISG-8 Revision 3 [2] as documented in NUREG/CR-7109 [13].

4.3 SDF SOURCES

The similarity assessment performed by TSUNAMI-IP requires a set of SDFs, which are typically generated using TSUNAMI-3D. The generation of SDFs can be time consuming, so identifying sources for SDFs to be used in this work is important. Three primary sources were considered: SDFs generated by the OECD/NEA, SDFs used in the preparation of NUREG/CR-7109, and SDFs in the SCALE validation library maintained at ORNL, known as the Verified, Archived Library of Inputs and Data (VALID) library [24]. Each of these sources is discussed briefly here. A complete list of the experiments considered in this validation work is provided in Appendix C. In total, over 1100 low-enriched uranium (LEU) experiments were considered in this work, as well as more than 575 mixed uranium/plutonium (MIX) experiments.

The generation of SDFs at the OECD/NEA is automated such that a large amount of sensitivity data is available in the public domain for use. These files are distributed in the IHECSBE. For the purposes of this report, sensitivity data from 1002 LEU-COMP-THERM (LCT) experiments data are used from this source, along with 200 MIX-COMP-THERM (MCT) and 26 MIX-SOL-THERM (MST) SDFs. This large collection of SDFs is a valuable resource for validation studies. The terms “COMP” and “SOL” indicate the fuel form (solid composition, e.g. UO_2 , and solution, respectively). The term “THERM” specifies the flux spectrum is thermal.

A number of SDFs available at ORNL were collected as part of the generation of NUREG/CR-7109 [13]. The inputs used to generate these SDFs are available for public download from the SCALE website [25]. This collection includes 124 LEU experiments and 194 MIX experiments. The 156 HTC experiments were also considered in NUREG/CR-7109 and in this validation effort. The HTC data are proprietary and are therefore not freely distributed; the data necessary to build models of the HTC experiments can be acquired from ORNL at no cost after an appropriate non-disclosure agreement has been signed. Some of these cases were superseded by SDFs available in the VALID library.

The VALID library is maintained at ORNL to provide a source of high fidelity reviewed models and other data, including SDFs. Each file contained within VALID has been created and reviewed by qualified subject matter experts to provide confidence that the SDFs are correct and

of high quality. A total of 123 LEU-COMP-THERM experiments from VALID are considered, along with 49 MIX-COMP-THERM cases.

Some experiments are included in multiple SDF sources. After elimination of duplicate experiments, a total of 1643 unique experiments are considered.

4.4 POTENTIALLY APPLICABLE EXPERIMENTS

TSUNAMI-3D models of the GBC-68 cask [10], loaded with full and vanished lattices, are used as applications for validation. Sensitivity data are generated for three GBC-68 cask models: the vanished lattice including AO and AFP compositions, and the full lattice with AFP compositions. These were calculated with an initial enrichment of 4.305 wt% ^{235}U , an approximately 7.5 GWd/MTU peak reactivity burnup, and a 5-year decay time.

These SDFs are compared against the critical experiments described in the previous section to determine which experiments have sufficiently high similarity to be applicable for benchmarking BWR peak reactivity cask models. The results of these comparisons are provided for each of these cases, followed by a summary at the end of this section. In addition, the SDF for the BWR SFP rack application from NUREG/CR-7109 [13], which used a different lattice design, is used for comparison with the GBC-68 models to provide an indication of the possible range of validation results from different design basis BWR lattices. Peak reactivity for the SFP rack lattice was at a burnup of approximately 11 GWd/MTU, and the fuel was modeled with AFP compositions.

4.4.1 Vanished Lattice with Actinide-Only Modeling

The complete set of 1643 critical experiment SDFs is compared against the GBC-68 model with the vanished lattice with AO nuclide modeling for the BWR assembly. A plot of the resulting c_k values is shown in Figure 4.1. Each category of experiments is shown as a different data set, regardless of the source of the SDF. As evident from the figure, only a limited number of experiments is similar enough to the BWR peak reactivity model to have a c_k value of 0.8 or greater. All of these suitably similar experiments are LEU-COMP-THERM cases. Seventy-six cases are identified as being similar and applicable for validation. Three cases are excluded because of aberrant k_{eff} results likely resulting from poorly quantified compositions in the experiment, and two cases are excluded because the fissile material is UF_6 instead of UO_2 . A list of the 71 remaining cases and their c_k values is included in Appendix D. A plot of the c_k values showing each evaluation as a different series is provided in Figure 4.2.

The highest c_k values come from LEU-COMP-THERM-008, followed by LEU-COMP-THERM-051 and then the LEU-COMP-THERM-011; the top 44 c_k values come from these three evaluations. This is of potential concern because all three evaluations were performed at the same laboratory, the Babcock and Wilcox (B&W) Lynchburg Research Center, using the same fuel rods [19]. Ideally, a variety of experiments from different facilities involving different fuel, experimental facilities, and experimenters would provide a broader population of similar experiments to consider. The potential for correlation among the experiments may need to be considered when a large number of experiments are used incorporating many similar features, though the impact of this is as yet unclear and is under investigation [26, 27, 28]. At this time, the applicable ANSI/ANS standard [17] requires validation with experiments that are as similar

as possible to the safety application, but the standard does not address the potential impact of experimental correlations. None of the experiments identified as being sufficiently similar to the GBC-68 cask contain plutonium, thus indicating that a penalty should be developed to cover the unvalidated nuclides. A discussion of this penalty factor is provided in Section 4.6.

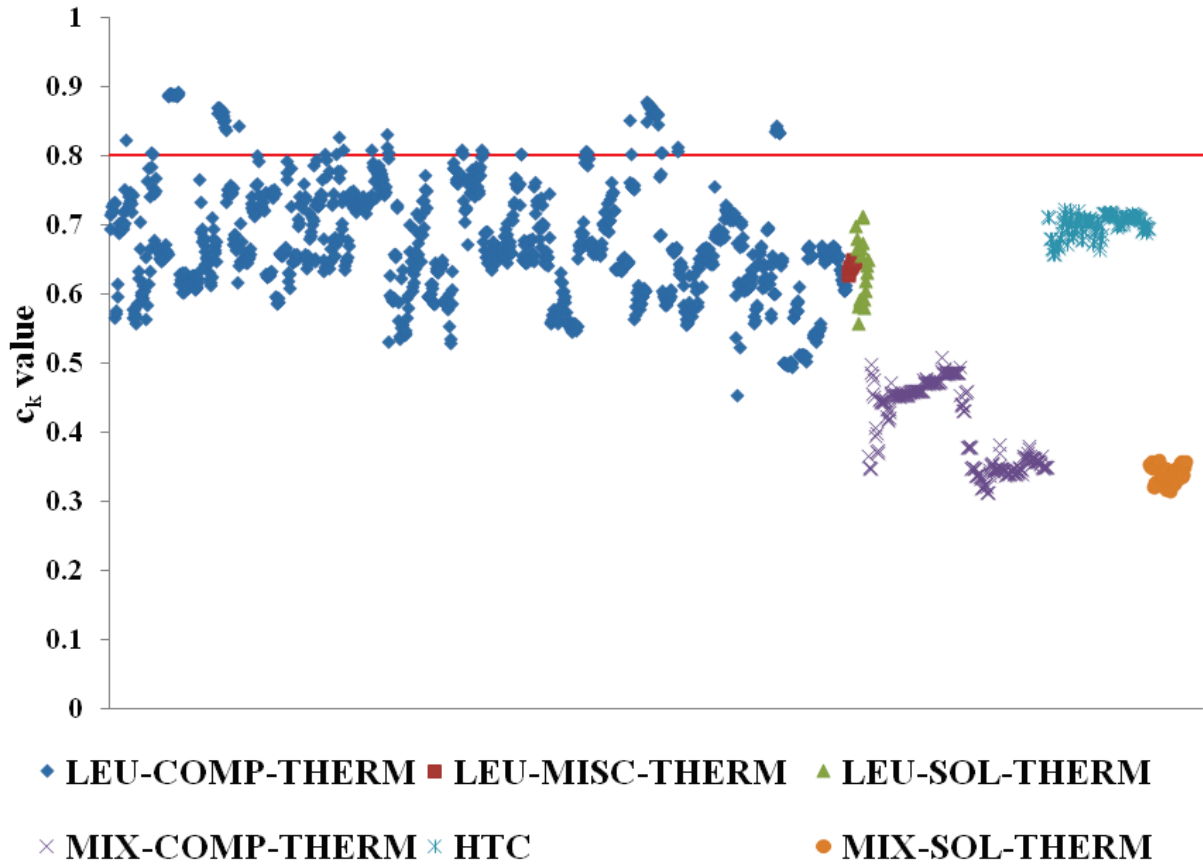


Figure 4.1. c_k values for critical experiments compared to GBC-68 with vanished lattice and AO nuclides.

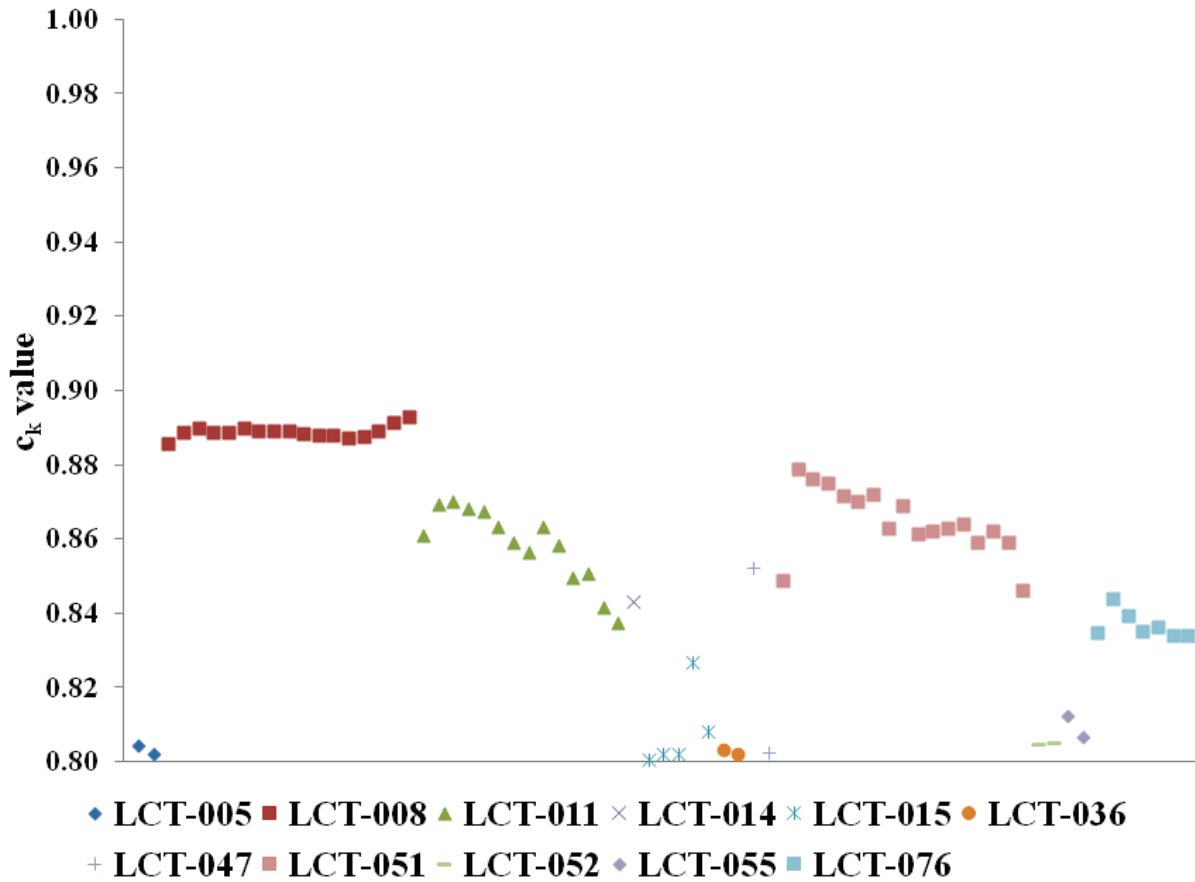


Figure 4.2. c_k values greater than or equal to 0.8 with vanished lattice and AO nuclides.

4.4.2 Vanished Lattice with Actinide and Fission Product Modeling

The complete set of 1643 critical experiment SDFs is also compared against the GBC-68 model with the vanished lattice with AFP nuclide modeling for the BWR assembly. A plot of the resulting c_k values is shown in Figure 4.3. The cases with a c_k value over 0.8 are nearly identical to those for the AO model. All suitably similar experiments are LEU-COMP-THERM cases. Sixty-seven cases are identified as being similar and applicable for validation. Three cases are excluded because of aberrant k_{eff} results likely resulting from poorly quantified compositions in the experiment, and two cases are excluded because the fissile material is UF_6 instead of UO_2 . A list of the 62 remaining cases and their c_k values is included in Appendix D. A plot of the c_k values showing each evaluation as a different series is provided in Figure 4.4.

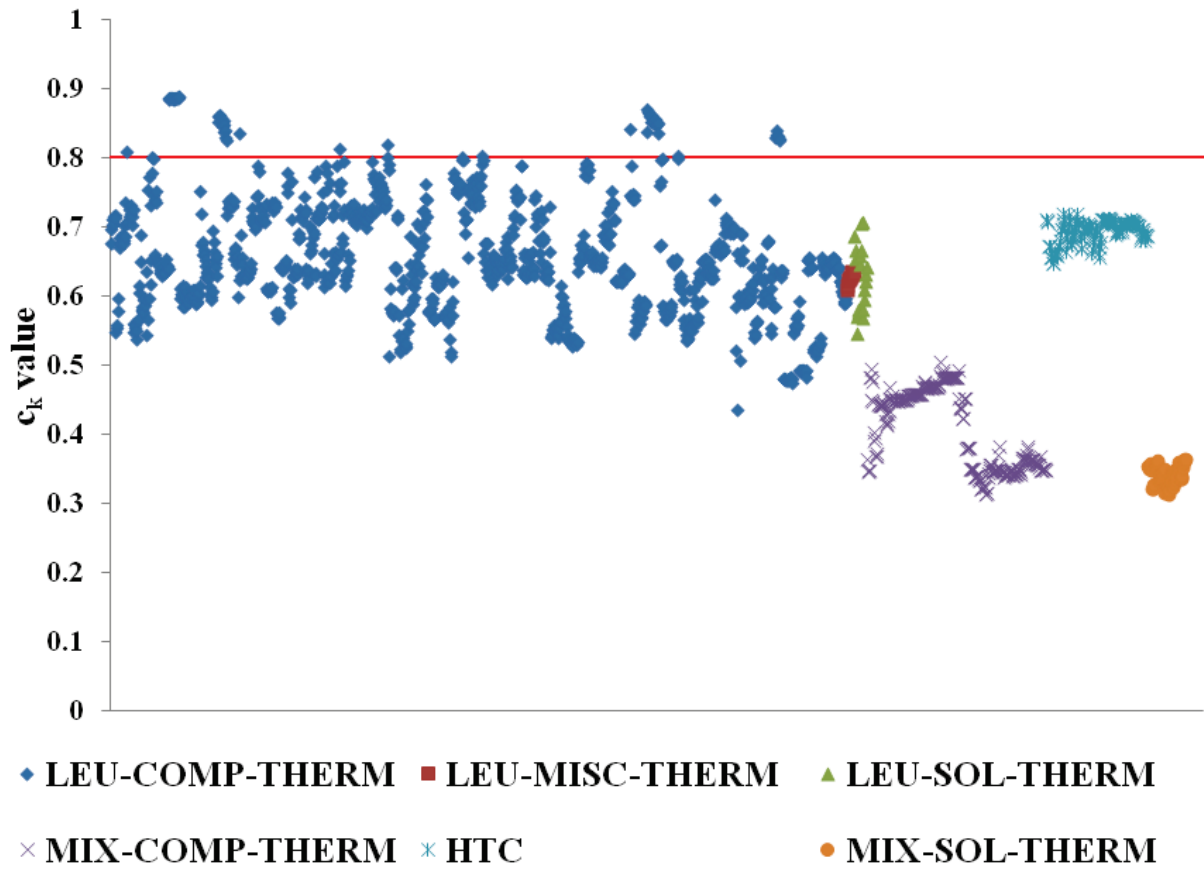


Figure 4.3. c_k values for critical experiments compared to GBC-68 with vanished lattice and AFP nuclides.

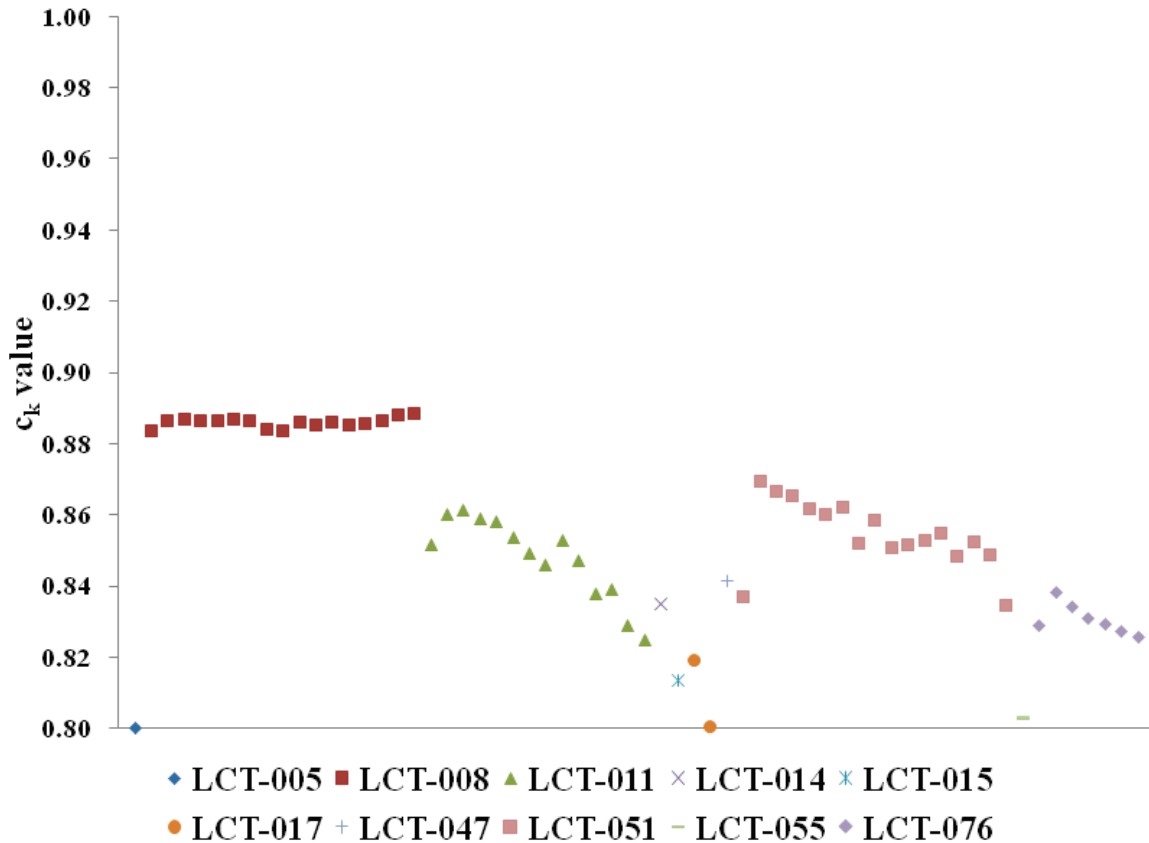


Figure 4.4. c_k values greater than or equal to 0.8 with vanished lattice and AFP nuclides.

The AFP validation cases contain the same potential weakness with regard to potential experiment correlations discussed in the previous section. Again, the top 44 cases come from the three evaluations based on the B&W experiments, though this makes up a larger fraction of the total population for this case than for the AO results discussed above.

There is a slight reduction in the number of experiments with acceptable similarity for use in validation compared to the AO case, and the cases that still exceed the 0.8 c_k threshold generally have lower c_k values. This is mostly a result of the addition of fission products to the model, most of which, as discussed further below, are not represented in the critical experiments. The effect is small, with c_k values dropping by 0.01 or less in most cases. Some cases show higher similarity with the fuel, including actinides and fission products condition, though this difference is also typically small.

Only one case, LEU-COMP-THERM-005-010, contains gadolinium. The gadolinium in the experiment was dissolved in the moderator and was not present in absorber rods. Another difficulty is that the experiment contained natural gadolinium, consisting of a range of nuclides including 14.8 atom% ^{155}Gd and 15.65 atom% ^{157}Gd [29]. Only ^{155}Gd is included in the AFP nuclide set, as shown in Table 3.1. The majority of the residual gadolinium poison at peak reactivity is also ^{155}Gd . Natural gadolinium does not have an appropriate isotopic mixture for

validating residual or fission product gadolinium in BWR fuel at peak reactivity. An additional problem is that validation is not possible with only a single benchmark case.

A comparison of the total ^{155}Gd sensitivity profiles for the GBC-68 model and LEU-COMP-THERM-005-010 are shown in Figure 4.5.

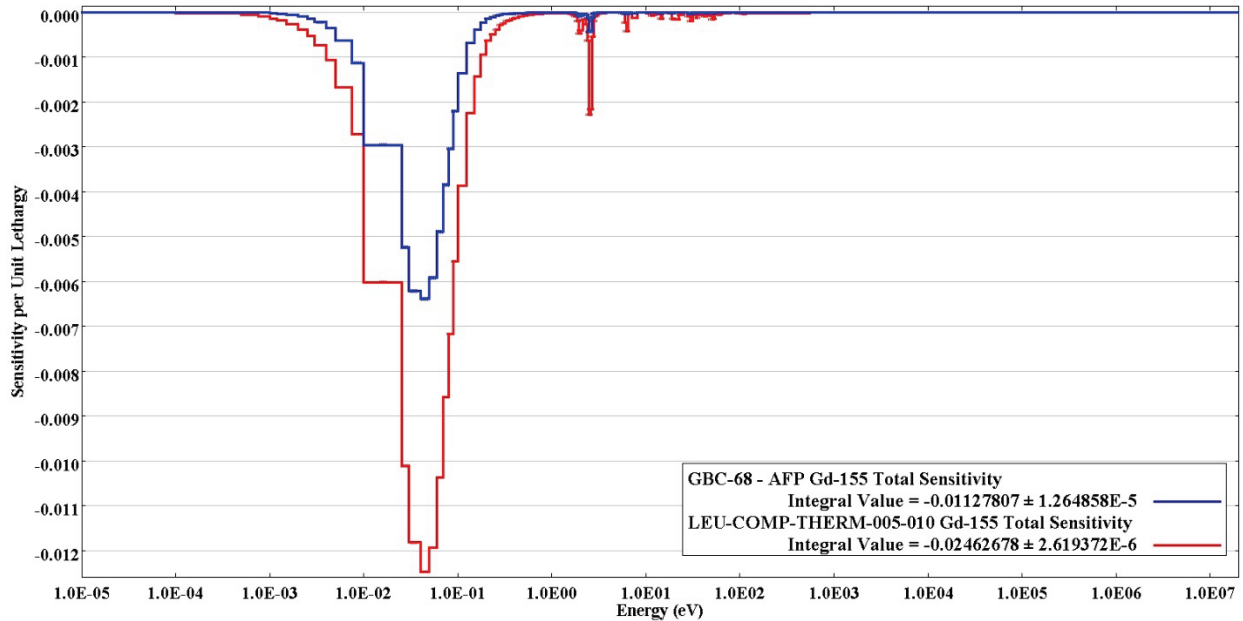


Figure 4.5. Sensitivity profile comparison for ^{155}Gd between GBC-68 with vanished lattice and LEU-COMP-THERM-005-010.

Approximately 93% of the ^{155}Gd sensitivity comes from the mixtures used to model the gadolinium-bearing fuel rods, so the majority of the sensitivity is contributed by residual gadolinium and not fission product gadolinium. There is no method to separate the two gadolinium sources within the TSUNAMI codes. As shown in the figure, the energy-dependent behavior of the profiles is in good agreement, but the sensitivity in the critical experiment is more than twice the magnitude of that in the GBC-68 model. The integral sensitivity in the critical experiment is approximately -0.025 as compared to -0.011 in the storage and transportation cask. A critical experiment with a lower gadolinium loading might show better agreement with the application sensitivity for ^{155}Gd .

As noted previously, none of the experiments identified as candidates for validation contain plutonium, so a penalty for extended area of applicability may be necessary, as well as for residual gadolinium poison. None of the experiments contain any fission products other than gadolinium, necessitating an evaluation of a potential validation penalty for unvalidated nuclides. A discussion of these penalty factors is provided in Section 4.6.

4.4.3 Full Lattice with Actinide and Fission Product Modeling

The complete set of 1643 critical experiment SDFs is also compared against the GBC-68 model with the full lattice with AFP nuclide modeling for the BWR assembly. A plot of the resulting c_k values is shown in Figure 4.6.

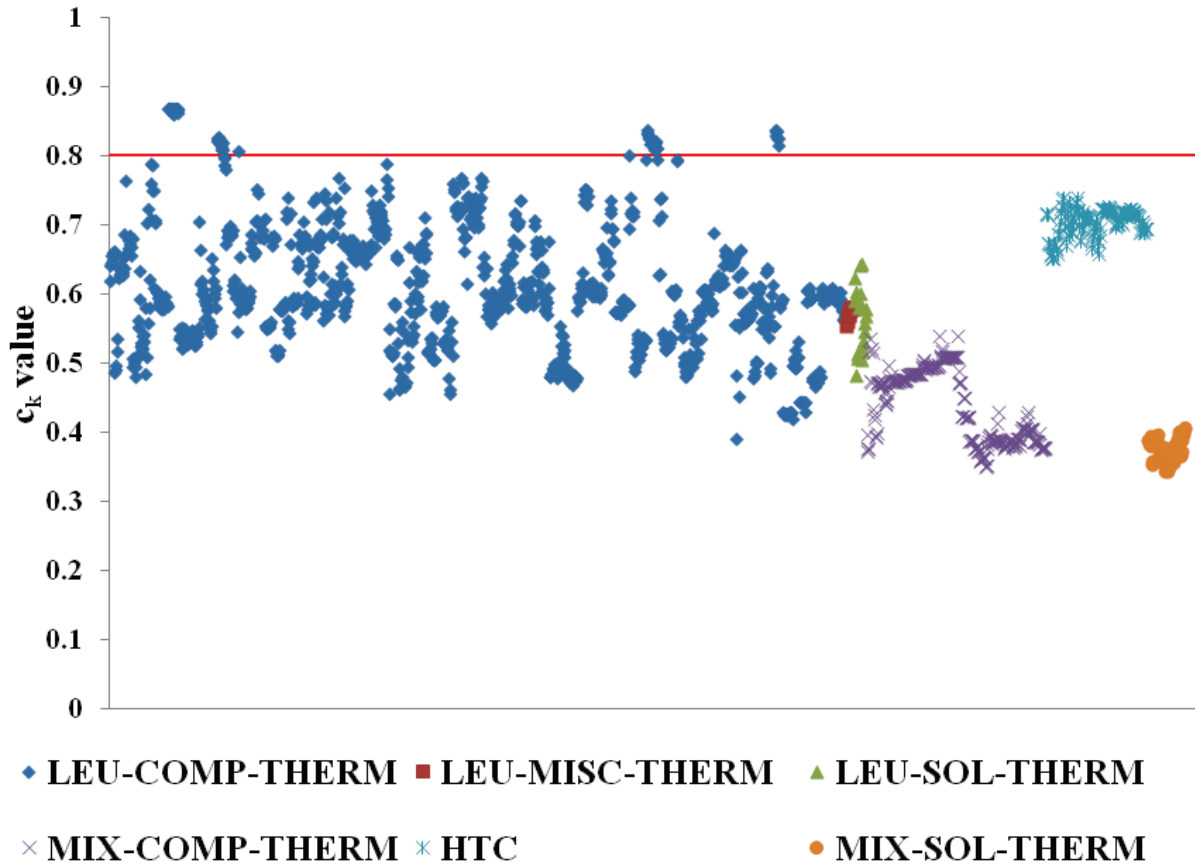


Figure 4.6. Values for critical experiments compared to GBC-68 with full lattice and AFP nuclides.

As in the two previous comparisons, only a limited number of experiments is similar enough to the BWR peak reactivity model to have a c_k value over 0.8. All of these suitably similar experiments are LEU-COMP-THERM cases. Fifty-three cases are identified as being similar and applicable for validation. Two cases are excluded because of aberrant k_{eff} results likely resulting from poorly quantified compositions in the experiment. A list of the 51 remaining cases and their c_k values is included in Appendix D. A plot of the c_k values showing each evaluation as a different series is provided in Figure 4.7.

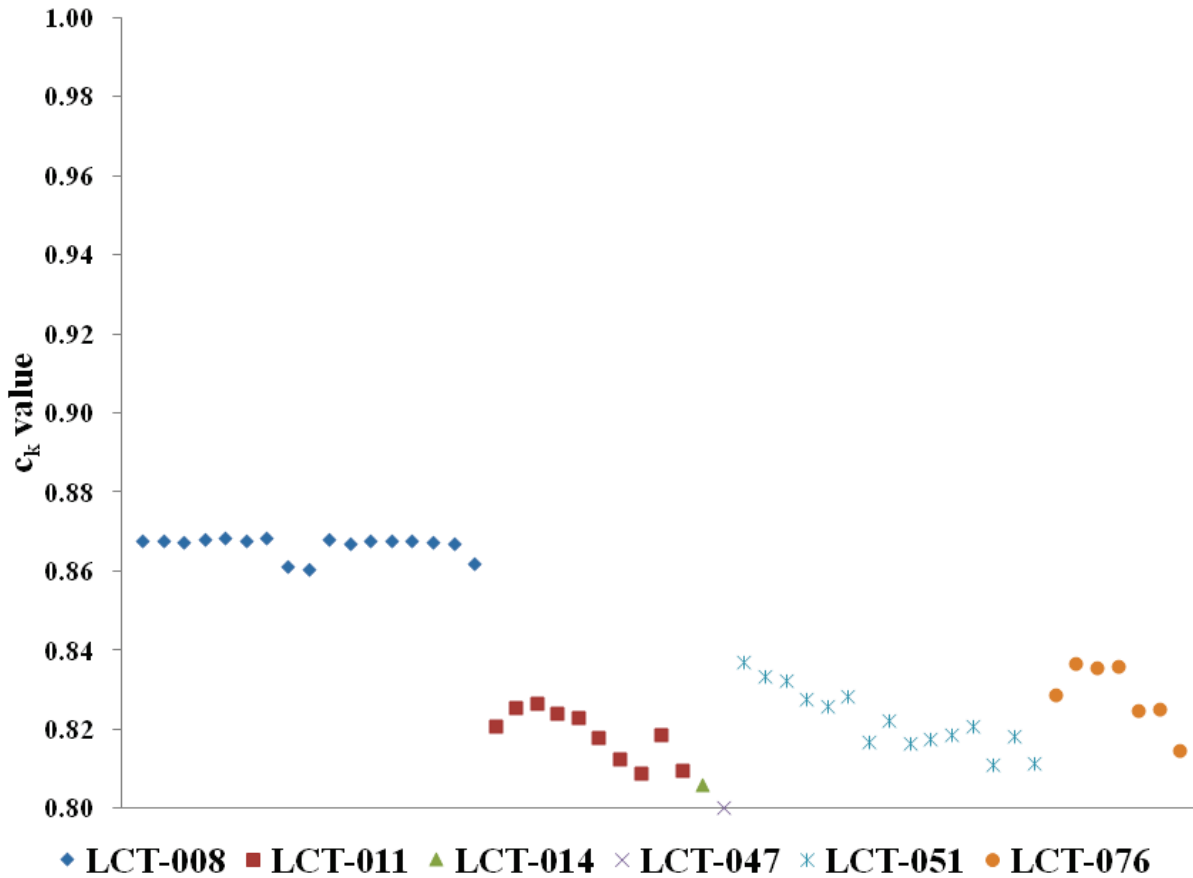


Figure 4.7. c_k values greater than or equal to 0.8 with full lattice and AFP nuclides.

The AFP validation cases contain the same potential weakness with regard to potential experiment correlations discussed in the previous two sections. The top 18 cases, and 42 of the 51 total cases, come from the three evaluations based on the B&W experiments. There is also a significant reduction in the number of evaluations that have at least one case with a c_k value over 0.8, potentially weakening the validation.

The number of experiments with an acceptable degree of similarity with the full lattice is lower than for the vanished lattice, even considering the same nuclide set. This change is largely driven by the differences in neutron spectrum between the vanished and full lattices. The full lattice has a significantly harder spectrum, with an energy-of-average-lethargy-of-fission (EALF) of 0.339 eV, compared with the vanished lattice, which has an EALF of 0.222 eV. The replacement of fuel rods with water in the vanished lattice introduces significant moderation within the lattice, thus softening the neutron spectrum. Figure 4.8 shows the change in c_k value for each of the 51 candidate experiments for validation of the full lattice model as a function of EALF.

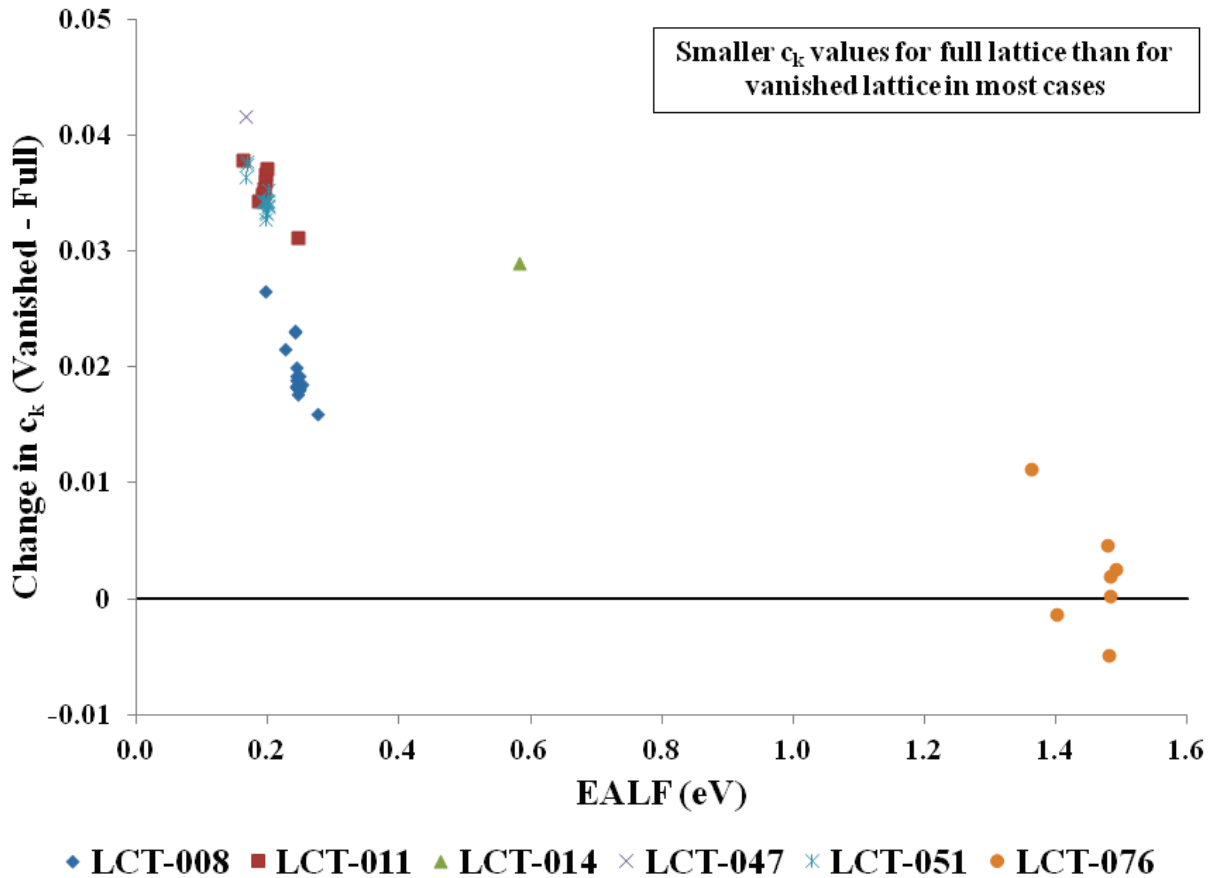


Figure 4.8. Changes in c_k values between vanished lattice and full lattice.

It is evident that experiments with an EALF around 0.25 eV have significant reductions in c_k for the full lattice, while experiments with EALF values around 1 eV show little change in c_k at all. This indicates that critical experiments with harder spectra could provide additional useful validation cases, if such cases can be identified.

As noted previously, none of the experiments identified as candidates for validation contain plutonium so a penalty for extended area of applicability may be necessary. None of the experiments contain any fission products, necessitating an evaluation of a potential validation penalty for unvalidated nuclides. A discussion of these penalty factors is provided in Section 4.6.

4.5 BIAS AND UNCERTAINTY DETERMINATION

One of the primary purposes of validation is to determine a bias and bias uncertainty associated with the computational method employed in a criticality safety analysis. The bias provides a measure of the difference between a computational result and the behavior of the real system. The bias is generally defined as shown in Equation 2 [22].

$$\beta = \overline{k_{eff}} - 1 \quad (2)$$

Where: β is the bias

$\overline{k_{eff}}$ is the average calculated k_{eff} for the experiments in the benchmark suite

One result of this definition is that a negative bias indicates that the computational method under predicts neutron multiplication, so this bias must be applied to the numerical results to ensure that a system predicted to be subcritical is in fact subcritical. Conversely, a positive bias indicates that the numerical simulation over predicts k_{eff} , though credit for this is generally not recommended [17].

This section provides a brief examination of the potential bias and bias uncertainty that could result from validation for a peak reactivity analysis of BWR fuel in a storage and transportation cask. The results presented here are not rigorous or complete and should not be used in lieu of performing an application-specific validation. Guidance on performing and documenting a complete validation can be found in References 22 and 23. Also, results are presented for only the vanished lattice with AFP modeling of the fuel composition; results for the AO model or the full lattice would be similar and thus are not presented. Results are presented for a non-trending method, a traditional trending analysis considering enrichment and EALF as trending parameters, and for a TSUNAMI-based validation based on c_k trending.

For each of the 62 experiments used in this sample validation, the calculated-to-expected (C/E) ratio is determined based on SCALE calculations using KENO V.a or KENO-VI in SCALE 6.1.2. As mentioned previously, multiple transport codes should not be pooled in a single validation because validation applies to a specific computational method. In this case, the practice is acceptable as a demonstration of methods and as an expediency to generate a large enough pool of acceptable candidates based on pre-existing models. Recent studies [30] have shown good agreement between KENO V.a and KENO-VI for identical models, so the pooling of results is not expected to have a significant effect on the results. The C/E ratio, enrichment, and EALF for each case considered in this sample validation are provided in Appendix D. The c_k values are provided in Appendix D.

The normality of the distribution of experiment set results was evaluated using 5- and 11-bin χ^2 normality tests. These tests show that there is greater than 95% confidence that the results are not normally distributed. This deficiency is not addressed here because this demonstration is not intended as a full validation example. For simplicity, a sample validation is performed as if normality had been demonstrated. Consideration of other methods, including a non-parametric approach, may be needed for validation of criticality safety calculations with a validation suite that fails normality tests. Given the fact that more than 50 experiments with acceptable similarity have been identified, the non-parametric penalty is likely to be negligible. Therefore, the bias and bias uncertainty could be determined by a straightforward process of evaluating several of the calculated benchmark cases with the least conservative k_{eff} values.

4.5.1 Bias and Uncertainty without Trending Analysis

Prior to examining the data set for trends, a non-trending bias and bias uncertainty should be established [22]. This bias and bias uncertainty would be used if no trends are identified or accepted, or if the non-trending bias and bias uncertainty have a larger magnitude than those resulting from trending analyses. The non-trending method used is the simultaneous one-sided lower tolerance limit with inverse variance weighting of the data points [22]. For the data considered here, the resulting bias is -0.00354, and the 95%/95% bias uncertainty is 0.00526, making the combined bias and uncertainty -0.00879.

4.5.2 Traditional Trending Analysis

Trending analysis is recommended for validation analyses [22, 17] and can be useful in determining the most appropriate bias to apply for a particular safety application case or providing insight on potential causes of bias. In most validations, the assessment of the validity of trends has been judged by the coefficient of determination, R^2 . This metric can be a poor measure of the validity of a trend in cases with significant scatter in the data set, as is typical for many validation sets. More robust statistical testing should be performed to determine the probability that a fit is better than random and to determine the probability that the slope is non-zero. These determinations can be made with an F-test and a Student's T-test, respectively. Many different system parameters can be used as the independent parameter for trending, including enrichment, fuel pin pitch, spectral measures, poison content, and others. In this analysis, two common bias trending parameters, enrichment and EALF, are used to examine potential bias and bias uncertainty values resulting from the validation of BWR fuel at peak reactivity in a storage and transportation cask. The confidence band with administrative margin method, upper safety limit (USL)-1, as determined by the Upper Safety Limit Statistics (USLSTATS) module in SCALE [23], is used to determine the bias and bias uncertainty in the trending analyses.

The bias and bias uncertainty values for both trending parameters are shown in Table 4.1.

Table 4.1. Bias and bias uncertainty values

Trend parameter	Parameter value	Bias	95%/95% bias uncertainty	Combined bias and uncertainty
Enrichment	3.51 wt% ^{235}U	-0.00136	0.00604	-0.00740
EALF	0.2217 eV	-0.00396	0.00577	-0.00973

The enrichment trend, combined bias, and bias uncertainty from both trending and non-trending methods are shown in Figure 4.9; the EALF trend and limits are shown in Figure 4.10. The limits in the figures are shown relative to a k_{eff} limit of 1 to facilitate the comparison of the limits to the data. The limits as implemented in a specific application would instead be applied relative to the subcritical limit.

The combined bias and uncertainty for the non-trending and trending methods are generally in good agreement, ranging from -0.00740 to -0.00973. The bias varies significantly, especially between the enrichment trend and the EALF trend, but the uncertainty values are largely consistent. Figure 4.9 shows that as the enrichment trend passes above 1, USL-1 stops increasing. Beyond this point, the uncertainty of 0.00604 is applied with no credit for the positive

bias. The trend relative to EALF does not get to a best estimate bias of 1, so there is no flat portion to USL-1 for that case. At the parameter values of interest, the bias and uncertainty resulting from the enrichment trend are smaller than the non-trending method, but the largest bias and largest combined bias and uncertainty result from the EALF trend. The overall results of all three methods show reasonable agreement in magnitude.

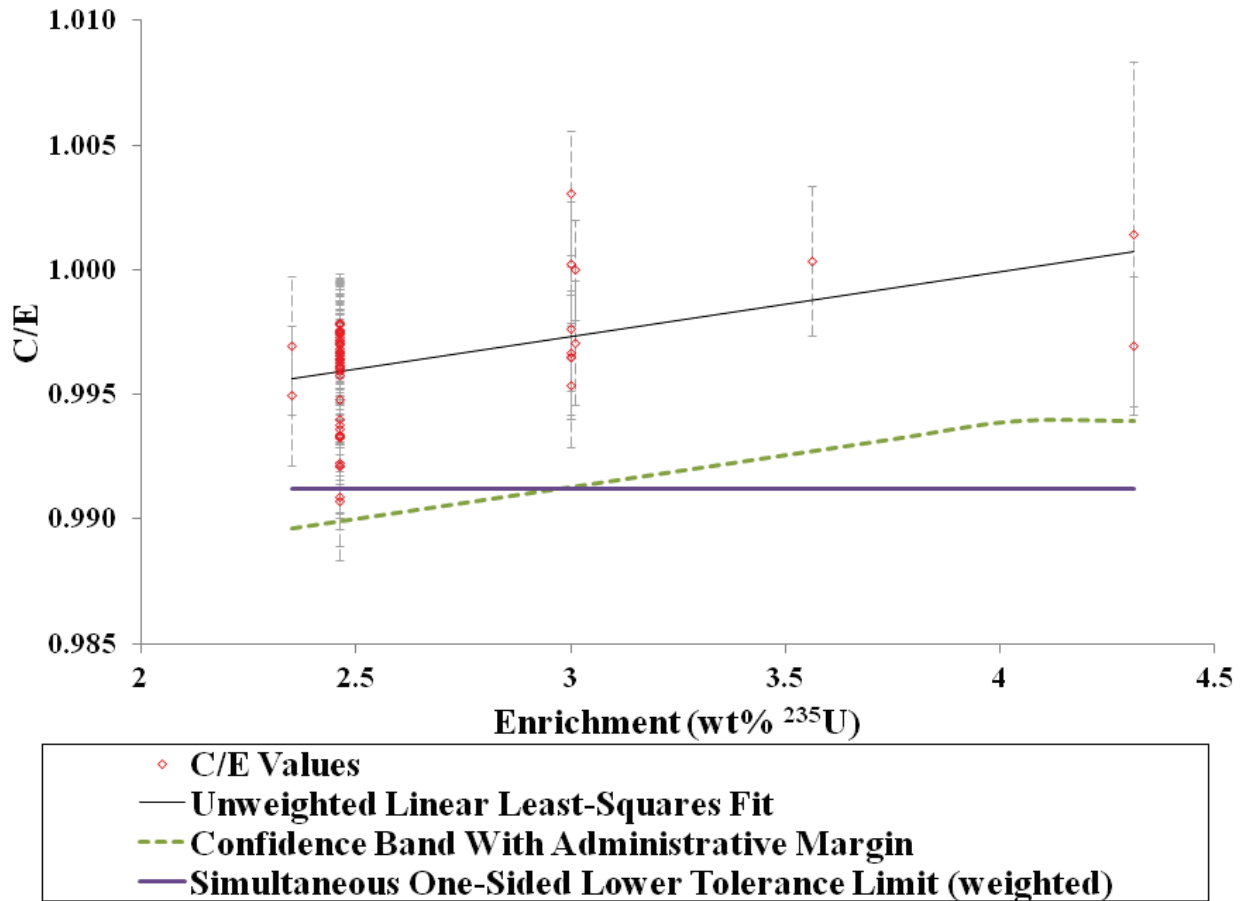


Figure 4.9. C/E trend and limits as a function of enrichment.

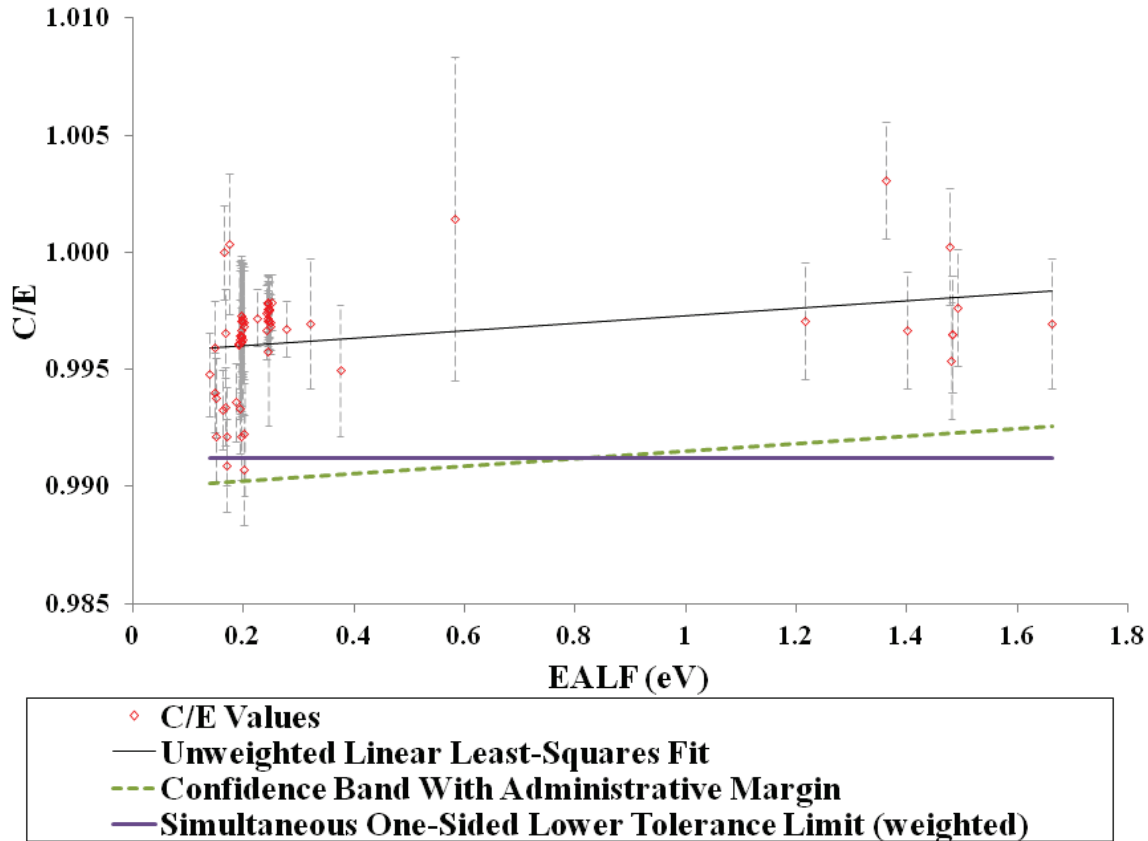


Figure 4.10. C/E trend and limits as a function of EALF.

4.5.3 c_k Trending

One nontraditional trending approach that can be used with TSUNAMI-IP results is c_k trending. This technique uses a linear least-squares fit of the C/E values as a function of c_k and extrapolates to determine the bias at a c_k value of 1.0. This c_k value represents perfect similarity, which can essentially only be achieved by the application system itself. This approach can also be interpreted as massively multi-parameter interpolation; all possible differences are removed from the critical experiment as the c_k approaches 1, whether they are caused by changes in enrichment, neutron energy spectrum, fissile materials or isotopic distributions, absorber materials, or any other causes. This method is described more fully in Section 9.1 of the TSUNAMI Primer [31].

There are potential disadvantages to c_k trending, some of which are potentially important to this sample validation. The primary potential weakness of this method is that it can lead to inaccurate estimates of the bias for experiment sets that do not have c_k values near 1. An example of this problem is provided in Reference 32. The bias for a sample validation system is calculated to be -0.0065 using experiments with c_k values greater than 0.95, but the bias estimate from experiments with c_k values between 0.8 and 0.9 is 0.0084. The change in the estimate of the system bias is more than 1% Δk ; the former estimate is known to be more accurate because the application in this system was a measured critical configuration. Another difficulty with this

technique is that the uncertainty band applied is non-linear, and it expands as the extrapolation grows. The uncertainty band can increase width quickly, and the resulting penalty can become significant.

The trend of C/E data as a function of c_k is shown in Figure 4.11. The best estimate of the bias is calculated using the linear fit of the C/E values, shown as the blue solid line. USL-1 is shown in the red dashed line, and it incorporates the best estimate of the bias and the 95%/95% uncertainty in the prediction for the C/E value of the next sample from this distribution. The non-linear behavior of the uncertainty is evident as USL-1 is dropping for c_k values higher than the known data points, despite the increasing bias trend. The estimate of the bias with a c_k value of 1 is -0.00275 with an uncertainty of 0.00695, which provides a combined bias and bias uncertainty of -0.00970. These results are in good agreement with the traditional trending and non-trending results presented previously.

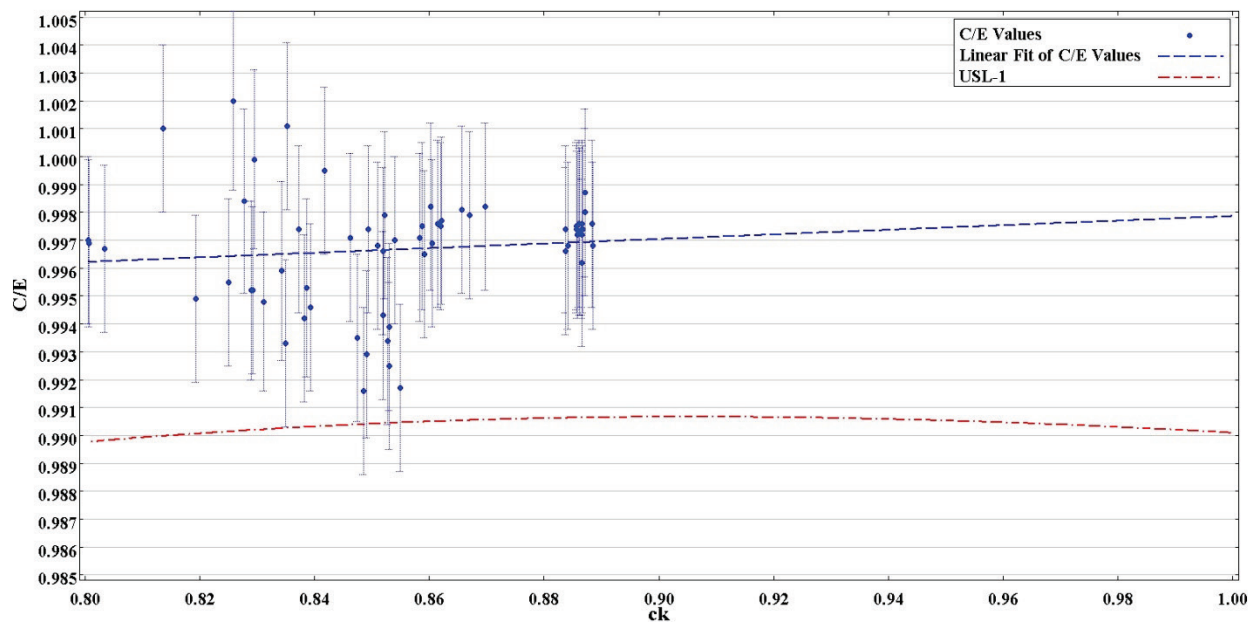


Figure 4.11. C/E trend and limits as a function of c_k .

4.6 PENALTIES FOR UNVALIDATED NUCLIDES

Any gaps in a validation must be identified and addressed [22, 23]. The sample validation results presented in the previous section all lack validation for several key nuclides, including plutonium, residual gadolinium, and fission products. A method for using TSUNAMI sensitivity/uncertainty (S/U) analysis to provide a quantitative estimate of such penalty factors is provided in NUREG/CR-7109 [13]. Similar techniques will be used in this section to illustrate the application of S/U tools for BWR fuel storage and transportation casks. The penalties will be estimated for the GBC-68 cask that has been used throughout this report, and the BWR SFP application case from NUREG/CR-7109 [13] will also be considered to provide an estimate of the potential range of the penalties. Penalties for plutonium, residual gadolinium, and fission products will be addressed separately in the following sections.

The S/U analysis approach is predicated on the assumptions that (1) the vast majority of the computational method-related biases will be captured by the validation study, (2) the primary cause of validation biases is nuclear data errors, and (3) these errors are bounded by the reported nuclear data uncertainties. The nuclear data uncertainty can then be multiplied by the sensitivity of the system k_{eff} to that nuclear data to translate the nuclear data uncertainty into a k_{eff} uncertainty. For this application, TSUNAMI performs this assessment in an energy-dependent manner using the SCALE covariance library and the sensitivities calculated by TSUNAMI-3D. As discussed in NUREG/CR-7109 [13], the nuclear data uncertainties are 1-sigma values from the covariance library, so the TSUNAMI-calculated results would need to be doubled to reach 2-sigma and hence 95% confidence. Comparisons of the TSUNAMI estimates of k_{eff} uncertainty resulting from nuclear data indicate that the nuclear data uncertainties are significantly overestimated [13], so this additional penalty (i.e., 2-sigma versus 1-sigma) may not be necessary, but it is expected to be conservative. The undercoverage penalty factors developed in this section are not generically applicable because only a limited number of lattices were considered. The factors should not be used directly in any licensing application.

4.6.1 Plutonium

All of the experiments identified as suitably similar for use in validation are LEU-COMP-THERM experiments and as such do not contain plutonium. Several options exist for addressing this validation gap, including adding experiments with plutonium to the validation suite despite low c_k values or S/U analysis to assess the potential bias due to unvalidated plutonium nuclides. An S/U analysis is presented in this section to generate a conservative estimate for a penalty for lack of validation coverage for plutonium in the validation experiments used in this report.

The uncertainty in system multiplication can be estimated, as mentioned above, by multiplying the nuclear data uncertainty by the reactivity sensitivity of any nuclide or reaction of interest. In this case, the plutonium nuclides credited in the GBC-68 cask model are the nuclides of interest. The uncertainty due to plutonium was determined for the GBC-68 model with the vanished lattice considering both AO and AFP compositions, the GBC-68 model with the full lattice and AFP compositions, and the BWR SFP application case from NUREG/CR-7109 [13] with AFP compositions. These cases were selected to examine the sensitivity of the plutonium uncertainty to different nuclide sets, different lattices, and different peak reactivity burnups. Peak reactivity for the GBC-68 models with actinides and fission products is at approximately 7.5 GWd/MTU; peak reactivity for the BWR SFP model is 11 GWd/MTU [13].

The uncertainty in system reactivity is determined by TSUNAMI-IP for each reaction for each nuclide in the model. These individual reaction contributions can be combined to determine the total uncertainty contribution by nuclide. The total plutonium contribution to reactivity uncertainty can be determined by combining the individual nuclides in the same manner.

The contributions for each of the plutonium nuclides and the total contribution for each of the models considered are shown in Table 4.2. The uncertainty contribution for ^{241}Am is also shown, but ^{239}Pu is the only relevant nuclide since the other transuranic nuclides have uncertainties at least two orders of magnitude lower.

Table 4.2. Uncertainty contributions from major transuranic nuclides

Nuclide	1-Sigma Uncertainty (% Δk)			
	GBC-68			SFP AFP
	Vanished AO	Vanished AFP	Full AFP	
²³⁸ Pu	6.55E-05	6.27E-05	8.76E-05	1.24E-04
²³⁹ Pu	1.38E-01	1.33E-01	1.53E-01	1.54E-01
²⁴⁰ Pu	7.83E-03	7.34E-03	9.10E-03	1.13E-02
²⁴¹ Pu	1.67E-03	1.64E-03	1.99E-03	3.28E-03
²⁴² Pu	1.74E-04	1.65E-04	2.58E-04	4.96E-04
²⁴¹ Am	8.84E-04	8.27E-04	1.17E-03	1.07E-04
Total	0.138	0.134	0.153	0.155

The results indicate that the system uncertainty due to plutonium is dependent on lattice type, but the uncertainty is not strongly dependent on the presence of fission products. The two vanished lattices have approximately 0.14% Δk uncertainty due to plutonium, while the two full lattices have slightly more uncertainty. The higher uncertainty in the full lattices is caused by larger plutonium sensitivities that result from larger plutonium number densities due to the harder neutron spectrum in the full lattice during depletion. The burnup of peak reactivity does not appear to have a strong effect on this result, as the difference in the full lattice uncertainties for GBC-68 vs. SFP is less than 0.005% Δk .

The uncertainties edited by TSUNAMI-IP represent 1-sigma confidence and thus should be doubled to represent 95% confidence of bounding the true bias for plutonium. Based on these results, a penalty of approximately 0.3% Δk should be sufficient to account for lack of plutonium validation in both full and vanished lattices. This penalty is applicable over most of the peak reactivity range for design basis lattices and would apply to AO or AFP analyses.

4.6.2 Residual Gadolinium

The AFP nuclide set contains ¹⁵⁵Gd, which is a component in natural gadolinium as loaded into BWR fuel as a burnable absorber. In the gadolinium rods, it is impossible to separate the sensitivity of the residual burnable absorber gadolinium from the fission product gadolinium, but it is possible to compare the reactivity sensitivity of the ¹⁵⁵Gd in the gadolinium rod mixtures to that of the SNF fission product ¹⁵⁵Gd to generate an estimate for the relative importance of fission product gadolinium compared to residual gadolinium.

From a comparison of ¹⁵⁵Gd in SNF at peak reactivity burnup with and without gadolinium poison after a five-year cooling time, approximately 93% of the ¹⁵⁵Gd sensitivity in the vanished lattice GBC-68 models comes from the fuel mixtures initially loaded with gadolinium poison, so it is apparent that the majority of the ¹⁵⁵Gd impact is due to residual burnable absorber. An S/U analysis can be used to generate a penalty factor for lack of coverage of the residual gadolinium in the validation suite based on the total ¹⁵⁵Gd sensitivity in the model, so it will conservatively include both fission product and residual gadolinium.

The uncertainty in system reactivity due to ¹⁵⁵Gd nuclear data uncertainties is shown in Table 4.3 for the GBC-68 model, with the vanished and full lattices with AFP representations of the fuel, and for the full lattice in the SFP application considered in NUREG/CR-7109 [13].

Table 4.3. Uncertainty contribution from ¹⁵⁵Gd

Model	Uncertainty (% Δk)
GBC-68 vanished	0.015
GBC-68 full	0.019
SFP full	0.024

The uncertainty contribution increases in the full lattice compared to the vanished lattice, and it is higher for the SFP model than for the GBC-68 model. However, these uncertainties are small for all three cases. In the GBC-68 models, this uncertainty represents about 1.25% of the ¹⁵⁵Gd worth for the vanished lattice and about 1.37% for the full lattice.

A bounding estimate for the 1-sigma uncertainty in system reactivity due to ¹⁵⁵Gd in the three models studied here is 0.025% Δk , which would result in a 2-sigma penalty of 0.05%. The penalty is relatively small, so added conservatism in this area will not significantly increase the conservatism of the analysis. Note that these uncertainties do not include the uncertainty in the calculation of residual gadolinium number densities. This depletion uncertainty is addressed in Section 5.

4.6.3 Fission Products and Minor Actinides

The worth of the major (i.e., top 16) fission products and minor actinides is approximately 3.6% Δk , as shown in Section 3.4.1. This section develops a penalty factor for major fission products and minor actinides for which no critical experiments are available. The penalty factor determined does not include consideration of ¹⁵⁵Gd, as that nuclide was considered explicitly in the previous section.

The major fission products considered in the AFP nuclide set are provided in Table 3.1 in Section 3.2.2. The minor actinides considered, ²³⁶U, ²³⁷Np, and ²⁴³Am, are also listed. The uncertainty contributions and totals for these 19 nuclides are provided in Table 4.4. The models considered are the GBC-68 with the vanished and full lattices and the BWR SFP application from NUREG/CR-7109 [13]. The main contributors to uncertainty are ¹⁴⁹Sm, ¹⁴³Nd, and ²³⁶U consistently across all three models. The uncertainties increase from vanished to full lattice and from the GBC-68 to the SFP. The higher uncertainties in the SFP model result from higher sensitivities caused by a higher burnup at peak reactivity. The uncertainty due to fission products and minor actinides ranges from 0.020% Δk for the GBC-68 model to 0.027% Δk for the SFP model.

A bounding estimate of the uncertainty due to minor actinides and major fission products based on the models examined here is 0.03% Δk , which would lead to a 2-sigma conservative estimate of 0.06% Δk . The 1-sigma uncertainty determined from fission products and minor actinides is equal to about 0.55% of their worth in the cask model. This would be bounded by the conservative bias estimate of 1.5% of the worth of the major fission products and minor actinides from recommendation 2 in Section 8 of NUREG/CR-7109 [13]. The total worth was less than 0.04 Δk , so the criterion that the total minor actinide and FP nuclide worth not exceed 0.1 Δk for application of recommendation 2 is also met. Implementation of this recommendation would add

a small additional penalty, but this would allow common treatment of this validation penalty between BWR and PWR analyses.

Table 4.4. Uncertainty contribution from major fission products and minor actinides

Nuclide	1-Sigma Uncertainty (% Δk)		
	GBC-68		SFP full
	Vanished	Full	
⁹⁵ Mo	1.31E-03	1.62E-03	1.70E-03
⁹⁹ Tc	1.96E-03	2.14E-03	2.99E-03
¹⁰¹ Ru	1.65E-03	2.05E-03	3.23E-03
¹⁰³ Rh	5.38E-03	6.75E-03	8.32E-03
¹⁰⁹ Ag	1.95E-04	2.65E-04	3.98E-04
¹³³ Cs	4.33E-03	5.25E-03	7.74E-03
¹⁴⁷ Sm	1.60E-03	1.90E-03	4.77E-04
¹⁴⁹ Sm	1.09E-02	1.13E-02	1.01E-02
¹⁵⁰ Sm	1.02E-03	1.14E-03	1.65E-03
¹⁵¹ Sm	6.02E-03	5.97E-03	6.06E-03
¹⁵² Sm	1.62E-03	1.95E-03	2.96E-03
¹⁴³ Nd	9.94E-03	1.04E-02	1.37E-02
¹⁴⁵ Nd	4.09E-03	5.10E-03	7.89E-03
¹⁵¹ Eu	1.13E-04	1.23E-04	6.71E-06
¹⁵³ Eu	7.86E-04	1.00E-03	1.65E-03
²³⁶ U	8.05E-03	9.79E-03	1.33E-02
²³⁷ Np	1.00E-03	1.26E-03	1.46E-03
²⁴³ Am	1.92E-06	3.58E-06	7.63E-06
Total	0.020	0.022	0.027

4.7 SUMMARY OF VALIDATION OF CASK REACTIVITY CALCULATIONS

A series of studies has been performed to investigate validation of cask k_{eff} calculations. This section presents the results of these studies and provides recommendations for BWR peak reactivity validations that are analogous to those provided in NUREG/CR-7109 [13] for PWR validations.

Several sources of SDFs have been used, as discussed in Section 4.3, providing a large number of candidate experiments. In total, over 1600 unique experiments were compared against cases ranging from application cases to experiment cases with c_k values of 0.8 or higher.

A range of potentially useful experiments has been identified in Section 4.4 for use in AO or AFP analyses. GBC-68 applications with both the full and vanished lattices were considered. More than 50 experiments have been identified for each of these applications, allowing a sufficient population for validation. All experiments selected are LEU-COMP-THERM experiments and thus provide no validation of cross sections for transuranics, residual gadolinium, or for fission products.

A sample validation was presented in Section 4.5 using a non-trending method, a traditional trending method for enrichment and EALF, and a c_k trending method. The resulting bias and bias

uncertainty values were similar for each of the methods. The bias was approximately $-0.00300 \Delta k$, with an uncertainty of about $0.00600 \Delta k$. The limiting combination of bias and bias uncertainty is $-0.00973 \Delta k$ and results from EALF trending.

Although the number of critical experiments with satisfactory similarity is sufficient for statistical analysis, the lack of several important nuclides in the validation suite is problematic. Penalty factors would therefore be required to extend the area of applicability to include these nuclides. A sensitivity/uncertainty analysis approach similar to that described in NUREG/CR-7109 [13] was used to develop these factors in Section 4.6. The calculations showed that a penalty factor of about $0.3\% \Delta k$ for transuranics, plutonium, and americium was appropriate for the sample validation. The factor for residual gadolinium was calculated to be $0.05\% \Delta k$. The factor for remaining fission products and minor actinides was calculated to be about $0.06\% \Delta k$. These penalty factors are fairly small, so it is unlikely that additional conservatism in them would have a noticeable impact on the overall conservatism of the analysis.

Validation calculations can be performed in compliance with the consensus ANSI/ANS standard [17] and with prior NUREG/CR recommendations [22, 23]. It has been demonstrated that penalty factors can be established that extend the validation area of applicability to account for some nuclides that cannot be validated with critical experiments at this time. Overall, the validation of cask reactivity calculations, including fuel at peak reactivity, does not present a technical barrier that would prevent implementation of peak reactivity methods for demonstrating the criticality safety of BWR SNF in storage and transportation casks.

5 VALIDATION OF SPENT FUEL NUCLIDE COMPOSITIONS

The approach for validating BWR BUC criticality safety analyses near peak reactivity investigated in this report consists of separately validating the cask reactivity calculations and the SNF compositions used in those calculations. These validation studies are based primarily on experimental data. Section 4 discusses the validation of cask reactivity calculations. This section provides a review of studies performed to establish a technical basis for validating the SNF nuclide concentration in BWR SNF at peak reactivity, and the bias and uncertainty in the cask reactivity calculations associated with uncertainties in the SNF composition.

Validation of calculated SNF compositions is performed by comparison of calculated nuclide contents against measured concentrations in SNF samples from BWR assemblies obtained by destructive radiochemical analysis. This approach to validating the SNF calculations for use in criticality analyses is broadly accepted and applied by the international nuclear criticality safety community [33, 34, 35, 36]. Validation of a depletion code using measured fuel sample compositions requires accurate local irradiation conditions at the location of the sample to avoid introducing significant modeling bias caused by uncertainties in the input data. Additional components of bias and uncertainty associated with this approach are introduced by uncertainties in the complex radiochemical analysis measurements themselves. The use of measured nuclide concentrations to validate burnup calculations is widely regarded as conservative because uncertainties in the measurements and in the reactor operating data cannot be eliminated or separated from other uncertainties in the calculations [36]. Recent comparisons of several different BUC validation approaches have corroborated that the uncertainties in criticality calculations using radiochemical assay (RCA) data as the basis for uncertainties were larger than alternate methods that did not rely on measured nuclide compositions [37].

This section provides an overview of an approach for validating SNF based on experimentally measured nuclide concentrations and the associated uncertainty in criticality calculations that apply these concentrations. Relevant characteristics of the application model are summarized in Section 5.1. The relative importance of actinide and fission product BUC nuclides, as well as the importance of residual ^{155}Gd near peak reactivity for the application model, is presented in Section 5.2. The computational methods and data are described in Section 5.3. A summary of the available experimental data applicable to validation of SNF nuclide concentrations is provided in Section 5.4, and a more detailed review and vetting of all available data is provided in Appendix F. Section 5.5 summarizes the results from a recent OECDNEA BWR computational benchmark that includes code assessments in the burnup range near peak reactivity. The bias and uncertainty determination is covered in Section 5.6, which is organized by the analysis of the nuclide uncertainties, analysis of the k_{eff} uncertainties associated with the nuclide uncertainties, and a summary of the uncertainty results. Conclusions and recommendations related to depletion code validation are provided in Section 5.7.

5.1 APPLICATION MODEL

The application model in this study is the GBC-68 cask model described in Section 3.2.3. The fuel lattice used with this application model is the vanished fuel lattice with actinide-only modeling that is described in Section 4.4.1. It has been shown previously that vanished lattices

result in the maximum peak reactivity value because the empty fuel rod locations provide more neutron moderation [4].

The fuel assembly nuclide concentrations in this application model were obtained using the depletion modeling approach described in Section 3.4.1. In this approach, the assembly-average initial enrichment is used in each fuel rod. However, the spatial effects related to the fuel rod location in the assembly are treated explicitly, i.e., the neutronic influence of channel moderator of the edge and corner rods, and the proximity of fuel rods to internal water rods. The UO_2 fuel rods are grouped into three different mixtures that deplete with the same compositions. Each group is assigned a unique mixture number to facilitate specification of different Dancoff factors [12] that account for the neutronic environment effect of adjacent fuel rods. The gadolinium-bearing $\text{Gd}_2\text{O}_3\text{-UO}_2$ fuel rods were represented as a unique material. These rods were subdivided into seven rings with identical volumes, and each ring was assigned a unique mixture. Subdivision of the gadolinium rods is required for accurate representation of the gadolinium isotopes depletion during irradiation.

The BWR fuel assembly model identifying the different fuel mixtures in the vanished lattice is illustrated in Figure 5.1. The fuel rods identified as 1–3 in this figure correspond to UO_2 fuel mixtures 1-3 and rods identified as 4 represent the $\text{Gd}_2\text{O}_3\text{-UO}_2$ fuel rods. Note that the $\text{Gd}_2\text{O}_3\text{-UO}_2$ fuel rods actually contain 7 depletion mixtures (numbered 4–10 in the depletion model) in the subdivided rod; however, they are shown as a single mixture 4 in the figure for illustration purposes.

The fuel compositions in the application model, which are identical to those in the model used in Section 4.4.1, correspond to an initial enrichment of 4.305 wt% ^{235}U , an approximately 7.5-GWd/MTU peak reactivity burnup, and a 5-year decay time.

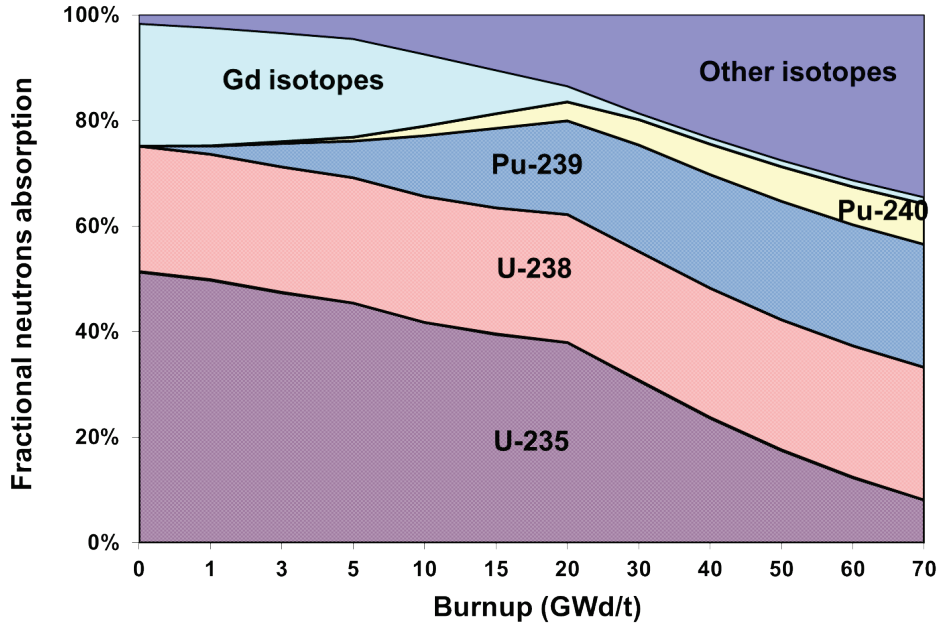


Figure 5.2. Relative neutron absorption fractions in typical UO_2 fuel with gadolinium. [38]

The importance of individual nuclides with respect to BWR fuel reactivity in the GBC-68 cask application model was determined using k_{eff} sensitivity coefficients calculated with TSUNAMI. The relative sensitivity coefficient S_n , defined as shown in Eq. 3 [11], is a relative measure of the first-order effect of changes in the nuclide concentration, N_n of nuclide n , on k_{eff} ,

$$S_n = \frac{\delta k_{eff} / k_{eff}}{\delta N_n / N_n} \quad (3)$$

The k_{eff} sensitivity coefficients for the application model with actinide, fission product, and residual ^{155}Gd nuclides are illustrated in Figure 5.3. The k_{eff} sensitivity to the ^{155}Gd concentration is observed to be larger than for any other single fission product isotope.

As discussed in Section 4.6.2, the majority of the reactivity effect in the assembly due to ^{155}Gd is from ^{155}Gd in gadolinium-bearing fuel rods and not from fission product ^{155}Gd in UO_2 fuel rods. This is an indication of the importance to fuel reactivity of residual ^{155}Gd in gadolinium-bearing fuel rods. For example, the reactivity worth of ^{155}Gd is approximately 1.25% (see Section 3.4.1) for the application model including ^{155}Gd from both the residual ^{155}Gd poison and fission product ^{155}Gd .

The presence of initial ^{157}Gd in the gadolinium poison rods also results in significant neutron absorption at low burnup. This nuclide has previously not been considered in BUC (Table 3.1) because ^{157}Gd is not an important fission product in BUC and is only significant when present as initial natural gadolinium poison. However, an analysis of gadolinium depletion indicates that ^{157}Gd depletes much more rapidly than ^{155}Gd , and that in the range of peak reactivity, neutron absorption by ^{157}Gd is significantly less than by ^{155}Gd . Therefore, ^{157}Gd has not been evaluated in the present study.

The sensitivity coefficients in Figure 5.3 show that the dominant actinides at low burnup include ^{235}U , ^{238}U , ^{239}Pu , and ^{240}Pu . The most important fission products are ^{149}Sm , ^{151}Sm , ^{143}Nd , and ^{103}Rh . The reactivity worth of minor actinides, residual ^{155}Gd , and the top 16 fission products is approximately 3.6%. (See Section 3.4.1.)

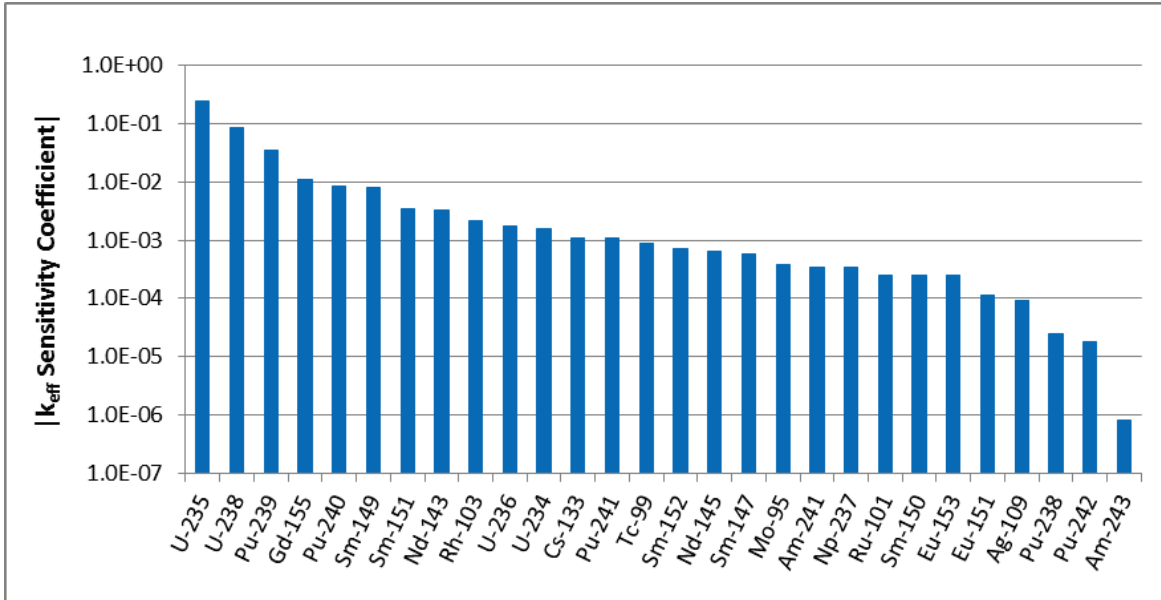


Figure 5.3. k_{eff} relative sensitivity coefficients (absolute) for the BWR application model at peak reactivity for actinides, fission products, and residual ^{155}Gd .

5.3 CODES AND METHODS

The computational analyses of the SNF nuclide compositions used in this work were performed using the SCALE 6.1.2 code system. The burnup calculations were performed using 2D assembly models developed for the NEWT deterministic multigroup neutron transport code, coupled with the ORIGEN code for isotope generation and depletion [39]. These calculations were performed using the TRITON (t-depl) depletion sequence (see Section 3.2.1). The ENDF/B-VII.0 238-group cross-section library [40] was used for all nuclide composition calculations.

TRITON was used to calculate nuclide concentrations for the application model (see Sections 3.2.3 and 4.4.1) and to evaluate the experimental radiochemical assay data used to develop bias and uncertainty associated with the calculated nuclide concentrations. This code has the capability of simulating depletion of individual fuel rods in the fuel assembly model, and spatial subdivisions within a fuel rod. This capability allows an accurate representation of the local flux distribution for a specific fuel rod within the fuel assembly, which is required when validating the computer code predictions with measurements performed using small samples obtained from a single fuel rod.

The depletion models for the measured fuel samples and the application model were developed using a consistent approach to ensure that the nuclide bias and uncertainty estimated from the experimental data are directly applicable to the application model. For example, fuel rods containing gadolinium were subdivided into seven rings with equal volumes to provide an accurate and consistent representation of the gadolinium depletion. For models of the measured UO_2 fuel samples, a burnup time step of 0.5 GWd/MTU was specified for burnups less than 15 GWd/MTU and larger depletion steps (1–1.5 GWd/MTU) were used beyond 15 GWd/MTU. A burnup step of 0.5 GWd/MTU was used to model the depletion of gadolinium-bearing fuel samples.

Details of the fuel assembly models used for validation with experimental data are described in Appendix F.

5.4 APPLICABLE EXPERIMENTAL DATA

Validation of calculated SNF compositions for BWR fuel is challenging due to a limited number of measured samples that are publicly available for code benchmarking. Experimental data for burnups near peak reactivity are further limited since these burnups are generally lower than typical burnup values of measured BWR fuel samples from discharged fuel assemblies. In addition, much of the applicable validation data identified in this study are available from experimental programs performed in the 1970s and 1980s. These studies involved older assembly designs, and the measurements did not include many of the fission products currently considered in BUC. The availability of applicable experimental data for validation has a direct impact on the ability to validate the nuclides considered in a criticality safety analysis, and it also influences the BUC approach (e.g., AO, AFP, or a reduced set of nuclides).

The main characteristics of the SNF samples identified in this study as applicable to depletion code validation are summarized in Table 5.1. The burnup range of the 16 BWR fuel samples is between 2.77 and 27.18 GWd/MTU, which encompasses the assembly peak reactivity burnup values (i.e., less than ~20 GWd/MTU) associated with different gadolinium concentrations and configurations analyzed in this report (see Figure 3.13). These data include samples with burnups exceeding the region of peak reactivity and were included to evaluate potential trends in the data in the low burnup regime.

- Twelve samples were obtained from BWR 6×6 fuel assemblies operated in the Japan Power Demonstration Reactor (JPDR) [41] and the German Gundremmingen reactor [42]. These assemblies are older BWR fuel assembly designs that did not contain gadolinium burnable poison rods.
- Four samples were obtained from a BWR 8×8-2 fuel assembly from the Japanese Fukushima-Daini-2 reactor [43]. This fuel contained gadolinium poison, though no ^{155}Gd measurements were performed for the gadolinium-bearing samples. However, these samples provide information on the accuracy of burnup calculations for actinides in the presence of gadolinium poison.
- Three samples from the Japanese Ohi-2 reactor [43] were evaluated as these are the only publicly available data identified for gadolinium-bearing fuel rods ($\text{UO}_2\text{-Gd}_2\text{O}_3$) that included gadolinium isotope measurements for the burnup range of interest. Ohi-2 is a

PWR reactor that operates with 17×17 assemblies; therefore the data are not necessarily applicable to void conditions of BWRs.

A more detailed review and vetting of the available SNF experimental data for application to validating BWR fuel reactivity near peak reactivity is provided in Appendix F. Note that a number of available BWR samples were not considered in this study due to incomplete operational information, including the void concentrations at the location of the measured samples, and incomplete information on control absorber exposure. Also, several low burnup samples obtained from the extreme ends of the active fuel length were excluded due to bias caused by the fuel rod end region hardware; 3D neutron transport methods would be needed to accurately model these samples. In this study, 2D models were used to represent the fuel assemblies.

The 16 BWR fuel samples provide measurement data for the major actinide nuclides ^{235}U , ^{238}U , ^{238}Pu , ^{239}Pu , ^{240}Pu , ^{241}Pu , and ^{242}Pu . Measurements of ^{234}U and ^{241}Am is available for a subset of the 16 fuel samples. Review of the ^{241}Am experimental data [34] indicates large analytical measurement uncertainties of ~20% that resulted in large deviations between calculations and measurements. The ^{241}Am data were therefore not considered in this study due to their measurement uncertainties that make a reliable validation of the calculated concentrations impractical.

The majority of the fission product nuclides generally considered in BUC (see Table 3.1) had no measurement data in the BWR experiments considered. Only two samples included measurements for the samarium nuclides — ^{149}Sm and ^{151}Sm — which represent the dominant fission products near peak reactivity (Figure 5.3). The limited fission product data derive from the fact that the early experimental programs were primarily motivated by actinide transmutation studies and radiological nuclides, and less by the stable and long-lived fission products important in BUC.

The lack of adequate measurement data precludes the consideration of fission products in BWR BUC near peak reactivity using methods based on destructive radiochemical analysis data. Alternate uncertainty analysis methods such as Monte Carlo nuclear data uncertainty sampling [45] could be considered for unvalidated fission product nuclides. This approach is similar to that used in the validation of reactivity calculations (Section 4.6). However, application of these methods to estimate nuclide uncertainties from burnup calculations has not been extensively validated by this time.

The lack of adequate fission product data associated with BWR fuel near peak reactivity does not extend to higher burnup fuel where significantly more complete experimental data exist. Many of the more recent experimental programs for BWR fuel [46] have focused primarily on high burnup fuel and include measurements for most of the fission products considered in criticality calculations.

An additional consideration unique to BWR fuel near peak reactivity is the importance of the residual ^{155}Gd in gadolinium-bearing fuel rods. The BWR experimental data considered do not include any fuel samples with measurements of ^{155}Gd . To provide some assessment of the ability of computer codes and data to predict the depletion of ^{155}Gd , surrogate measurement data for

¹⁵⁵Gd in gadolinium-bearing PWR fuel rods were considered in this validation study. Only three such measurements from the Ohi-2 reactor were available within the burnup range < 30 GWd/MTU. The rationale for applying PWR surrogate ¹⁵⁵Gd measurement data to the BWR isotopic validation is that the PWR fuel samples were irradiated in an environment similar to that of the bottom section of a BWR fuel assembly (i.e., the subcooled region of the assembly near the core coolant inlet). However, these ¹⁵⁵Gd measurement data may be nonrepresentative of the middle and upper sections of a BWR fuel assembly containing void.

The available measurement data for the actinide nuclides ²³⁴U, ²³⁵U, ²³⁸U, ²³⁸Pu, ²³⁹Pu, ²⁴⁰Pu, ²⁴¹Pu, and ²⁴²Pu in BWR fuel samples within the burnup range associated with peak reactivity provide the technical basis for the depletion code validation in terms of *k_{eff}* uncertainty presented in this report.

Table 5.1. Evaluated experimental spent fuel nuclide data

Reactor name	Reactor type	Lattice type	Measured fuel rod type	Number of samples	Enrichment (wt % ²³⁵ U)	Burnup (GWd/MTU)	Gadolinium isotope measurements
Gundremmingen-A	BWR	6×6	UO ₂	8	2.53	14.39	No
						15.84	No
						17.49	No
						21.24	No
						22.25	No
						22.97	No
						23.51	No
JPDR	BWR	6×6	UO ₂	4	2.597	2.77	No
						3.38	No
						4.13	No
						4.35	No
Fukushima-Daini-2	BWR	8×8-2 ^b	UO ₂ -Gd ₂ O ₃	4	3.41	16.65	No
						21.83	No
						22.63	No
			UO ₂	1	3.91	27.18	No
Ohi-2 ^a	PWR	17×17	UO ₂ -Gd ₂ O ₃	3	3.20	21.92	Yes
						29.45	Yes
						25.73	Yes

^a PWR fuel samples analyzed to obtain data on residual ¹⁵⁵Gd in gadolinium-bearing fuel rods.

^b An 8×8 lattice design with two water rods.

5.5 OECD/NEA BWR BENCHMARK

International computational benchmarks represent an important means for comparing the performance of nuclear analysis codes, models, and nuclear data, particularly when experimental data are limited or not available. These benchmarks provide opportunities to compare analysis/simulation codes, which use different methodologies, different nuclear data sets, and different modeling techniques. The Expert Group on Burnup Credit Criticality Safety (EGBUC) of the Working Party of Nuclear Criticality Safety (WPNCS) under the Nuclear Science Committee (NSC) of OECD/NEA is conducting the Phase III C benchmark on BWR fuel assembly burnup calculations to assess assembly peak reactivity [47]. The benchmark is being coordinated by Japan and was primarily motivated by the requirement to assess computational methods for BUC in support of fuel handling activities at the damaged Fukushima reactors and spent fuel pools.

The benchmark model consists of an ATRIUM9, 9×9 BWR fuel assembly, with fuel rod enrichments in the assembly that vary from 2.1 to 4.9 wt% ²³⁵U. Twelve gadolinium rods contain 5 wt% Gd₂O₃ with 3.4 wt% ²³⁵U enrichment. The assembly eigenvalue and isotopic concentrations were calculated for 40 nuclides as a function of burnup for 0%, 40% and 70% coolant void fractions. In addition, the participants calculated the eigenvalue at peak reactivity for each void fraction and the peak reactivity burnup. Benchmark results from more than 20 different computer codes and nuclear data libraries have been submitted.

A preliminary finding of the BWR benchmark is the variability in the predicted residual ¹⁵⁵Gd concentration in the fuel. The uncertainty (2 sigma) in the ¹⁵⁵Gd content for a burnup of 12 GWd/MTU was observed to be between approximately 35% and 50% for the different void conditions, indicating that the results have a large dependence on the computer code, modeling, and/or the nuclear data used in the calculations. The large variability in the calculated results reinforces the need for additional code validation for residual ¹⁵⁵Gd before it can be reliably used in BUC calculations.

Another important finding is the variability in the code predictions of peak reactivity and on the burnup associated with peak reactivity. The variability in the calculated peak k-infinity results (2 sigma) was less than 1%, indicating relatively consistent agreement between codes. However, variability in the burnup value where peak reactivity occurs ranged from about 2.8% to 5.5% (2 sigma) and was greatest for zero-void conditions.

Although the OECD/NEA Phase III C BWR Benchmark is not based on experimental data, it will provide important information on the consistency of different code and nuclear data library performance in areas where validation data is lacking. These benchmarks also highlight areas where additional work is needed to assess code performance.

5.6 BIAS AND UNCERTAINTY DETERMINATION

5.6.1 Nuclide Uncertainty Analysis

The bias and bias uncertainty values associated with BWR nuclide compositions within the burnup range characteristic to a BWR assembly reactivity peak are presented in this section. The nuclides with available validation data that are considered in this study include ^{234}U , ^{235}U , ^{238}U , ^{238}Pu , ^{239}Pu , ^{240}Pu , ^{241}Pu , ^{242}Pu , and ^{155}Gd (residual). The analysis does not include ^{241}Am due to large measurement uncertainties. In addition, fission products are not included due to the lack of adequate measurement data. The bias and uncertainty in the calculated nuclide compositions are derived directly from comparisons of the calculated and measured nuclide concentrations. The nuclide bias, X_i^j , is calculated with Eq. (4),

$$X_i^j = M_i^j / C_i^j, \quad (4)$$

where

- i = the index of a burnup-credit nuclide,
- j = the index of a measured fuel sample in a set of N_s samples,
- M_i^j = the measured concentration of nuclide i in fuel sample j ,
- C_i^j = the calculated concentration of nuclide i in fuel sample j .

Provided that the X_i^j values have a normal distribution, the probability frequency distributions of the X_i^j values may be characterized by the sample mean \bar{X}_i and standard deviation s_i given by Eqs. (5) and (6), respectively.

$$\bar{X}_i = \sum_{j=1}^{N_s} X_i^j / N_s. \quad (5)$$

$$s_i = \sqrt{\frac{\sum_{j=1}^{N_s} (X_i^j - \bar{X}_i)^2}{N_s - 1}}. \quad (6)$$

Standard practice [48] in criticality safety evaluations does not credit biases that result in an overprediction of the effective neutron multiplication factor, k_{eff} . Hence, in this analysis, no credit is applied for the overprediction of fissile nuclides (i.e., ^{235}U , ^{239}Pu , and ^{241}Pu) or the underprediction of neutron absorbing nuclides. With this approach, the mean for an isotope, or isotopic bias, \bar{X}_i' , is defined as shown in Eqs. (7) and (8) for fissile and neutron absorbing nuclides, respectively:

$$\bar{X}_i' = \begin{cases} \bar{X}_i, & \text{if } \bar{X}_i > 1 \\ 1, & \text{if } \bar{X}_i \leq 1 \end{cases}, \quad (7)$$

$$\bar{X}_i' = \begin{cases} \bar{X}_i, & \text{if } \bar{X}_i < 1 \\ 1, & \text{if } \bar{X}_i \geq 1 \end{cases}. \quad (8)$$

Data normality of the X_i^j values for each actinide isotope i and the N_s fuel samples was assessed with the Shapiro-Wilk normality test at the 0.05 significance level [49]. The nuclide bias and uncertainty for the measured nuclides are summarized in Table 5.2. All the actinides pass the normality test except for ^{238}U and ^{238}Pu . The uncertainty associated with the calculated ^{238}U concentration values is very small (e.g., standard deviation of the measured-to-calculated values was ~ 0.001) and has insignificant impact on k_{eff} uncertainty. For example, by applying the ^{238}U bias uncertainty values of 0.001 and 0.002 (i.e., twice as much as the standard deviation value) to the calculated ^{238}U concentration, the corresponding k_{eff} values differed by 13 pcm, a negligible impact. In this report, the effect on k_{eff} uncertainty of the normality assumption for the ^{238}Pu results is considered to be negligible because k_{eff} has a very small sensitivity to the ^{238}Pu content, as illustrated by the k_{eff} sensitivity coefficients in Figure 5.3.

There are additional uncertainties in the estimation of the mean bias \bar{X}_i and standard deviation s_i due to the limited number of the measurements considered. As the number increases, there is increased confidence that the parameters \bar{X}_i and s_i are good estimates of the actual probability distribution. However, when the size is small, there is less confidence that the estimated parameters represent the population parameters, in a statistical sense, and the uncertainties in these estimates should be increased accordingly. In this study, statistical tolerance-limit factors were applied based on the number of measurements (fuel samples) available for each nuclide. Tolerance limits correspond to an interval, or range, within which a specified percentage of the population is expected to reside with a given confidence. In this report, the 95%/95% interval is defined such that 95% of the population is expected to reside within this range with 95% confidence. The development of the tolerance intervals is accomplished using tolerance-limit factors that are multipliers on the estimated standard deviation s_i . In this work, the one-sided 95%/95% tolerance limit factor (k_l) is used to define the upper or lower limit of the population above which 95% of the population resides.

Table 5.2. Isotopic bias and bias uncertainty values associated with calculated BWR isotopic concentrations

Isotope	No. of samples	Burnup range (GWd/MTU)	Mean \bar{X}_i	Nuclide bias (\bar{X}_i)	Standard Deviation (s_i)	One-sided tolerance limit factor ^c (k_l)
^{234}U	8	2.77–27.18	0.969	0.969	0.040	3.187
^{235}U	16	2.77–27.18	0.985	1.000	0.023	2.524
^{238}U	16	2.77–27.18	1.000	1.000	0.002 ^b	2.524
^{238}Pu	16	2.77–27.18	1.039	1.000	0.098	2.524
^{239}Pu	16	2.77–27.18	0.950	1.000	0.039	2.524
^{240}Pu	16	2.77–27.18	0.967	0.967	0.048	2.524
^{241}Pu	16	2.77–27.18	1.059	1.059	0.129	2.524
^{242}Pu	16	2.77–27.18	1.012	1.000	0.121	2.524
^{155}Gd ^a	3	21.47–29.45	2.440	1.000	1.719	7.656

^a Surrogate isotopic validation data from gadolinium-bearing PWR UO_2 fuel samples.

^b Standard deviation for ^{238}U values was doubled to account for the non-normality of the distribution.

^c One-sided 95%/95% tolerance limit factors.

Both the bias and the standard deviation associated with ^{155}Gd concentration based on the three evaluated PWR fuel samples are very large. This is caused by erratic behavior in the measurement data, which may be due to very low isotopic abundances of ^{155}Gd in the fuel, that are challenging to measure with mass spectrometry.

5.6.2 k_{eff} Bias and Uncertainty Analysis

A number of methods for calculating k_{eff} uncertainty associated with uncertainties in calculated nuclide concentrations in SNF have previously been explored. The methods investigated in NUREG/CR-6811 [50] include both conservative bounding and best estimate approaches to uncertainty estimation. The bounding method applies bias and uncertainty associated with calculated isotopic concentrations in a way that maximizes the k_{eff} uncertainty value. This method increases the concentrations of the fissile nuclides based on their individual nuclide uncertainties estimated from validation studies, and it decreases the concentrations of the neutron absorbing nuclides. The best estimate methods previously applied to the analysis of uncertainty for PWR BUC [51] provide a more realistic representation of the uncertainties but are very computationally intensive.

The bounding method for uncertainty determination was applied for BWR fuel near peak reactivity in this study. Specifically, the predicted concentrations of the fissile nuclides in Table 5.2 (i.e., ^{235}U , ^{239}Pu , and ^{241}Pu) are adjusted to their upper one-sided 95%/95% tolerance limit values [52] to account for the uncertainty in the calculations as determined from the experimental data. The concentrations of all neutron-absorbing nuclides (i.e., ^{234}U , ^{238}U , ^{238}Pu , ^{240}Pu , ^{242}Pu , ^{155}Gd) are adjusted to their lower one-sided tolerance limit values. This conservative approach maximizes the reactivity in the application model. The nuclide concentrations adjusted for bias and uncertainty, c_i' are determined as:

$$c_i' = \begin{cases} c_i \times (\bar{X}_i' + k_1 \times s_i), & \text{for fissile nuclides} \\ c_i \times (\bar{X}_i' - k_1 \times s_i), & \text{for neutron absorbing nuclides} \end{cases} \quad (9)$$

where

- i = the index of a BUC nuclide,
- c_i = calculated nuclide concentration,
- \bar{X}_i' = bias in the predicted fuel concentration for nuclide i [see Eqs. (5), (7), and (8)],
- k_1 = one-sided tolerance limit factor for 95% confidence and 95% of the population (Table 5.2),
- s_i = standard deviation in the predicted nuclide concentration as determined from the spent fuel sample data for nuclide i [see Eq. (5)].

This approach requires two criticality calculations to be performed for the application model. The first calculation applies the nuclide concentrations as calculated directly by the depletion code without any corrections. The second calculation applies nuclide concentrations that have been adjusted for estimated bias and uncertainty according to Eq. (9). The difference in the system eigenvalues between these calculations provides a direct and bounding estimate of the bias and uncertainty associated with the calculated nuclide compositions.

The large variability in the validation results for ^{155}Gd and the statistical penalty associated with the small number of measurements, as defined by the tolerance limit factor (Table 5.2), results in a calculated ^{155}Gd concentration after adjusting for bias and uncertainty (c_i') that is negative. In effect, the uncertainty in the concentration is larger than the concentration value, eliminating ^{155}Gd from consideration in the BUC analysis based on the limited experimental data currently available.

The bounding method was used in this work to provide a conservative approach that maximizes the system reactivity and k_{eff} uncertainty for the following reasons:

1. The number of measured BWR fuel samples (see Section 5.2) in the burnup range of peak reactivity is limited. Only three different experimental programs were identified as sources of experimental data. While the tolerance limit factors statistically account for the low number of available measurements, there is reduced confidence in the nuclide experimental data, as there is an increased likelihood that any single set of measured data could potentially bias the results.
2. The BWR measurement data were limited to 6×6 and 8×8 assembly designs. No data were identified for modern assembly designs (e.g., 9×9 and 10×10) for low burnup fuel.
3. There is limited BWR data for fuel assemblies containing gadolinium-bearing fuel rods.
4. This method is easily applied to a heterogeneous fuel assembly in an application model that contains both UO_2 and $\text{Gd}_2\text{O}_3\text{-UO}_2$ fuel rods (i.e., described in Section 5.1).

5.6.3 k_{eff} Bias and Uncertainty Results

The uncertainty in k_{eff} associated with nuclide biases and bias uncertainties was determined for the GBC-68 cask application model using the bounding method described in Section 5.6.2. The k_{eff} margin for uncertainty was calculated as the difference between the k_{eff} value using nuclide concentrations adjusted for bias and uncertainty (see Eq. 9) and the k_{eff} value using calculated nuclide concentrations (i.e., base case). The bias and uncertainty values used in Eq. 9 and the one-sided tolerance limit factors for 95% probability and 95% confidence level are listed in Table 5.2 [53]. The calculated k_{eff} values and uncertainty are presented in Table 5.3. The calculated k_{eff} margin for uncertainty due to the calculated nuclide concentrations is 0.0165 (1.65% Δk).

The BWR SNF composition used in this study consisted of actinides only (see Table 3.1), excluding ^{241}Am . The large measurement uncertainty of ^{241}Am in the experiments considered precludes its reliable use for code validation.

Table 5.3. k_{eff} results and margin for uncertainty for the GBC-68 cask model

Description	k_{eff} ^a
Calculated concentrations (AO base case)	0.9363
Adjusted concentrations as shown in Eq. (9)	0.9528
Δk_{eff} margin for nuclide uncertainty ^b	0.0165 (1.65% Δk)

^a Standard deviation from the Monte Carlo simulation = 0.0001.

^b 95% probability, 95% confidence level.

5.7 CONCLUSIONS AND RECOMMENDATIONS

A method for determining the uncertainty in k_{eff} calculations associated with the BWR SNF nuclide concentrations near peak reactivity has been demonstrated for the GBC-68 cask model described in Section 3.2.3 and the vanished lattice configuration (see Section 5.1 for details). This method is based on the direct application of measured BWR SNF composition data to estimate the uncertainties associated with the calculated nuclide composition used in BUC application models.

The available experimental nuclide data for BWR fuel near peak reactivity currently limits BUC analyses to consider AO fuel compositions. Present radiochemical assay data lack sufficient fission product data that would enable validation for AFPs. Similarly, applicable data for residual ¹⁵⁵Gd are limited, and only three samples obtained from PWR fuel samples were evaluated in this work. However, the large variability in the validation results for ¹⁵⁵Gd and the statistical penalty associated with the low number of measurements effectively eliminates any potential credit that can be obtained based on the existing measurement data.

The reactivity worth of ¹⁵⁵Gd in the GBC-68 cask model at BWR fuel peak reactivity for the vanished assembly lattice was approximately 1.25% relative to crediting AO nuclides listed in Table 3.1. The margin for k_{eff} uncertainty in the calculated actinide compositions for the AO cask configuration is estimated to be 0.0165 with a 95% confidence level. The actinide compositions exclude ²⁴¹Am due to large measurement uncertainties. Addition of fission product measurement data and improved ¹⁵⁵Gd data in the range of peak reactivity could support credit for a substantial fraction of the reactivity worth from the omitted BUC nuclides, which represent approximately 3.64% of the total reactivity worth.

Although the analysis in this work was limited by the available validation data to consider AO compositions, the approach is applicable to fission products and residual ¹⁵⁵Gd provided sufficient measurement data are obtained to support validation of the nuclide concentrations. The Belgian nuclear research center Studiecentrum voor Kernenergie (SCK•CEN) recently initiated a new research program called Rod Extremity and Gadolinia AnaLysis (REGAL) [54] to measure an extensive list of actinides and fission products in the burnup range of peak reactivity and also to measure residual gadolinium nuclides to validate gadolinium depletion. These commercial data could be acquired to increase the number of fuel samples in the burnup range of interest and dramatically expand the measured nuclides that could potentially be credited and reduce current levels of nuclide uncertainty.

BUC programs in Japan are relatively advanced and have focused heavily on the acquisition of experimental data to support BWR BUC validation [43]. The Japan Nuclear Regulation Authority (NRA) also recently contributed new nuclide assay data to the OECD/NEA SNF assay database, the Spent Fuel Isotopic Composition Database (SFCOMPO) [55]. These new data should be reviewed and evaluated to assess possible applicability to the present studies. The Japanese Atomic Energy Agency (JAEA) and other research organizations have additional BWR validation data that could be acquired through international cooperation agreements. The Spanish Nuclear Safety Council, or Consejo de Seguridad Nuclear (CSN), has an active research program, has conducted several experimental studies [56, 57], and currently has a research initiative in the area of BWR fuel BUC. Collaboration with these international organizations could be used to leverage limited experimental data, and cooperation on future research projects could further validate BWR BUC methodologies.

An emerging methodology for uncertainty analysis is the use of nuclear data uncertainty information (covariance matrices) to predict reactor physics parameters [58]. This method has recently been applied to the analysis of nuclide composition uncertainties [45]. This approach is based on Monte Carlo sampling of the underlying nuclear data uncertainties used in the calculation to estimate the uncertainties in calculated parameters. The methodology has been implemented in SCALE in the Sampler code, which performs stochastic sampling of the nuclear data. This approach is similar to that used by TSUNAMI, and in fact applies the same nuclear data covariance data files used by TSUNAMI as discussed in Section 4.1. Data uncertainty files have been recently expanded to include uncertainties in the nuclear decay data and fission product yields to provide a comprehensive uncertainty evaluation for spent fuel analyses. Preliminary studies [37] comparing this methodology with methods based on nuclide assay data and an independent approach proposed by industry show promising results. Such an approach may be valuable to support validation in situations of limited experimental data; however additional validation of these methods is needed before they can be used to support licensing analyses.

6 SUMMARY AND CONCLUSIONS

This report provides a technical basis for the use of peak reactivity methods to credit burnup in the criticality safety analysis of BWR storage casks and transportation systems. It presents an overview of current peak reactivity methods used in SNF pools as background for the evaluation of peak reactivity BUC in casks. Parameter studies were performed to identify the most important factors affecting peak reactivity analysis and the conservative direction for each of these parameters for various sets of nuclides modeled in the GBC-68 cask. Validation of criticality calculations for peak reactivity BWR fuel was performed with calculation of bias, uncertainties, and penalty factors. Validation is also presented for SNF isotopic inventories using RCA measurements of low burnup BWR fuel. A brief summary of each of these sections is presented here, followed by overall conclusions of this assessment of a technical basis for peak reactivity methods in storage and transportation casks.

6.1 CURRENT PEAK REACTIVITY METHODS FOR SPENT FUEL POOLS

The SCCG-limit-with-gadolinium-credit method gives credit for residual gadolinium and examines several different lattices including a range of enrichments, gadolinium loadings, and gadolinium patterns over multiple burnups. This method provides a fairly straightforward approach to demonstrating safe storage of BWR fuel assemblies. While this method requires a large number of lattice designs, the use of real lattice designs provides a degree of accuracy in the analysis that is lacking in some other methods.

The SCCG-limit-with-gadolinium-credit method has some potential shortcomings as well. The use of a sizeable number of real lattice designs may be problematic for implementation by a cask vendor without ready access to a reliable collection of such design information. The SCCG-limit-with-gadolinium-credit method attempts to balance some of the conservatisms of the peak reactivity methods, such as considering all assemblies to be identical and all at peak reactivity, with a less conservative depletion analysis including nonlimiting depletion conditions and lattices. Finally, the use of nonlimiting lattices and depletion conditions may also bias the correlation of k_{rack} and SCCG k_{inf} in the low, potentially unconservative direction.

In comparison, the SCCG-limit-without-gadolinium-credit method has some advantages in terms of conservatism and is simple to implement in power plant operations. There are subtle but important differences between this method and the SCCG-limit-with-gadolinium-credit method. The primary difference is that in this method, the SCCG limit is based on a correlation created without credit for gadolinium.

The SCCG-limit-without-gadolinium-credit method also suffers from some potential areas of concern. The storage of fresh and low burnup fuel requires that a separate gadolinium requirement be determined and met in the burnup range in which the reactivity of unpoisoned fuel exceeds limits. This adds additional complexity, especially in the selection of fuel assemblies that are qualified for storage in a cask or package. The range of depletion conditions will also require more effort for validation of both criticality and composition calculations.

6.2 PEAK REACTIVITY ANALYSIS SUMMARY

A range of parameters was studied to identify the important parameters for BWR peak reactivity and to quantify the potential sensitivity of calculated cask reactivity to these parameters. A BWR BUC methodology would require a set of selected nuclides and the associated depletion conditions to ensure a conservative analysis. Those found to give the most reactive results are summarized in Tables 3.32 and 3.33 in Section 3.5.1. The most important operating conditions are void fraction and control blade insertion. For AO analyses, both high void fractions and control blade insertion increase reactivity. For AFP analyses, low void fractions increase reactivity at the peak; control blade insertion was also shown to be a positive reactivity effect in these studies, but is likely dependent on gadolinium rod pattern. Other parameters, including gadolinium pattern, fuel temperature, specific power, and operating history have smaller impacts on peak reactivity.

One set of conclusions that can be drawn from these studies relates to which parameters are sufficiently variable or interdependent so that examination is recommended for each licensing analysis performed. The primary parameters of interest in this category are the gadolinium pattern used in the analysis and the way it interacts with control blade insertion. It is conceivable that some gadolinium patterns will be more reactive than others. More importantly, the power distribution shifts caused by control blade insertion drive changes in residual gadolinium, and hence discharged fuel reactivity. These effects will be sensitive to the gadolinium pattern. Certain other key parameters do not need to be studied further to identify the direction of conservatism, but justification of the values used should be provided as part of an application. The parameters that do not need further investigation for the GE14 fuel assembly design considered in this work include initial or depleted composition modeling, void fraction, fuel temperature, and operating history.

Several areas related to peak reactivity BUC could be further studied to provide additional confidence in the results generated in this report, clarify causes and relationships among parameters, or extend the area of applicability beyond the parameters, ranges, and fuel types studied here. Other areas that could be studied further include the following:

- A wider range of lattice enrichment zoning patterns
- Additional gadolinium patterns, potentially including less constrained pattern development
- Expansion of the study of the interaction between gadolinium patterns and control blade effects
- Control blade programs, including both rodded and unrodded depletion during operation
- Additional fuel assembly design types
- 3D depletion calculations to investigate interactions between lattices
- Fuel assembly orientation within the cask
- Depletion effects of symmetric gaps between assemblies in the core
- Parameter interdependencies and potential competing effects.

6.3 VALIDATION OF CASK REACTIVITY CALCULATIONS SUMMARY

Section 4 presents a series of studies that investigate validation of cask reactivity calculations. As discussed in Section 4.3, several sources of SDFs have been used, providing a large number of candidate experiments. In total, over 1600 unique experiments were compared against a range of application cases to experiment cases with c_k values of 0.8 or higher.

A range of potentially useful experiments has been identified in Section 4.4 for use in AO or AFP analyses. More than 50 experiments have been identified for each application, allowing a sufficient population for validation. All experiments selected are LEU-COMP-THERM experiments and thus provide no validation of cross sections for plutonium or americium, residual gadolinium, or fission products. The experiments identified for use in validation are listed in Appendix C. A sample validation was presented in Section 4.5 using multiple methods; the results on which the validation is based are listed in Appendix D. The resulting bias and bias uncertainty values, of the single application model examined, were similar among each of the methods, and the limiting combination of bias and bias uncertainty was $-0.00973 \Delta k$.

Several important nuclides are not present in the validation suite used for the sample validation, as mentioned previously. A sensitivity/uncertainty analysis approach was used to develop these factors in Section 4.6. The calculations showed that a penalty factor of about 0.3% Δk for transuranics, plutonium, and americium was appropriate for the sample validation. The factor for residual gadolinium was calculated to be 0.05% Δk . The factor for remaining fission products and minor actinides was calculated to be about 0.06% Δk . These penalty factors are fairly small, so it is unlikely that additional conservatism in them would have a noticeable impact on the overall conservatism of the analysis.

Validation calculations can be performed in compliance with the consensus ANSI/ANS standard [17] and prior NUREG/CR recommendations [22, 23]. Modest penalty factors have been established that can extend the validation area of applicability to account for nuclides that cannot be validated with critical experiments at this time. Overall, the validation of cask reactivity calculations does not present a technical barrier that would prevent implementation of peak reactivity methods for demonstrating the criticality safety of BWR fuel in storage and transportation casks.

6.4 ISOTOPIC VALIDATION SUMMARY

A method for determining the uncertainty in k_{eff} calculations associated with the BWR SNF nuclide concentrations near peak reactivity has been demonstrated for the GBC-68 cask model and the vanished fuel assembly lattice configuration. This method is based on the direct application of measured BWR SNF composition data to estimate the uncertainties associated with the calculated nuclide composition used in BUC application models.

The available experimental nuclide data for BWR fuel near peak reactivity currently limits BUC analyses to consider AO fuel compositions. Present radiochemical assay data lack sufficient fission product data that would enable validation for actinide and fission product compositions. Similarly, applicable data for residual ^{155}Gd are limited, and only three samples obtained from

PWR fuel samples were evaluated in this work. However, the large variability in the validation results for ^{155}Gd and the statistical penalty associated with the low number of measurements effectively eliminates any credit that can be obtained based on the existing measurement data.

Addition of fission product measurement data and improved ^{155}Gd data in the range of peak reactivity could support credit for a substantial fraction of the reactivity worth from the omitted BUC nuclides which represent approximately 4% of the total reactivity worth.

Although the analysis in this work was limited by the available validation data to consider AO compositions, the approach is applicable to fission products and residual ^{155}Gd provided sufficient measurement data are obtained to support validation of the nuclide concentrations. BUC programs in Belgium, Japan, and Spain currently have research initiatives in the area of BWR fuel BUC in which collaboration with international organizations could be used to leverage limited experimental data and cooperate on future research projects to validate BWR BUC methodologies.

6.5 CONCLUSIONS

The primary purpose of this report is to provide a technical basis for applying peak reactivity methods for BWR BUC in SNF storage and transportation casks. The results summarized above support several important conclusions.

- The physics of BWR fuel depletion are well understood, reliable, and predictable in their effects on discharged fuel reactivity near peak reactivity. A conservative set of analysis conditions can be identified and implemented to allow criticality safety analysis of BWR SNF at peak reactivity in storage and transportation casks.
- The conservative set of depletion parameters used in any analysis will be dependent on the methodology developed and implemented by an applicant, including the specific set of nuclides credited in the analysis.
- A suitable number of UO_2 critical experiments can be identified to support validation of peak reactivity analysis of BWR SNF. All the experiments identified in this report are LEU, water-moderated pin array experiments.
- There is a need for critical experiment data with plutonium and/or gadolinium that have adequate similarity to low burnup BWR fuel. No such experiments were identified in this study.
- Penalty factors have been developed for the unvalidated transuranic, gadolinium, and fission product nuclides included in GBC-68 models used in this report. The sum of these three factors is less than 0.5% Δk .
- Isotopic validation for AO BUC near peak reactivity has been demonstrated with identified radiochemical assay data. A method for determining the uncertainty in k_{eff} calculations associated with the BWR SNF nuclide concentrations near peak reactivity has been verified for the GBC-68 cask model and the vanished fuel assembly lattice configuration.
- Additional radiochemical assay data are needed for modern design low burnup BWR fuel with gadolinium poison and fission product measurements. The addition of fission product measurement data and improved ^{155}Gd data in the range of peak reactivity could support credit for a substantial fraction of the reactivity worth from the omitted BUC

nuclides which represent approximately 4% of the total reactivity worth. Collaboration with international organizations could be used to leverage limited experimental data and to cooperate on future research projects to validate BWR BUC methodologies.

7 REFERENCES

1. U.S. Code of Federal Regulations, Title 10, “Energy,” U.S. Nuclear Regulatory Commission, Washington, D.C., 2014.
2. Division of Spent Fuel Storage and Transportation, *Interim Staff Guidance – 8, Revision 3, Burnup Credit in the Criticality Safety Analyses of PWR Spent Fuel in Transportation and Storage Casks*, U.S. Nuclear Regulatory Commission, September 26, 2012.
3. J. C. Hannah, W. A. Metwally, and V. W. Mills, *Uncertainty Contribution to Final In-Rack $k(95/95)$ from the In-Core k_{∞} Criterion Methodology for Spent Fuel Storage Rack Criticality Safety Analyses*, Proceedings of PHYSOR 2010, Pittsburgh, PA, May 9–14, 2010.
4. K. W. Cummings and S. E. Turner, *Design of Wet Storage Racks for Spent BWR Fuel*, Topical Meeting on Practical Implementation of Nuclear Criticality Safety, Reno, NV, November 11–15, 2001.
5. M. L. Fensin, *Optimum Boiling Water Reactor Fuel Design Strategies to Enhance Reactor Shutdown by the Standby Liquid Control System*, Master of Engineering Thesis, University of Florida, 2004.
6. L. Kopp, *Guidance on the Regulatory Requirements for Criticality Analysis of Fuel Storage at Light-Water Reactor Power Plants*, Letter from L. Kopp to T. Collins, U.S. Nuclear Regulatory Commission, August 19, 1998, ADAMS ML072710248.
7. *Criticality Safety Evaluation for the Nine Mile Point 2 Rack Installation Project*, Holtec Report Number HI-2012621, Revision 1, December 13, 2010, ADAMS ML103500365.
8. *Licensing Report on the Wet Fuel Storage Capacity Expansion at Cooper Nuclear Station*, Holtec Report HI-2043224, Revision 1, April 7, 2006, ADAMS ML062990432.
9. M. Tardy, S. Kitsos, L. Picard, L. Milet, M. Lein, G. Grassi, *Gadolinium Credit Application for Transportation and Storage Casks loaded with BWR UO₂ Assemblies*, Proceedings of the 17th International Symposium on the Packaging and Transportation of Radioactive Materials (PATRAM 2013), San Francisco, CA, August 18–23, 2013.
10. D. E. Mueller, J. M. Scaglione, J. C. Wagner, and S. M. Bowman, *Computational Benchmark for Estimated Reactivity Margin from Fission Products and Minor Actinides in BWR Burnup Credit*, NUREG/CR-7157, ORNL/TM-2012/96, U.S. Nuclear Regulatory Commission, Oak Ridge National Laboratory, 2013.
11. *SCALE: A Comprehensive Modeling and Simulation Suite for Nuclear Safety Analysis and Design*, ORNL/TM-2005/39, Version 6.1, Oak Ridge National Laboratory, June, 2011. Available from Radiation Safety Information Computational Center at Oak Ridge National Laboratory as CCC-785.
12. B. J. Ade, *SCALE/TRITON Primer: A Primer for Light Water Reactor Lattice Physics Calculations*, Oak Ridge National Laboratory, NUREG-7041, ORNL/TM-2011/21, U.S. Nuclear Regulatory Commission, Oak Ridge National Laboratory, 2012.
13. J. M. Scaglione, D. E. Mueller, J. C. Wagner, and W. J. Marshall, *An Approach for Validating Actinide and Fission Product Burnup Credit Criticality Safety Analyses – Criticality (k_{eff}) Predictions*, NUREG/CR-7109, ORNL/TM-2011/514, U.S. Nuclear Regulatory Commission, Oak Ridge National Laboratory, 2012.
14. D.E. Mueller, S. M. Bowman, W. J. Marshall, and J. M. Scaglione, *Review and Prioritization of Technical Issues Related to Burnup Credit for BWR Fuel*, NUREG/CR-

- 7158, ORNL/TM-2012/261, U.S. Nuclear Regulatory Commission, Oak Ridge National Laboratory, 2013.
15. J. Rhodes, K. Smith, and D. Lee, "CASMO-5 Development and Applications," PHYSOR – ANS Topical Meeting on Reactor Physics, Vancouver, BC, 2006.
 16. C. V. Parks, M. D. DeHart, and J. C. Wagner, *Review and Prioritization of Technical Issues Related to Burnup Credit for LWR Fuel*, NUREG/CR-6665, ORNL/TM-1999/303, U.S. Nuclear Regulatory Commission, Oak Ridge National Laboratory, 2000.
 17. "Validation of Neutron Transport Methods for Nuclear Criticality Safety Calculations," ANSI/ANS-8.24-2007:R2012, an American National Standard, published by the American Nuclear Society, La Grange Park, IL, 2007.
 18. D. E. Mueller, K. R. Elam, and P. B. Fox, *Evaluation of the French Haut Taux de Combustion (HTC) Critical Experiment Data*, NUREG/CR-6979, ORNL/TM-2007/083, U.S. Nuclear Regulatory Commission, Oak Ridge National Laboratory, September 2008.
 19. *International Handbook of Evaluated Criticality Safety Benchmark Experiments*, NEA/NSC/DOC(95)03, NEA Nuclear Science Committee, September 2013.
 20. B. T. Rearden, M. L. Williams, M. A. Jessee, D. E. Mueller, and D. A. Wiarda, *Sensitivity and Uncertainty Analysis Capabilities and Data in SCALE*, Nucl. Technol. Volume 174, Issue 2, pp. 236–288, May 2011.
 21. I. Hill, J. Gulliford, J. B. Briggs, B.T. Rearden, and T. Ivanova, *Generation of 1800 New Sensitivity Data Files for ICSBEP Using SCALE 6.0*, Transactions of the American Nuclear Society, Volume 109, Number 1, pp. 867–869, November, 2013.
 22. J. C. Dean, R. W. Tayloe, Jr., *Guide for Validation of Nuclear Criticality Safety Computational Methodology*, NUREG/CR-6698, U.S. Nuclear Regulatory Commission, Science Applications International Corporation, 2001.
 23. J. J. Lichtenwalter, S. M. Bowman, M. D. DeHart, and C. M. Hopper, *Criticality Benchmark Guide for Light-Water-Reactor Fuel in Transportation and Storage Packages*, NUREG/CR-6361, ORNL/TM-13211, U.S. Nuclear Regulatory Commission, Oak Ridge National Laboratory, 1997.
 24. W. J. Marshall and B. T. Rearden, *The SCALE Verified, Archived Library of Inputs and Data – VALID*, ANS Nuclear Criticality Safety Division Topical Meetings (NCSD2013), Wilmington, NC, September 29–October 3, 2013.
 25. *SCALE 5 and 5.1 Criticality Safety Validation Input Files–Validation and Benchmarks–SCALE*, http://scale.ornl.gov/validation_input.shtml, retrieved June 9, 2014.
 26. B. T. Rearden, K. J. Dugan, and F. Havljū, *Quantification of Uncertainties and Correlations in Criticality Experiments with SCALE*, ANS Nuclear Criticality Safety Division Topical Meetings (NCSD2013), Wilmington, NC, September 29–October 3, 2013.
 27. M. Bock and M. Stuke, *Determination of Correlations among Benchmark Experiments by Monte Carlo Sampling Techniques*, ANS Nuclear Criticality Safety Division Topical Meetings (NCSD2013), Wilmington, NC, September 29–October 3, 2013.
 28. M. Bock and M. Behler, *Impact of Correlated Benchmark Experiments on the Computational Bias in Criticality Safety Assessment*, ANS Nuclear Criticality Safety Division Topical Meetings (NCSD2013), Wilmington, NC, September 29–October 3, 2013.
 29. E. M. Baum, M. C. Ernesti, H. D. Knox, T. R. Miller, and A. M. Watson, *Chart of the Nuclides*, 17th edition, Knolls Atomic Power Laboratory, 2010.

30. W. J. Marshall, D. Wiarda, C. Celik, B. T. Rearden, and D. R. Wentz, *Validation of Criticality Safety Calculations with SCALE 6.2*, ANS Nuclear Criticality Safety Division Topical Meetings (NCSD2013), Wilmington, NC, September 29–October 3, 2013.
31. B. T. Rearden, D. E. Mueller, S. M. Bowman, R. D. Busch, and S. J. Emerson, *TSUNAMI Primer: A Primer for Sensitivity/Uncertainty Calculations with SCALE*, ORNL/TM-2009/027, Oak Ridge National Laboratory, 2009.
32. B. T. Rearden, *A Criticality Code Validation Exercise with TSUNAMI*, Proceedings of ICNC2007, Volume 1, St. Petersburg, Russia, May 28–June 1, 2007.
33. *Workshop Proceedings – The Need for Post Irradiation Experiments to Validate Depletion Calculation Methodologies*, Prague, Czech Republic, May 11–12, 2006, Nuclear Energy Agency, NEA/NSC/DOC(2006)31, 2007.
34. *Technical Meeting Proceedings, Advances in Applications of Burnup Credit to Enhance Spent Fuel Transportation, Storage, Reprocessing and Disposition*, Proceedings of a Technical Meeting held in, London, August 29–September 2, 2005, International Atomic Energy Agency, IAEA-TECDOC-1547, 2007.
35. Y. Rugama et al., *Fuel Cycle Associated Activities of the OECD/NEA/NSC Working Party on Nuclear Criticality Safety*, GLOBAL 2009, “The Nuclear Fuel Cycle: Sustainable Options & Industrial Perspectives,” September 6–11, 2009, Paris, France.
36. *Spent Nuclear Fuel Assay Data for Isotopic Validation*, NEA/NSC/WPNC/DOC(2011)5, Nuclear Energy Agency, Organisation for Economic Co-operation and Development, 2011.
37. W. A. Wieselquist, K. S. Kim, G. Ilas, and I. C. Gauld, *Comparison of Burnup Credit Uncertainty Quantification Methods*, ANS Nuclear Criticality Safety Division Topical Meetings, 2013, Wilmington, NC, September 29–October 3, 2013.
38. Andrius Slavickas, et al., “Decomposition Analysis of Void Reactivity Coefficient for Innovative and Modified BWR Assemblies,” Hindawi Publishing Corporation, *Science and Technology of Nuclear Installations*, Volume 2014, Article ID 132737, March 2014. (<http://dx.doi.org/10.1155/2014/132737>).
39. I. C. Gauld, G. Radulescu, G. Ilas, B. D. Murphy, M. L. Williams, and D. Wiarda, *Isotopic Depletion and Decay Methods and Analysis Capabilities in SCALE*, Nucl. Technol. Volume 174, Issue 2, pp. 169–195, May 2011.
40. M. B. Chadwick et al., “ENDF/B-VII.0: Next Generation Evaluated Nuclear Data Library for Nuclear Science and Technology,” *Nuclear Data Sheets*, Volume 107, Issue 12, pp. 2931–3059, December 2006.
41. O. W. Hermann and M. D. DeHart, *Validation of SCALE (SAS2H) Isotopic Predictions for BWR Spent Fuel*, ORNL/TM-13315, Oak Ridge National Laboratory, September 1998.
42. “Post-Irradiation Analysis of the Gundremmingen BWR Spent Fuel,” *Nucl. Sci. and Tech.*, Commission of the European Communities, ISBN 92-825-1099-9, 1979.
43. Y. Nakahara, K. Suyama, and T. Suzuki, *Technical Development on Burnup Credit for Spent LWR Fuels*, JAERI-Tech 2000-071, ORNL/TR-2001/01, English Translation, Oak Ridge National Laboratory, 2002.
44. K. Suyama, M. Murazaki, K. Ohkubo, Y. Nakahara, G. Uchiyama, “Re-evaluation of Assay Data of Spent Nuclear Fuel Obtained at Japan Atomic Energy Research Institute for Validation of Burnup Calculation Code Systems.” *Annals of Nuclear Energy*, Volume 38, pp. 930–941, 2011.

45. M. Williams, F. Havluj, M. Pigni, I. Gauld, *SCALE Uncertainty Quantification Methodology for Criticality Safety Analysis of Used Nuclear Fuel*, ANS Topical Meetings, Wilmington, NC, September 29–October 3, 2013.
46. H. J. Smith, I. C. Gauld, and U. Mertyurek, *Analysis of Experimental Data for High Burnup BWR Spent Fuel Isotopic Validation—SVEA-96 and GE14 Assembly Designs*, NUREG/CR-7162, ORNL/TM-2013/18, U.S. Nuclear Regulatory Commission, Oak Ridge National Laboratory, 2013.
47. K. Suyama et al., *OECD/NEA Burnup Credit Criticality Benchmark Phase IIIC: Nuclide Composition and Neutron Multiplication Factor of BWR Spent Fuel Assembly for Burnup Credit and Criticality Control of Damaged Nuclear Fuel*, Benchmark Proposal, 2012.
48. H. R. Dyer and C. V. Parks, *Recommendations for Preparing the Criticality Safety Evaluation of Transportation Packages*, NUREG/CR-5661, ORNL/TM-11936, U.S. Nuclear Regulatory Commission, Oak Ridge National Laboratory, 1997.
49. S. S. Shapiro and M. B. Wilk, “An Analysis of Variance Test for Normality,” *Biometrika*, Volume 52, pp. 591–611, 1965.
50. I. C. Gauld, *Strategies for Application of Isotopic Uncertainties in Burnup Credit*, NUREG/CR-6811, ORNL/TM-2001/257, U.S. Nuclear Regulatory Commission, Oak Ridge National Laboratory, 2003.
51. G. Radulescu, I. C. Gauld, G. Ilas, and J. C. Wagner, *An Approach for Validating Actinide and Fission Product Burnup Credit Criticality Safety Analyses-Isotopic Composition Predictions*, NUREG/CR-7108, ORNL/TM-2011/509, U.S. Nuclear Regulatory Commission, Oak Ridge National Laboratory, 2012.
52. NIST/SEMATECH *e-Handbook of Statistical Methods*, available from <http://www.itl.nist.gov/div898/handbook/>, April 2010.
53. R. E. Odeh and D. B. Owen, *Tables for Normal Tolerance Limits, Sampling Plans, and Screening, Statistics: Textbooks and Monographs*, Volume 32. Marcel Dekker, Inc., New York, 1980.
54. K. Govers, M. Gysemans, and M. Verwerft, *New Spent Fuel Characterization Proposal: REGAL – Rod Extremity and Gadolinia AnaLysis*, SCK•CEN SCK•CEN-ER-110, December 2009.
55. SFCOMPO - Spent Fuel Isotopic Composition Database, <https://www.oecd-nea.org/sfcompo/>.
56. J. M. Conde and M. Recio, Evaluation of Burnup Credit for Fuel Storage Analysis—Experience in Spain, *Nuclear Technology* Volume 110, Issue 1, pp. 22 April 1995, pp. 22–32.
57. J. M. Alonso et al., *Spanish R&D Program on Spent Fuel Dry Storage*, TopFuel Conference 2006, Transactions of the International Meeting on LWR Fuel Performance, Salamanca, Spain, October 22–26, 2006.
58. M. Klein, L. Gallner, B. Krzykacz-Hausmann, I. Pasichnyk, A. Pautz, and W. Zwermann, *Influence of Nuclear Data Covariance on Reactor Core Calculations*, International Conference on Mathematics and Computational Methods Applied to Nuclear Science and Engineering, Rio de Janeiro, Brazil, May 8–12, 2011.

APPENDIX A. TRITON DEPLETION MODELING DETAILS

A.1 TRITON DEPLETION MODELING DETAILS

Four different options were used for modeling the isotopic depletion of the fuel assemblies in TRITON in Section 3: (1) pin-wise enrichment with pin-wise isotopics (PEPI), (2) pin-wise enrichment with average isotopics (PEAI), (3) average-enrichment with pin-wise isotopics (AEPI), and (4) average-enrichment with average isotopics (AEAI). These four options were chosen in an effort to cover all options that an analyst might select for isotopic modeling. In the interest of clarity, these four options are further explained in this section.

The four isotopic modeling options are a combination of two different sets of assumptions. The user can either assume that the fuel pins in a lattice contain their actual as-designed enrichment (pin-wise enrichment [PE]), or the user can assume that a single, lattice-average enrichment is used in each fuel pin (average enrichment [AE]). For either of these two assumptions, the user can then choose to either deplete a set of like-enrichment fuel pins as individual depletion regions (pin-wise isotopics, [PI]), or as a single average depletion region (average isotopics [AI]). The combinations of these different options provide the four options used throughout this work: PEPI, PEA, AEPI, and AEAI. Although other modeling options exist, these four are likely to cover the range from least conservative to most conservative options.

A further complication is the need to specify user-defined Dancoff factors for certain fuel pins in a boiling water reactor (BWR) fuel lattice when using SCALE [A1]. Accurate results for BWR lattices can be obtained by specifying user-defined Dancoff factors for fuel corner-, edge-, and water rod-adjacent fuel pins. The default Dancoff factor treatment in SCALE provides sufficient accuracy for all other fuel pins in the lattice. A plot illustrating the Dancoff factor treatment is shown in Figure A.1. The numbers indicate the ^{235}U enrichment for each pin. Fuel pin locations that result in similar Dancoff factors have been shaded pink with single underlined numbers or blue with double underlined numbers. The unshaded boxes without underlined numbers signify a fuel pin location in which the SCALE default Dancoff factor treatment is used.

<u>1.60</u>	<u>2.80</u>	<u>3.20</u>	<u>3.95</u>	<u>3.95</u>	<u>3.95</u>	<u>3.95</u>	<u>3.95</u>	<u>3.95</u>	<u>2.80</u>
<u>2.80</u>	2.80	3.20	3.95	3.60	3.95	3.95	4.40	3.95	<u>3.95</u>
<u>3.20</u>	3.20	4.40	4.40	4.90	<u>4.40</u>	<u>4.40</u>	4.40	4.40	<u>4.90</u>
<u>3.95</u>	3.95	4.40	4.90	<u>3.95</u>	WR		<u>4.90</u>	4.90	<u>4.90</u>
<u>3.95</u>	3.60	4.90	<u>3.95</u>	<u>4.40</u>	WR		<u>4.90</u>	4.90	<u>4.90</u>
<u>3.95</u>	3.95	<u>4.40</u>	WR		<u>4.90</u>	<u>4.90</u>	4.90	4.90	<u>4.90</u>
<u>3.95</u>	3.95	<u>4.40</u>	WR		<u>4.90</u>	4.90	4.90	4.90	<u>4.90</u>
<u>3.95</u>	4.40	4.40	<u>4.90</u>	<u>4.90</u>	4.90	4.90	4.90	4.90	<u>4.90</u>
<u>3.95</u>	3.95	4.40	4.90	4.90	4.90	4.90	4.90	4.90	<u>4.90</u>
<u>2.80</u>	<u>3.95</u>	<u>4.90</u>	<u>3.20</u>						

Figure A.1. Lattice layout highlighting the three different sets of Dancoff factors used in this SCALE/TRITON analysis.

PEPI uses the as-designed fuel enrichment in each fuel pin location, and each fuel pin is depleted as a separate mixture. The Dancoff factors are applied as described in Figure A.1. Figure A.2 illustrates the PEPI lattice layout and SCALE/TRITON visualization of the lattice. (Double underlined numbers indicate special Dancoff factor treatment.)

In the lattice layout, all fuel pin locations are unshaded, signifying that the fuel location uses a different depletion mixture than all other locations. This is also illustrated in the SCALE/TRITON representation in Figure A.2, which shows a different color for each fuel mixture in each diagonally symmetric location.

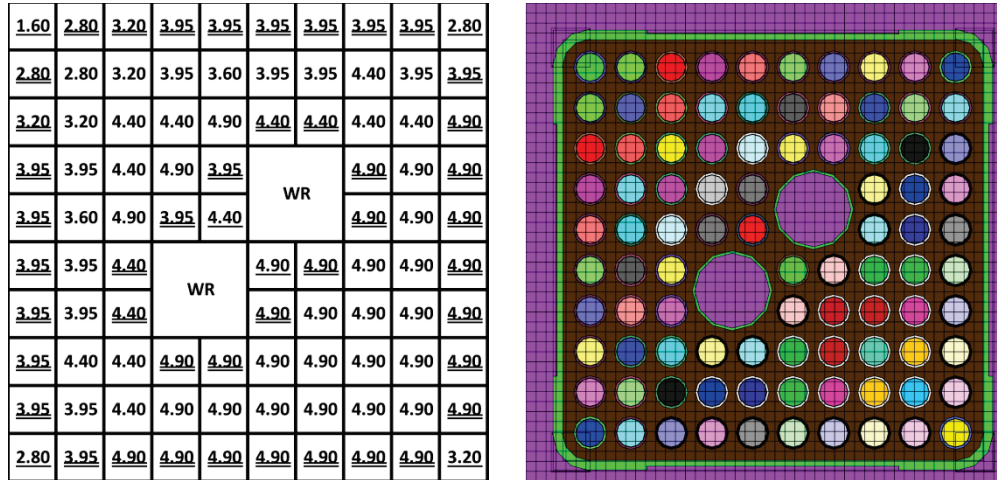


Figure A.2. PEPI lattice layout (left) and SCALE/TRITON representation (right).

AEPI uses the lattice-average enrichment in all fuel locations; each fuel pin is depleted as a separate mixture. (Double underlining signifies special Dancoff factor treatment.) Figure A.3 shows the AEPI lattice layout and SCALE/TRITON visualization of the lattice can be found in Figure A.3. In the lattice layout, all fuel pin locations are unshaded, signifying that each fuel location uses a different depletion mixture than all other locations, assuming diagonal symmetry from upper left to lower right corner. This is also illustrated in the SCALE/TRITON representation in Figure A.3, which shows a different color for each fuel mixture in each diagonally symmetric location.

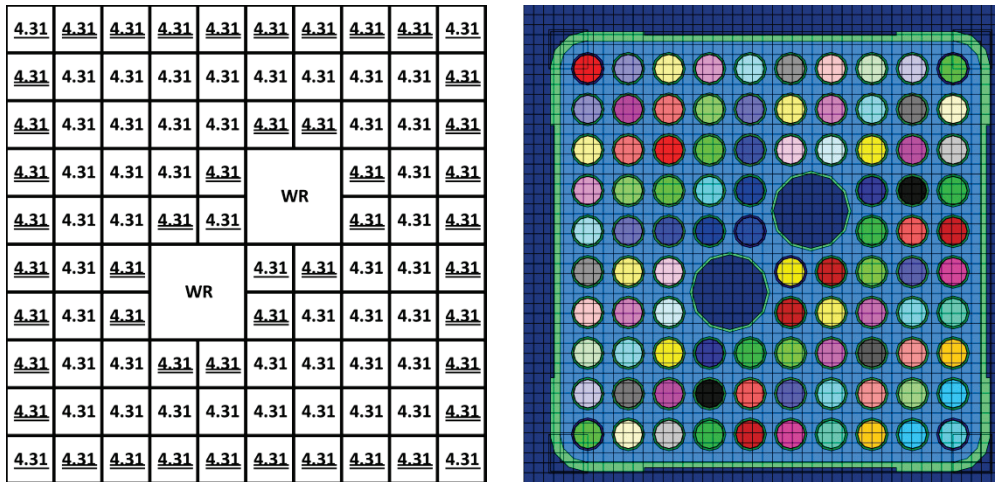


Figure A.3. AEPI lattice layout (left) and SCALE/TRITON representation (right).

Because separate Dancoff factors cannot be applied to a single fuel mixture, the AI option divides a set of like-enrichment fuel pins into three different depletion regions based on the Dancoff factor. The cross-section processing, and thus depletion, for these fuel pins must be separated by Dancoff factor grouping. For example, for the 4.40 wt% enriched set of fuel pins, three different fuel mixtures are required: as nine fuel pins receive the default Dancoff factor treatment, four receive a specialized Dancoff factor corresponding to the fuel pins along the assembly edge and near water rods, and one fuel pin receives a specialized Dancoff factor corresponding to the fuel location adjacent to both water rods. Figure A.4 presents a lattice layout highlighting this treatment using different shading for each set of depletion mixtures. In Figure A.4 a single depletion mixture is used for the green-shaded fuel locations (no underlined text), a second depletion mixture is used for the blue-shaded fuel locations (double underlined text), and a third depletion mixture is used for the orange-shaded fuel location (single underlined text).

<u>1.60</u>	<u>2.80</u>	<u>3.20</u>	<u>3.95</u>	<u>2.80</u>						
<u>2.80</u>	2.80	3.20	3.95	3.60	3.95	3.95	4.40	3.95	<u>3.95</u>	
<u>3.20</u>	3.20	4.40	4.40	4.90	<u>4.40</u>	<u>4.40</u>	4.40	4.40	<u>4.90</u>	
<u>3.95</u>	3.95	4.40	4.90	<u>3.95</u>	WR		<u>4.90</u>	4.90	<u>4.90</u>	
<u>3.95</u>	3.60	4.90	<u>3.95</u>	<u>4.40</u>			<u>4.90</u>	4.90	<u>4.90</u>	
<u>3.95</u>	3.95	<u>4.40</u>	WR		<u>4.90</u>	<u>4.90</u>	4.90	4.90	<u>4.90</u>	
<u>3.95</u>	3.95	<u>4.40</u>			<u>4.90</u>	4.90	4.90	4.90	<u>4.90</u>	
<u>3.95</u>	4.40	4.40	<u>4.90</u>	<u>4.90</u>	4.90	4.90	4.90	4.90	<u>4.90</u>	
<u>3.95</u>	3.95	4.40	4.90	4.90	4.90	4.90	4.90	4.90	<u>4.90</u>	
<u>2.80</u>	<u>3.95</u>	<u>4.90</u>	<u>3.20</u>							

Figure A.4. Visual depiction of the grouping of depletion mixtures based on Dancoff factor for 4.40 wt% fuel.

PEAI uses the as-designed fuel enrichment in each fuel pin location, and fuel is depleted in separate groups based on fuel enrichment and Dancoff factor. The lattice layout and SCALE/TRITON representation of the PEA1 options are shown in Figure A.5. Similar to Figure A.4, the shading in the boxes of the lattice layout signify different depletion mixtures – the same color is used for each

enrichment group, but the opacity is adjusted and the text is underlined in order to signify different groups of depletion mixtures that are required for separated Dancoff factor treatment. In the SCALE/TRITON layout of Figure A.5 (right), a large number of like-colored fuel pin locations are observed, indicating that the same mixture is used in each of those fuel pins.

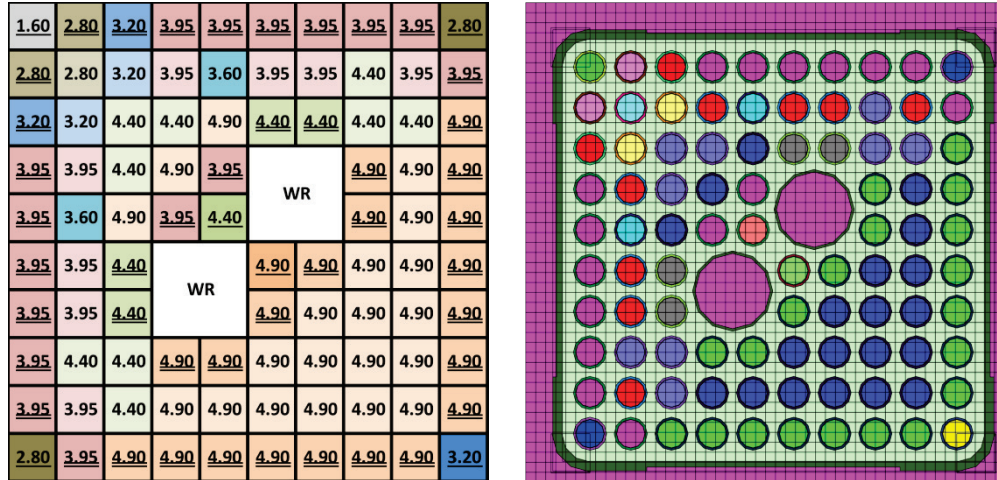


Figure A.5. PEAI lattice layout (left) and SCALE/TRITON representation (right).

AEAI uses the lattice-average enrichment in all fuel locations, and fuel is depleted by Dancoff factor groups. Figure A.6 shows the lattice layout and SCALE/TRITON representation of the AEA I option.

As in Figure A.5, the shading in the boxes of the lattice layout signify different depletion mixtures—the same color is used for each enrichment group, but the opacity is adjusted and the numbers are underlined in order to signify different groups of depletion mixtures.

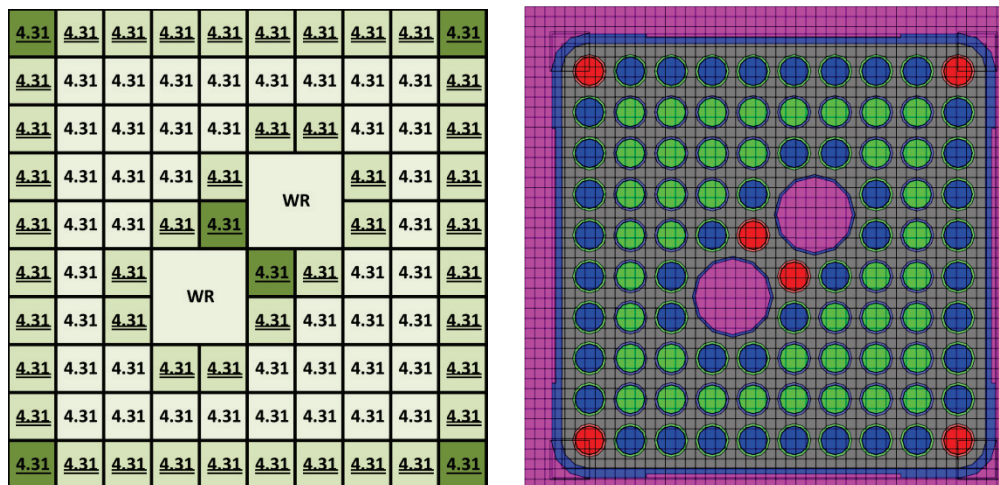


Figure A.6. AEA I lattice layout (left) and SCALE/TRITON representation (right).

None of the lattices discussed in this appendix have described the treatment when gadolinium fuel pins are present in the lattice. The treatment is very similar; for all non-gadolinium-bearing fuel locations, the same treatment as previously described as applied. In all studies in Section 3 of this report, only the 4.9% -enriched fuel pins were allowed to contain gadolinium. In these cases, each gadolinium-bearing pin was

modeled using seven radial rings. In each gadolinium-bearing fuel pin, each individual fuel ring corresponds to all other gadolinium-bearing fuel pins: the outer rings are identical between all gadolinium-bearing fuel pins; the second rings are identical between all fuel pins, etc.

A.2 APPENDIX A REFERENCE

- A1 B. J. Ade, *SCALE/TRITON Primer: A Primer for Light Water Reactor Lattice Physics Calculations*, NUREG/CR-7041, ORNL/TM-2011/21, U.S. Nuclear Regulatory Commission, Oak Ridge National Laboratory, November 2012.

APPENDIX B. GADOLINIUM PATTERNS

B.1 GADOLINIUM PATTERNS

This appendix contains the 15 gadolinium patterns used in the pattern study documented in Section 3.4.3. The base case pattern used in all sections is shown in Figure B.1; the subsequent 14 figures (B.2–B.15) show the alternate patterns considered. All patterns contain six gadolinium fuel rods containing 2 wt% gadolinium. Only pins with 4.90 weight-percent ^{235}U enrichment are considered for gadolinium in this study. The fuel enrichment and gadolinium layout for the full and vanished lattices are illustrated; a box with a single number signifies the fuel pin enrichment in wt% ^{235}U , and a box with two numbers signifies the enrichment (top) and gadolinium content in wt% gadolinium (bottom). The large boxes containing “WR” specify the large central water rod and boxes with a “V” specify a vanished fuel pin.

1.60	2.80	3.20	3.95	3.95	3.95	3.95	3.95	3.95	3.95	2.80
2.80	2.80	3.20	3.95	3.60	3.95	3.95	4.40	3.95	3.95	
3.20	3.20	4.40	4.40	4.90 Gd	4.40	4.40	4.40	4.40	4.90	
3.95	3.95	4.40	4.90	3.95	WR		4.90	4.90	4.90	
3.95	3.60	4.90 Gd	3.95	4.40	WR		4.90	4.90	4.90	
3.95	3.95	4.40	WR		4.90	4.90	4.90	4.90 Gd	4.90	
3.95	3.95	4.40	WR		4.90	4.90	4.90	4.90	4.90	
3.95	4.40	4.40	4.90	4.90	4.90	4.90	4.90	4.90 Gd	4.90	
3.95	3.95	4.40	4.90	4.90	4.90 Gd	4.90	4.90 Gd	4.90	4.90	
2.80	3.95	4.90	4.90	4.90	4.90	4.90	4.90	4.90	3.20	

1.60	2.80	3.20	3.95	3.95	3.95	3.95	3.95	3.95	2.80	
2.80	V	3.20	V	3.60	3.95	V	4.40	V	3.95	
3.20	3.20	4.40	4.40	4.90 Gd	4.40	4.40	4.40	4.40	4.90	
3.95	V	4.40	4.90	3.95	WR		4.90	V	4.90	
3.95	3.60	4.90 Gd	3.95	V	WR		4.90	4.90	4.90	
3.95	3.95	4.40	WR		V	4.90	4.90	4.90 Gd	4.90	
3.95	V	4.40	WR		4.90	4.90	4.90	V	4.90	
3.95	4.40	4.40	4.90	4.90	4.90	4.90	4.90	4.90 Gd	4.90	
3.95	V	4.40	V	4.90	4.90 Gd	V	4.90 Gd	V	4.90	
2.80	3.95	4.90	4.90	4.90	4.90	4.90	4.90	4.90	3.20	

Figure B.1. Gadolinium patterns 0 (same as used in the Gd-loading study, P0).

1.60	2.80	3.20	3.95	3.95	3.95	3.95	3.95	3.95	2.80	
2.80	2.80	3.20	3.95	3.60	3.95	3.95	4.40	3.95	3.95	
3.20	3.20	4.40	4.40	4.90 Gd	4.40	4.40	4.40	4.40	4.90	
3.95	3.95	4.40	4.90	3.95	WR		4.90	4.90	4.90	
3.95	3.60	4.90 Gd	3.95	4.40	WR		4.90	4.90	4.90	
3.95	3.95	4.40	WR		4.90	4.90	4.90 Gd	4.90	4.90	
3.95	3.95	4.40	WR		4.90	4.90	4.90	4.90	4.90	
3.95	4.40	4.40	4.90	4.90	4.90 Gd	4.90	4.90	4.90 Gd	4.90	
3.95	3.95	4.40	4.90	4.90	4.90	4.90	4.90 Gd	4.90	4.90	
2.80	3.95	4.90	4.90	4.90	4.90	4.90	4.90	4.90	3.20	

1.60	2.80	3.20	3.95	3.95	3.95	3.95	3.95	3.95	2.80	
2.80	V	3.20	V	3.60	3.95	V	4.40	V	3.95	
3.20	3.20	4.40	4.40	4.90 Gd	4.40	4.40	4.40	4.40	4.90	
3.95	V	4.40	4.90	3.95	WR		4.90	V	4.90	
3.95	3.60	4.90 Gd	3.95	V	WR		4.90	4.90	4.90	
3.95	3.95	4.40	WR		V	4.90	4.90	4.90 Gd	4.90	
3.95	V	4.40	WR		4.90	4.90	4.90	V	4.90	
3.95	4.40	4.40	4.90	4.90	4.90 Gd	4.90	4.90	4.90 Gd	4.90	
3.95	V	4.40	V	4.90	4.90	V	4.90 Gd	V	4.90	
2.80	3.95	4.90	4.90	4.90	4.90	4.90	4.90	4.90	3.20	

Figure B.2. Gadolinium patterns 1 (P1).

1.60	2.80	3.20	3.95	3.95	3.95	3.95	3.95	3.95	2.80
2.80	2.80	3.20	3.95	3.60	3.95	3.95	4.40	3.95	3.95
3.20	3.20	4.40	4.40	4.90 Gd	4.40	4.40	4.40	4.40	4.90
3.95	3.95	4.40	4.90	3.95	WR		4.90	4.90	4.90
3.95	3.60	4.90 Gd	3.95	4.40	WR		4.90	4.90 Gd	4.90
3.95	3.95	4.40	WR		4.90	4.90	4.90	4.90	4.90
3.95	3.95	4.40	WR		4.90	4.90	4.90	4.90	4.90
3.95	4.40	4.40	4.90	4.90	4.90	4.90	4.90	4.90 Gd	4.90
3.95	3.95	4.40	4.90	4.90 Gd	4.90	4.90	4.90 Gd	4.90	4.90
2.80	3.95	4.90	4.90	4.90	4.90	4.90	4.90	4.90	3.20

1.60	2.80	3.20	3.95	3.95	3.95	3.95	3.95	3.95	2.80
2.80	V	3.20	V	3.60	3.95	V	4.40	V	3.95
3.20	3.20	4.40	4.40	4.90 Gd	4.40	4.40	4.40	4.40	4.90
3.95	V	4.40	4.90	3.95	WR		4.90	V	4.90
3.95	3.60	4.90 Gd	3.95	V	WR		4.90	4.90 Gd	4.90
3.95	3.95	4.40	WR		V	4.90	4.90	4.90	4.90
3.95	V	4.40	WR		4.90	4.90	4.90	V	4.90
3.95	4.40	4.40	4.90	4.90	4.90	4.90	4.90	4.90 Gd	4.90
3.95	V	4.40	V	4.90 Gd	4.90	V	4.90 Gd	V	4.90
2.80	3.95	4.90	4.90	4.90	4.90	4.90	4.90	4.90	3.20

Figure B.3. Gadolinium patterns 2 (P2).

1.60	2.80	3.20	3.95	3.95	3.95	3.95	3.95	3.95	2.80
2.80	2.80	3.20	3.95	3.60	3.95	3.95	4.40	3.95	3.95
3.20	3.20	4.40	4.40	4.90 Gd	4.40	4.40	4.40	4.40	4.90
3.95	3.95	4.40	4.90	3.95	WR		4.90	4.90	4.90
3.95	3.60	4.90 Gd	3.95	4.40	WR		4.90 Gd	4.90	4.90
3.95	3.95	4.40	WR		4.90	4.90	4.90	4.90	4.90
3.95	3.95	4.40	WR		4.90	4.90	4.90	4.90	4.90
3.95	4.40	4.40	4.90	4.90 Gd	4.90	4.90	4.90	4.90 Gd	4.90
3.95	3.95	4.40	4.90	4.90	4.90	4.90	4.90 Gd	4.90	4.90
2.80	3.95	4.90	4.90	4.90	4.90	4.90	4.90	4.90	3.20

1.60	2.80	3.20	3.95	3.95	3.95	3.95	3.95	3.95	2.80
2.80	V	3.20	V	3.60	3.95	V	4.40	V	3.95
3.20	3.20	4.40	4.40	4.90 Gd	4.40	4.40	4.40	4.40	4.90
3.95	V	4.40	4.90	3.95	WR		4.90	V	4.90
3.95	3.60	4.90 Gd	3.95	V	WR		4.90 Gd	4.90	4.90
3.95	3.95	4.40	WR		V	4.90	4.90	4.90	4.90
3.95	V	4.40	WR		4.90	4.90	4.90	V	4.90
3.95	4.40	4.40	4.90	4.90 Gd	4.90	4.90	4.90	4.90 Gd	4.90
3.95	V	4.40	V	4.90	4.90	V	4.90 Gd	V	4.90
2.80	3.95	4.90	4.90	4.90	4.90	4.90	4.90	4.90	3.20

Figure B.4. Gadolinium patterns 3 (P3).

1.60	2.80	3.20	3.95	3.95	3.95	3.95	3.95	3.95	2.80
2.80	2.80	3.20	3.95	3.60	3.95	3.95	4.40	3.95	3.95
3.20	3.20	4.40	4.40	4.90 Gd	4.40	4.40	4.40	4.40	4.90
3.95	3.95	4.40	4.90	3.95	WR		4.90	4.90	4.90
3.95	3.60	4.90 Gd	3.95	4.40	WR		4.90 Gd	4.90	4.90
3.95	3.95	4.40	WR		4.90	4.90	4.90	4.90	4.90
3.95	3.95	4.40	WR		4.90	4.90	4.90 Gd	4.90	4.90
3.95	4.40	4.40	4.90	4.90 Gd	4.90	4.90 Gd	4.90	4.90	4.90
3.95	3.95	4.40	4.90	4.90	4.90	4.90	4.90	4.90	4.90
2.80	3.95	4.90	4.90	4.90	4.90	4.90	4.90	4.90	3.20

1.60	2.80	3.20	3.95	3.95	3.95	3.95	3.95	3.95	2.80
2.80	V	3.20	V	3.60	3.95	V	4.40	V	3.95
3.20	3.20	4.40	4.40	4.90 Gd	4.40	4.40	4.40	4.40	4.90
3.95	V	4.40	4.90	3.95	WR		4.90	V	4.90
3.95	3.60	4.90 Gd	3.95	V	WR		4.90 Gd	4.90	4.90
3.95	3.95	4.40	WR		V	4.90	4.90	4.90	4.90
3.95	V	4.40	WR		4.90	4.90	4.90 Gd	V	4.90
3.95	4.40	4.40	4.90	4.90 Gd	4.90	4.90 Gd	4.90	4.90	4.90
3.95	V	4.40	V	4.90	4.90	V	4.90	V	4.90
2.80	3.95	4.90	4.90	4.90	4.90	4.90	4.90	4.90	3.20

Figure B.5. Gadolinium patterns 4 (P4).

1.60	2.80	3.20	3.95	3.95	3.95	3.95	3.95	3.95	2.80
2.80	2.80	3.20	3.95	3.60	3.95	3.95	4.40	3.95	3.95
3.20	3.20	4.40	4.40	4.90	4.40	4.40	4.40	4.40	4.90
3.95	3.95	4.40	4.90 Gd	3.95	WR		4.90	4.90	4.90
3.95	3.60	4.90	3.95	4.40	WR		4.90	4.90	4.90
3.95	3.95	4.40	WR		4.90	4.90	4.90	4.90 Gd	4.90
3.95	3.95	4.40	WR		4.90	4.90 Gd	4.90	4.90	4.90
3.95	4.40	4.40	4.90	4.90	4.90	4.90	4.90	4.90 Gd	4.90
3.95	3.95	4.40	4.90	4.90	4.90 Gd	4.90	4.90 Gd	4.90	4.90
2.80	3.95	4.90	4.90	4.90	4.90	4.90	4.90	4.90	3.20

1.60	2.80	3.20	3.95	3.95	3.95	3.95	3.95	3.95	2.80
2.80	V	3.20	V	3.60	3.95	V	4.40	V	3.95
3.20	3.20	4.40	4.40	4.90	4.40	4.40	4.40	4.40	4.90
3.95	V	4.40	4.90 Gd	3.95	WR		4.90	V	4.90
3.95	3.60	4.90	3.95	V	WR		4.90	4.90	4.90
3.95	3.95	4.40	WR		V	4.90	4.90	4.90 Gd	4.90
3.95	V	4.40	WR		4.90	4.90 Gd	4.90	V	4.90
3.95	4.40	4.40	4.90	4.90	4.90	4.90	4.90	4.90 Gd	4.90
3.95	V	4.40	V	4.90	4.90 Gd	V	4.90 Gd	V	4.90
2.80	3.95	4.90	4.90	4.90	4.90	4.90	4.90	4.90	3.20

Figure B.6. Gadolinium patterns 5 (P5).

1.60	2.80	3.20	3.95	3.95	3.95	3.95	3.95	3.95	2.80
2.80	2.80	3.20	3.95	3.60	3.95	3.95	4.40	3.95	3.95
3.20	3.20	4.40	4.40	4.90	4.40	4.40	4.40	4.40	4.90
3.95	3.95	4.40	4.90 Gd	3.95	WR		4.90	4.90	4.90
3.95	3.60	4.90	3.95	4.40	WR		4.90 Gd	4.90	4.90
3.95	3.95	4.40	WR		4.90	4.90	4.90	4.90	4.90
3.95	3.95	4.40	WR		4.90	4.90 Gd	4.90	4.90	4.90
3.95	4.40	4.40	4.90	4.90 Gd	4.90	4.90	4.90	4.90 Gd	4.90
3.95	3.95	4.40	4.90	4.90	4.90	4.90	4.90 Gd	4.90	4.90
2.80	3.95	4.90	4.90	4.90	4.90	4.90	4.90	4.90	3.20

1.60	2.80	3.20	3.95	3.95	3.95	3.95	3.95	3.95	2.80
2.80	V	3.20	V	3.60	3.95	V	4.40	V	3.95
3.20	3.20	4.40	4.40	4.90	4.40	4.40	4.40	4.40	4.90
3.95	V	4.40	4.90 Gd	3.95	WR		4.90	V	4.90
3.95	3.60	4.90	3.95	V	WR		4.90 Gd	4.90	4.90
3.95	3.95	4.40	WR		V	4.90	4.90	4.90	4.90
3.95	V	4.40	WR		4.90	4.90 Gd	4.90	V	4.90
3.95	4.40	4.40	4.90	4.90 Gd	4.90	4.90	4.90	4.90 Gd	4.90
3.95	V	4.40	V	4.90	4.90	V	4.90 Gd	V	4.90
2.80	3.95	4.90	4.90	4.90	4.90	4.90	4.90	4.90	3.20

Figure B.7. Gadolinium patterns 6 (P6).

1.60	2.80	3.20	3.95	3.95	3.95	3.95	3.95	3.95	2.80
2.80	2.80	3.20	3.95	3.60	3.95	3.95	4.40	3.95	3.95
3.20	3.20	4.40	4.40	4.90	4.40	4.40	4.40	4.40	4.90
3.95	3.95	4.40	4.90 Gd	3.95	WR		4.90	4.90	4.90
3.95	3.60	4.90	3.95	4.40	WR		4.90	4.90	4.90
3.95	3.95	4.40	WR		4.90	4.90 Gd	4.90	4.90 Gd	4.90
3.95	3.95	4.40	WR		4.90 Gd	4.90	4.90	4.90	4.90
3.95	4.40	4.40	4.90	4.90	4.90	4.90	4.90 Gd	4.90	4.90
3.95	3.95	4.40	4.90	4.90	4.90 Gd	4.90	4.90	4.90	4.90
2.80	3.95	4.90	4.90	4.90	4.90	4.90	4.90	4.90	3.20

1.60	2.80	3.20	3.95	3.95	3.95	3.95	3.95	3.95	2.80
2.80	V	3.20	V	3.60	3.95	V	4.40	V	3.95
3.20	3.20	4.40	4.40	4.90	4.40	4.40	4.40	4.40	4.90
3.95	V	4.40	4.90 Gd	3.95	WR		4.90	V	4.90
3.95	3.60	4.90	3.95	V	WR		4.90	4.90	4.90
3.95	3.95	4.40	WR		V	4.90 Gd	4.90	4.90 Gd	4.90
3.95	V	4.40	WR		4.90 Gd	4.90	4.90	V	4.90
3.95	4.40	4.40	4.90	4.90	4.90	4.90	4.90 Gd	4.90	4.90
3.95	V	4.40	V	4.90	4.90 Gd	V	4.90	V	4.90
2.80	3.95	4.90	4.90	4.90	4.90	4.90	4.90	4.90	3.20

Figure B.8. Gadolinium patterns 7 (P7).

1.60	2.80	3.20	3.95	3.95	3.95	3.95	3.95	3.95	2.80
2.80	2.80	3.20	3.95	3.60	3.95	3.95	4.40	3.95	3.95
3.20	3.20	4.40	4.40	4.90	4.40	4.40	4.40	4.40	4.90
3.95	3.95	4.40	4.90 Gd	3.95	WR		4.90	4.90	4.90
3.95	3.60	4.90	3.95	4.40	WR		4.90	4.90 Gd	4.90
3.95	3.95	4.40	WR		4.90	4.90 Gd	4.90	4.90	4.90
3.95	3.95	4.40	WR		4.90 Gd	4.90	4.90	4.90	4.90
3.95	4.40	4.40	4.90	4.90	4.90	4.90	4.90 Gd	4.90	4.90
3.95	3.95	4.40	4.90	4.90 Gd	4.90	4.90	4.90	4.90	4.90
2.80	3.95	4.90	4.90	4.90	4.90	4.90	4.90	4.90	3.20

1.60	2.80	3.20	3.95	3.95	3.95	3.95	3.95	3.95	2.80
2.80	V	3.20	V	3.60	3.95	V	4.40	V	3.95
3.20	3.20	4.40	4.40	4.90	4.40	4.40	4.40	4.40	4.90
3.95	V	4.40	4.90 Gd	3.95	WR		4.90	V	4.90
3.95	3.60	4.90	3.95	V	WR		4.90	4.90 Gd	4.90
3.95	3.95	4.40	WR		V	4.90 Gd	4.90	4.90	4.90
3.95	V	4.40	WR		4.90 Gd	4.90	4.90	V	4.90
3.95	4.40	4.40	4.90	4.90	4.90	4.90	4.90 Gd	4.90	4.90
3.95	V	4.40	V	4.90 Gd	4.90	V	4.90	V	4.90
2.80	3.95	4.90	4.90	4.90	4.90	4.90	4.90	4.90	3.20

Figure B.9. Gadolinium patterns 8 (P8).

1.60	2.80	3.20	3.95	3.95	3.95	3.95	3.95	3.95	2.80
2.80	2.80	3.20	3.95	3.60	3.95	3.95	4.40	3.95	3.95
3.20	3.20	4.40	4.40	4.90	4.40	4.40	4.40	4.40	4.90
3.95	3.95	4.40	4.90 Gd	3.95	WR		4.90 Gd	4.90	4.90
3.95	3.60	4.90	3.95	4.40	WR		4.90	4.90	4.90
3.95	3.95	4.40	WR		4.90	4.90 Gd	4.90	4.90	4.90
3.95	3.95	4.40	WR		4.90 Gd	4.90	4.90	4.90	4.90
3.95	4.40	4.40	4.90 Gd	4.90	4.90	4.90	4.90 Gd	4.90	4.90
3.95	3.95	4.40	4.90	4.90	4.90	4.90	4.90	4.90	4.90
2.80	3.95	4.90	4.90	4.90	4.90	4.90	4.90	4.90	3.20

1.60	2.80	3.20	3.95	3.95	3.95	3.95	3.95	3.95	2.80
2.80	V	3.20	V	3.60	3.95	V	4.40	V	3.95
3.20	3.20	4.40	4.40	4.90	4.40	4.40	4.40	4.40	4.90
3.95	V	4.40	4.90 Gd	3.95	WR		4.90 Gd	V	4.90
3.95	3.60	4.90	3.95	V	WR		4.90	4.90	4.90
3.95	3.95	4.40	WR		V	4.90 Gd	4.90	4.90	4.90
3.95	V	4.40	WR		4.90 Gd	4.90	4.90	V	4.90
3.95	4.40	4.40	4.90 Gd	4.90	4.90	4.90	4.90 Gd	4.90	4.90
3.95	V	4.40	V	4.90	4.90	V	4.90	V	4.90
2.80	3.95	4.90	4.90	4.90	4.90	4.90	4.90	4.90	3.20

Figure B.10. Gadolinium patterns 9 (P9).

1.60	2.80	3.20	3.95	3.95	3.95	3.95	3.95	3.95	2.80
2.80	2.80	3.20	3.95	3.60	3.95	3.95	4.40	3.95	3.95
3.20	3.20	4.40	4.40	4.90	4.40	4.40	4.40	4.40	4.90
3.95	3.95	4.40	4.90	3.95	WR		4.90	4.90	4.90
3.95	3.60	4.90	3.95	4.40	WR		4.90	4.90	4.90
3.95	3.95	4.40	WR		4.90	4.90 Gd	4.90	4.90 Gd	4.90
3.95	3.95	4.40	WR		4.90 Gd	4.90	4.90	4.90	4.90
3.95	4.40	4.40	4.90	4.90	4.90	4.90	4.90	4.90 Gd	4.90
3.95	3.95	4.40	4.90	4.90	4.90 Gd	4.90	4.90 Gd	4.90	4.90
2.80	3.95	4.90	4.90	4.90	4.90	4.90	4.90	4.90	3.20

1.60	2.80	3.20	3.95	3.95	3.95	3.95	3.95	3.95	2.80
2.80	V	3.20	V	3.60	3.95	V	4.40	V	3.95
3.20	3.20	4.40	4.40	4.90	4.40	4.40	4.40	4.40	4.90
3.95	V	4.40	4.90	3.95	WR		4.90	V	4.90
3.95	3.60	4.90	3.95	V	WR		4.90	4.90	4.90
3.95	3.95	4.40	WR		V	4.90 Gd	4.90	4.90 Gd	4.90
3.95	V	4.40	WR		4.90 Gd	4.90	4.90	V	4.90
3.95	4.40	4.40	4.90	4.90	4.90	4.90	4.90	4.90 Gd	4.90
3.95	V	4.40	V	4.90	4.90 Gd	V	4.90 Gd	V	4.90
2.80	3.95	4.90	4.90	4.90	4.90	4.90	4.90	4.90	3.20

Figure B.11. Gadolinium patterns 10 (P10).

1.60	2.80	3.20	3.95	3.95	3.95	3.95	3.95	3.95	2.80
2.80	2.80	3.20	3.95	3.60	3.95	3.95	4.40	3.95	3.95
3.20	3.20	4.40	4.40	4.90	4.40	4.40	4.40	4.40	4.90
3.95	3.95	4.40	4.90	3.95	WR		4.90	4.90	4.90
3.95	3.60	4.90	3.95	4.40	WR		4.90	4.90 Gd	4.90
3.95	3.95	4.40	WR		4.90	4.90 Gd	4.90	4.90	4.90
3.95	3.95	4.40	WR		4.90 Gd	4.90	4.90	4.90	4.90
3.95	4.40	4.40	4.90	4.90	4.90	4.90	4.90	4.90 Gd	4.90
3.95	3.95	4.40	4.90	4.90 Gd	4.90	4.90	4.90 Gd	4.90	4.90
2.80	3.95	4.90	4.90	4.90	4.90	4.90	4.90	4.90	3.20

1.60	2.80	3.20	3.95	3.95	3.95	3.95	3.95	3.95	2.80
2.80	V	3.20	V	3.60	3.95	V	4.40	V	3.95
3.20	3.20	4.40	4.40	4.90	4.40	4.40	4.40	4.40	4.90
3.95	V	4.40	4.90	3.95	WR		4.90	V	4.90
3.95	3.60	4.90	3.95	V	WR		4.90	4.90 Gd	4.90
3.95	3.95	4.40	WR		V	4.90 Gd	4.90	4.90	4.90
3.95	V	4.40	WR		4.90 Gd	4.90	4.90	V	4.90
3.95	4.40	4.40	4.90	4.90	4.90	4.90	4.90	4.90 Gd	4.90
3.95	V	4.40	V	4.90 Gd	4.90	V	4.90 Gd	V	4.90
2.80	3.95	4.90	4.90	4.90	4.90	4.90	4.90	4.90	3.20

Figure B.12. Gadolinium patterns 11 (P11).

1.60	2.80	3.20	3.95	3.95	3.95	3.95	3.95	3.95	2.80
2.80	2.80	3.20	3.95	3.60	3.95	3.95	4.40	3.95	3.95
3.20	3.20	4.40	4.40	4.90	4.40	4.40	4.40	4.40	4.90
3.95	3.95	4.40	4.90	3.95	WR		4.90 Gd	4.90	4.90
3.95	3.60	4.90	3.95	4.40			4.90	4.90	4.90
3.95	3.95	4.40	WR		4.90	4.90 Gd	4.90	4.90	4.90
3.95	3.95	4.40			4.90 Gd	4.90	4.90	4.90	4.90
3.95	4.40	4.40	4.90 Gd	4.90	4.90	4.90	4.90 Gd	4.90	
3.95	3.95	4.40	4.90	4.90	4.90	4.90	4.90 Gd	4.90	
2.80	3.95	4.90	4.90	4.90	4.90	4.90	4.90	3.20	

1.60	2.80	3.20	3.95	3.95	3.95	3.95	3.95	3.95	2.80
2.80	V	3.20	V	3.60	3.95	V	4.40	V	3.95
3.20	3.20	4.40	4.40	4.90	4.40	4.40	4.40	4.40	4.90
3.95	V	4.40	4.90	3.95	WR		4.90 Gd	V	4.90
3.95	3.60	4.90	3.95	V			4.90	4.90	4.90
3.95	3.95	4.40	WR		V	4.90 Gd	4.90	4.90	4.90
3.95	V	4.40			4.90 Gd	4.90	4.90	V	4.90
3.95	4.40	4.40	4.90 Gd	4.90	4.90	4.90	4.90	4.90 Gd	4.90
3.95	V	4.40	V	4.90	4.90	V	4.90 Gd	V	4.90
2.80	3.95	4.90	4.90	4.90	4.90	4.90	4.90	4.90	3.20

Figure B.13. Gadolinium patterns 12 (P12).

1.60	2.80	3.20	3.95	3.95	3.95	3.95	3.95	3.95	2.80
2.80	2.80	3.20	3.95	3.60	3.95	3.95	4.40	3.95	3.95
3.20	3.20	4.40	4.40	4.90	4.40	4.40	4.40	4.40	4.90
3.95	3.95	4.40	4.90	3.95	WR		4.90 Gd	4.90	4.90
3.95	3.60	4.90	3.95	4.40			4.90	4.90 Gd	4.90
3.95	3.95	4.40	WR		4.90	4.90	4.90	4.90	4.90
3.95	3.95	4.40			4.90	4.90	4.90	4.90	4.90
3.95	4.40	4.40	4.90 Gd	4.90	4.90	4.90	4.90 Gd	4.90	
3.95	3.95	4.40	4.90	4.90 Gd	4.90	4.90	4.90 Gd	4.90	
2.80	3.95	4.90	4.90	4.90	4.90	4.90	4.90	4.90	3.20

1.60	2.80	3.20	3.95	3.95	3.95	3.95	3.95	3.95	2.80
2.80	V	3.20	V	3.60	3.95	V	4.40	V	3.95
3.20	3.20	4.40	4.40	4.90	4.40	4.40	4.40	4.40	4.90
3.95	V	4.40	4.90	3.95	WR		4.90 Gd	V	4.90
3.95	3.60	4.90	3.95	V			4.90	4.90 Gd	4.90
3.95	3.95	4.40	WR		V	4.90	4.90	4.90	4.90
3.95	V	4.40			4.90	4.90	4.90	V	4.90
3.95	4.40	4.40	4.90 Gd	4.90	4.90	4.90	4.90	4.90 Gd	4.90
3.95	V	4.40	V	4.90 Gd	4.90	V	4.90 Gd	V	4.90
2.80	3.95	4.90	4.90	4.90	4.90	4.90	4.90	4.90	3.20

Figure B.14. Gadolinium patterns 13 (P13).

1.60	2.80	3.20	3.95	3.95	3.95	3.95	3.95	3.95	2.80
2.80	2.80	3.20	3.95	3.60	3.95	3.95	4.40	3.95	3.95
3.20	3.20	4.40	4.40	4.90	4.40	4.40	4.40	4.40	4.90
3.95	3.95	4.40	4.90	3.95	WR		4.90 Gd	4.90	4.90
3.95	3.60	4.90	3.95	4.40			4.90	4.90	4.90
3.95	3.95	4.40	WR		4.90	4.90	4.90 Gd	4.90	4.90
3.95	3.95	4.40			4.90	4.90	4.90	4.90	4.90
3.95	4.40	4.40	4.90 Gd	4.90	4.90 Gd	4.90	4.90 Gd	4.90	4.90
3.95	3.95	4.40	4.90	4.90	4.90	4.90	4.90 Gd	4.90	4.90
2.80	3.95	4.90	4.90	4.90	4.90	4.90	4.90	4.90	3.20

1.60	2.80	3.20	3.95	3.95	3.95	3.95	3.95	3.95	2.80
2.80	V	3.20	V	3.60	3.95	V	4.40	V	3.95
3.20	3.20	4.40	4.40	4.90	4.40	4.40	4.40	4.40	4.90
3.95	V	4.40	4.90	3.95	WR		4.90 Gd	V	4.90
3.95	3.60	4.90	3.95	V			4.90	4.90	4.90
3.95	3.95	4.40	WR		V	4.90	4.90 Gd	4.90	4.90
3.95	V	4.40			4.90	4.90	4.90	V	4.90
3.95	4.40	4.40	4.90 Gd	4.90	4.90 Gd	4.90	4.90	4.90 Gd	4.90
3.95	V	4.40	V	4.90	4.90	V	4.90 Gd	V	4.90
2.80	3.95	4.90	4.90	4.90	4.90	4.90	4.90	4.90	3.20

Figure B.15. Gadolinium patterns 14 (P14).

APPENDIX C. EXPERIMENTS CONSIDERED

C.1 EXPERIMENTS CONSIDERED

This appendix contains the full list of critical experiments considered as candidates for validation in Table C.1. This list was compiled from the three sources discussed in Section 4.3 and contains 1643 unique critical experiments.

Table C.1. Critical experiments considered for validation

LEU-COMP-THERM-001-001	LEU-COMP-THERM-033-025	LEU-COMP-THERM-090-007
LEU-COMP-THERM-001-002	LEU-COMP-THERM-033-026	LEU-COMP-THERM-090-008
LEU-COMP-THERM-001-003	LEU-COMP-THERM-033-027	LEU-COMP-THERM-090-009
LEU-COMP-THERM-001-004	LEU-COMP-THERM-033-028	LEU-COMP-THERM-091-001
LEU-COMP-THERM-001-005	LEU-COMP-THERM-033-029	LEU-COMP-THERM-091-002
LEU-COMP-THERM-001-006	LEU-COMP-THERM-033-030	LEU-COMP-THERM-091-003
LEU-COMP-THERM-001-007	LEU-COMP-THERM-033-031	LEU-COMP-THERM-091-004
LEU-COMP-THERM-001-008	LEU-COMP-THERM-033-032	LEU-COMP-THERM-091-005
LEU-COMP-THERM-002-001	LEU-COMP-THERM-033-033	LEU-COMP-THERM-091-006
LEU-COMP-THERM-002-002	LEU-COMP-THERM-033-034	LEU-COMP-THERM-091-007
LEU-COMP-THERM-002-003	LEU-COMP-THERM-033-035	LEU-COMP-THERM-091-008
LEU-COMP-THERM-002-004	LEU-COMP-THERM-033-036	LEU-COMP-THERM-091-009
LEU-COMP-THERM-002-005	LEU-COMP-THERM-033-037	LEU-COMP-THERM-092-001
LEU-COMP-THERM-003-001	LEU-COMP-THERM-033-038	LEU-COMP-THERM-092-002
LEU-COMP-THERM-003-002	LEU-COMP-THERM-033-039	LEU-COMP-THERM-092-003
LEU-COMP-THERM-003-003	LEU-COMP-THERM-033-040	LEU-COMP-THERM-092-004
LEU-COMP-THERM-003-004	LEU-COMP-THERM-033-041	LEU-COMP-THERM-092-005
LEU-COMP-THERM-003-005	LEU-COMP-THERM-033-042	LEU-COMP-THERM-092-006
LEU-COMP-THERM-003-006	LEU-COMP-THERM-033-043	LEU-COMP-THERM-094-001
LEU-COMP-THERM-003-007	LEU-COMP-THERM-033-044	LEU-COMP-THERM-094-002
LEU-COMP-THERM-003-008	LEU-COMP-THERM-033-045	LEU-COMP-THERM-094-003
LEU-COMP-THERM-003-009	LEU-COMP-THERM-033-046	LEU-COMP-THERM-094-004
LEU-COMP-THERM-003-010	LEU-COMP-THERM-033-047	LEU-COMP-THERM-094-005
LEU-COMP-THERM-003-011	LEU-COMP-THERM-033-048	LEU-COMP-THERM-094-006
LEU-COMP-THERM-003-012	LEU-COMP-THERM-033-049	LEU-COMP-THERM-094-007
LEU-COMP-THERM-003-013	LEU-COMP-THERM-033-050	LEU-COMP-THERM-094-008
LEU-COMP-THERM-003-014	LEU-COMP-THERM-033-051	LEU-COMP-THERM-094-009
LEU-COMP-THERM-003-015	LEU-COMP-THERM-033-052	LEU-COMP-THERM-094-010
LEU-COMP-THERM-003-016	LEU-COMP-THERM-034-001	LEU-COMP-THERM-094-011
LEU-COMP-THERM-003-017	LEU-COMP-THERM-034-002	LEU-MISC-THERM-005-001
LEU-COMP-THERM-003-018	LEU-COMP-THERM-034-003	LEU-MISC-THERM-005-002
LEU-COMP-THERM-003-019	LEU-COMP-THERM-034-004	LEU-MISC-THERM-005-003
LEU-COMP-THERM-003-020	LEU-COMP-THERM-034-005	LEU-MISC-THERM-005-004
LEU-COMP-THERM-003-021	LEU-COMP-THERM-034-006	LEU-MISC-THERM-005-005
LEU-COMP-THERM-003-022	LEU-COMP-THERM-034-007	LEU-MISC-THERM-005-006
LEU-COMP-THERM-004-001	LEU-COMP-THERM-034-008	LEU-MISC-THERM-005-007
LEU-COMP-THERM-004-002	LEU-COMP-THERM-034-009	LEU-MISC-THERM-005-008
LEU-COMP-THERM-004-003	LEU-COMP-THERM-034-010	LEU-MISC-THERM-005-009
LEU-COMP-THERM-004-004	LEU-COMP-THERM-034-011	LEU-MISC-THERM-005-010
LEU-COMP-THERM-004-005	LEU-COMP-THERM-034-012	LEU-MISC-THERM-005-011

Table C.1. Continued

LEU-COMP-THERM-004-006	LEU-COMP-THERM-034-013	LEU-MISC-THERM-005-012
LEU-COMP-THERM-004-007	LEU-COMP-THERM-034-014	LEU-SOL-THERM-002-001
LEU-COMP-THERM-004-008	LEU-COMP-THERM-034-015	LEU-SOL-THERM-002-002
LEU-COMP-THERM-004-009	LEU-COMP-THERM-034-016	LEU-SOL-THERM-002-003
LEU-COMP-THERM-004-010	LEU-COMP-THERM-034-017	LEU-SOL-THERM-003-001
LEU-COMP-THERM-004-011	LEU-COMP-THERM-034-018	LEU-SOL-THERM-003-002
LEU-COMP-THERM-004-012	LEU-COMP-THERM-034-019	LEU-SOL-THERM-003-003
LEU-COMP-THERM-004-013	LEU-COMP-THERM-034-020	LEU-SOL-THERM-003-004
LEU-COMP-THERM-004-014	LEU-COMP-THERM-034-021	LEU-SOL-THERM-003-005
LEU-COMP-THERM-004-015	LEU-COMP-THERM-034-022	LEU-SOL-THERM-003-006
LEU-COMP-THERM-004-016	LEU-COMP-THERM-034-023	LEU-SOL-THERM-003-007
LEU-COMP-THERM-004-017	LEU-COMP-THERM-034-024	LEU-SOL-THERM-003-008
LEU-COMP-THERM-004-018	LEU-COMP-THERM-035-001	LEU-SOL-THERM-003-009
LEU-COMP-THERM-004-019	LEU-COMP-THERM-035-002	LEU-SOL-THERM-004-001
LEU-COMP-THERM-004-020	LEU-COMP-THERM-035-003	LEU-SOL-THERM-004-002
LEU-COMP-THERM-005-001	LEU-COMP-THERM-036-001	LEU-SOL-THERM-004-003
LEU-COMP-THERM-005-002	LEU-COMP-THERM-036-002	LEU-SOL-THERM-004-004
LEU-COMP-THERM-005-003	LEU-COMP-THERM-036-003	LEU-SOL-THERM-004-005
LEU-COMP-THERM-005-004	LEU-COMP-THERM-036-004	LEU-SOL-THERM-004-006
LEU-COMP-THERM-005-005	LEU-COMP-THERM-036-005	LEU-SOL-THERM-004-007
LEU-COMP-THERM-005-006	LEU-COMP-THERM-036-006	MIX-COMP-THERM-001-001
LEU-COMP-THERM-005-007	LEU-COMP-THERM-036-007	MIX-COMP-THERM-001-002
LEU-COMP-THERM-005-008	LEU-COMP-THERM-036-008	MIX-COMP-THERM-001-003
LEU-COMP-THERM-005-009	LEU-COMP-THERM-036-009	MIX-COMP-THERM-001-004
LEU-COMP-THERM-005-010	LEU-COMP-THERM-036-010	MIX-COMP-THERM-002-001S
LEU-COMP-THERM-005-011	LEU-COMP-THERM-036-011	MIX-COMP-THERM-002-002S
LEU-COMP-THERM-005-012	LEU-COMP-THERM-036-012	MIX-COMP-THERM-002-003S
LEU-COMP-THERM-005-013	LEU-COMP-THERM-036-013	MIX-COMP-THERM-002-004S
LEU-COMP-THERM-005-014	LEU-COMP-THERM-036-014	MIX-COMP-THERM-002-005S
LEU-COMP-THERM-005-015	LEU-COMP-THERM-036-015	MIX-COMP-THERM-002-006S
LEU-COMP-THERM-005-016	LEU-COMP-THERM-036-016	MIX-COMP-THERM-003-001
LEU-COMP-THERM-006-001	LEU-COMP-THERM-036-017	MIX-COMP-THERM-003-002
LEU-COMP-THERM-006-002	LEU-COMP-THERM-036-018	MIX-COMP-THERM-003-003
LEU-COMP-THERM-006-003	LEU-COMP-THERM-036-019	MIX-COMP-THERM-003-004
LEU-COMP-THERM-006-004	LEU-COMP-THERM-036-020	MIX-COMP-THERM-003-005
LEU-COMP-THERM-006-005	LEU-COMP-THERM-036-021	MIX-COMP-THERM-003-006
LEU-COMP-THERM-006-006	LEU-COMP-THERM-036-022	MIX-COMP-THERM-004-001
LEU-COMP-THERM-006-007	LEU-COMP-THERM-036-023	MIX-COMP-THERM-004-002
LEU-COMP-THERM-006-008	LEU-COMP-THERM-036-024	MIX-COMP-THERM-004-003
LEU-COMP-THERM-006-009	LEU-COMP-THERM-036-025	MIX-COMP-THERM-004-004
LEU-COMP-THERM-006-010	LEU-COMP-THERM-036-026	MIX-COMP-THERM-004-005
LEU-COMP-THERM-006-011	LEU-COMP-THERM-036-027	MIX-COMP-THERM-004-006
LEU-COMP-THERM-006-012	LEU-COMP-THERM-036-028	MIX-COMP-THERM-004-007
LEU-COMP-THERM-006-013	LEU-COMP-THERM-036-029	MIX-COMP-THERM-004-008
LEU-COMP-THERM-006-014	LEU-COMP-THERM-036-030	MIX-COMP-THERM-004-009
LEU-COMP-THERM-006-015	LEU-COMP-THERM-036-031	MIX-COMP-THERM-004-010
LEU-COMP-THERM-006-016	LEU-COMP-THERM-036-032	MIX-COMP-THERM-004-011

Table C.1. Continued

LEU-COMP-THERM-006-017	LEU-COMP-THERM-036-033	MIX-COMP-THERM-005-01
LEU-COMP-THERM-006-018	LEU-COMP-THERM-036-034	MIX-COMP-THERM-005-02
LEU-COMP-THERM-008-001	LEU-COMP-THERM-036-035	MIX-COMP-THERM-005-03
LEU-COMP-THERM-008-002	LEU-COMP-THERM-036-036	MIX-COMP-THERM-005-04
LEU-COMP-THERM-008-003	LEU-COMP-THERM-036-037	MIX-COMP-THERM-005-05
LEU-COMP-THERM-008-004	LEU-COMP-THERM-036-038	MIX-COMP-THERM-005-06
LEU-COMP-THERM-008-005	LEU-COMP-THERM-036-039	MIX-COMP-THERM-005-07
LEU-COMP-THERM-008-006	LEU-COMP-THERM-036-040	MIX-COMP-THERM-006-001
LEU-COMP-THERM-008-007	LEU-COMP-THERM-036-041	MIX-COMP-THERM-006-002
LEU-COMP-THERM-008-008	LEU-COMP-THERM-036-042	MIX-COMP-THERM-006-003
LEU-COMP-THERM-008-009	LEU-COMP-THERM-036-043	MIX-COMP-THERM-006-004
LEU-COMP-THERM-008-010	LEU-COMP-THERM-036-044	MIX-COMP-THERM-006-005
LEU-COMP-THERM-008-011	LEU-COMP-THERM-036-045	MIX-COMP-THERM-006-006
LEU-COMP-THERM-008-012	LEU-COMP-THERM-036-046	MIX-COMP-THERM-006-007
LEU-COMP-THERM-008-013	LEU-COMP-THERM-036-047	MIX-COMP-THERM-006-008
LEU-COMP-THERM-008-014	LEU-COMP-THERM-036-048	MIX-COMP-THERM-006-009
LEU-COMP-THERM-008-015	LEU-COMP-THERM-036-049	MIX-COMP-THERM-006-010
LEU-COMP-THERM-008-016	LEU-COMP-THERM-036-050	MIX-COMP-THERM-006-011
LEU-COMP-THERM-008-017	LEU-COMP-THERM-036-051	MIX-COMP-THERM-006-012
LEU-COMP-THERM-009-001	LEU-COMP-THERM-036-052	MIX-COMP-THERM-006-013
LEU-COMP-THERM-009-002	LEU-COMP-THERM-036-053	MIX-COMP-THERM-006-014
LEU-COMP-THERM-009-003	LEU-COMP-THERM-036-054	MIX-COMP-THERM-006-015
LEU-COMP-THERM-009-004	LEU-COMP-THERM-036-055	MIX-COMP-THERM-006-016
LEU-COMP-THERM-009-005	LEU-COMP-THERM-036-056	MIX-COMP-THERM-006-017
LEU-COMP-THERM-009-006	LEU-COMP-THERM-036-057	MIX-COMP-THERM-006-018
LEU-COMP-THERM-009-007	LEU-COMP-THERM-036-058	MIX-COMP-THERM-006-019
LEU-COMP-THERM-009-008	LEU-COMP-THERM-036-059	MIX-COMP-THERM-006-020
LEU-COMP-THERM-009-009	LEU-COMP-THERM-036-060	MIX-COMP-THERM-006-021
LEU-COMP-THERM-009-010	LEU-COMP-THERM-036-061	MIX-COMP-THERM-006-022
LEU-COMP-THERM-009-011	LEU-COMP-THERM-036-062	MIX-COMP-THERM-006-023
LEU-COMP-THERM-009-012	LEU-COMP-THERM-036-063	MIX-COMP-THERM-006-024
LEU-COMP-THERM-009-013	LEU-COMP-THERM-036-064	MIX-COMP-THERM-006-025
LEU-COMP-THERM-009-014	LEU-COMP-THERM-036-065	MIX-COMP-THERM-006-026
LEU-COMP-THERM-009-015	LEU-COMP-THERM-036-066	MIX-COMP-THERM-006-027
LEU-COMP-THERM-009-016	LEU-COMP-THERM-036-067	MIX-COMP-THERM-006-028
LEU-COMP-THERM-009-017	LEU-COMP-THERM-036-068	MIX-COMP-THERM-006-029
LEU-COMP-THERM-009-018	LEU-COMP-THERM-036-069	MIX-COMP-THERM-006-030
LEU-COMP-THERM-009-019	LEU-COMP-THERM-037-001	MIX-COMP-THERM-006-031
LEU-COMP-THERM-009-020	LEU-COMP-THERM-037-002	MIX-COMP-THERM-006-032
LEU-COMP-THERM-009-021	LEU-COMP-THERM-037-003	MIX-COMP-THERM-006-033
LEU-COMP-THERM-009-022	LEU-COMP-THERM-037-004	MIX-COMP-THERM-006-034
LEU-COMP-THERM-009-023	LEU-COMP-THERM-037-005	MIX-COMP-THERM-006-035
LEU-COMP-THERM-009-024	LEU-COMP-THERM-037-006	MIX-COMP-THERM-006-036
LEU-COMP-THERM-009-025	LEU-COMP-THERM-037-007	MIX-COMP-THERM-006-037
LEU-COMP-THERM-009-026	LEU-COMP-THERM-037-008	MIX-COMP-THERM-006-038
LEU-COMP-THERM-009-027	LEU-COMP-THERM-037-009	MIX-COMP-THERM-006-039
LEU-COMP-THERM-010-001	LEU-COMP-THERM-037-010	MIX-COMP-THERM-006-040

Table C.1. Continued

LEU-COMP-THERM-010-002	LEU-COMP-THERM-037-011	MIX-COMP-THERM-006-041
LEU-COMP-THERM-010-003	LEU-COMP-THERM-038-001	MIX-COMP-THERM-006-042
LEU-COMP-THERM-010-004	LEU-COMP-THERM-038-002	MIX-COMP-THERM-006-043
LEU-COMP-THERM-010-005	LEU-COMP-THERM-038-003	MIX-COMP-THERM-006-044
LEU-COMP-THERM-010-006	LEU-COMP-THERM-038-004	MIX-COMP-THERM-006-045
LEU-COMP-THERM-010-007	LEU-COMP-THERM-038-005	MIX-COMP-THERM-006-046
LEU-COMP-THERM-010-008	LEU-COMP-THERM-038-006	MIX-COMP-THERM-006-047
LEU-COMP-THERM-010-009	LEU-COMP-THERM-038-007	MIX-COMP-THERM-006-048
LEU-COMP-THERM-010-010	LEU-COMP-THERM-038-008	MIX-COMP-THERM-006-049
LEU-COMP-THERM-010-011	LEU-COMP-THERM-038-009	MIX-COMP-THERM-006-050
LEU-COMP-THERM-010-012	LEU-COMP-THERM-038-010	MIX-COMP-THERM-007-001
LEU-COMP-THERM-010-013	LEU-COMP-THERM-038-011	MIX-COMP-THERM-007-002
LEU-COMP-THERM-010-014	LEU-COMP-THERM-038-012	MIX-COMP-THERM-007-003
LEU-COMP-THERM-010-015	LEU-COMP-THERM-038-013	MIX-COMP-THERM-007-004
LEU-COMP-THERM-010-016	LEU-COMP-THERM-038-014	MIX-COMP-THERM-007-005
LEU-COMP-THERM-010-017	LEU-COMP-THERM-039-001	MIX-COMP-THERM-007-006
LEU-COMP-THERM-010-018	LEU-COMP-THERM-039-002	MIX-COMP-THERM-007-007
LEU-COMP-THERM-010-019	LEU-COMP-THERM-039-003	MIX-COMP-THERM-007-008
LEU-COMP-THERM-010-020	LEU-COMP-THERM-039-004	MIX-COMP-THERM-007-009
LEU-COMP-THERM-010-021	LEU-COMP-THERM-039-005	MIX-COMP-THERM-007-010
LEU-COMP-THERM-010-022	LEU-COMP-THERM-039-006	MIX-COMP-THERM-007-011
LEU-COMP-THERM-010-023	LEU-COMP-THERM-039-007	MIX-COMP-THERM-007-012
LEU-COMP-THERM-010-024	LEU-COMP-THERM-039-008	MIX-COMP-THERM-007-013
LEU-COMP-THERM-010-025	LEU-COMP-THERM-039-009	MIX-COMP-THERM-007-014
LEU-COMP-THERM-010-026	LEU-COMP-THERM-039-010	MIX-COMP-THERM-007-015
LEU-COMP-THERM-010-027	LEU-COMP-THERM-039-011	MIX-COMP-THERM-007-016
LEU-COMP-THERM-010-028	LEU-COMP-THERM-039-012	MIX-COMP-THERM-007-017
LEU-COMP-THERM-010-029	LEU-COMP-THERM-039-013	MIX-COMP-THERM-007-018
LEU-COMP-THERM-010-030	LEU-COMP-THERM-039-014	MIX-COMP-THERM-007-019
LEU-COMP-THERM-011-001	LEU-COMP-THERM-039-015	MIX-COMP-THERM-007-020
LEU-COMP-THERM-011-002	LEU-COMP-THERM-039-016	MIX-COMP-THERM-007-021
LEU-COMP-THERM-011-003	LEU-COMP-THERM-039-017	MIX-COMP-THERM-007-022
LEU-COMP-THERM-011-004	LEU-COMP-THERM-040-001	MIX-COMP-THERM-007-023
LEU-COMP-THERM-011-005	LEU-COMP-THERM-040-002	MIX-COMP-THERM-007-024
LEU-COMP-THERM-011-006	LEU-COMP-THERM-040-003	MIX-COMP-THERM-007-025
LEU-COMP-THERM-011-007	LEU-COMP-THERM-040-004	MIX-COMP-THERM-007-026
LEU-COMP-THERM-011-008	LEU-COMP-THERM-040-005	MIX-COMP-THERM-007-027
LEU-COMP-THERM-011-009	LEU-COMP-THERM-040-006	MIX-COMP-THERM-008-001
LEU-COMP-THERM-011-010	LEU-COMP-THERM-040-007	MIX-COMP-THERM-008-002
LEU-COMP-THERM-011-011	LEU-COMP-THERM-040-008	MIX-COMP-THERM-008-003
LEU-COMP-THERM-011-012	LEU-COMP-THERM-040-009	MIX-COMP-THERM-008-004
LEU-COMP-THERM-011-013	LEU-COMP-THERM-040-010	MIX-COMP-THERM-008-005
LEU-COMP-THERM-011-014	LEU-COMP-THERM-042-001	MIX-COMP-THERM-008-006
LEU-COMP-THERM-011-015	LEU-COMP-THERM-042-002	MIX-COMP-THERM-008-007
LEU-COMP-THERM-012-001	LEU-COMP-THERM-042-003	MIX-COMP-THERM-008-008
LEU-COMP-THERM-012-002	LEU-COMP-THERM-042-004	MIX-COMP-THERM-008-009
LEU-COMP-THERM-012-003	LEU-COMP-THERM-042-005	MIX-COMP-THERM-008-010

Table C.1. Continued

LEU-COMP-THERM-012-004	LEU-COMP-THERM-042-006	MIX-COMP-THERM-008-011
LEU-COMP-THERM-012-005	LEU-COMP-THERM-042-007	MIX-COMP-THERM-008-012
LEU-COMP-THERM-012-006	LEU-COMP-THERM-043-001	MIX-COMP-THERM-008-013
LEU-COMP-THERM-012-007	LEU-COMP-THERM-043-002	MIX-COMP-THERM-008-014
LEU-COMP-THERM-012-008	LEU-COMP-THERM-043-003	MIX-COMP-THERM-008-015
LEU-COMP-THERM-012-009	LEU-COMP-THERM-043-004	MIX-COMP-THERM-008-016
LEU-COMP-THERM-012-010	LEU-COMP-THERM-043-005	MIX-COMP-THERM-008-017
LEU-COMP-THERM-013-001	LEU-COMP-THERM-043-006	MIX-COMP-THERM-008-018
LEU-COMP-THERM-013-002	LEU-COMP-THERM-043-007	MIX-COMP-THERM-008-019
LEU-COMP-THERM-013-003	LEU-COMP-THERM-043-008	MIX-COMP-THERM-008-020
LEU-COMP-THERM-013-004	LEU-COMP-THERM-043-009	MIX-COMP-THERM-008-021
LEU-COMP-THERM-013-005	LEU-COMP-THERM-044-001	MIX-COMP-THERM-008-022
LEU-COMP-THERM-013-006	LEU-COMP-THERM-044-002	MIX-COMP-THERM-008-023
LEU-COMP-THERM-013-007	LEU-COMP-THERM-044-003	MIX-COMP-THERM-008-024
LEU-COMP-THERM-014-001	LEU-COMP-THERM-044-004	MIX-COMP-THERM-008-025
LEU-COMP-THERM-014-002	LEU-COMP-THERM-044-005	MIX-COMP-THERM-008-026
LEU-COMP-THERM-014-005	LEU-COMP-THERM-044-006	MIX-COMP-THERM-008-027
LEU-COMP-THERM-014-006	LEU-COMP-THERM-044-007	MIX-COMP-THERM-008-028
LEU-COMP-THERM-014-007	LEU-COMP-THERM-044-008	MIX-COMP-THERM-009-01
LEU-COMP-THERM-015-001	LEU-COMP-THERM-044-009	MIX-COMP-THERM-009-02
LEU-COMP-THERM-015-002	LEU-COMP-THERM-044-010	MIX-COMP-THERM-009-03
LEU-COMP-THERM-015-003	LEU-COMP-THERM-045-001	MIX-COMP-THERM-009-04
LEU-COMP-THERM-015-004	LEU-COMP-THERM-045-002	MIX-COMP-THERM-009-05
LEU-COMP-THERM-015-005	LEU-COMP-THERM-045-003	MIX-COMP-THERM-009-06
LEU-COMP-THERM-015-006	LEU-COMP-THERM-045-004	MIX-COMP-THERM-011-01
LEU-COMP-THERM-015-007	LEU-COMP-THERM-045-005	MIX-COMP-THERM-011-02
LEU-COMP-THERM-015-008	LEU-COMP-THERM-045-006	MIX-COMP-THERM-011-03
LEU-COMP-THERM-015-009	LEU-COMP-THERM-045-007	MIX-COMP-THERM-011-04
LEU-COMP-THERM-015-010	LEU-COMP-THERM-045-008	MIX-COMP-THERM-011-05
LEU-COMP-THERM-015-011	LEU-COMP-THERM-045-009	MIX-COMP-THERM-011-06
LEU-COMP-THERM-015-012	LEU-COMP-THERM-045-010	MIX-COMP-THERM-012-001
LEU-COMP-THERM-015-013	LEU-COMP-THERM-045-011	MIX-COMP-THERM-012-002
LEU-COMP-THERM-015-014	LEU-COMP-THERM-045-012	MIX-COMP-THERM-012-003
LEU-COMP-THERM-015-015	LEU-COMP-THERM-045-013	MIX-COMP-THERM-012-004
LEU-COMP-THERM-015-016	LEU-COMP-THERM-045-014	MIX-COMP-THERM-012-005
LEU-COMP-THERM-015-017	LEU-COMP-THERM-045-015	MIX-COMP-THERM-012-006
LEU-COMP-THERM-015-018	LEU-COMP-THERM-045-016	MIX-COMP-THERM-012-007
LEU-COMP-THERM-015-019	LEU-COMP-THERM-045-017	MIX-COMP-THERM-012-008
LEU-COMP-THERM-015-020	LEU-COMP-THERM-045-018	MIX-COMP-THERM-012-009
LEU-COMP-THERM-015-021	LEU-COMP-THERM-045-019	MIX-COMP-THERM-012-010
LEU-COMP-THERM-015-022	LEU-COMP-THERM-045-020	MIX-COMP-THERM-012-011
LEU-COMP-THERM-015-023	LEU-COMP-THERM-045-021	MIX-COMP-THERM-012-012
LEU-COMP-THERM-015-024	LEU-COMP-THERM-046-001	MIX-COMP-THERM-012-013
LEU-COMP-THERM-015-025	LEU-COMP-THERM-046-002	MIX-COMP-THERM-012-014
LEU-COMP-THERM-015-026	LEU-COMP-THERM-046-003	MIX-COMP-THERM-012-015
LEU-COMP-THERM-015-027	LEU-COMP-THERM-046-004	MIX-COMP-THERM-012-016
LEU-COMP-THERM-015-028	LEU-COMP-THERM-046-005	MIX-COMP-THERM-012-017

Table C.1. Continued

LEU-COMP-THERM-015-029	LEU-COMP-THERM-046-006	MIX-COMP-THERM-012-018
LEU-COMP-THERM-015-030	LEU-COMP-THERM-046-007	MIX-COMP-THERM-012-019
LEU-COMP-THERM-015-031	LEU-COMP-THERM-046-008	MIX-COMP-THERM-012-020
LEU-COMP-THERM-015-032	LEU-COMP-THERM-046-009	MIX-COMP-THERM-012-021
LEU-COMP-THERM-015-033	LEU-COMP-THERM-046-010	MIX-COMP-THERM-012-022
LEU-COMP-THERM-015-034	LEU-COMP-THERM-046-011	MIX-COMP-THERM-012-023
LEU-COMP-THERM-015-035	LEU-COMP-THERM-046-012	MIX-COMP-THERM-012-024
LEU-COMP-THERM-015-036	LEU-COMP-THERM-046-013	MIX-COMP-THERM-012-025
LEU-COMP-THERM-015-037	LEU-COMP-THERM-046-014	MIX-COMP-THERM-012-026
LEU-COMP-THERM-015-038	LEU-COMP-THERM-046-015	MIX-COMP-THERM-012-027
LEU-COMP-THERM-015-039	LEU-COMP-THERM-046-016	MIX-COMP-THERM-012-028
LEU-COMP-THERM-015-040	LEU-COMP-THERM-046-017	MIX-COMP-THERM-012-029
LEU-COMP-THERM-015-041	LEU-COMP-THERM-046-018	MIX-COMP-THERM-012-030
LEU-COMP-THERM-015-042	LEU-COMP-THERM-046-019	MIX-COMP-THERM-012-031
LEU-COMP-THERM-015-043	LEU-COMP-THERM-046-020	MIX-COMP-THERM-012-032
LEU-COMP-THERM-015-044	LEU-COMP-THERM-046-021	MIX-COMP-THERM-012-033
LEU-COMP-THERM-015-045	LEU-COMP-THERM-046-022	MIX-COMP-THERM-013-001
LEU-COMP-THERM-015-046	LEU-COMP-THERM-047-001	MIX-COMP-THERM-013-002
LEU-COMP-THERM-015-047	LEU-COMP-THERM-047-002	MIX-COMP-THERM-013-003
LEU-COMP-THERM-015-048	LEU-COMP-THERM-047-003	MIX-COMP-THERM-013-004
LEU-COMP-THERM-015-049	LEU-COMP-THERM-048-001	MIX-COMP-THERM-013-005
LEU-COMP-THERM-015-050	LEU-COMP-THERM-048-002	MIX-COMP-THERM-013-006
LEU-COMP-THERM-015-051	LEU-COMP-THERM-048-003	MIX-COMP-THERM-013-007
LEU-COMP-THERM-015-052	LEU-COMP-THERM-048-004	MIX-COMP-THERM-013-008
LEU-COMP-THERM-015-053	LEU-COMP-THERM-048-005	MIX-COMP-THERM-013-009
LEU-COMP-THERM-015-054	LEU-COMP-THERM-050-001	MIX-COMP-THERM-013-010
LEU-COMP-THERM-015-055	LEU-COMP-THERM-050-002	MIX-COMP-THERM-013-011
LEU-COMP-THERM-015-056	LEU-COMP-THERM-050-003	MIX-COMP-THERM-013-012
LEU-COMP-THERM-015-057	LEU-COMP-THERM-050-004	MIX-COMP-THERM-013-013
LEU-COMP-THERM-015-058	LEU-COMP-THERM-050-005	MIX-COMP-THERM-013-014
LEU-COMP-THERM-015-059	LEU-COMP-THERM-050-006	MIX-COMP-THERM-013-015
LEU-COMP-THERM-015-060	LEU-COMP-THERM-050-007	MIX-COMP-THERM-013-016
LEU-COMP-THERM-015-061	LEU-COMP-THERM-050-008	MIX-COMP-THERM-013-017
LEU-COMP-THERM-015-062	LEU-COMP-THERM-050-009	MIX-COMP-THERM-013-018
LEU-COMP-THERM-015-063	LEU-COMP-THERM-050-010	MIX-COMP-THERM-013-019
LEU-COMP-THERM-015-064	LEU-COMP-THERM-050-011	MIX-COMP-THERM-013-020
LEU-COMP-THERM-015-065	LEU-COMP-THERM-050-012	MIX-COMP-THERM-013-021
LEU-COMP-THERM-015-066	LEU-COMP-THERM-050-013	MIX-COMP-THERM-013-022
LEU-COMP-THERM-015-067	LEU-COMP-THERM-050-014	MIX-COMP-THERM-013-023
LEU-COMP-THERM-015-068	LEU-COMP-THERM-050-015	MIX-COMP-THERM-013-024
LEU-COMP-THERM-015-069	LEU-COMP-THERM-050-016	MIX-COMP-THERM-013-025
LEU-COMP-THERM-015-070	LEU-COMP-THERM-050-017	MIX-COMP-THERM-013-026
LEU-COMP-THERM-015-071	LEU-COMP-THERM-050-018	MIX-COMP-THERM-013-027
LEU-COMP-THERM-015-072	LEU-COMP-THERM-051-001	MIX-COMP-THERM-013-028
LEU-COMP-THERM-015-073	LEU-COMP-THERM-051-002	MIX-COMP-THERM-013-029
LEU-COMP-THERM-015-074	LEU-COMP-THERM-051-003	MIX-COMP-THERM-013-030
LEU-COMP-THERM-015-075	LEU-COMP-THERM-051-004	MIX-COMP-THERM-014-001

Table C.1. Continued

LEU-COMP-THERM-015-076	LEU-COMP-THERM-051-005	MIX-COMP-THERM-014-002
LEU-COMP-THERM-015-077	LEU-COMP-THERM-051-006	MIX-COMP-THERM-014-003
LEU-COMP-THERM-015-078	LEU-COMP-THERM-051-007	MIX-COMP-THERM-014-004
LEU-COMP-THERM-015-079	LEU-COMP-THERM-051-008	MIX-COMP-THERM-014-005
LEU-COMP-THERM-015-080	LEU-COMP-THERM-051-009	MIX-COMP-THERM-014-006
LEU-COMP-THERM-015-081	LEU-COMP-THERM-051-010	MIX-COMP-THERM-014-007
LEU-COMP-THERM-015-082	LEU-COMP-THERM-051-011	MIX-COMP-THERM-014-008
LEU-COMP-THERM-015-083	LEU-COMP-THERM-051-012	MIX-COMP-THERM-014-009
LEU-COMP-THERM-015-084	LEU-COMP-THERM-051-013	MIX-COMP-THERM-014-010
LEU-COMP-THERM-015-085	LEU-COMP-THERM-051-014	MIX-COMP-THERM-014-011
LEU-COMP-THERM-015-086	LEU-COMP-THERM-051-015	MIX-COMP-THERM-014-012
LEU-COMP-THERM-015-087	LEU-COMP-THERM-051-016	MIX-COMP-THERM-014-013
LEU-COMP-THERM-015-088	LEU-COMP-THERM-051-017	MIX-COMP-THERM-014-014
LEU-COMP-THERM-015-089	LEU-COMP-THERM-051-018	MIX-COMP-THERM-014-015
LEU-COMP-THERM-015-090	LEU-COMP-THERM-051-019	MIX-COMP-THERM-014-016
LEU-COMP-THERM-015-091	LEU-COMP-THERM-052-001	MIX-COMP-THERM-014-017
LEU-COMP-THERM-015-092	LEU-COMP-THERM-052-002	MIX-COMP-THERM-014-018
LEU-COMP-THERM-015-093	LEU-COMP-THERM-052-003	MIX-COMP-THERM-014-019
LEU-COMP-THERM-015-094	LEU-COMP-THERM-052-004	MIX-COMP-THERM-014-020
LEU-COMP-THERM-015-095	LEU-COMP-THERM-052-005	MIX-COMP-THERM-014-021
LEU-COMP-THERM-015-096	LEU-COMP-THERM-052-006	MIX-COMP-THERM-014-022
LEU-COMP-THERM-015-097	LEU-COMP-THERM-053-001	MIX-COMP-THERM-016-001
LEU-COMP-THERM-015-098	LEU-COMP-THERM-053-002	MIX-COMP-THERM-016-002
LEU-COMP-THERM-015-099	LEU-COMP-THERM-053-003	MIX-COMP-THERM-016-003
LEU-COMP-THERM-015-100	LEU-COMP-THERM-053-004	MIX-COMP-THERM-016-004
LEU-COMP-THERM-015-101	LEU-COMP-THERM-053-005	MIX-COMP-THERM-016-005
LEU-COMP-THERM-015-102	LEU-COMP-THERM-053-006	MIX-COMP-THERM-016-006
LEU-COMP-THERM-015-103	LEU-COMP-THERM-053-007	MIX-COMP-THERM-016-007
LEU-COMP-THERM-015-104	LEU-COMP-THERM-053-008	MIX-COMP-THERM-016-008
LEU-COMP-THERM-015-105	LEU-COMP-THERM-053-009	MIX-COMP-THERM-016-009
LEU-COMP-THERM-015-106	LEU-COMP-THERM-053-010	MIX-COMP-THERM-016-010
LEU-COMP-THERM-015-107	LEU-COMP-THERM-053-011	MIX-COMP-THERM-016-011
LEU-COMP-THERM-015-108	LEU-COMP-THERM-053-012	MIX-COMP-THERM-016-012
LEU-COMP-THERM-015-109	LEU-COMP-THERM-053-013	MIX-COMP-THERM-016-013
LEU-COMP-THERM-015-110	LEU-COMP-THERM-053-014	MIX-COMP-THERM-016-014
LEU-COMP-THERM-015-111	LEU-COMP-THERM-054-001	MIX-COMP-THERM-016-015
LEU-COMP-THERM-015-112	LEU-COMP-THERM-054-002	MIX-COMP-THERM-016-016
LEU-COMP-THERM-015-113	LEU-COMP-THERM-054-003	MIX-COMP-THERM-016-017
LEU-COMP-THERM-015-114	LEU-COMP-THERM-054-004	MIX-COMP-THERM-016-018
LEU-COMP-THERM-015-115	LEU-COMP-THERM-054-005	MIX-COMP-THERM-016-019
LEU-COMP-THERM-015-116	LEU-COMP-THERM-054-006	MIX-COMP-THERM-017-001
LEU-COMP-THERM-015-117	LEU-COMP-THERM-054-007	MIX-COMP-THERM-017-002
LEU-COMP-THERM-015-118	LEU-COMP-THERM-054-008	MIX-COMP-THERM-017-003
LEU-COMP-THERM-015-119	LEU-COMP-THERM-055-001	MIX-COMP-THERM-017-004
LEU-COMP-THERM-015-120	LEU-COMP-THERM-055-002	MIX-COMP-THERM-017-005
LEU-COMP-THERM-015-121	LEU-COMP-THERM-057-001	MIX-COMP-THERM-017-006
LEU-COMP-THERM-015-122	LEU-COMP-THERM-057-002	MIX-COMP-THERM-017-007

Table C.1. Continued

LEU-COMP-THERM-015-123	LEU-COMP-THERM-057-003	MIX-COMP-THERM-017-008
LEU-COMP-THERM-015-124	LEU-COMP-THERM-057-004	MIX-COMP-THERM-017-009
LEU-COMP-THERM-015-125	LEU-COMP-THERM-057-005	MIX-COMP-THERM-017-010
LEU-COMP-THERM-015-126	LEU-COMP-THERM-057-006	MIX-COMP-THERM-017-011
LEU-COMP-THERM-015-127	LEU-COMP-THERM-057-007	MIX-COMP-THERM-017-012
LEU-COMP-THERM-015-128	LEU-COMP-THERM-057-008	MIX-COMP-THERM-017-013
LEU-COMP-THERM-015-129	LEU-COMP-THERM-057-009	MIX-COMP-THERM-017-014
LEU-COMP-THERM-015-130	LEU-COMP-THERM-057-010	MIX-COMP-THERM-017-015
LEU-COMP-THERM-015-131	LEU-COMP-THERM-057-011	MIX-COMP-THERM-017-016
LEU-COMP-THERM-015-132	LEU-COMP-THERM-057-012	MIX-COMP-THERM-017-017
LEU-COMP-THERM-015-133	LEU-COMP-THERM-057-013	MIX-COMP-THERM-017-018
LEU-COMP-THERM-015-134	LEU-COMP-THERM-057-014	MIX-COMP-THERM-017-019
LEU-COMP-THERM-015-135	LEU-COMP-THERM-057-015	HTC1_001
LEU-COMP-THERM-015-136	LEU-COMP-THERM-057-016	HTC1_002
LEU-COMP-THERM-015-137	LEU-COMP-THERM-057-017	HTC1_003
LEU-COMP-THERM-015-138	LEU-COMP-THERM-057-018	HTC1_004
LEU-COMP-THERM-015-139	LEU-COMP-THERM-057-019	HTC1_005
LEU-COMP-THERM-015-140	LEU-COMP-THERM-057-020	HTC1_006
LEU-COMP-THERM-015-141	LEU-COMP-THERM-057-021	HTC1_007
LEU-COMP-THERM-015-142	LEU-COMP-THERM-057-022	HTC1_008
LEU-COMP-THERM-015-143	LEU-COMP-THERM-057-023	HTC1_009
LEU-COMP-THERM-015-144	LEU-COMP-THERM-057-024	HTC1_010
LEU-COMP-THERM-015-145	LEU-COMP-THERM-057-025	HTC1_011
LEU-COMP-THERM-015-146	LEU-COMP-THERM-057-026	HTC1_012
LEU-COMP-THERM-015-147	LEU-COMP-THERM-057-027	HTC1_013
LEU-COMP-THERM-015-148	LEU-COMP-THERM-057-028	HTC1_014
LEU-COMP-THERM-015-149	LEU-COMP-THERM-057-029	HTC1_015
LEU-COMP-THERM-015-150	LEU-COMP-THERM-057-030	HTC1_016
LEU-COMP-THERM-015-151	LEU-COMP-THERM-057-031	HTC1_017
LEU-COMP-THERM-015-152	LEU-COMP-THERM-057-032	HTC1_018
LEU-COMP-THERM-015-153	LEU-COMP-THERM-057-033	HTC2B_001
LEU-COMP-THERM-015-154	LEU-COMP-THERM-057-034	HTC2B_002
LEU-COMP-THERM-015-155	LEU-COMP-THERM-057-035	HTC2B_003
LEU-COMP-THERM-015-156	LEU-COMP-THERM-057-036	HTC2B_004
LEU-COMP-THERM-015-157	LEU-COMP-THERM-058-001	HTC2B_005
LEU-COMP-THERM-015-158	LEU-COMP-THERM-058-002	HTC2B_006
LEU-COMP-THERM-015-159	LEU-COMP-THERM-058-003	HTC2B_007
LEU-COMP-THERM-015-160	LEU-COMP-THERM-058-004	HTC2B_008
LEU-COMP-THERM-015-161	LEU-COMP-THERM-058-005	HTC2B_009
LEU-COMP-THERM-015-162	LEU-COMP-THERM-058-006	HTC2B_010
LEU-COMP-THERM-015-163	LEU-COMP-THERM-058-007	HTC2B_011
LEU-COMP-THERM-015-164	LEU-COMP-THERM-058-008	HTC2B_012
LEU-COMP-THERM-015-165	LEU-COMP-THERM-058-009	HTC2B_014
LEU-COMP-THERM-016-001	LEU-COMP-THERM-061-001	HTC2B_015
LEU-COMP-THERM-016-002	LEU-COMP-THERM-061-002	HTC2B_016
LEU-COMP-THERM-016-003	LEU-COMP-THERM-061-003	HTC2B_017
LEU-COMP-THERM-016-004	LEU-COMP-THERM-061-004	HTC2B_018

Table C.1. Continued

LEU-COMP-THERM-016-005	LEU-COMP-THERM-061-005	HTC2B_019
LEU-COMP-THERM-016-006	LEU-COMP-THERM-061-006	HTC2B_020
LEU-COMP-THERM-016-007	LEU-COMP-THERM-061-007	HTC2B_021
LEU-COMP-THERM-016-008	LEU-COMP-THERM-061-008	HTC2G_001
LEU-COMP-THERM-016-009	LEU-COMP-THERM-061-009	HTC2G_002
LEU-COMP-THERM-016-010	LEU-COMP-THERM-061-010	HTC2G_003
LEU-COMP-THERM-016-011	LEU-COMP-THERM-062-001	HTC2G_004
LEU-COMP-THERM-016-012	LEU-COMP-THERM-062-002	HTC2G_005
LEU-COMP-THERM-016-013	LEU-COMP-THERM-062-003	HTC2G_006
LEU-COMP-THERM-016-014	LEU-COMP-THERM-062-004	HTC2G_007
LEU-COMP-THERM-016-015	LEU-COMP-THERM-062-005	HTC2G_008
LEU-COMP-THERM-016-016	LEU-COMP-THERM-062-006	HTC2G_009
LEU-COMP-THERM-016-017	LEU-COMP-THERM-062-007	HTC2G_010
LEU-COMP-THERM-016-018	LEU-COMP-THERM-062-008	HTC2G_011
LEU-COMP-THERM-016-019	LEU-COMP-THERM-062-009	HTC2G_012
LEU-COMP-THERM-016-020	LEU-COMP-THERM-062-010	HTC2G_013
LEU-COMP-THERM-016-021	LEU-COMP-THERM-062-011	HTC2G_014
LEU-COMP-THERM-016-022	LEU-COMP-THERM-062-012	HTC2G_015
LEU-COMP-THERM-016-023	LEU-COMP-THERM-062-013	HTC2G_016
LEU-COMP-THERM-016-024	LEU-COMP-THERM-062-014	HTC2G_017
LEU-COMP-THERM-016-025	LEU-COMP-THERM-062-015	HTC2G_018
LEU-COMP-THERM-016-026	LEU-COMP-THERM-065-001	HTC2G_019
LEU-COMP-THERM-016-027	LEU-COMP-THERM-065-002	HTC2G_020
LEU-COMP-THERM-016-028	LEU-COMP-THERM-065-003	HTC3_001
LEU-COMP-THERM-016-029	LEU-COMP-THERM-065-004	HTC3_002
LEU-COMP-THERM-016-030	LEU-COMP-THERM-065-005	HTC3_003
LEU-COMP-THERM-016-031	LEU-COMP-THERM-065-006	HTC3_004
LEU-COMP-THERM-016-032	LEU-COMP-THERM-065-007	HTC3_005
LEU-COMP-THERM-017-001	LEU-COMP-THERM-065-008	HTC3_006
LEU-COMP-THERM-017-002	LEU-COMP-THERM-065-009	HTC3_007
LEU-COMP-THERM-017-003	LEU-COMP-THERM-065-010	HTC3_008
LEU-COMP-THERM-017-004	LEU-COMP-THERM-065-011	HTC3_009
LEU-COMP-THERM-017-005	LEU-COMP-THERM-065-012	HTC3_010
LEU-COMP-THERM-017-006	LEU-COMP-THERM-065-013	HTC3_011
LEU-COMP-THERM-017-007	LEU-COMP-THERM-065-014	HTC3_012
LEU-COMP-THERM-017-008	LEU-COMP-THERM-065-015	HTC3_013
LEU-COMP-THERM-017-009	LEU-COMP-THERM-065-016	HTC3_014
LEU-COMP-THERM-017-010	LEU-COMP-THERM-065-017	HTC3_015
LEU-COMP-THERM-017-011	LEU-COMP-THERM-066-004	HTC3_016
LEU-COMP-THERM-017-012	LEU-COMP-THERM-066-005	HTC3_017
LEU-COMP-THERM-017-013	LEU-COMP-THERM-066-006	HTC3_018
LEU-COMP-THERM-017-014	LEU-COMP-THERM-066-007	HTC3_019
LEU-COMP-THERM-017-015	LEU-COMP-THERM-066-008	HTC3_020
LEU-COMP-THERM-017-016	LEU-COMP-THERM-066-009	HTC3_021
LEU-COMP-THERM-017-017	LEU-COMP-THERM-066-010	HTC3_022
LEU-COMP-THERM-017-018	LEU-COMP-THERM-069-001	HTC3_023
LEU-COMP-THERM-017-019	LEU-COMP-THERM-069-002	HTC3_024

Table C.1. Continued

LEU-COMP-THERM-017-020	LEU-COMP-THERM-069-003	HTC3_025
LEU-COMP-THERM-017-021	LEU-COMP-THERM-069-004	HTC3_026
LEU-COMP-THERM-017-022	LEU-COMP-THERM-069-005	HTC4FE_001
LEU-COMP-THERM-017-023	LEU-COMP-THERM-070-001	HTC4FE_002
LEU-COMP-THERM-017-024	LEU-COMP-THERM-070-002	HTC4FE_003
LEU-COMP-THERM-017-025	LEU-COMP-THERM-070-003	HTC4FE_004
LEU-COMP-THERM-017-026	LEU-COMP-THERM-070-004	HTC4FE_005
LEU-COMP-THERM-017-027	LEU-COMP-THERM-070-005	HTC4FE_006
LEU-COMP-THERM-017-028	LEU-COMP-THERM-070-006	HTC4FE_007
LEU-COMP-THERM-017-029	LEU-COMP-THERM-070-007	HTC4FE_008
LEU-COMP-THERM-018-001	LEU-COMP-THERM-070-008	HTC4FE_009
LEU-COMP-THERM-020-001	LEU-COMP-THERM-070-009	HTC4FE_010
LEU-COMP-THERM-020-002	LEU-COMP-THERM-070-010	HTC4FE_011
LEU-COMP-THERM-020-003	LEU-COMP-THERM-070-011	HTC4FE_012
LEU-COMP-THERM-020-004	LEU-COMP-THERM-070-012	HTC4FE_013
LEU-COMP-THERM-020-005	LEU-COMP-THERM-071-001	HTC4FE_014
LEU-COMP-THERM-020-006	LEU-COMP-THERM-071-002	HTC4FE_015
LEU-COMP-THERM-020-007	LEU-COMP-THERM-071-003	HTC4FE_016
LEU-COMP-THERM-021-001	LEU-COMP-THERM-071-004	HTC4FE_017
LEU-COMP-THERM-021-002	LEU-COMP-THERM-072-001	HTC4FE_018
LEU-COMP-THERM-021-003	LEU-COMP-THERM-072-002	HTC4FE_019
LEU-COMP-THERM-021-004	LEU-COMP-THERM-072-003	HTC4FE_020
LEU-COMP-THERM-021-005	LEU-COMP-THERM-072-004	HTC4FE_021
LEU-COMP-THERM-021-006	LEU-COMP-THERM-072-005	HTC4FE_022
LEU-COMP-THERM-022-001	LEU-COMP-THERM-072-006	HTC4FE_023
LEU-COMP-THERM-022-002	LEU-COMP-THERM-072-007	HTC4FE_024
LEU-COMP-THERM-022-003	LEU-COMP-THERM-072-008	HTC4FE_025
LEU-COMP-THERM-022-004	LEU-COMP-THERM-072-009	HTC4FE_026
LEU-COMP-THERM-022-005	LEU-COMP-THERM-073-001	HTC4FE_027
LEU-COMP-THERM-022-006	LEU-COMP-THERM-073-002	HTC4FE_028
LEU-COMP-THERM-022-007	LEU-COMP-THERM-073-003	HTC4FE_029
LEU-COMP-THERM-023-001	LEU-COMP-THERM-073-004	HTC4FE_030
LEU-COMP-THERM-023-002	LEU-COMP-THERM-073-005	HTC4FE_031
LEU-COMP-THERM-023-003	LEU-COMP-THERM-073-006	HTC4FE_032
LEU-COMP-THERM-023-004	LEU-COMP-THERM-073-007	HTC4FE_033
LEU-COMP-THERM-023-005	LEU-COMP-THERM-073-008	HTC4PB_001
LEU-COMP-THERM-023-006	LEU-COMP-THERM-073-009	HTC4PB_002
LEU-COMP-THERM-024-001	LEU-COMP-THERM-073-010	HTC4PB_003
LEU-COMP-THERM-024-002	LEU-COMP-THERM-073-011	HTC4PB_004
LEU-COMP-THERM-026-001	LEU-COMP-THERM-073-012	HTC4PB_005
LEU-COMP-THERM-026-002	LEU-COMP-THERM-073-013	HTC4PB_006
LEU-COMP-THERM-026-003	LEU-COMP-THERM-073-014	HTC4PB_007
LEU-COMP-THERM-026-004	LEU-COMP-THERM-074-001	HTC4PB_008
LEU-COMP-THERM-026-005	LEU-COMP-THERM-074-002	HTC4PB_009
LEU-COMP-THERM-026-006	LEU-COMP-THERM-074-003	HTC4PB_010
LEU-COMP-THERM-027-001	LEU-COMP-THERM-074-004	HTC4PB_011
LEU-COMP-THERM-027-002	LEU-COMP-THERM-075-001	HTC4PB_012

Table C.1. Continued

LEU-COMP-THERM-027-003	LEU-COMP-THERM-075-002	HTC4PB_013
LEU-COMP-THERM-027-004	LEU-COMP-THERM-075-003	HTC4PB_014
LEU-COMP-THERM-028-001	LEU-COMP-THERM-075-004	HTC4PB_015
LEU-COMP-THERM-028-002	LEU-COMP-THERM-075-005	HTC4PB_016
LEU-COMP-THERM-028-003	LEU-COMP-THERM-075-006	HTC4PB_017
LEU-COMP-THERM-028-004	LEU-COMP-THERM-076-001	HTC4PB_018
LEU-COMP-THERM-028-005	LEU-COMP-THERM-076-002	HTC4PB_019
LEU-COMP-THERM-028-006	LEU-COMP-THERM-076-003	HTC4PB_020
LEU-COMP-THERM-028-007	LEU-COMP-THERM-076-004	HTC4PB_021
LEU-COMP-THERM-028-008	LEU-COMP-THERM-076-005	HTC4PB_022
LEU-COMP-THERM-028-009	LEU-COMP-THERM-076-006	HTC4PB_023
LEU-COMP-THERM-028-010	LEU-COMP-THERM-076-007	HTC4PB_024
LEU-COMP-THERM-028-011	LEU-COMP-THERM-077-001	HTC4PB_025
LEU-COMP-THERM-028-012	LEU-COMP-THERM-077-002	HTC4PB_026
LEU-COMP-THERM-028-013	LEU-COMP-THERM-077-003	HTC4PB_027
LEU-COMP-THERM-028-014	LEU-COMP-THERM-077-004	HTC4PB_028
LEU-COMP-THERM-028-015	LEU-COMP-THERM-077-005	HTC4PB_029
LEU-COMP-THERM-028-016	LEU-COMP-THERM-078-001	HTC4PB_030
LEU-COMP-THERM-028-017	LEU-COMP-THERM-078-002	HTC4PB_031
LEU-COMP-THERM-028-018	LEU-COMP-THERM-078-003	HTC4PB_032
LEU-COMP-THERM-028-019	LEU-COMP-THERM-078-004	HTC4PB_033
LEU-COMP-THERM-028-020	LEU-COMP-THERM-078-005	HTC4PB_034
LEU-COMP-THERM-029-001	LEU-COMP-THERM-078-006	HTC4PB_035
LEU-COMP-THERM-029-002	LEU-COMP-THERM-078-007	HTC4PB_036
LEU-COMP-THERM-029-003	LEU-COMP-THERM-078-008	HTC4PB_037
LEU-COMP-THERM-029-004	LEU-COMP-THERM-078-009	HTC4PB_038
LEU-COMP-THERM-029-005	LEU-COMP-THERM-078-010	MIX-SOL-THERM-001-001
LEU-COMP-THERM-029-006	LEU-COMP-THERM-078-011	MIX-SOL-THERM-001-002
LEU-COMP-THERM-029-007	LEU-COMP-THERM-078-012	MIX-SOL-THERM-001-003
LEU-COMP-THERM-029-008	LEU-COMP-THERM-078-013	MIX-SOL-THERM-001-004
LEU-COMP-THERM-029-009	LEU-COMP-THERM-078-014	MIX-SOL-THERM-001-005
LEU-COMP-THERM-029-010	LEU-COMP-THERM-078-015	MIX-SOL-THERM-001-006
LEU-COMP-THERM-029-011	LEU-COMP-THERM-079-001	MIX-SOL-THERM-001-007
LEU-COMP-THERM-029-012	LEU-COMP-THERM-079-002	MIX-SOL-THERM-001-008
LEU-COMP-THERM-030-001	LEU-COMP-THERM-079-003	MIX-SOL-THERM-001-009
LEU-COMP-THERM-030-002	LEU-COMP-THERM-079-004	MIX-SOL-THERM-001-010
LEU-COMP-THERM-030-003	LEU-COMP-THERM-079-005	MIX-SOL-THERM-001-011
LEU-COMP-THERM-030-004	LEU-COMP-THERM-079-006	MIX-SOL-THERM-001-012
LEU-COMP-THERM-030-005	LEU-COMP-THERM-079-007	MIX-SOL-THERM-001-013
LEU-COMP-THERM-030-006	LEU-COMP-THERM-079-008	MIX-SOL-THERM-002-001
LEU-COMP-THERM-030-007	LEU-COMP-THERM-079-009	MIX-SOL-THERM-002-002
LEU-COMP-THERM-030-008	LEU-COMP-THERM-079-010	MIX-SOL-THERM-002-003
LEU-COMP-THERM-030-009	LEU-COMP-THERM-080-001	MIX-SOL-THERM-003-001
LEU-COMP-THERM-030-010	LEU-COMP-THERM-080-002	MIX-SOL-THERM-003-002
LEU-COMP-THERM-030-011	LEU-COMP-THERM-080-003	MIX-SOL-THERM-003-003
LEU-COMP-THERM-030-012	LEU-COMP-THERM-080-004	MIX-SOL-THERM-003-004
LEU-COMP-THERM-031-001	LEU-COMP-THERM-080-005	MIX-SOL-THERM-003-005

Table C.1. Continued

LEU-COMP-THERM-031-002	LEU-COMP-THERM-080-006	MIX-SOL-THERM-003-006
LEU-COMP-THERM-031-003	LEU-COMP-THERM-080-007	MIX-SOL-THERM-003-007
LEU-COMP-THERM-031-004	LEU-COMP-THERM-080-008	MIX-SOL-THERM-003-008
LEU-COMP-THERM-031-005	LEU-COMP-THERM-080-009	MIX-SOL-THERM-003-009
LEU-COMP-THERM-031-006	LEU-COMP-THERM-080-010	MIX-SOL-THERM-003-010
LEU-COMP-THERM-032-001	LEU-COMP-THERM-080-011	MIX-SOL-THERM-004-001
LEU-COMP-THERM-032-002	LEU-COMP-THERM-082-002	MIX-SOL-THERM-004-002
LEU-COMP-THERM-032-003	LEU-COMP-THERM-082-003	MIX-SOL-THERM-004-003
LEU-COMP-THERM-032-004	LEU-COMP-THERM-082-004	MIX-SOL-THERM-004-004
LEU-COMP-THERM-032-005	LEU-COMP-THERM-082-005	MIX-SOL-THERM-004-005
LEU-COMP-THERM-032-006	LEU-COMP-THERM-082-006	MIX-SOL-THERM-004-006
LEU-COMP-THERM-032-007	LEU-COMP-THERM-083-001	MIX-SOL-THERM-004-007
LEU-COMP-THERM-032-008	LEU-COMP-THERM-083-002	MIX-SOL-THERM-004-008
LEU-COMP-THERM-032-009	LEU-COMP-THERM-083-003	MIX-SOL-THERM-004-009
LEU-COMP-THERM-033-001	LEU-COMP-THERM-084-001	MIX-SOL-THERM-005-001
LEU-COMP-THERM-033-002	LEU-COMP-THERM-085-001	MIX-SOL-THERM-005-002
LEU-COMP-THERM-033-003	LEU-COMP-THERM-085-002	MIX-SOL-THERM-005-003
LEU-COMP-THERM-033-004	LEU-COMP-THERM-085-003	MIX-SOL-THERM-005-004
LEU-COMP-THERM-033-005	LEU-COMP-THERM-085-004	MIX-SOL-THERM-005-005
LEU-COMP-THERM-033-006	LEU-COMP-THERM-085-005	MIX-SOL-THERM-005-006
LEU-COMP-THERM-033-007	LEU-COMP-THERM-085-006	MIX-SOL-THERM-005-007
LEU-COMP-THERM-033-008	LEU-COMP-THERM-085-007	MIX-SOL-THERM-007-001
LEU-COMP-THERM-033-009	LEU-COMP-THERM-085-008	MIX-SOL-THERM-007-002
LEU-COMP-THERM-033-010	LEU-COMP-THERM-085-009	MIX-SOL-THERM-007-003
LEU-COMP-THERM-033-011	LEU-COMP-THERM-085-010	MIX-SOL-THERM-007-004
LEU-COMP-THERM-033-012	LEU-COMP-THERM-085-011	MIX-SOL-THERM-007-005
LEU-COMP-THERM-033-013	LEU-COMP-THERM-085-012	MIX-SOL-THERM-007-006
LEU-COMP-THERM-033-014	LEU-COMP-THERM-085-013	MIX-SOL-THERM-007-007
LEU-COMP-THERM-033-015	LEU-COMP-THERM-089-001	MIX-SOL-THERM-010-001
LEU-COMP-THERM-033-016	LEU-COMP-THERM-089-002	MIX-SOL-THERM-010-002
LEU-COMP-THERM-033-017	LEU-COMP-THERM-089-003	MIX-SOL-THERM-010-003
LEU-COMP-THERM-033-018	LEU-COMP-THERM-089-004	MIX-SOL-THERM-010-004
LEU-COMP-THERM-033-019	LEU-COMP-THERM-090-001	MIX-SOL-THERM-010-005
LEU-COMP-THERM-033-020	LEU-COMP-THERM-090-002	MIX-SOL-THERM-010-006
LEU-COMP-THERM-033-021	LEU-COMP-THERM-090-003	MIX-SOL-THERM-010-007
LEU-COMP-THERM-033-022	LEU-COMP-THERM-090-004	MIX-SOL-THERM-010-008
LEU-COMP-THERM-033-023	LEU-COMP-THERM-090-005	MIX-SOL-THERM-010-009
LEU-COMP-THERM-033-024	LEU-COMP-THERM-090-006	

**APPENDIX D. CRITICAL EXPERIMENTS WITH C_k VALUES NO
LESS THAN 0.8**

D1. CRITICAL EXPERIMENTS WITH C_k VALUES NO LESS THAN 0.8

This appendix provides the cases with c_k values of 0.8 or more for GBC-68 models. The results for the vanished lattice are contained in Tables D.1 and D.2 for AO and AFP compositions. The results for the full lattice with AFP modeling are contained in Table D.3.

Table D.1. Experiments with a c_k no less than 0.8, vanished lattice – actinide only

Experiment	c_k	Experiment	c_k
LEU-COMP-THERM-005-010	0.8044	LEU-COMP-THERM-015-146	0.8021
LEU-COMP-THERM-005-011	0.8020	LEU-COMP-THERM-015-151	0.8268
LEU-COMP-THERM-008-001	0.8859	LEU-COMP-THERM-015-158	0.8083
LEU-COMP-THERM-008-002	0.8889	LEU-COMP-THERM-036-025	0.8032
LEU-COMP-THERM-008-003	0.8900	LEU-COMP-THERM-036-026	0.8023
LEU-COMP-THERM-008-004	0.8889	LEU-COMP-THERM-047-001	0.8522
LEU-COMP-THERM-008-005	0.8888	LEU-COMP-THERM-047-003	0.8025
LEU-COMP-THERM-008-006	0.8900	LEU-COMP-THERM-051-001	0.8488
LEU-COMP-THERM-008-007	0.8892	LEU-COMP-THERM-051-002	0.8789
LEU-COMP-THERM-008-008	0.8892	LEU-COMP-THERM-051-003	0.8763
LEU-COMP-THERM-008-009	0.8891	LEU-COMP-THERM-051-004	0.8752
LEU-COMP-THERM-008-010	0.8883	LEU-COMP-THERM-051-005	0.8718
LEU-COMP-THERM-008-011	0.8880	LEU-COMP-THERM-051-006	0.8702
LEU-COMP-THERM-008-012	0.8881	LEU-COMP-THERM-051-007	0.8719
LEU-COMP-THERM-008-013	0.8873	LEU-COMP-THERM-051-008	0.8628
LEU-COMP-THERM-008-014	0.8878	LEU-COMP-THERM-051-009	0.8690
LEU-COMP-THERM-008-015	0.8892	LEU-COMP-THERM-051-010	0.8613
LEU-COMP-THERM-008-016	0.8913	LEU-COMP-THERM-051-011	0.8621
LEU-COMP-THERM-008-017	0.8929	LEU-COMP-THERM-051-012	0.8631
LEU-COMP-THERM-011-002	0.8610	LEU-COMP-THERM-051-015	0.8642
LEU-COMP-THERM-011-003	0.8694	LEU-COMP-THERM-051-016	0.8591
LEU-COMP-THERM-011-004	0.8703	LEU-COMP-THERM-051-017	0.8620
LEU-COMP-THERM-011-005	0.8682	LEU-COMP-THERM-051-018	0.8592
LEU-COMP-THERM-011-006	0.8674	LEU-COMP-THERM-051-019	0.8464
LEU-COMP-THERM-011-007	0.8635	LEU-COMP-THERM-052-003	0.8049
LEU-COMP-THERM-011-008	0.8593	LEU-COMP-THERM-052-006	0.8053
LEU-COMP-THERM-011-009	0.8563	LEU-COMP-THERM-055-001	0.8124
LEU-COMP-THERM-011-010	0.8634	LEU-COMP-THERM-055-002	0.8067
LEU-COMP-THERM-011-011	0.8584	LEU-COMP-THERM-076-001	0.8347
LEU-COMP-THERM-011-012	0.8498	LEU-COMP-THERM-076-002	0.8440
LEU-COMP-THERM-011-013	0.8509	LEU-COMP-THERM-076-003	0.8394
LEU-COMP-THERM-011-014	0.8416	LEU-COMP-THERM-076-004	0.8353
LEU-COMP-THERM-011-015	0.8375	LEU-COMP-THERM-076-005	0.8364
LEU-COMP-THERM-014-005	0.8432	LEU-COMP-THERM-076-006	0.8339
LEU-COMP-THERM-015-026	0.8007	LEU-COMP-THERM-076-007	0.8340
LEU-COMP-THERM-015-129	0.8023		

Table D.2. Experiments with a c_k no less than 0.8, vanished lattice – actinides and fission products

Experiment	c_k	Experiment	c_k
LEU-COMP-THERM-005-010	0.8005	LEU-COMP-THERM-011-015	0.8250
LEU-COMP-THERM-008-001	0.8838	LEU-COMP-THERM-014-005	0.8352
LEU-COMP-THERM-008-002	0.8866	LEU-COMP-THERM-015-151	0.8136
LEU-COMP-THERM-008-003	0.8872	LEU-COMP-THERM-017-026	0.8193
LEU-COMP-THERM-008-004	0.8866	LEU-COMP-THERM-017-027	0.8007
LEU-COMP-THERM-008-005	0.8866	LEU-COMP-THERM-047-001	0.8418
LEU-COMP-THERM-008-006	0.8871	LEU-COMP-THERM-051-001	0.8373
LEU-COMP-THERM-008-007	0.8867	LEU-COMP-THERM-051-002	0.8698
LEU-COMP-THERM-008-008	0.8841	LEU-COMP-THERM-051-003	0.8670
LEU-COMP-THERM-008-009	0.8838	LEU-COMP-THERM-051-004	0.8657
LEU-COMP-THERM-008-010	0.8862	LEU-COMP-THERM-051-005	0.8620
LEU-COMP-THERM-008-011	0.8856	LEU-COMP-THERM-051-006	0.8602
LEU-COMP-THERM-008-012	0.8861	LEU-COMP-THERM-051-007	0.8622
LEU-COMP-THERM-008-013	0.8856	LEU-COMP-THERM-051-008	0.8522
LEU-COMP-THERM-008-014	0.8858	LEU-COMP-THERM-051-009	0.8587
LEU-COMP-THERM-008-015	0.8866	LEU-COMP-THERM-051-010	0.8510
LEU-COMP-THERM-008-016	0.8884	LEU-COMP-THERM-051-011	0.8519
LEU-COMP-THERM-008-017	0.8885	LEU-COMP-THERM-051-012	0.8530
LEU-COMP-THERM-011-002	0.8519	LEU-COMP-THERM-051-015	0.8549
LEU-COMP-THERM-011-003	0.8605	LEU-COMP-THERM-051-016	0.8486
LEU-COMP-THERM-011-004	0.8615	LEU-COMP-THERM-051-017	0.8527
LEU-COMP-THERM-011-005	0.8591	LEU-COMP-THERM-051-018	0.8491
LEU-COMP-THERM-011-006	0.8583	LEU-COMP-THERM-051-019	0.8349
LEU-COMP-THERM-011-007	0.8540	LEU-COMP-THERM-055-001	0.8034
LEU-COMP-THERM-011-008	0.8494	LEU-COMP-THERM-076-001	0.8290
LEU-COMP-THERM-011-009	0.8462	LEU-COMP-THERM-076-002	0.8386
LEU-COMP-THERM-011-010	0.8531	LEU-COMP-THERM-076-003	0.8343
LEU-COMP-THERM-011-011	0.8474	LEU-COMP-THERM-076-004	0.8311
LEU-COMP-THERM-011-012	0.8382	LEU-COMP-THERM-076-005	0.8295
LEU-COMP-THERM-011-013	0.8393	LEU-COMP-THERM-076-006	0.8277
LEU-COMP-THERM-011-014	0.8293	LEU-COMP-THERM-076-007	0.8259

Table D.3. Experiments with a c_k no less than 0.8, full lattice – actinides and fission products

Experiment	c_k	Experiment	c_k
LEU-COMP-THERM-008-001	0.8679	LEU-COMP-THERM-011-011	0.8095
LEU-COMP-THERM-008-002	0.8677	LEU-COMP-THERM-014-005	0.8062
LEU-COMP-THERM-008-003	0.8672	LEU-COMP-THERM-047-001	0.8002
LEU-COMP-THERM-008-004	0.8682	LEU-COMP-THERM-051-002	0.8371
LEU-COMP-THERM-008-005	0.8683	LEU-COMP-THERM-051-003	0.8336
LEU-COMP-THERM-008-006	0.8679	LEU-COMP-THERM-051-004	0.8324
LEU-COMP-THERM-008-007	0.8684	LEU-COMP-THERM-051-005	0.8277
LEU-COMP-THERM-008-008	0.8611	LEU-COMP-THERM-051-006	0.8260
LEU-COMP-THERM-008-009	0.8606	LEU-COMP-THERM-051-007	0.8283
LEU-COMP-THERM-008-010	0.8680	LEU-COMP-THERM-051-008	0.8169
LEU-COMP-THERM-008-011	0.8671	LEU-COMP-THERM-051-009	0.8223
LEU-COMP-THERM-008-012	0.8677	LEU-COMP-THERM-051-010	0.8166
LEU-COMP-THERM-008-013	0.8679	LEU-COMP-THERM-051-011	0.8175
LEU-COMP-THERM-008-014	0.8678	LEU-COMP-THERM-051-012	0.8188
LEU-COMP-THERM-008-015	0.8673	LEU-COMP-THERM-051-015	0.8209
LEU-COMP-THERM-008-016	0.8669	LEU-COMP-THERM-051-016	0.8111
LEU-COMP-THERM-008-017	0.8620	LEU-COMP-THERM-051-017	0.8184
LEU-COMP-THERM-011-002	0.8207	LEU-COMP-THERM-051-018	0.8114
LEU-COMP-THERM-011-003	0.8255	LEU-COMP-THERM-076-001	0.8287
LEU-COMP-THERM-011-004	0.8267	LEU-COMP-THERM-076-002	0.8367
LEU-COMP-THERM-011-005	0.8241	LEU-COMP-THERM-076-003	0.8356
LEU-COMP-THERM-011-006	0.8229	LEU-COMP-THERM-076-004	0.8359
LEU-COMP-THERM-011-007	0.8179	LEU-COMP-THERM-076-005	0.8249
LEU-COMP-THERM-011-008	0.8127	LEU-COMP-THERM-076-006	0.8251
LEU-COMP-THERM-011-009	0.8090	LEU-COMP-THERM-076-007	0.8147
LEU-COMP-THERM-011-010	0.8187		

APPENDIX E. VALIDATION DATA

E.1 VALIDATION DATA

The data used for the sample validation presented in Section 4.5 are provided here. The C/E ratios, enrichments, and EALF values are provided for each experiment in Table E.1. The c_k values are provided in Table D.2.

Table E.1. Validation data for vanished lattice with actinides and fission products

Experiment	C/E	C/E Uncertainty	Enrichment (wt% ^{235}U)	EALF (eV)
LEU-COMP-THERM-005-010	0.99697	0.00279	4.31	1.663
LEU-COMP-THERM-008-001	0.99672	0.00120	2.46	0.277
LEU-COMP-THERM-008-002	0.99757	0.00120	2.46	0.244
LEU-COMP-THERM-008-003	0.99784	0.00120	2.46	0.244
LEU-COMP-THERM-008-004	0.99745	0.00120	2.46	0.244
LEU-COMP-THERM-008-005	0.99719	0.00120	2.46	0.244
LEU-COMP-THERM-008-006	0.99780	0.00120	2.46	0.243
LEU-COMP-THERM-008-007	0.99705	0.00120	2.46	0.243
LEU-COMP-THERM-008-008	0.99666	0.00120	2.46	0.242
LEU-COMP-THERM-008-009	0.99739	0.00120	2.46	0.241
LEU-COMP-THERM-008-010	0.99707	0.00120	2.46	0.247
LEU-COMP-THERM-008-011	0.99786	0.00120	2.46	0.252
LEU-COMP-THERM-008-012	0.99753	0.00120	2.46	0.246
LEU-COMP-THERM-008-013	0.99759	0.00120	2.46	0.246
LEU-COMP-THERM-008-014	0.99702	0.00120	2.46	0.248
LEU-COMP-THERM-008-015	0.99686	0.00120	2.46	0.248
LEU-COMP-THERM-008-016	0.99721	0.00120	2.46	0.226
LEU-COMP-THERM-008-017	0.99646	0.00120	2.46	0.197
LEU-COMP-THERM-011-002	0.99578	0.00319	2.46	0.245
LEU-COMP-THERM-011-003	0.99607	0.00319	2.46	0.192
LEU-COMP-THERM-011-004	0.99644	0.00319	2.46	0.193
LEU-COMP-THERM-011-005	0.99627	0.00319	2.46	0.194
LEU-COMP-THERM-011-006	0.99616	0.00319	2.46	0.195
LEU-COMP-THERM-011-007	0.99640	0.00319	2.46	0.196
LEU-COMP-THERM-011-008	0.99666	0.00319	2.46	0.197
LEU-COMP-THERM-011-009	0.99631	0.00319	2.46	0.198
LEU-COMP-THERM-011-010	0.99359	0.00169	2.46	0.187
LEU-COMP-THERM-011-011	0.99328	0.00169	2.46	0.163
LEU-COMP-THERM-011-012	0.99341	0.00169	2.46	0.167
LEU-COMP-THERM-011-013	0.99401	0.00169	2.46	0.147
LEU-COMP-THERM-011-014	0.99380	0.00169	2.46	0.151
LEU-COMP-THERM-011-015	0.99478	0.00179	2.46	0.139
LEU-COMP-THERM-014-005	1.00143	0.00691	4.31	0.583
LEU-COMP-THERM-015-151	1.00034	0.00300	3.56	0.175
LEU-COMP-THERM-017-026	0.99496	0.00279	2.35	0.375
LEU-COMP-THERM-017-027	0.99696	0.00279	2.35	0.321
LEU-COMP-THERM-047-001	1.00000	0.00200	3.01	0.165
LEU-COMP-THERM-051-001	0.99594	0.00199	2.46	0.147

Table E.1. (continued)

Experiment	C/E	C/E Uncertainty	Enrichment (wt% ²³⁵U)	EALF (eV)
LEU-COMP-THERM-051-002	0.99730	0.00239	2.46	0.197
LEU-COMP-THERM-051-003	0.99708	0.00239	2.46	0.196
LEU-COMP-THERM-051-004	0.99709	0.00239	2.46	0.198
LEU-COMP-THERM-051-005	0.99709	0.00239	2.46	0.198
LEU-COMP-THERM-051-006	0.99718	0.00239	2.46	0.200
LEU-COMP-THERM-051-007	0.99682	0.00239	2.46	0.200
LEU-COMP-THERM-051-008	0.99700	0.00239	2.46	0.201
LEU-COMP-THERM-051-009	0.99655	0.00189	2.46	0.167
LEU-COMP-THERM-051-010	0.99609	0.00189	2.46	0.192
LEU-COMP-THERM-051-011	0.99332	0.00189	2.46	0.193
LEU-COMP-THERM-051-012	0.99213	0.00189	2.46	0.195
LEU-COMP-THERM-051-015	0.99070	0.00238	2.46	0.201
LEU-COMP-THERM-051-016	0.99088	0.00198	2.46	0.169
LEU-COMP-THERM-051-017	0.99226	0.00268	2.46	0.202
LEU-COMP-THERM-051-018	0.99215	0.00208	2.46	0.169
LEU-COMP-THERM-051-019	0.99213	0.00189	2.46	0.151
LEU-COMP-THERM-055-001	0.99707	0.00249	3.01	1.216
LEU-COMP-THERM-076-001	0.99653	0.00249	3.00	1.482
LEU-COMP-THERM-076-002	0.99653	0.00249	3.00	1.482
LEU-COMP-THERM-076-003	0.99668	0.00249	3.00	1.400
LEU-COMP-THERM-076-004	0.99540	0.00249	3.00	1.481
LEU-COMP-THERM-076-005	1.00027	0.00250	3.00	1.477
LEU-COMP-THERM-076-006	0.99762	0.00250	3.00	1.491
LEU-COMP-THERM-076-007	1.00308	0.00251	3.00	1.362

APPENDIX F. ISOTOPIC VALIDATION DATA

F.1 SELECTION OF DATA FOR BWR ISOTOPIC VALIDATION

A review of the Spent Fuel Isotopic Composition Database (SFCOMPO) [F1] and the literature was performed to identify radiochemical assay (RCA) data for boiling water reactor (BWR) spent nuclear fuel (SNF) in the burnup range of interest for this report. The samples considered were expanded to encompass RCA data that included gadolinium measurements of PWR SNF samples selected from gadolinium fuel rods since the data available for BWR fuel was limited. The results of the review are summarized in Table F.1, which presents the RCA data that were further evaluated for applicability in this report. This table shows 14 sets of RCA data, 11 of which contain samples irradiated in BWRs.

Table F.1. Sources of RCA data for BWR isotopic validation

Reactor name	Reactor type	Lattice type	Measured fuel rod type(s)	Number of samples	Sample burnup (GWd/MTU)	Gd rods in assembly?	Gd nuclides measured?
JPDR	BWR	6×6	UO ₂	30	2.2–7.2	No	No
Fukushima-Daini-2	BWR	8×8	UO ₂ , UO ₂ -Gd ₂ O ₃	18	4.1–44.0	Yes	No
Fukushima-Daichi-3	BWR	8×8	UO ₂ , UO ₂ -Gd ₂ O ₃	36	4.1–33.6	Yes	No
Garigliano	BWR	9×9	UO ₂	30	8.0–13.7	No	No
Tsuruga-1	BWR	7×7	UO ₂	10	8.6–27.7	No	No
Gundremmingen-A	BWR	6×6	UO ₂	12	14.4–27.4	No	No
Cooper	BWR	7×7	UO ₂	6	17.8–33.9	No	No
Fukushima-Daini-1	BWR	9×9	UO ₂ , UO ₂ -Gd ₂ O ₃	8	35.6–68.3	Yes	No
Forsmark3	BWR	10×10	UO ₂	6	38.3–56.0	Yes	Yes
Monticello	BWR	8×8	UO ₂ , UO ₂ -Gd ₂ O ₃	30	40.3–58.7	Yes	No
Dodeward	BWR	6×6	UO ₂	1	54.4	Yes	No
Takahama-3	PWR	17×17	UO ₂ , UO ₂ -Gd ₂ O ₃	16	7.8–47.3	Yes	No
Ohi-2	PWR	17×17	UO ₂ , UO ₂ -Gd ₂ O ₃	3	21.5–25.1	Yes	Yes

Many of the BWR samples in Table F.1 correspond to older lattice designs that do not contain gadolinium fuel rods. The pressurized water reactor (PWR) data sets were selected because they include measurement data performed for gadolinium fuel rods. The sample burnups range from 2.2 to 68.3 gigawatt days per metric ton of uranium (GWd/MTU).

Older measurements, such as those for SNF from the Japan Power Demonstration Reactor (JPDR) and the Gundremmingen-A reactor, include only major actinides and limited fission product data. Only three of the measurement sets in Table F.1 include gadolinium measurements. Measurement data from the Forsmark-3 reactor include gadolinium; however the measured fuel rod did not contain any gadolinium poison. The only samples where gadolinium measurements were performed on fuel containing gadolinium poison were the PWR samples from Takahama-3 and Ohi-2.

The measurement data included in Table F.1 represent a wide range of burnups and assembly types. The burnup and enrichment ranges for the BWR samples included in this table are illustrated in Figure F.1. Each color in the figure represents samples from one of the reactors listed in Table F.1. Not all of these measurements would be applicable to validating nuclide compositions near peak reactivity burnup credit (BUC). The uncertainties and biases calculated from isotopic validation can vary as a function of fuel burnup and core conditions. The measurement data listed in Table F.1 were evaluated using several selection criteria, as further presented in this section, for applicability to the analyses discussed in the current report.

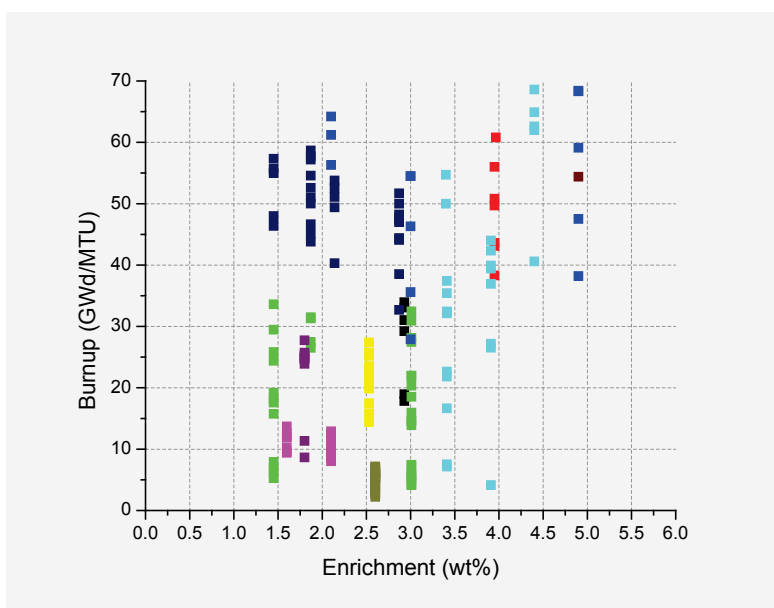


Figure F.1. Burnup vs. enrichment for available BWR RCA data.

The first criterion for sample selection was the burnup of the measured samples. Peak reactivity can generally occur at burnups up to ~20 GWd/MTU, but the reactivity effects in assemblies with high gadolinium content can extend to ~30 GWd/MTU. Therefore, all samples with burnups less than 30 GWd/MTU were selected for inclusion in the isotopic validation set. Gadolinium measurements were only available at burnups greater than 20 GWd/MTU, with a few of these data corresponding to burnups larger than 25 GWd/MTU. Seven BWR RCA data sets listed in Table F.1 meet this selection criterion.

Another sample selection criterion relates to the availability of adequate operation data for the measured samples to enable accurate depletion modeling. The older RCA measurements usually lack detailed operating history data for the measured samples. Depending on the reactor type and isotope of interest, the effect of the missing data on the isotopic prediction, and consequently on the calculated bias and uncertainty for that isotope, can vary. For example, the fuel temperature history generally has a small effect on isotopic prediction, whereas the coolant void fraction history can be a very important factor in prediction of major actinides.

Unlike PWRs, the axial change in the coolant density in BWRs is large, leading to isotopic variations along the axial direction of the fuel rod due to the hardening of the neutron spectrum with increased void fraction. Figure F.2 illustrates the high sensitivity to void fraction of calculated plutonium isotopic contents. This example shows the percent change in the isotopic content of selected actinides and fission products due to a 10% decrease in the void fraction for a JPDR fuel sample with a 5 GWd/MTU burnup. This example emphasizes the importance of void fraction data availability to accurately model the fuel

depletion. The samples from the Cooper, Fukushima-Daichi-3, and Tsuruga reactors listed in Table F.1 were not included in the final isotopic validation data set because no void fraction information was available for these samples.

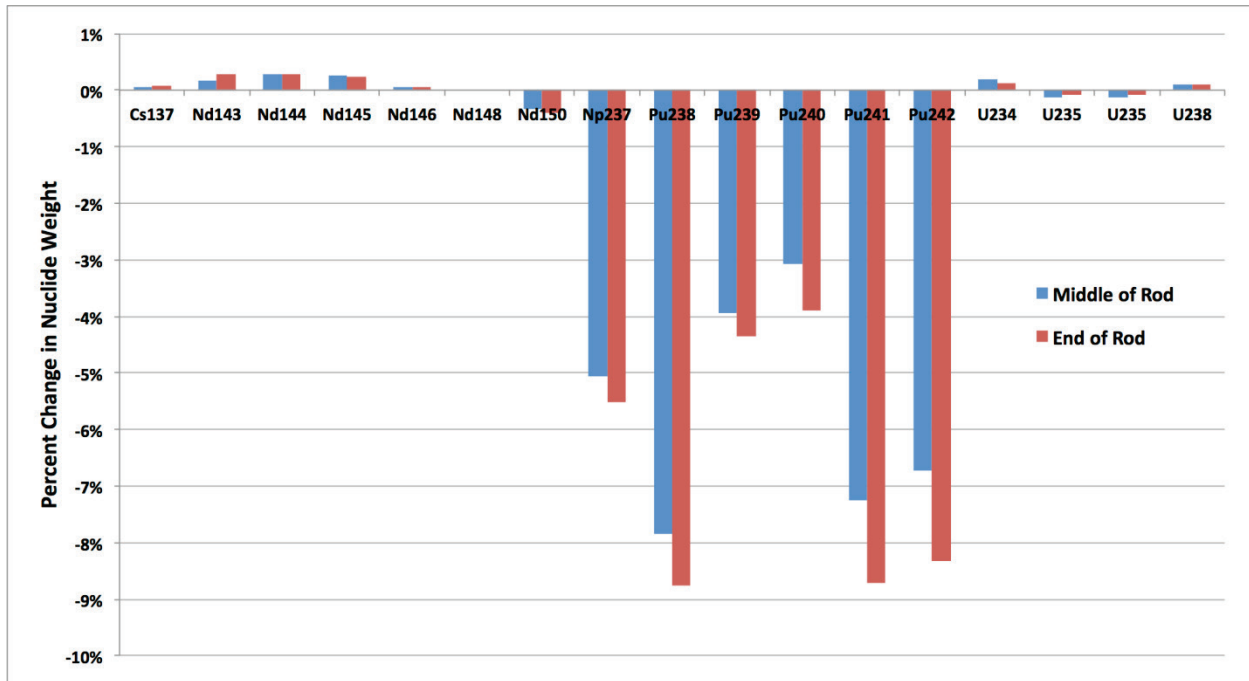


Figure F.2. Effect of void fraction change (-10%) on isotopic content for 5 GWd/MTU BWR fuel.

A third criterion for sample selection was the availability of complete design data important to the accuracy of the depletion models. All samples from the Garigliano reactor and some of the samples from the JPDR were eliminated due to unavailability of relevant design data. The Garigliano reactor and the JPDR employed first generation BWR designs, with boron curtains and erbium-loaded fuel rods used as burnable poisons in the reactor cycle at the times the samples were irradiated. However, no specifications for the boron curtains or the erbium loading of the fuel rods are available. Because both of these burnable absorbers—boron and erbium—are expected to change the neutron spectrum significantly, the samples adjacent to the boron curtains in JPDR assemblies were eliminated from the validation data set in this study, as were all Garigliano samples.

The samples that resulted from the down-selection process are listed in Table F.2. Sixteen of the 19 samples are from BWRs. However, none of these BWR samples include gadolinium nuclide measurements, and only four samples (Fukushima-Daini-2) are from gadolinium-loaded assemblies. Clearly there is a need for additional RCA measurements of BWR SNF with burnup in the peak reactivity burnup range.

Table F.2. Selected RCA isotopic validation data set

Reactor name	Lattice type	Reactor type	Measured fuel rod type	Number of samples	Sample burnup (GWd/MTU)	Gadolinium nuclides measurements
Gundremmingen-A	6×6	BWR	UO ₂	8	14.4 - 25.2	No
JPDR	6×6	BWR	UO ₂	4	2.8 - 4.4	No
Fukushima-Daini-2	8×8	BWR	UO ₂ , UO ₂ - Gd ₂ O ₃	4	16.6 - 26.5	No
Ohi-2 ^a	17×17	PWR	UO ₂ , UO ₂ - Gd ₂ O ₃	3	21.5 - 28.7	Yes

^a fuel samples analyzed to obtain isotopic validation data for ¹⁵⁵Gd

To provide additional data for validating gadolinium depletion three samples from the Ohi-2 PWR were included in the isotopic validation dataset. This PWR assembly included gadolinium-loaded fuel rods, which are also present in modern BWR assemblies. The Ohi-2 samples are the only available RCA data that include gadolinium isotope measurements at relatively low burnups for fuel rods that include gadolinium poison. Although BWRs and PWRs differ in their fuel assembly design and operation, the fuel-to-moderator ratio for the Ohi-2 and a modern GE14 10×10 assembly are similar, and these particular PWR samples provide data representative of non-boiling regions of a BWR assembly.

F.2 ISOTOPIC VALIDATION MODELING

This section presents the modeling assumptions used for BWR depletion modeling in the peak reactivity burnup range. The SCALE depletion simulation models used for isotopic validation include several assumptions in cases of missing operation and design data for the validation samples. These assumptions are listed below.

1. It is assumed that the in-channel void fraction is radially uniform across the sample axial node. Although high or low power fuel rods may exhibit gradients from the average value, in-channel radial void fraction distribution data are not available.
2. It is assumed that the void fraction is constant with burnup. The available void history is averaged over irradiation time.
3. Unless specified, the clad temperature is set equal to the moderator temperature. In normal reactor operations, the clad temperature is at a value between the temperature of the fuel pin outer surface and the coolant temperature. However, the sensitivity of the clad neutron absorption to the clad temperature is negligible.
4. The fuel temperature is assumed to be radially uniform across the fuel assembly and constant over the irradiation history of the assembly. The basis for this assumption is that the effect of fuel temperature history on fuel isotopics diminishes over long assembly exposures.
5. It is assumed that the modeling of the fuel channel as a square has a negligible impact on the calculated isotopic results. Although the fuel channel corners are rounded, this geometrical approximation would impact only the corner fuel rods to some extent, and not the non-corner fuel rods. None of the samples included in the isotopic validation set were selected from rods located at the corner of the assembly.

F.3 ANALYSIS OF ISOTOPIC MEASUREMENTS

F.3.1 JPDR

The Japanese Power Demonstration Reactor (JPDR) was a small, natural circulation BWR operated at the Japanese Atomic Energy Research Institute (JAERI). The RCA measurements of the JPDR samples were performed by JAERI. These JPDR samples offer a unique set of data for the validation of major actinides at very low burnups [F1, F2]. Note that the poison rods used in this reactor, as discussed in Section F.1, are an early implementation of burnable poison rods in BWRs. The void history data are available for these samples. However, there are missing data on the use of boron poison curtains, as no information was provided about the material content of the curtains.

The JPDR measured samples were extracted from three assemblies with locations in the core as illustrated in Figure F.3. Based on the assembly locations, the samples from the A-20 assembly were not included in the isotopic validation set. The A-20 assembly is located adjacent to poison curtains on two sides and a control blade nearby. The missing control blade information increases the uncertainty in modeling the depletion of the samples. Considering that the majority of the samples are located at the edge of the assembly, the samples from A-20 are not included in the analysis for this report.

The fuel assembly design data and operating characteristics are listed in Table F.3. The operating data for the samples from A-14 and A-18 assemblies are given in Table F.4. The samples' axial locations are shown in Figure F.4. The SCALE/TRITON assembly model used for depletion simulations is illustrated in Figure F.5. This figure indicates the location of the measured rod in the assembly. As indicated in the figure by different colors for fuel zones, the measured fuel rod and each of its nearest neighbors are depleted individually.

The TRITON-calculated isotopic contents for the four considered samples were compared with reported isotopic measured data. As shown in Table F.5, there is very good agreement between calculation and measurement for the major actinide ^{235}U . The Pu nuclides are generally overpredicted. The largest discrepancies for Pu are seen for sample A18-5, which is near a Dy_2O_3 pellet. The effect of this pellet cannot be modeled in the TRITON 2D model of A18-5 and likely contributes to the larger discrepancies in results for this sample.

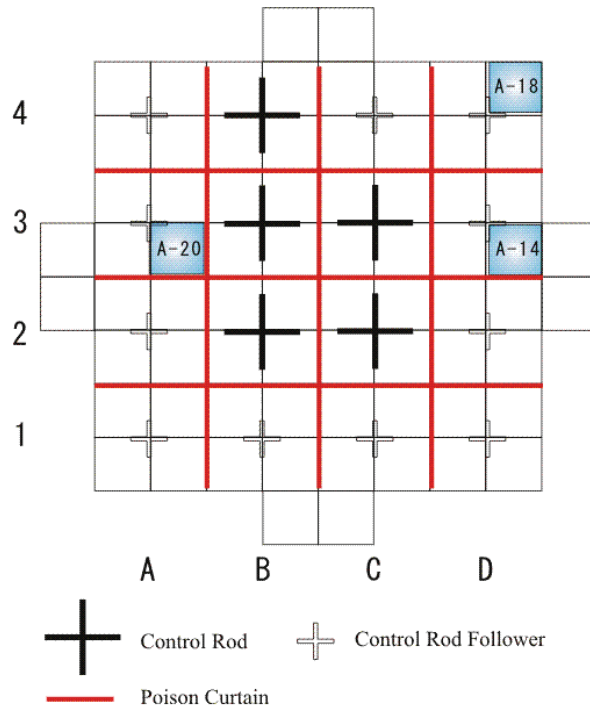


Figure F.3. JPDR core map [F1].

Table F.3. JPDR assembly design data [F1, F2]

Parameter	Data
Fuel Rod Data	
Fuel Type	UO ₂
Fuel Density (g/cm ³)	10.4
Fuel Pitch (cm)	1.956
Fuel Diameter (cm)	1.25
Fuel Temperature (K)	840
Initial U Isotopics	²³⁴ U 0.0153 wt%
	²³⁵ U 2.5966 wt%
	²³⁶ U 0.0161 wt%
	²³⁸ U 97.372 wt%
Clad Inner Diameter (cm)	1.26
Clad Thickness (mm)	0.76
Clad Material	Zircaloy-2
Clad Temperature (K)	620
Moderator Data	
Temperature (K)	550
Assembly Data	
Assembly Pitch (cm)	13.26
Channel Material	Zircaloy-4
Assembly Pitch (cm)	11.736
Fuel Rod Active Height (cm)	366

Table F.4. JPDR samples data [F1, F2]

Sample	Assembly	Burnup (GWd/MTU)	Void fraction (%)	Coolant density (g/cm ³)	Sample location (cm)*
A14-1	A14	4.13	0	0.7541	-293
A14-3		3.38	20.0	0.6075	+538
A18-5	A18	4.35	11.8	0.6700	+49
A18-6		2.77	26.6	0.5629	+538

* See Figure F.12

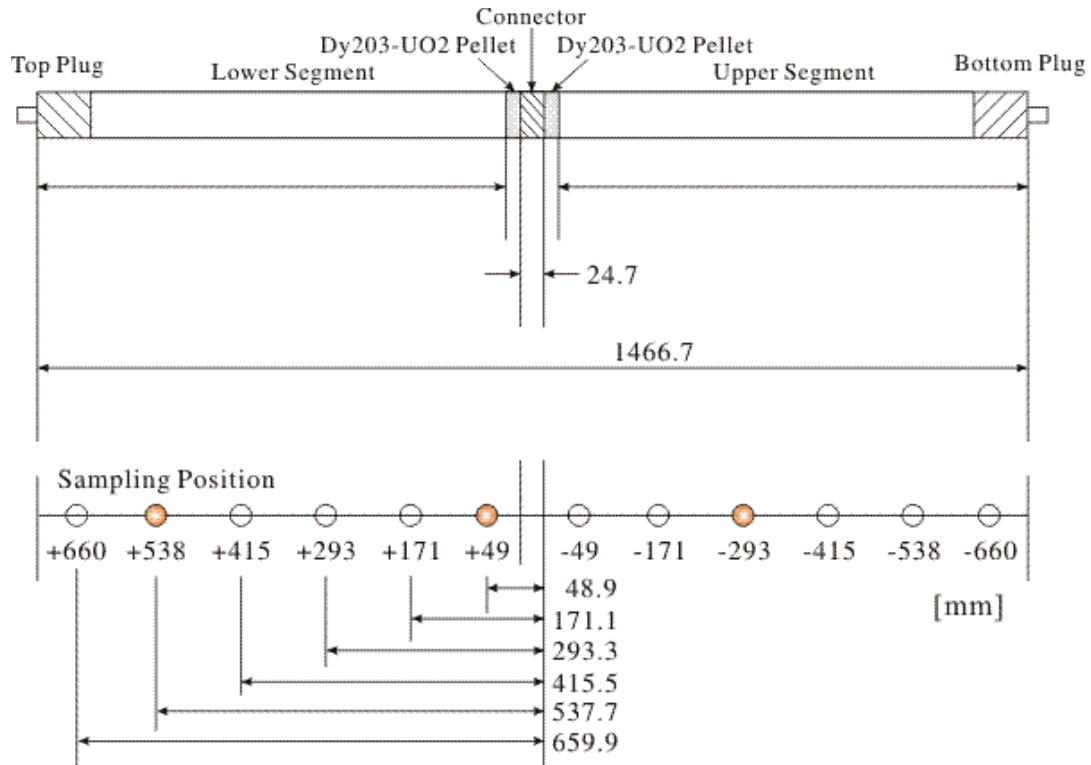


Figure F.4. JPDR samples axial locations [F1].

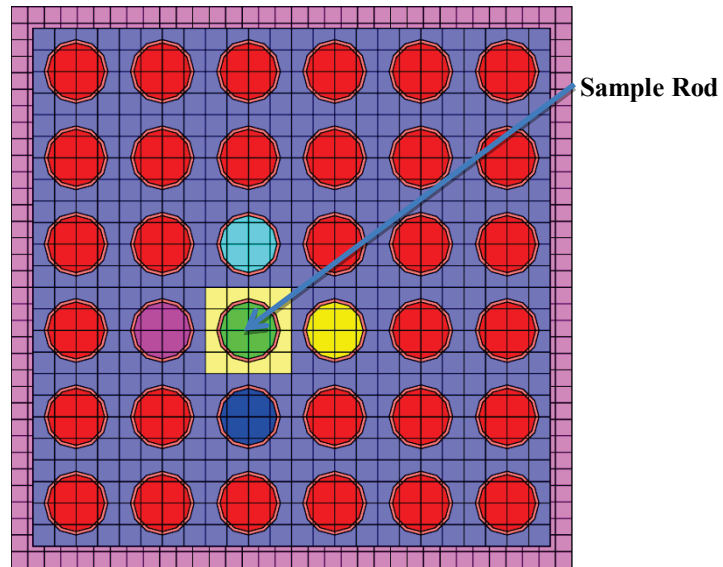


Figure F.5. Illustration of SCALE/TRITON model for JPDR assembly.

Table F.5. Comparison calculation-measurement for JPDR samples

Sample ID	C/M-1 (%)			
	A14-1	A14-3	A18-5	A18-6
GWd/MTU	4.13	3.38	4.35	2.77
U ²³⁴	1.79	-0.92	-1.31	0.12
U ²³⁵	0.31	-0.67	0.90	0.00
U ²³⁶	0.01	-0.64	2.78	-1.18
U ²³⁸	0.00	0.03	0.11	-0.01
Pu ²³⁸	-5.52	-8.68	3.98	36.92
Pu ²³⁹	8.66	9.07	15.39	6.45
Pu ²⁴⁰	7.51	10.54	16.09	8.90
Pu ²⁴¹	11.79	10.45	25.66	3.09
Pu ²⁴²	8.45	10.76	20.26	35.23
Nd ¹⁴³	-0.08	-0.05	0.01	0.00
Nd ¹⁴⁴	-1.21	-0.62	-1.19	-0.51
Nd ¹⁴⁵	0.46	0.13	0.32	0.43
Nd ¹⁴⁶	0.65	0.53	0.92	0.66
Nd ¹⁴⁸	1.18	0.70	1.37	0.44
Nd ¹⁵⁰	0.58	0.20	1.48	-1.06
Cs ¹³⁷	-10.70	-11.01	-7.59	-6.95

F.3.2 Gundremmingen-A

Located in Germany, the Gundremmingen power plant was one of the first commercial BWRs. Like the JPDR plant, the Gundremmingen employed poison curtains in the reactor core. The poison curtains were boron-loaded, stainless steel plates located along the narrow gap edges of the fuel assembly [F1, F2].

Post-irradiation examination of two 6×6 fuel assemblies from Gundremmingen Unit A was performed by the Karlsruhe and Ispra institutes [F3]. Both assemblies—identified as B23 and C16—had low assembly average burnups of 22 GWd/MTU and 17 GWd/MTU, respectively, and they also had similar enrichment profiles. Each assembly had seven fuel rods with 1.87 wt% ²³⁵U enrichment and 29 fuel rods with 2.53 wt% ²³⁵U enrichment. The configuration of the assemblies, including the location of the measured fuel rods, is illustrated in Figure F.6. All measured samples were selected from rods with 2.53 wt% ²³⁵U enrichment.

Relevant assembly design data are listed in Table F.6. Burnup, coolant density, and sample location for the eight samples analyzed in this report are shown in Table F.7. The majority of the design information used for modeling was obtained from a report released by the European Commission Joint Research Center [F3], with other modeling data gathered from several other sources [F1, F4]. An example of the SCALE/TRITON models used for analysis of these samples is illustrated in Figure F.7, which corresponds to sample C16-B3 analysis. Note that the model makes use of the symmetry along the assembly diagonal. The measured rod and its nearest neighbor rods are depleted individually as indicated by the use of different colors in Figure F.7.

Table F.8 presents a comparison of the calculated and measured data. The major actinides show good agreement, while some of the minor actinides show larger discrepancies, especially ²⁴¹Am, which requires further investigation.

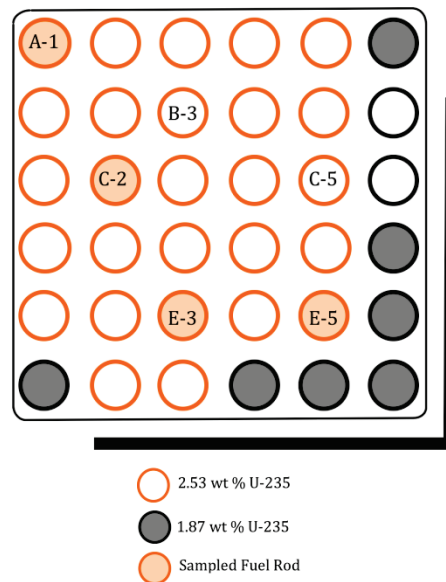


Figure F.6. Diagram of assembly C16 enrichment profile [F1].

Table F.6. Gundremmingen-A assembly design data

Parameter	Data
Assembly and reactor data	
Lattice type	6×6
Active core height (m)	3.302
Assembly pitch wide-wide (cm)	13.098
Assembly pitch narrow-narrow (cm)	12.303
Fuel rod data	
Fuel material	UO ₂
Fresh fuel pellet density (g/cm ³)	10.5
Smearred fuel pellet density (g/cm ³)	10.07
Fuel pellet diameter (cm)	1.224
Rod pitch (cm)	1.78
Fuel temperature (K)	923
Clad material	Zircaloy-2
Pellet-cladding gap (cm)	0.01375
Clad thickness (cm)	0.0889
Clad inner diameter (cm)	1.25
Moderator data	
Nominal pressure (bar)	69
Nominal outlet temperature (K)	559
Channel box data	
Channel box outside width (cm)	11.352
Channel box thickness (cm)	0.15
Channel box material	Zircaloy-4

Table F.7. Gundremmingen-A samples data

Sample	Assembly	Burnup (GWd/MTU)	Coolant density (g/cm ³)	Sample location (cm)*
C16-B3	C16	14.39	0.388	268
C16-C5		15.84	0.388	268
C16-E5		17.49	0.388	268
B23-B3	B23	21.24	0.388	268
B23-B4		22.25	0.388	268
B23-C5		22.97	0.388	268
B23-E3		23.51	0.388	268
B23-E5		25.19	0.388	268

* axial distance from bottom of active length

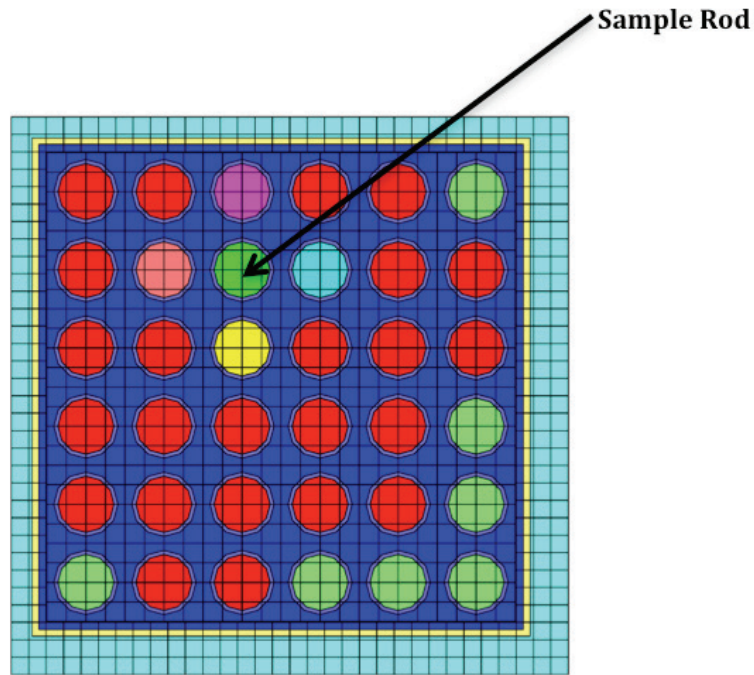


Figure F.7. Illustration of SCALE/TRITON model for Gundremmingen sample C16-B3.

Table F.8. Comparison calculation-measurement for Gundremmingen-A samples

Sample ID	C/M-1 (%)							
	C16-B3	C16-C5	C16-E5	B23-B3	B23-B4	B23-C5	B23-E3	B23-E5
GWd/MTU	14.39	15.84	17.49	21.24	22.25	22.97	23.51	25.19
U ²³⁵	2.16	-1.61	3.71	0.23	3.24	0.44	-2.80	4.86
U ²³⁶	-7.78	-3.73	-5.98	-3.81	-2.69	-5.76	-4.13	-4.91
U ²³⁸	-0.02	0.01	0.00	-0.04	-0.09	0.00	0.01	0.07
Pu ²³⁸	-6.56	-3.50	-9.94	-7.64	-10.65	-8.33	1.41	-9.92
Pu ²³⁹	3.18	2.57	1.11	4.70	9.37	3.79	6.77	1.64
Pu ²⁴⁰	-0.26	2.94	-3.52	-0.56	4.00	-0.31	8.72	-0.79
Pu ²⁴¹	-16.13	-11.91	-17.47	-13.57	-10.39	-14.89	-11.49	-16.41
Pu ²⁴²	-9.31	-0.14	-16.88	-8.09	-3.02	-8.34	4.74	-10.05
Am ¹⁴¹	-11.04	167.88	-28.14	-51.78			-20.26	-8.54
Cm ²⁴²	-99.18	-98.82	-98.96	-98.94	-99.00	-99.06	-99.55	-99.03
Cm ²⁴⁴	-21.35	-17.26	-25.06	-16.94	-10.02	-18.75	3.66	-23.82
Nd ¹⁴⁸	-0.89	0.75	-1.07	-0.68	-0.41	-0.45	-3.09	-3.24
Cs ¹³⁷	-13.28	-18.36	-6.08	-9.28	-7.04	-15.50	-4.71	-9.73

F.3.3 Fukushima Daini-2

The Fukushima Daini-2 Nuclear Power Station, operated by Tokyo Electric Power Company (TEPCO), used Hitachi BWR fuel bundles with an 8×8 lattice for the reactor cycles considered in this report [0]. A nuclide composition benchmark data set was generated by JAERI as part of a BUC research project [F5]. The JAERI-generated data set included 18 BWR samples which were selected from two rods with initial ²³⁵U enrichments of 3.41 and 3.91 wt%, respectively. The samples had burnups ranging from 4.2 to 44.0 GWd/MTU. The two measured rods, identified as SF98 and SF99, were part of the same assembly—2F2DN23—which was irradiated in the reactor for a total of 1174 days.

The layout of assembly 2F2DN23 and its axially averaged enrichment distribution are shown in Figure F.8. The SF98 rod corresponds to position B-2 within the assembly. The SF99 rod corresponds to position C-2 and contains gadolinium as a burnable poison. Both fuel rods contain a natural uranium blanket segment at the upper and lower tips of the rods.

Destructive and non-destructive analyses were performed at JAERI from 1995 through 1997. The destructive analyses were conducted to determine nuclide compositions. Non-destructive gamma scans were performed to determine axial burnup distributions. For destructive analyses, the samples were collected by cutting 0.5 mm-thick slices axially at different locations along the rod, as shown in Figure F.9. Based on the reported sample burnups [0], four of the SF98 and SF99 samples have burnups smaller than 20 GWd/MTU; however, three of these samples are located in the natural uranium blanket region and are therefore not applicable for the study in this report.

Relevant design and operation data used in the SCALE models of the considered samples are presented in Tables F.9 and F.10 [0, F4, F5, F6]. The SCALE/TRITON model for SF99 samples is illustrated in Figure F.10. The comparison of calculated and measured isotopic concentrations is presented in Table F.11.

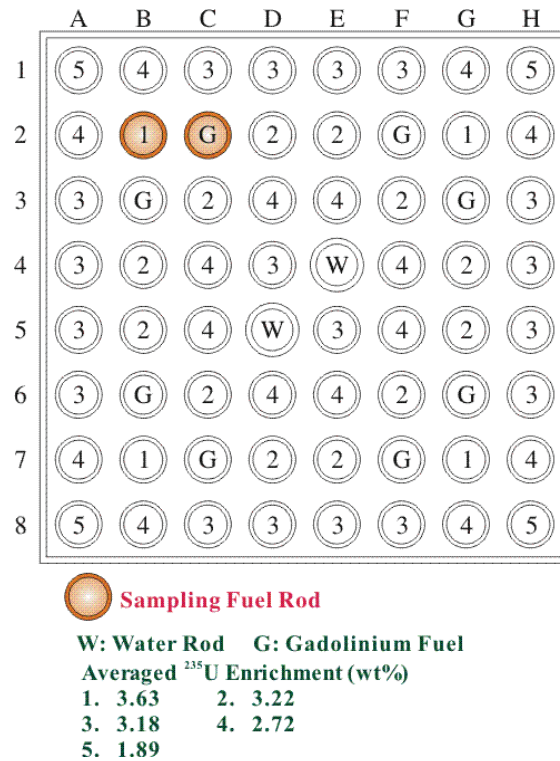


Figure F.8. Radial loading diagram of assembly 2F2DN23.

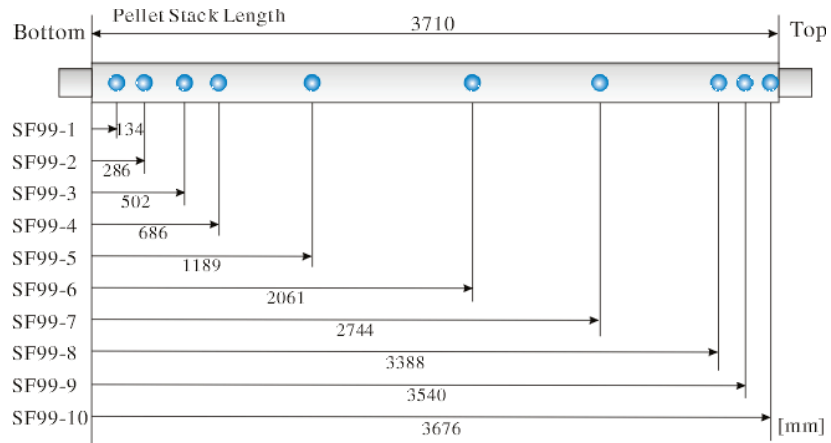


Figure F.9. Measurement positions for rod SF99.

Table F.9. Fukushima-Daini-2 assembly design data

Parameter	Data
Assembly and reactor data	
Lattice type	8×8-2
Active core height (m)	3.71
Assembly pitch (cm)	15.2
Fuel rod data	
Fuel material	UO ₂ , UO ₂ -Gd ₂ O ₃
Fuel density (g/cm ³)	10.412
Smear fuel pellet density (g/cm ³)*	9.943
Fuel pellet diameter (cm)	1.03
Pellet-clad gap clearance (cm)	0.024
Clad material	Zircaloy-2
Clad thickness (cm)	0.086
Clad outer diameter (cm)	1.23
Rod pitch (cm)	1.63
Fuel temperature (K)	900
Water rod data	
Water rod material	Zircaloy
Water rod inner diameter (cm)	1.35
Water rod outer diameter (cm)	1.50
Channel Box Data	
Channel box inner width (cm)	13.4
Channel box thickness (cm)	0.203

*Based on fresh fuel diameter + gap distance.

Table F.10. Fukushima-Daini-2 samples data

Sample	Burnup (GWd/MTU)	Enrichment (wt% ²³⁵U)	Coolant density (g/cm³)	Sample location* (cm)
SF99-9	16.65	3.41	0.2272	354.0
SF99-8	21.83	3.41	0.2356	338.8
SF99-2	22.63	3.41	0.7303	28.6
SF98-8	27.18	3.91	0.2265	339.7

* distance from bottom of active fuel

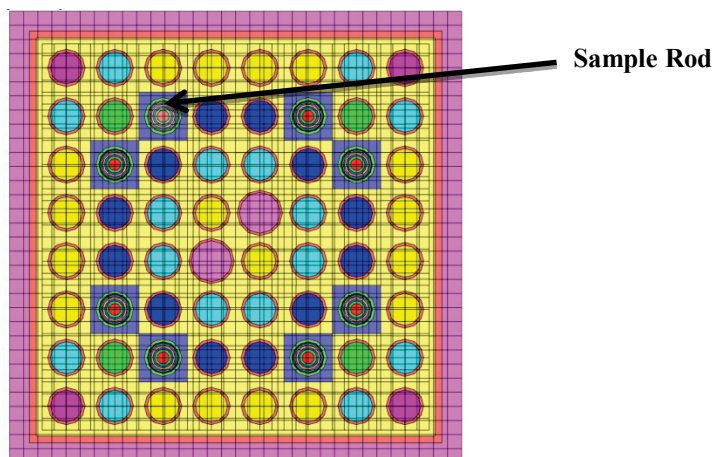


Figure F.10. Illustration of SCALE/TRITON model for Fukushima Daini-2 SF99 samples.

Table F.11. Comparison calculation-measurement for Fukushima Daini-2 samples

Sample ID	C/M-1 (%)			
	SF99-9	SF99-8	SF99-2	SF98-8
GWd/MTU	16.65	21.83	22.63	27.18
U ²³⁴	4.85	7.86	10.77	3.47
U ²³⁵	4.53	5.20	2.47	1.97
U ²³⁶	-1.82	-2.84	-2.30	-1.99
U ²³⁸	-0.14	-0.09	0.30	-0.07
Np ²³⁷	-10.03	-9.74	-13.14	6.50
Pu ²³⁸	2.09	-3.58	-1.47	-12.38
Pu ²³⁹	9.99	3.98	-2.71	2.09
Pu ²⁴⁰	4.70	1.65	-1.50	0.49
Pu ²⁴¹	7.27	-1.23	-10.28	-0.34
Pu ²⁴²	2.53	-4.86	-13.03	-4.08
Am ²⁴¹	0.87	7.88	30.05	16.11
Am ^{242m}	-13.44	-26.49	-35.11	-31.35
Am ²⁴³	13.98	1.03	-7.27	13.27
Cm ²⁴⁴	4.06	-15.05	-22.92	-4.31
Nd ¹⁴³	-2.71	-1.20	0.23	1.39
Nd ¹⁴⁴	-3.09	5.40	0.32	5.88
Nd ¹⁴⁵	-1.88	-0.59	1.13	1.68
Nd ¹⁴⁶	-0.79	-0.53	1.42	2.34
Nd ¹⁴⁸	-0.65	-0.42	0.65	1.86
Nd ¹⁵⁰	0.38	-0.53	-0.20	1.46
Cs ¹³⁷	-6.87	-6.92	-5.04	3.95
Cs ¹³⁴	-11.06	-14.64	-11.96	4.69
Eu ¹⁵⁴	-3.11	-6.73	-10.29	-0.93
Ce ¹⁴⁴	-6.19	-21.25	-0.64	-12.13
Ru ¹⁰⁶	2.34	73.27	111.58	23.16
Sm ¹⁴⁷	-2.07	-2.02		-7.49
Sm ¹⁴⁸	-5.54	-12.53		-14.66
Sm ¹⁴⁹	7.27	-3.60		-26.18
Sm ¹⁵⁰	-1.74	-4.21		-6.23
Sm ¹⁵¹	3.61	-4.60		-9.07
Sm ¹⁵²	-2.20	-2.08		-7.66
Sm ¹⁵⁴	-2.41	-4.71		-12.00

F.3.4 Ohi-2

The Ohi-2 reactor is a PWR operated in Japan by JAERI. Post irradiation evaluation of five samples from fuel irradiated in this reactor was performed by JAERI [F7]. All samples were cut from three fuel rods located in the same 17×17 fuel assembly, identified as 17G. Although the assembly's average burnup is relatively high, the samples located at the top of the fuel have burnups less than 30 GWd/MTU. Three of these samples were selected from two gadolinium fuel rods placed at symmetric locations in the fuel assembly.

The measurements include data for actinides (U, Pu, Am, Cm) and fission products (selected nuclides of Nd, Ru, Ag, Sb, Cs, Ce, Eu, Gd). The experimental actinides data are reported for discharge time, whereas the fission products data are reported at a cooling time in the range 1100–1390 days after discharge. All the measurement data except for gadolinium are expressed in grams of measured nuclide per initial MTU. For the gadolinium nuclides, the data are reported as atomic ratios of a gadolinium isotope relative to the total gadolinium content.

Relevant design and operating data for the analyzed gadolinium rod samples are listed in Tables F.12 and F.13. The SCALE/TRITON model used for the depletion simulations is illustrated in Figure F.11.

The results of the calculated to measured isotopic comparisons for actinides and the burnup indicator fission product ^{148}Nd are presented in Table F.14. As seen from this table, the prediction for actinides is similar to that observed for other reported data for PWR fuel. However, for UO_2 , ^{235}U is slightly overpredicted for the gadolinium rod. The calculated and measured data for ^{148}Nd are in very good agreement.

The experimental and the calculated data for the gadolinium nuclides are presented in Table F.15. The results shown in this table indicate a systematic large underestimation for ^{155}Gd . This underestimation is consistent with other published results for these samples, which were obtained using the Step Wise Burnup Analysis Code System (SWAT) with the Japanese Evaluated Nuclear Data Library (JENDL)-3.2 cross sections [F7]. Note that the ^{155}Gd content in the measured samples is less than 2% of the total gadolinium content.

Table F.12. Ohi-2 assembly design data [F7]

Parameter	Data
Fuel rod data	
Fuel Type	UO ₂ , UO ₂ - Gd ₂ O ₃
Pellet Density (g/cm ³)	10.4
Pin Pitch (cm)	1.265
Fuel Pellet Diameter. (cm)	0.805
Fuel Temperature (K)	900
Fuel Enrichment (UO ₂)	3.2 wt % ²³⁵ U
Fuel Enrichment (UO ₂ -Gd ₂ O ₃)	1.68 wt % ²³⁵ U, 6wt% Gd ₂ O ₃
Clad Inner Diameter (cm)	0.822
Clad Outer Diameter (cm)	0.950
Clad Material	Zircaloy-4
Clad Temperature (K)	600
Moderator data	
Coolant Inlet Temperature (K)	289
Coolant Outlet Temperature (K)	325
Assembly data	
Assembly Pitch (cm)	21.4
Channel Material	Zircaloy-4
Operating Pressure (kg/cm ²)	32
Fuel Active Height (cm)	364.8

Table F.13. Ohi-2 samples data

Sample ID	Burnup (GWd/MTU)	Coolant density (g/cm³)	Sample location* (mm)
89G01	21.92	0.740	267
89G03	29.45	0.726	737
89G05	25.73	0.726	733

* with respect to bottom of active fuel

Sample Rod

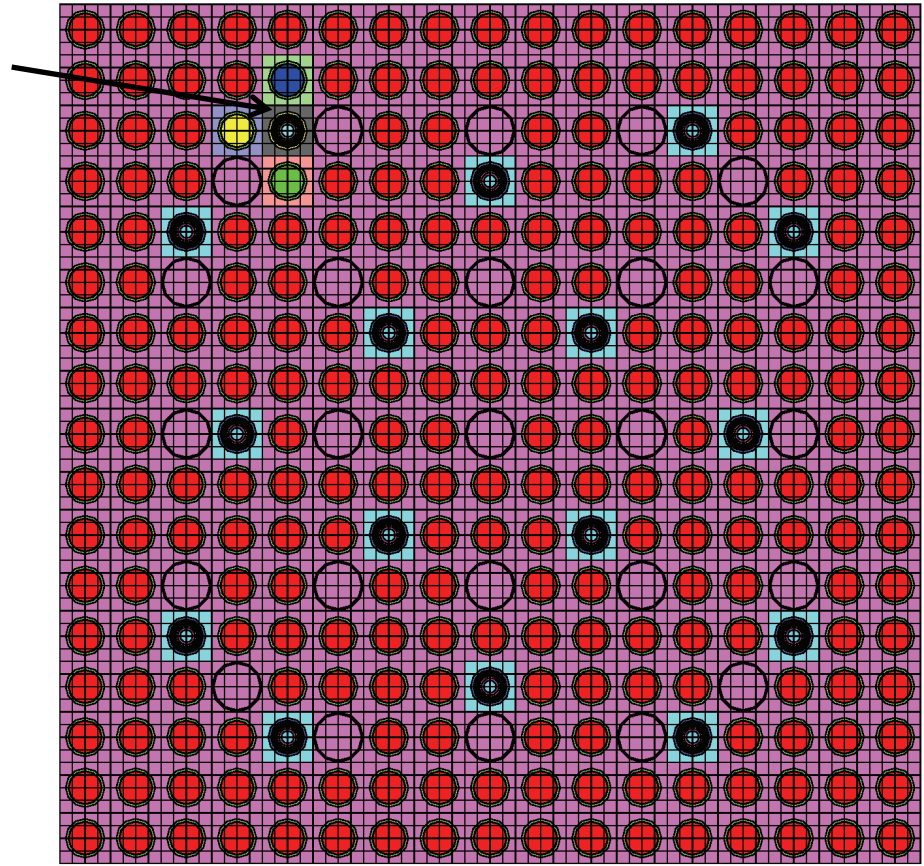


Figure F.11. Illustration of SCALE/TRITON model for Ohi-2 assembly.

Table F.14. Comparison calculation-measurement for Ohi-2 samples (actinides)

Sample ID	C/M-1 (%)			
	89G01	89G05	89G03	Average
GWd/MTU	21.47	25.14	28.72	
U ²³⁴	2.5	2.3	3.6	2.8
U ²³⁵	4.1	5.2	4.7	4.7
U ²³⁸	0.1	0.2	0.1	0.1
Np ²³⁷	-5.1	0.9	-0.5	-1.6
Pu ²³⁸	-10.8	-15.9	-14.5	-13.7
Pu ²³⁹	-1.7	-2.9	-1.8	-2.1
Pu ²⁴⁰	-1.5	-2.5	-1.9	-2.0
Pu ²⁴¹	-4.4	-6.0	-5.3	-5.2
Pu ²⁴²	-5.5	-9.2	-7.9	-7.5
Am ²⁴¹	13.0	3.5	-6.7	3.3
Am ²⁴³	6.2	-14.8	1.6	-2.3
Nd ¹⁴⁸	-0.7	-0.3	-0.2	-0.4

Table F.15. Comparison calculation-measurement for Ohi-2 samples (Gd)

	89G01				89G05				89G03			
GWd/MTU	21.47				25.14				28.72			
	M (measured data)*		C	C/M	M (measured data)		C	C/M	M (measured data)		C	C/M
	Gd ⁿ /Gd ^{total}	uncert			Gd ⁿ /Gd ^{total}	uncert			Gd ⁿ /Gd ^{total}	uncert		
Gd ¹⁵²	0.056	0.001	0.057	1.024	0.044	0.001	0.046	1.340	0.034	0.001	0.036	0.828
Gd ¹⁵⁴	1.818	0.002	1.863	1.025	1.748	0.002	1.806	1.079	1.674	0.002	1.754	1.003
Gd ¹⁵⁵	0.018	0.001	0.012	0.675	0.019	0.001	0.012	0.226	0.053	0.003	0.013	0.707
Gd ¹⁵⁶	34.600	0.020	34.665	1.002	34.545	0.023	34.567	1.009	34.26	0.030	34.467	0.998
Gd ¹⁵⁷	0.007	0.001	0.007	0.964	0.009	0.001	0.007	0.843	0.008	0.001	0.007	0.745
Gd ¹⁵⁸	41.520	0.020	41.406	0.997	41.640	0.030	41.556	0.992	41.870	0.030	41.699	1.001
Gd ¹⁶⁰	21.990	0.010	21.990	1.000	21.994	0.004	22.008	0.996	22.100	0.010	22.023	1.001

* reported measured data consists of the ratio of atoms of a Gd isotope and total number of Gd atoms.

F.4 STATISTICAL ANALYSIS OF THE BWR ISOTOPIC VALIDATION DATA

Relevant statistical data for the analyzed BWR samples are shown in Table F.16. For each of the BUC nuclides, the table includes the mean, the standard deviation around the mean, and the number of samples. The variation with burnup in the 16 considered samples of (C/M-1) is presented in Figure F.12 for the major actinides ²³⁵U and ²³⁹Pu. On average, the comparison calculation-measurement for these two major actinides, obtained for the 16 BWR samples with burnups less than 27 GWd/MTU, is quite similar with the data obtained for PWR fuel. For the considered 16 BWR samples, ²³⁵U and ²³⁹Pu are predicted on average within 1.6 and 5.4% of the measurement, respectively. Corresponding standard deviations are 2.4 and 4.4%. Results reported [F8] for 92 PWR fuel samples with burnups in the range of 7–70 GWd/MTU, based on calculations performed with SCALE6.1 and ENDF/B-VII.0 cross sections,

show predictions for ^{235}U and ^{239}Pu that are on average within 1.2 and 4.1% of the measurement, respectively; the corresponding standard deviations are 3.5 and 3.5%.

Table F.16. Statistical data for the BWR samples (BUC nuclides)

Nuclide	Average % (C/M-1)	Standard deviation	Number of samples
U^{234}	3.33	4.32	8
U^{235}	1.56	2.36	16
U^{236}	-2.92	2.58	16
U^{238}	0.00	0.10	16
Pu^{238}	-2.74	11.64	16
Pu^{239}	5.38	4.40	16
Pu^{240}	3.66	5.37	16
Pu^{241}	-4.12	12.72	16
Pu^{242}	0.26	13.40	16
Am^{241}	10.30	60.02	10
Am^{243}	5.25	10.25	4
Nd^{143}	-0.30	1.20	8
Nd^{145}	0.21	1.08	8
Sm^{147}	-3.86	3.14	3
Sm^{149}	-7.50	17.06	3
Sm^{150}	-4.06	2.25	3
Sm^{151}	-3.35	6.43	3
Sm^{152}	-3.98	3.19	3

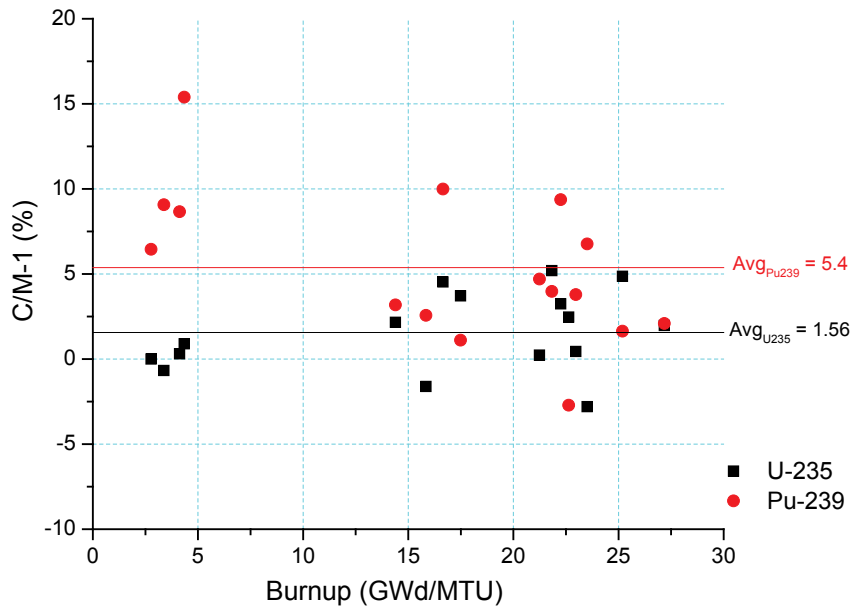


Figure F.12. Variation with burnup of (C/M-1) for ^{235}U and ^{239}Pu .

F.5 APPENDIX F REFERENCES

- F1. SFCOMPO - Spent Fuel Isotopic Composition Database, <http://www.nea.fr/sfcompo/>, retrieved November 2014.
- F2. O. W. Hermann and M. D. DeHart, "Validation of SCALE (SAS2H) Isotopic Predictions for BWR Spent Fuel," ORNL/TM-13315, Oak Ridge National Laboratory, September 1998.
- F3. "Post-Irradiation Analysis of the Gundremmingen BWR Spent Fuel," *Nucl. Sci. and Tech.*, Commission of the European Communities, ISBN 92-825-1099-9, 1979.
T. Yamamoto, "Compilation of Measurement and Analysis Results of Isotopic Inventories of Spent BWR Fuels,"
<https://www.oecd-nea.org/science/wpncs/ADSNF/reports/JNES/JNESreport2009.pdf>.
- F4. T. Yamamoto and M. Yamamoto, "Nuclear Analysis of [Postirradiation Examination] PIE Data of Irradiated BWR 8×8-2 and 8x8-4 UO₂ Fuel Assemblies," *Journal of Nuclear Science and Technology*, Vol. 45, No.11, (November 2008).
- F5. Y. Nakahara, K. Suyama, and T. Suzaki, "Technical Development on Burnup Credit for Spent LWR Fuels," JAERI-Tech 2000-071, ORNL/TR-2001/01, English Translation, Oak Ridge National Laboratory, January 2002.
- F6. U. Mertzyurek, M. W. Francis, and I. C. Gauld, "SCALE 5 Analysis of BWR Spent Nuclear Fuel Isotopic Compositions for Safety Studies," ORNL/TM-2010/286, Oak Ridge National Laboratory, December 2010.
- F7. K. Suyama, M. Murazaki, K. Ohkubo, Y. Nakahara, G. Uchiyama, "Re-evaluation of Assay Data of Spent Nuclear Fuel obtained at Japan Atomic Energy Research Institute for Validation of Burnup Calculation Code Systems," *Annals of Nuclear Energy*, Volume 38, pp. 930–941, 2011.
- F8. G. Ilas, I. C. Gauld, and G. Radulescu, "Validation of new depletion capabilities and ENDF/VII data libraries in SCALE," *Annals of Nuclear Energy* Volume 46, pp. 43–55, August 2012.

BIBLIOGRAPHIC DATA SHEET

(See instructions on the reverse)

NUREG/CR-7194
ORNL/TM-2014/240

2. TITLE AND SUBTITLE

Technical Basis for Peak Reactivity Burnup Credit for BWR Spent Nuclear Fuel in Storage and Transportation Systems

3. DATE REPORT PUBLISHED

MONTH	YEAR
04	2015

4. FIN OR GRANT NUMBER
NRC JCN V6452

5. AUTHOR(S)

William (B.J.) Marshall, Brian J. Ade, Stephen M. Bowman, Ian C. Gauld, Germina Ilas, Ugur Mertuyrek, Georgeta Radulescu

6. TYPE OF REPORT
Technical

7. PERIOD COVERED (Inclusive Dates)

8. PERFORMING ORGANIZATION - NAME AND ADDRESS (If NRC, provide Division, Office or Region, U.S. Nuclear Regulatory Commission, and mailing address; if contractor, provide name and mailing address)

Oak Ridge National Laboratory
Managed by UT-Battelle, LLC
Oak Ridge, TN 37831-6170

9. SPONSORING ORGANIZATION - NAME AND ADDRESS (If NRC, type "Same as above"; if contractor, provide NRC Division, Office or Region, U.S. Nuclear Regulatory Commission, and mailing address)

Division of System Analysis and Regulatory Effectiveness
Office of Nuclear Regulatory Research
U. S. Nuclear Regulatory Commission, Washington, DC 20555-0001

10. SUPPLEMENTARY NOTES

11. ABSTRACT (200 words or less)

This report describes studies performed to provide a technical basis for the application of burnup credit in criticality safety analyses of storage and transportation casks for boiling-water reactor (BWR) spent nuclear fuel (SNF) using BWR peak reactivity methods. Most BWR fuel assemblies contain gadolinium oxide burnable absorber in some fuel rods. The gadolinium absorber depletes more rapidly than the fuel, which causes the fuel assembly reactivity to reach a maximum value at an assembly average burnup typically less than 20 gigawatt days per metric ton of uranium (GWd/MTU).

This report reviews the most commonly used peak reactivity methods in spent fuel pool analyses for BWR SNF to provide technical background for potential application to storage and transportation casks, including (1) an examination of the fuel assembly lattice design and operating parameters that affect the burnup and reactivity of the peak reactivity in storage and transportation configurations, (2) validation of these reactivity calculations, and (3) validation of the depleted isotopic inventories in BWR SNF at burnups associated with peak reactivity. This report focuses on fuel assemblies with average burnups of approximately 20 GWd/MTU or less. Burnup credit for BWR fuel assemblies with typical discharge burnups will be addressed in future reports.

12. KEY WORDS/DESCRIPTORS (List words or phrases that will assist researchers in locating the report)

burnup credit
BWR
fission products
actinides
peak reactivity
gadolinium
spent fuel

13 AVAILABILITY STATEMENT
unlimited

14 SECURITY CLASSIFICATION
(This Page)
unclassified

(This Report)
unclassified

15. NUMBER OF PAGES

16. PRICE



Federal Recycling Program



**UNITED STATES
NUCLEAR REGULATORY COMMISSION**
WASHINGTON, DC 20555-0001

OFFICIAL BUSINESS



NUREG/CR-7194

**Technical Basis for Peak Reactivity Burnup Credit for BWR Spent Nuclear
Fuel in Storage and Transportation Systems**

April 2015